

DYNAMIC NUMERICAL RUN-OUT MODELING FOR
QUANTITATIVE LANDSLIDE RISK ASSESSMENT

Byron Rene Quan Luna

Examining committee:

Prof. Tom Veldkamp	University of Twente
Prof. Freek van der Meer	University of Twente
Prof. Michel Jaboyedoff	UNIL, Switzerland
Dr. Jean-Philippe Malet	CNRS, France
Dr. Farrokh Nadim	NGI, Norway

ITC dissertation number 206
ITC, P.O. Box 6, 7500 AA Enschede, The Netherlands

ISBN 978-90-6164-330-2
Cover designed by Job Duim / Benno Masselink
Printed by ITC Printing Department
Copyright © 2012 by Byron Rene Quan Luna



DYNAMIC NUMERICAL RUN-OUT MODELING FOR QUANTITATIVE LANDSLIDE RISK ASSESSMENT

DISSERTATION

to obtain
the degree of doctor at the University of Twente,
on the authority of the Rector Magnificus,
prof.dr. H. Brinksma,
on account of the decision of the graduation committee,
to be publicly defended
on Friday May 11, 2012 at 14:45 hrs

by

Byron Rene Quan Luna

born on March 30, 1975

in Guatemala, Guatemala

This thesis is approved by

Prof. dr. Victor G. Jetten

Dr. Cees van Westen

Dr. Theo van Asch

promoter

assistant promoter

assistant promoter

Abstract

Landslides and debris flows are geomorphologic events that may pose danger to different components of mountainous societies. This danger is not only the result of the process as such, but of the interaction with human systems and their associated vulnerabilities. Understanding, forecasting and controlling the hazard associated to this type of slope movements is still an empirical task which requires a mix of qualitative and quantitative analyses. The development of numerical dynamic run-out models has made a dramatic change in the study of hazardous processes, as these allow the simulation of possible future scenarios, including ones that have no historical evidences. Dynamic computer models have the potential to simulate geomorphologic processes with an acceptable degree of accuracy. Once this is achieved, a range of potential hazard scenarios can be analyzed and the results can be used to inform local authorities and the population in order to respond to these hazards and plan to reduce the associated risks. For this reason, it is important to evaluate the reliability and consistency of these dynamic models that integrate the physical descriptions of the landslide process in a numerical scheme, embedded in a Geographical Information System (GIS).

A variety of models exists for simulating and for identifying the hazard that the different mass-flow phenomena present. Dynamic run-out models are able to forecast the propagation of material after the initial failure and to delineate the zone where the elements-at-risk will suffer an impact with a certain level of intensity. The results of these models are an appropriate input for vulnerability and risk assessments. An important feature of using run-out models is the possibility to perform forward analyses and forecast changes in hazards. However, still most of the work using these models is based on the calibration of parameters doing a back calculation of past events. Given the number of unknown parameters and the fact that most of the rheological parameters cannot be measured in the laboratory or field, it is very difficult to parameterize the run-out models. For this reason the application of run-out models is mostly used for back analysis of past events and very few studies attempts to achieve a forward modelling with the available run-out models. A reason for this is the substantial degree of uncertainty that still characterizes the definition of the run-out model parameters.

The main objective of this research was to apply, improve and optimize the use of dynamic run-out models in quantitative risk assessment, focusing on the parameterization of the models, and the analysis of uncertainty. Since a variety of models exists for simulating mass-flows and for identifying the intensity of the hazardous phenomena, it is important to assess these models, perform a parameterization and reduce their uncertainties. This will enable to improve the understanding to assess the hazard and will provide

the link with vulnerability curves that will lead eventually to generate risk curves and quantify the risk.

This research describes the state of the art in dynamic run-out modelling focusing on continuum depth-average models. Three different dynamic run-out models (MassMov2D, DAN3D and RAMMS) were selected for a sensitivity analysis of their resistance parameters using the Voellmy rheology. Three test sites were used: Barcelonnette in France, Valtellina di Tirano in Italy, and a site in Kerala, India.

A special consideration was given to the entrainment mechanism. The increase of volume once a failed mass is in movement due to entrainment enhances the mobility of the flow and can significantly influence the size of the potential impact area. In view of this, a 1-D run-out model is presented with an entrainment concept based on limit equilibrium considerations and the generation of excess pore water pressure through undrained loading of the bed material.

An extensive database was made which includes the rheological parameters (Voellmy and Bingham rheologies), release volumes, the type of movement, the environmental setting and other physical characteristics of previously back-calibrated events that have been described by other authors. Using the database, the variability for the rheological parameters was represented as probability density functions. The PDFs were used in a probabilistic framework based on a Monte Carlo simulation to analyze the effect of the uncertainty of input parameters. Combined probability density functions of the Voellmy and Bingham rheology were sampled and a large number (5000) of run-out scenarios were generated. The result was a Gamma probability distribution of possible intensities in selected points of the deposition area. The result obtained from the application of this methodology was the probability of a selected location being affected by a landslide in terms of intensity factors (height or velocity). The generated probability density functions were also applied to a newly developed medium scale model called "AschFlow", which is a 2-D one-phase continuum model that simulates the spreading, entrainment and deposition process of landslides or debris flows at a medium scale in the French test site.

Complexity arises with the interaction of the modelling intensity outputs with the affected elements at risk. For this reason, three physical vulnerability curves that relate the intensity of debris flows and the economic losses were derived from a well documented debris flow event. The event was back analyzed with a dynamic-run out model and the outputs were related to the damage data of elements at risk in order to generate the vulnerability functions. A quantitative risk assessment was carried out using run-out

modelling for the Italian study site. Based on the historical events and susceptibility maps, three potential debris flows initiation zones were delimited. These selected areas were modelled with the dynamic run-out model FLO-2D to assess the run-out intensity. The methodology used in this analysis consisted of several components, such as a detailed analysis of rainfall return periods (10, 50, 100 years return period), the modelling of rainfall-runoff, the analysis of soil samples in the laboratory, the analysis of terrain characteristics, the modelling of the run-out of the debris flows, the application of debris flow height and impact pressure vulnerability curves and the generation of risk curves based on the economic losses.

This research has contributed to a better understanding of the use of run-out modelling of debris flows, and provides a number of new avenues for the incorporation of uncertainty in this type of analysis, in order to be better make an estimation of potential losses. The results can be applied in cost benefit analysis for the design of risk reduction measures.

The main part of this research was carried out as an Early Stage Researcher inside the European Commission Marie Curie Actions Research Training Network: "Mountain Risks: from prediction to management and governance" within the 6th Framework Programme (<http://mountain-risks.eu/>). The last part and completion of this research was executed inside the "SafeLand" project within the 7th Framework Programme for research and technological development of the European Commission. (<http://www.safeland-fp7.eu/>).

Acknowledgements

This thesis would have never been accomplished without the help, support and dedication of many wonderful people. Their patience and tolerance with me during this whole period is highly appreciated. These acknowledgments are for all of them.

I would like to say a special thanks to Cees van Westen my supervisor and tutor. He was always available when needed with the right solution and smart approach for every situation. He made this work an exciting challenge and I have learned a lot during this time under his supervision. Personally, I am extremely proud to be one of his students. I am very grateful for his support during this whole period. Also a special mention and thanks to my co-supervisor Theo van Asch. Theo is the kindest and coolest person to work with. With Theo around, there is no boring minute and it is always something new to learn from his vast experience. This thesis was completed thanks to his inputs and amazing ideas. Thanks also to my promotor Victor Jetten for his trust in me and nice discussions. Victor was always supportive and had continuous faith in this work. To the three of them (my supervising team), thanks a lot! Thanks for going through every word of this thesis and make the right comments at the right moment and place. You were incredible and I admire your work.

Another special thanks to Kaare Høeg. His teaching at the University of Oslo and his supervision during my Master studies were immensely valuable for the completion of this thesis. He is an inspiration and one of the reasons I follow this research topic. I will always be grateful for his kindness, his support and his constant interest during this period.

I am also very grateful to all the people involved in the Mountain Risk project. They were an excellent group to work with. Mountain Risk was not only a training network where great research and collaboration between institutions was carried out but also a place where long lasting friendships were forged. I had an awesome time working with all of them. Thanks to Jean Philippe Malet for coordinating the project and making every activity inside the project a success. A special mention to the debris flow guru Alexandre Remaître (my Firenze roommate), Simone Frigerio (my step brother ever since Luciana, Antonio and Kikinha adopted me in Albavilla), my good friend Simone Sterlacchini, Jan "Buznito" Blahut, Alessandro Pasuto and H. Cross. Thanks also to the leading scientists inside the project which with their experience made this a great project to be in: Michel Jaboyedoff, Thomas Glade, Olivier Maquarie, Dorian Castaldini, Denis Jongmans, Jordi Corominas, Filippo Catani, Thom Bogaard, Santiago Begueria, Gianluca Marcato and Alessandro Corsini. Thanks to all the ER's and ESR's too, for all

the great memories: Melanie, Marjorie, Carolina, Graciela, Ulrich, Jacopo, Ping, Alessio, Olga, Alexander, Dominika, Julien, Anke and Suen Wong.

Thanks to all the people from ITC-UT that helped me unconditionally during this period. Thanks to Lyande for always being there and her friendship. Also special thanks to Jeroen Jansen for his assistance ever since I arrive to ITC. I am also grateful to Herman Baltink for all his help. To all the marvelous people in ITC like Freek, Theresa, Cecille (and Marjolijn), Benno, Job, Esther, Christie, Dinand, Janneke, Nanette, Sekhar, Rob, Bart, Menno, Harald, Mark, Chris, Petra, Malgosia, Tsehaie, Robert, Norman, David, John and Sabine, I will always cherish their support and guidance. Also big thanks to Loes for her patience, her help in finishing the thesis and all the arrangements that were made at the end.

To my PhD colleagues sitting at ITC, I encourage them to make the best of this experience and to keep on going strong with the great job they are doing at the moment. Each of them are special and I wish them the biggest of success. Thanks to Mila (for her company and having the time to hear me when I needed it), Andre, Haydar, Tolga, Xuanmei, Sharon, Anandita, Khamarrul, Frederick, Nugroho, Pablo and Sanaz. Good luck to all of you in the future.

A very special thanks to Farrokh Nadim and Bjørn Kalsnes for letting me finish my thesis at ICG/NGI. They have made a nice and comfortable environment for me to work there. I am very grateful for their support; patience and making me feel welcome. Thanks for everything. I would also like to thanks Jose Cepeda for his continuous help, his words of encouragement and his friendship. Besides them, thanks to all the people at NGI (like Dieter, Ulrik, Regula, Haakon, Bjørn Vidar) that had made my stay at NGI a fruitful and productive one.

My utmost gratitude goes to the Molenaar family. Thanks to Noortje for absolutely everything. Without her being there, nothing would have worked out. Noortje should get a trophy for her outstanding behavior, patience and her constant support. Muchos gracias, je bent geweldig in alle opzichten! A big thanks to Arnold, Rieneke, Inge and Thijs for making me feel at home in The Netherlands and for each and every small thing you have done for me. Thanks Rieneke for making the cover of the thesis.

My eternal gratitude to my mom and my dad (Doña Sara and Don Hernan). It has been as much as my effort as it has been theirs. Their love, sacrifice and support has no boundaries or distance. Thanks also to my brothers and sisters for their cheers: Aileen, Sara, Kenneth and Erick. Also big thanks to Rodrigo for his insights in difficult situations.

A special mention to the small angel Miguel, no matter how long I was far away; he always received me back with a smile and a stor bjørn klem. After all this time, vi klarte det flink gutt!! I am very proud of us.

Thank God for giving me choices and the possibility to decide. Thanks for the freedom and the responsibility that this brings. Thanks for everything.

Last but not least, thanks also to the people that I could not mention here but that were also involved in my work during this period. I am sorry but due to the limited space, I can not mention all of you. As I said in the beginning, this thesis would have never been accomplished without the help, support and dedication of many wonderful people and if you are reading this, I am sure you are one of them.

This research was carried out thanks to the financial support of: - The European Commission Marie Curie Actions Research Training Network: "Mountain Risks: from prediction to management and governance" within the 6th Framework Programme; -The "SafeLand" project within the 7th Framework Programme for research and technological development of the European Commission; and – ITC, Faculty of Geo-Information Science and Earth Observation of the University of Twente.

Table of Contents

Abstract.....	i
Acknowledgements	iv
Table of Contents.....	vii
Chapter 1: Introduction	1
1.1 Background	1
1.2 Quantitative landslide and debris flow risk assessment	2
1.3 Run-out hazard analysis.....	5
1.4 Problem definition	6
1.5 Research objectives	7
1.6 Research questions.....	9
1.7 Framework of the thesis and outline of the methodology	10
Chapter 2: Test areas.....	15
2.1 Barcelonnette basin, France	15
2.1.1 <i>Faucon torrent</i>	19
2.2 Valtellina di Tirano, Italy	22
2.2.1 <i>Selvetta debris flow event</i>	25
2.2.2 <i>Tresenda debris flow events</i>	29
2.3 Peringalam, Kerala, India	31
2.4 Summary	32
Chapter 3: Dynamic run-out models: an overview	35
3.1 Introduction.....	35
3.1.1 <i>Empirical methods</i>	36
3.1.2 <i>Analytical methods</i>	37
3.1.3 <i>Numerical methods</i>	38
3.2 Classification of dynamic run-out models	40
3.3 An overview of several dynamic run-out models.....	43
3.4 Dynamic run-out models used in this research	45
3.4.1 <i>MassMov2D model</i>	47
3.4.2 <i>DAN3D model</i>	49
3.4.3 <i>MassMov2D and DAN3D sensitivity of the resistance parameters</i>	51
3.4.4 <i>RAMMS model</i>	53
3.4.4 <i>FLO-2D model</i>	55
Chapter 4: A run-out model with an entrainment module	59
4.1 Introduction.....	59
4.2 Entrainment mechanism analysis - brief summary of previous work	60
4.2.1 <i>Experimental investigations</i>	61
4.2.2 <i>Empirical analyses</i>	62
4.2.3 <i>Numerical analyses</i>	63
4.3 Model description	65
4.3.1 <i>An entrainment model based on static equilibrium conditions and undrained loading</i>	66
4.4 Sensitivity analysis	69

4.5	Testing the model in the Faucon test area.....	71
4.6	Discussion and conclusions	75
Chapter 5:	Parameterization of dynamic run-out models.....	77
5.1	Introduction.....	77
5.2	Parameters used in run-out modelling – a brief summary	78
5.3	Database compilation and description	80
5.4	Design of probability density functions	83
5.4.1	<i>Coupled distribution functions</i>	87
5.5	Discussion and conclusions	89
Chapter 6:	Application of a Monte Carlo method to debris flow run-out modeling	91
6.1	Introduction.....	91
6.2	Methodology	94
6.3	Results	96
6.3.1	<i>The Faucon catchment in the Barcelonnette Basin</i>	96
6.3.2	<i>Tresenda village in the Valtellina Valley</i>	103
6.4	Discussion	109
6.5	Conclusions	112
Chapter 7:	A dynamic run-out model for medium scale hazard analysis	115
7.1	Introduction.....	115
7.1.1	Brief summary of regional run-out modelling and past work	116
7.2	Description of the model	121
7.2.1	<i>Dynamic routines inside the model</i>	121
7.2.2	<i>Rheologies and entrainment mechanisms</i>	122
7.2.3	<i>Model setup and initial conditions</i>	122
7.3	Case studies	123
7.3.1	<i>Barcelonnette Basin, France</i>	123
7.3.2	<i>The Valtellina Valley in Italy</i>	130
7.4	Discussion and Conclusions.....	135
Chapter 8:	Local scale run-out modelling for vulnerability assessment..	139
8.1	Introduction.....	139
8.2	Numerical modelling for hazard analysis in a quantitative risk assessment (QRA)	140
8.3	Physical vulnerability assessment	141
8.4	Modelling the Selvetta 2008 event for determining vulnerability curves	144
8.4.1	<i>Rainfall modelling</i>	145
8.4.2	<i>Debris flow modelling</i>	145
8.5	Generation of vulnerability curves.....	147
8.5.1	<i>Methodology</i>	148
8.5.2	<i>Generation of a vulnerability curve using accumulation heights</i>	150
8.5.3	<i>Generation of a vulnerability curve using impact pressures</i>	151
8.5.4	<i>Generation of a vulnerability curve using kinematic viscosity</i>	152
8.6	Discussion and conclusions	153

Chapter 9: Use of run-out models for a quantitative risk assessment at a local scale.....	157
9.1 Introduction	157
9.2 Methodology	161
9.2.1 Estimation of rainfall return periods.....	161
9.2.2 <i>Rainfall-runoff simulation and threshold estimation</i>	162
9.2.3 <i>Laboratory analysis</i>	163
9.2.4 Debris flow modelling	164
9.3 Quantitative risk analysis	165
9.3.1 <i>Elements at risk in the study area</i>	165
9.3.2 <i>Loss estimation</i>	166
9.3.3 <i>10-year return period</i>	166
9.3.4 <i>50-year return period</i>	168
9.3.5 <i>100-year return period</i>	168
9.4 Results	170
9.6 Discussion and conclusions	172
Chapter 10: Conclusions	175
10.1 Future scope of research and practical needs of dynamic run-out models	180
References	183
Curriculum Vitae	201
List of publications	202
Samenvatting	203
Appendices.....	207
Appendix 1	207
Appendix 2	225
Appendix 3	228
Appendix 4	231
Appendix 5	235
ITC Dissertation List	238

Chapter 1: Introduction

1.1 Background

Debris flows are geomorphological events that may pose danger to different components of our societies. This danger is not only the result of the process as such, but of the interaction with human systems and their associated vulnerabilities. When both hazard and vulnerability have the same coordinates in space and time, natural disasters can occur (Alcantara-Ayala, 2002). Mass movements which are commonly triggered in mountainous area represents one of the most destructive natural hazards in terms of economical losses and the amount of human casualties, and are often underestimated (Petley, 2011)(Fig.1.1).

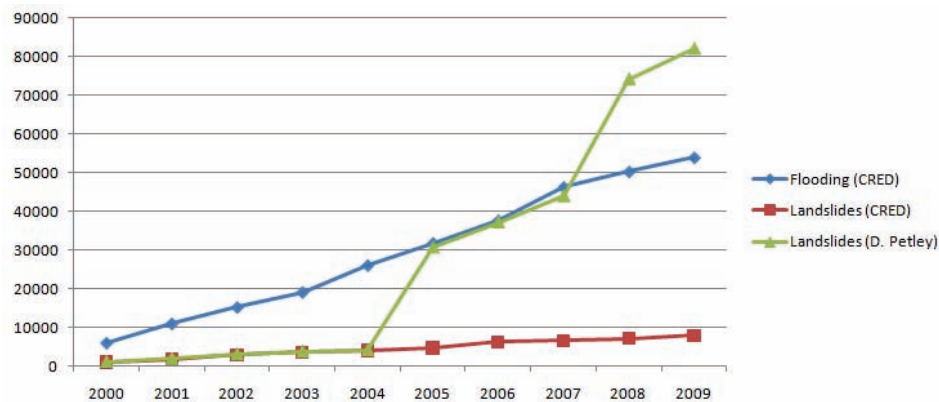


Fig. 1.1: Worldwide landslide fatalities are much higher than represented in the official CRED database, (EM-DAT: The CRED International Disaster Database, 2011) as many landslides fatalities are included in those of the triggering events. A study by Petley (2011) reveals that during the last 10 years landslides killed more people than flooding, particularly as a result of earthquake-induced landslides.

This research focused mainly on rapid geomorphologic mass movements such as debris flows and mud flows. These flows generally occur during periods of intense rainfall or rapid snow melt. These processes usually starts on steep hillsides as shallow landslides that liquefy and accelerate to speeds that are typically about 15 km/h, but can reach as much as 60 km/h (Iverson, 2005). Debris and mud flows can originate from many different sources and converge in channels where they may have a large destructive power (Hung *et al.*, 2001). The three main initiation mechanisms of debris flows are: landslide-type failures (which may also result in hillslope debris flows), channel-bed failure (erosion), and temporary blockage of sediment and water flows in the channel, enhancing the surge-like flow behaviour (Rickenmann and Zimmermann, 1993). Flow-like behaviour events are a mixture of water, poorly sorted sediment and other debris, typically flowing rapidly, with one or

more surges and a coarse-grained front, down steep mountain channels to a fan (Iverson and Denlinger, 2001). The materials involved in these flows usually include sediment from clay-size up to boulders, and organic components (Glade, 2005). Their non-homogeneous, non-Newtonian and transient fluid properties can change significantly as they flow down steep watershed channels or across alluvial fans (Hutchinson, 1986). Their behaviour is a function of the fluid matrix properties, channel geometry, slope and roughness. The fluid matrix consists of water and fine sediments. At sufficiently high concentrations, the fine sediments alter the properties of the fluid including density, viscosity and yield stress (O'Brien and Julien, 1988).

Debris and mud flows are complex phenomena which are influenced by many external (e.g. rainfall, groundwater levels, and topography) and intrinsic factors (e.g. geotechnical properties) both in their initiation and run-out processes. Understanding, forecasting and controlling the hazard associated to this type of slope movements is still an empirical task which requires a mix of qualitative and quantitative analyses. Analysis can be performed at several spatial and temporal scales according to the objective of the hazard assessment (van Asch *et al.*, 2004). In the case of attempting to forecast the spatial and temporal probability of occurrence and the intensity of these types of slope movements, a vast amount of different methods has been proposed in the past in order to characterize and analyze quantitatively the hazard in an area. These methods can be classified in general terms in: *heuristic, statistical, and deterministic approaches* (van Westen *et al.*, 1997). This research attempts to present the different approaches, developments and difficulties inside dynamic run-out modelling of debris flows, mud flows and landslide hazard at a local and medium scale with a focus on physically-based approaches. Special focus was given to the application and implementation of this type of models in a quantitative risk assessment. The deterministic characteristics of these models and the possibility to obtain direct intensity values make the run-out models an interesting tool to be used in these types of analyses.

1.2 Quantitative landslide and debris flow risk assessment

The main essence of a geomorphological risk assessment is to be able to quantify the probability of losses (either monetary values or fatalities) caused by geomorphologic process (hazards) in a specific area and within a specific period (Dai *et al.*, 2002; Fell and Hartford, 1997). The final result of this analysis is a risk curve that relates all the events with different probabilities and the corresponding losses. In this research we follow the most commonly used and straightforward approach for risk quantification; where the risk can

be quantified as the product of vulnerability, cost or amount of the elements at risk and the probability of occurrence of the event with a given magnitude/intensity. The hazard is multiplied with the expected losses for all different types of elements at risk (vulnerability amount), and this is done for all event types (Fig 1.2).

When trying to quantify risk, the hazard factor is one of the most complicated to estimate. This is mostly because of the spatial variation of the features that actively play a role in determining the type, magnitude and probability of occurrence of an event. For example in a landslide hazard assessment, the common approach is to calculate the stability of individual slopes with a static approach calculating the "Factor of Safety", which determines whether a slope can generate a landslide with a specific volume. Based on this estimated volume, the run-out zones can be assessed with dynamic or statistical models. Problems occur frequently in this type of calculations when confronted with a general lack of information on magnitude-frequency relations, surface topography, lithology, water table variations, soil depth and strength of materials. All of these can be added to the uncertainty of the intensity and probability of the triggering event, and the behavioural movement of the failed material down the slope.

Another important factor inside a quantitative risk assessment is the vulnerability component. Vulnerability is defined as the level of potential damage, or degree of loss, of a given element (expressed on a scale of 0 to 1) subjected to a hazard of a given intensity (Fell and Hartford, 1997). Vulnerability assessment involves the understanding of the interaction between a given hazard and the affected elements. In the case of a landslide risk assessment, the vulnerability depends on (a) the run-out distance; (b) the volume and velocity of sliding; and (c) the characteristics of the elements at risk and their exposure to the hazard. The assessment of vulnerability is somewhat subjective and largely based on historic records, or expert opinion. Landslide risk assessment involves the estimation of the level of risk, deciding whether or not it is acceptable, and exercising appropriate control measures to reduce the risk when the risk level cannot be accepted. In general, it requires the following issues to be addressed: (a) probability of landsliding, (b) run out behaviour of landslide debris, (c) vulnerability of property and people, (d) landslide risk to property and people, and (e) management strategies and decision-making (Ho *et al.*, 2000).

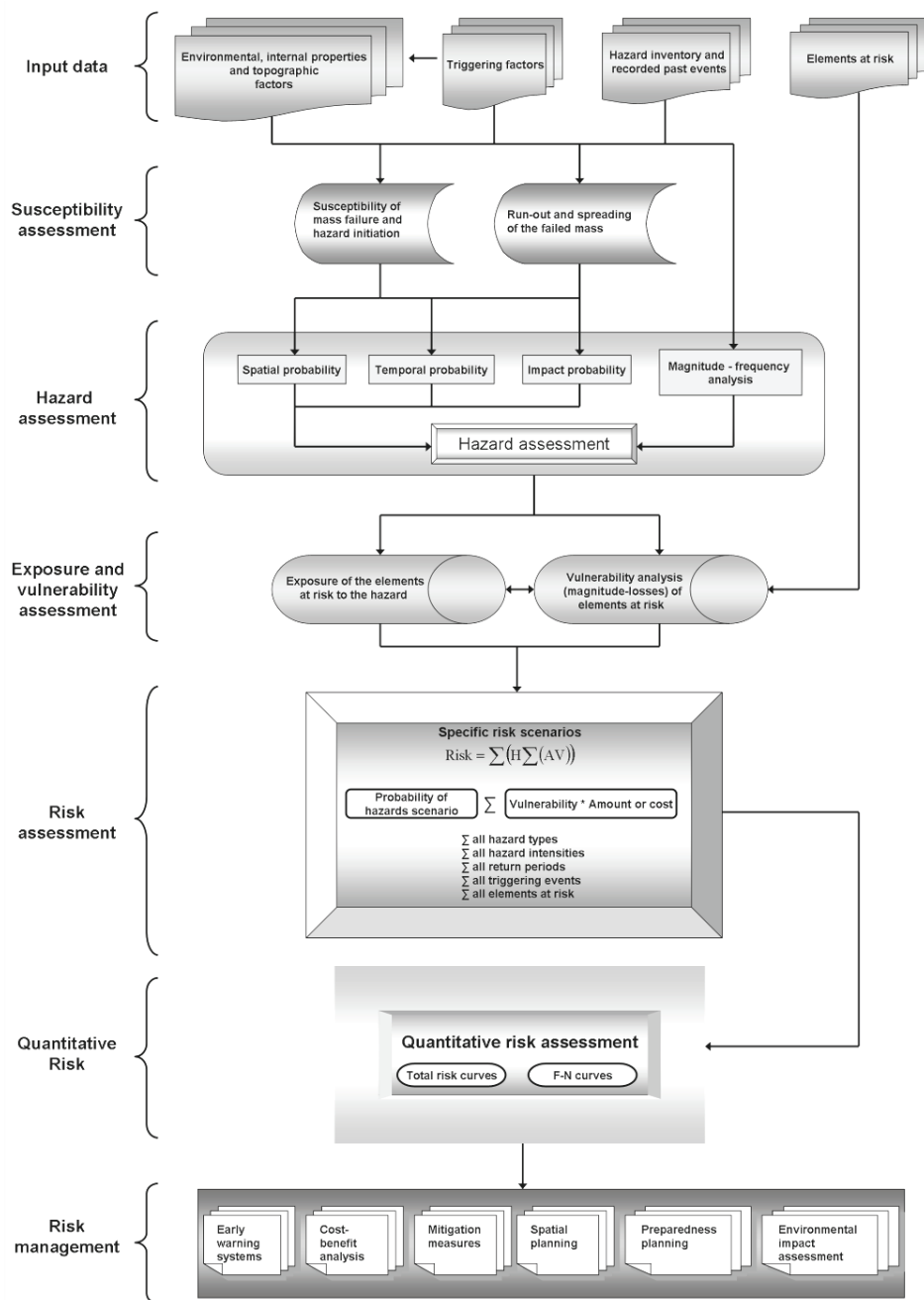


Fig 1.2: Framework of a multi-hazard risk assessment (after van Westen *et al*, 2010).

In spite all the difficulties and the uncertainties involved inside a quantitative risk assessment; regarding the topic of landslides and debris flows, recent advances and guidelines have provided a systematic approach for the whole process (Dai *et al.*, 2002; Fell *et al.*, 2008; van Westen *et al.*, 2008). These past efforts provide valuable information for a better understanding of the landslide risk and to develop risk acceptability criteria for a specific place.

1.3 Run-out hazard analysis

It is essential in a quantitative hazard assessment to know the extent of the endangered area. This requires accurate prediction of the run-out behaviour of a landslide, which include (Hung, 1995): run-out distance, run-out width, velocity, pressures, depth of the moving mass, and depth of deposits. The main factors that determine the run-out of a failed mass are the released volume of the landslide, the propagation behaviour/mechanism and the topographical characteristics of the path.

A variety of techniques have been developed to analyze the behaviour of the failed mass, its travel distance and the velocity at which it progresses down slope. It should be understood that the movement of a flow is complex and more than one phenomenon may be occurring at the same time, and different phenomena may prevail at different locations of a given event. These variations are dependent of the type of material and their response to external factors (e.g. loose granular soils tend to collapse when sheared, which under undrained condition results in an increase in pore water pressure). This can result in an evolution of the released mass into a debris flows that may travel great distances or to stop in a sudden manner. Once a failed mass is mobilized, the variation in the modes of movement and the different processes occurring while the flow is in movement (e.g. entrainment) influences the flow velocity and travel distance. For this reason, no universal run-out model exists, this means that no single model can adequately describes all the landslide types. However, the developed methods give a good systematic approach to assess the spreading, extension and impact that a landslide can generate. These methods (which will be further explained in chapter 3) can be divided in: *empirical methods* (Corominas, 1996); *analytical methods* (Hürlimann *et al.*, 2007); and *numerical methods* (Denlinger and Iverson, 2004; Mangeney *et al.*, 2005; Pudasaini and Hutter, 2007; Hung and McDougall, 2009; Crosta *et al.*, 2009; Pastor *et al.*, 2009).

One of the advantages of the numerical methods is that they have the ability of computing (with a good compromise between computing effort time and accuracy) the movement of the flow over irregular topographic terrains. In addition, the computed outputs of the models can be coupled directly to vulnerability or stage-damage functions for a quantitative risk assessment.

Numerical models also provide the opportunity to investigate run-out frequencies and magnitudes of landslides in the absence of documentation of former events.

1.4 Problem definition

The main aspect of run-out modelling is to reproduce accurately the dynamics of the geomorphologic processes and to forecast the potential area that might be affected. Post-failure movement is controlled by a complex interaction between mechanical and fluid properties that reflect spatio-temporal trends in the rheological properties of the material (Vulliet, 2000). Because of the complex interactions during the flow phase, the parameterization of hydrological and geotechnical factors is not sufficient to describe the post-failure movement patterns and not all the processes can be included in detail in the simulation.

One of these processes which is still difficult to include inside a run-out model and that plays an important role in the run-out phase of the flow is the entrainment. Entrainment mechanisms are able to change significantly the mobility of the flow, through rapid changes of the volume and its rheological behaviour (Iverson *et al.*, 1997; McDougall and Hungr, 2005, Takahashi, 2009). Models using both a constant rheology and a constant volume cannot yield accurate forecasts of debris flows characteristics (Chen *et al.*, 2006, Remaitre, 2006). After the failure at the source zone, the entrained materials may accumulate 10 - 50 times in volume with respect to the initially mobilized mass (Vandine and Bovis, 2002). Some efforts have already been made to quantify the erosion processes and entrained volumes, trying to propose a physical explanation for the extreme bulking rates (e.g. McDougall and Hungr, 2005; Sovilla *et al.*, 2007; Mangeney *et al.*, 2010). However, the introduction of entrainment in the models requires additional parameters, which will certainly complicate calculations even further.

Given the number of unknown parameters and the fact that most of the rheological parameters cannot be measured in the laboratory or field, it is very difficult to parameterize the run-out models. This leads to the problem of equifinality, as several combination of these unknown parameters might give results that resemble actual events. For this reason the application of run-out models is mostly used for back analysis of past events and very few studies (Calvo and Savi, 2008) attempts to achieve a forward modeling with the available run-out models. A reason for this is the substantial degree of uncertainty that still characterizes the definition of the run-out model parameters. Consequently all models are based on simplified descriptions that attempts to reproduce the general features of the failed mass motion through the use of parameters (restricted to friction coefficients) which account for aspects not explicitly described or oversimplified. At the moment,

a relatively complete and well-established calibration for most of the models is still lacking or not enough reliable to be applied in practical applications. This represents one of the basic limitations with the use of dynamic run-out models, since they are very sensitive to the frictional coefficients. Uncertainties involved in the run-out process have to be approached in a stochastic manner. It is of significant importance to develop methods for quantifying and properly handling the uncertainties in dynamic run-out models, in order to allow more appropriate quantitative risk assessment procedures to be defined

Most of the work done regarding dynamic run-out modeling in the past has been done at a local scale. Medium or small scale landslide run-out modeling that includes many possible landslide initiation areas in an area simultaneously has been a difficult task because of the complexity to define the initiation and volume of the released mass. In addition, modeling the displacements with a large amount of information becomes computational exhaustive. In many cases where the scale plays an important role in the limitation of the understanding of the material properties and the information about the flow characteristics (e.g. behavior of the flow), empirical methods have been used as a practical means to predict landslide mobility (Rickenmann, 1999; Devoli *et al.*, 2009). Statistical approaches (described in Chapter 3) are based on field observations and can be used to produce indices expressing, directly or indirectly, landslide mobility. However, there is still a large debate regarding the applicability of empirical methods as they require comprehensive datasets with the identification of both source point and end point of the movement (for geometrical characterization). Another drawback of these methods is the uncertainty caused by statistical regressions, the large scatter usually found inside the data and that they are not able to provide an estimate of the flow velocities or pressures, which is important in any type of quantitative risk assessment (van Westen *et al.*, 2006)

Due to these reasons there are still few attempts to use run-out models as an important tool inside a risk assessment (e.g. to create vulnerability curves) and to fully incorporate them inside a quantitative analysis. Even though, the run-out of a landslide or debris flow accounts for most of the damage to the elements at risk.

1.5 Research objectives

The main objective of this research was to apply, improve and optimize the use of dynamic run-out models in quantitative risk assessment, focusing on the parameterization of the models, and the analysis of uncertainty. Since a variety of models exists for simulating mass-flows and for identifying the intensity of the hazardous phenomena, it is important to assess these

models, perform a parameterization and reduce their uncertainties. This will enable to improve the understanding to assess the hazard and will provide the link with vulnerability curves that will lead eventually to generate risk curves and quantify the risk.

In order to reach the main objective, a number of sub-objectives have been formulated:

1. Evaluation and assessment of existing run-out models.

- To identify the characteristic features of different run-out models, the implementation of the numerical scheme, and the pre- and post-processing. This will allow understanding the simplifications and the assumptions of each model and their relevance to the type of the event.
- Assess the functionality of the models and their accuracy in reproducing past events by back analysis.
- Conduct a sensitivity analysis of the resistance parameters used in run-out models.

2. Entrainment process inside a run-out model

- Identify the past work done regarding the process of entrainment.
- Enhancement of a run-out model by the inclusion of the entrainment process in a dynamic manner.
- Validating the developed model with a back calibration of a well documented past event.

3. Parameterization of run-out models.

- To collect a detailed database of case studies that used back analysis of past events.
- Conduct a statistical analysis of the compiled database.
- Creation of probability density functions of the resistance parameters of two rheological models that direct the range of parameters to be used in forward analysis.

4. Application of a stochastic method to run-out models.

- Integrating the uncertainties related to the rheological parameters in a run-out model at a detailed scale
- Application of a Monte Carlo approach for a run-out model in order to obtain the probability of the intensity parameters at a certain location.

5. Medium scale run-out assessment

- Optimization of a run-out model to be applied for medium scale analysis for a quantitative hazard assessment.
- Perform an evaluation of the efficiency of the run-out model.

- Application of the model in areas with limited information at a catchment scale with stochastic techniques for the parameter uncertainty estimation.

6. Generation of vulnerability curves using numerical run-out models.

- Revision of the past work regarding physical vulnerability
- Application of numerical run-out models for a historical run-out site where damage information can be collected.
- Model the intensity values which will be related to the damage data in order to generate intensity-vulnerability curves which can be used in a subsequent risk assessment.

7. Quantitative risk assessment.

- Use a combination of stochastic and deterministic techniques in order to obtain the spatial and temporal probabilities of a hazard assessment.
- Link the output results from the run-out modelling with the generated physical vulnerability curves
- Assess the economic losses based on the impact of the hazard in the elements at risk
- Generation of risk curves

1.6 Research questions

The limited use and development of techniques for the application of run-out models for hazards and risk in a quantitative assessment lead to the formulation of a number of questions that this research intended to investigate.

- 1) Can run-out models be used as a significant tool to quantify risk and how can they be linked inside a risk assessment process?
- 2) Based on their characteristics, which of the different existing run-out models, which type of rheological model and which rheological parameters can be used consistently for a landslide or debris flow risk assessment?
- 3) How to quantify the amount of volume entrained by a flow event and is it possible to model this process inside a run-out model?
- 4) 4) How to represent the uncertainty of the input parameters that are involved in run-out modelling and can these uncertainties be approached in a stochastic manner?
- 5) Can a stochastic approach be applied to a run-out model and how?

- 6) At local and medium scale, can run-out models be applied with confidence where there is limited data about landslide events in the past and can run out models be used as predictive tools in areas where no event has happened before?
- 7) Are the outputs of the run-out models sufficiently reliable in order to use them as a tool to create physical vulnerability curves?
- 8) What consistent methodology allows quantifying the run-out processes in a consistent way that they can be applied regularly in a hazard analysis?

1.7 Framework of the thesis and outline of the methodology

The main part of this research was carried out as an Early Stage Researcher inside the European Commission Marie Curie Actions Research Training Network: "Mountain Risks: from prediction to management and governance" within the 6th Framework Programme (<http://mountain-risks.eu/>). The last part and completion of this research was executed inside the "SafeLand" project within the 7th Framework Programme for research and technological development of the European Commission. (<http://www.safeland-fp7.eu/>). This research attempts to acknowledge the advantages but at the same time points out the difficulties of using run-out models to perform a quantitative risk assessment. Special attention is given to the uncertainties involved in this process. A variety of run-out models exists to assess the hazard attempting to simulate the complexity of the flow phenomenon in different manners. For this reason, it was relevant to evaluate and optimize them with real applications and parameterize them. This research highlights the capacity of the dynamic run-out models to forecast the propagation of material and to delineate the zone where the elements at risk will suffer a certain impact with a known intensity. The results of these models are an appropriate input for vulnerability and risk assessments.

The methodology used in this research is illustrated by a flow diagram described in Figure 1.3 based on a quantitative risk assessment scheme. Given the developments and the time frame of the research some of the components were carried out with different models in diverse test areas. This was influenced by the conditions of the availability and characteristics of the models and the data. Apart from introduction and conclusion chapters (Chapter 1 and 10), the other 8 chapters are based on peer reviewed ISI journals publications, conference proceedings, presentations and articles in that are currently under review process for publication.

Chapter 2 – This chapter describes in general terms the characteristics of the selected test areas which are relevant for this research. General information regarding the geo-environmental conditions such as geology and geomorphology is presented. A description of the most relevant past debris flow events and their characteristics is provided. These events were the basis to back calibrate the run-out models and validate the obtained results. An overview of the data used for each test site is given.

Chapter 3 - In this chapter an overview of the methods for run-out assessment of debris flows is presented. Different run-out models are described and classified into empirical (statistical) and dynamic (analytical or numerical) methods. A description of the different and most used rheologies inside the run-out models is provided. This chapter gives also a short summary of the models and their set-up used in this research with their respective calibrated rheological parameters. Three different dynamic run-out models (MassMov2D, DAN3D and RAMMS) were selected for a sensitivity analysis of their resistance parameters.

Chapter 4 – This chapter presents and evaluates the performance of a 1D debris flow model with a material entrainment concept based on limit equilibrium considerations and the generation of excess pore water pressure through undrained loading of the in-situ bed material. The debris flow propagation model is based on a one dimensional continuum mechanics approach using a depth-integrated approximation based on the shallow water assumption (Saint–Venant equations). The flow is treated as a laminar one-phase material, in which behaviour is controlled by a visco-plastic Coulomb–Bingham rheology. A sensitivity test was performed for the model rheological parameters and the in-situ soil parameters. To validate the model, a back-analysis of the Faucon 2003 debris flow and calibration of the model was carried out. The main goal to present a run-out model that takes into account an entrainment mechanism was to identify and state the advantages of including this process in the calculation of debris flow intensities for hazard analysis.

Chapter 5 – This chapter describes the characteristics of an extensive database that was compiled from past-analyzed events reported in the literature. This database includes the rheological parameters (Voellmy and Bingham rheologies), release volumes, the type of movement, the environmental setting and other physical characteristics of previously back-calibrated events that have been described by other authors. Within the database, the variability for the rheological parameters was represented as a probability density function (PDF). The density functions can indicate the range of parameters to be used and is a first step for a stochastic approach

to be implemented for dynamic run-out models in order to assess hazard and risk at a specific locality

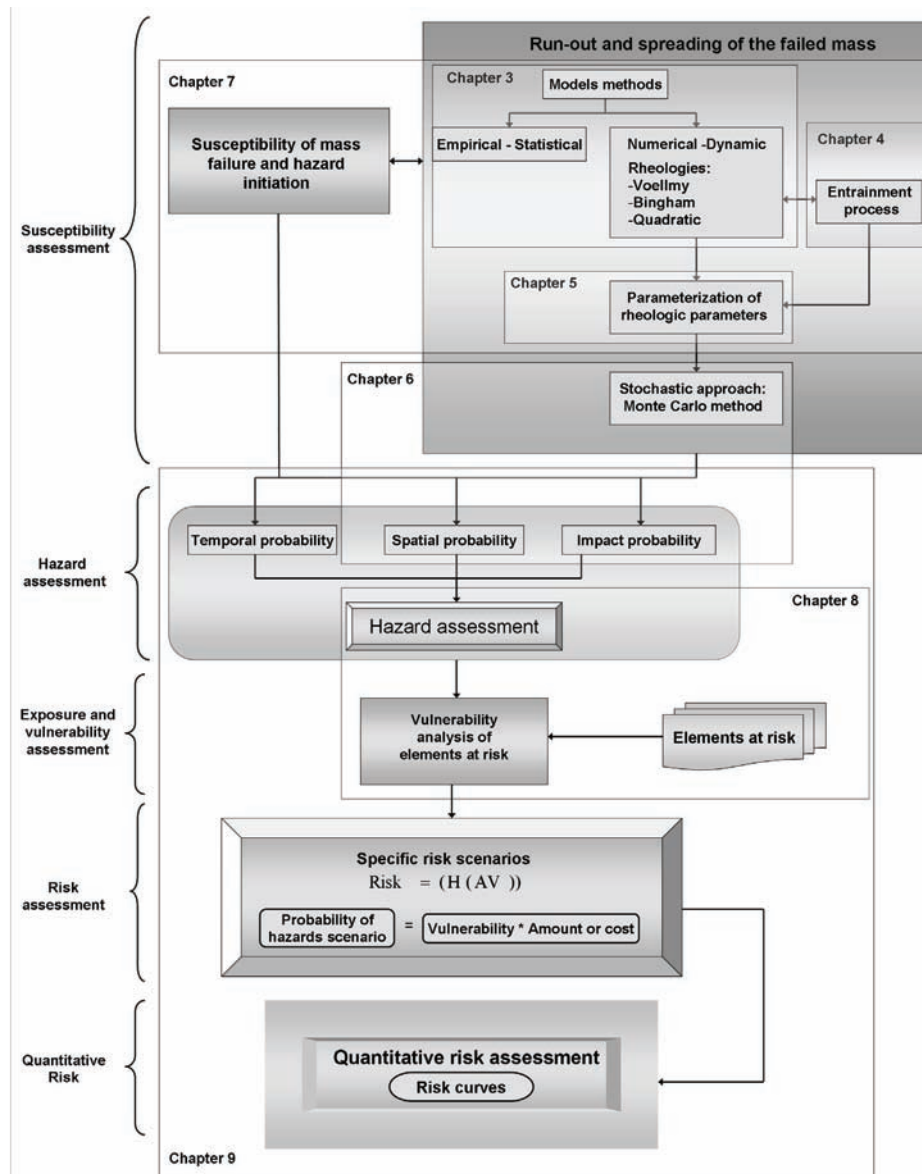


Fig. 1.3: Framework of the organization of the thesis chapters inside a quantitative risk assessment scheme proposed by van Westen *et al.* (2010).

Chapter 6 – In this chapter a method was applied to compute the variation in run-out intensities of debris flows by using a dynamic run-out model (MassMov2D) and a probabilistic framework based on a Monte Carlo

simulation to analyze the effect of the uncertainty of input parameters. The probability density functions of the Voellmy and Bingham rheology that were generated in Chapter 5 were sampled and a large number of run-out scenarios were generated. This methodology was applied in two study sites: the Faucon catchment and the Tresenda village using the Bingham and Voellmy rheology, respectively. In the application of the Monte Carlo method, 5,000 values were sampled at random from the input probability distributions that fitted a Gaussian copula distribution. Each set of samples was an iteration of the model, and the resulting outcome from the samples was analyzed. The result was a Gamma probability distribution of possible intensities in selected points of the deposition area.

Chapter 7 – This chapter presents the implementation of the model “AschFlow”. This model is a 2-D one-phase continuum model that simulates the spreading, entrainment and deposition process of a landslide or debris flow at a medium scale. “AschFlow” is based on an infinite slope model without any lateral or active-passive forces assuming that the forces are hydrostatic. The flow is thus treated as a single phase material, whose behaviour is controlled by rheology (e.g. Voellmy or Bingham). The medium-scale model “AschFlow” was applied and evaluated in two test site areas: the Faucon catchment using the Bingham rheology and the Tresenda village using the Voellmy rheology. The results of the “AschFlow” model are compared with other regional model results in order to evaluate the advantages and disadvantages of the two different modelling approaches and to make an assessment of the obtained modelling outputs.

Chapter 8 – This chapter presents an integrated approach that uses dynamic run-out modelling for the reconstruction of the debris flow intensities caused by a past event in the test site of Selvetta applying the FLO-2D model and to use this information in combination with damage data for the construction of physical vulnerability curves for buildings. Three physical vulnerability curves were prepared based on the flow depth, impact pressures, and kinematic viscosity. These curves relate the physical outputs of the modelling and the economic values of the elements at risk. The resulting vulnerability curves were compared with other vulnerability functions presented by other authors in the past.

Chapter 9 - In this chapter, a quantitative risk assessment using run-out modelling was carried out for the Tresenda Village study site. Based on the historical events and susceptibility maps, three potential debris flows initiation zones were delimited. These selected areas were modelled with the dynamic run-out model FLO-2D to assess the run-out intensity. The methodology used in this analysis consisted of several components, such as a detailed analysis of rainfall return periods (10, 50, 100 years return period),

the modelling of rainfall-runoff, the analysis of soil samples in the laboratory, the analysis of terrain characteristics, the modelling of the run-out of the debris flows, the application of debris flow height and impact pressure vulnerability curves (presented in chapter 8) and the generation of risk curves based on the economic losses.

Chapter 2: Test areas

Three different landslides and debris flow prone test areas were selected in order to pursue the objectives of this research: the Barcelonnette Basin located in the Southern Alps of France, the Valtellina Valley located in the Central Italian Alps and Peringalam in Kerala, India (Fig. 2.1). The areas were selected because of their importance in the scope of this research. The criteria applied to choose these areas were based on: well documented debris flow events; possibility to gather information on the field; information availability from other sources and institutions; and good quality and the quantity of data (e.g. DEMs, maps, images).

The Barcelonnette Basin and the Valtellina Valley were also selected as they were part of the study sites included inside the European Commission and Marie Curie Actions Research Training Network: "Mountain Risks: from prediction to management and governance" within the 6th Framework Programme. In the case of the Peringalam, India area, it was selected because the quality and good resolution of the data, and other related research (Kuriakose, 2010).

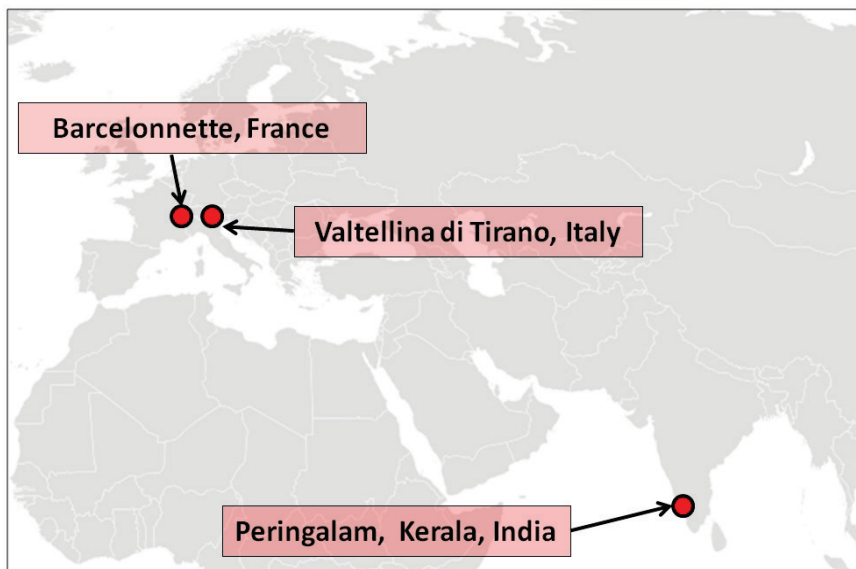


Fig. 2.1: Location of the three study areas: Barcelonnette (France), Valtellina di Tirano (Italy) and Peringalam, Kerala (India).

2.1 *Barcelonnette basin, France*

The Barcelonnette Basin is located in the Southern French Alps and has an elevation ranging from 1100 to 3000 m.a.s.l. The basin is a geological window in two Eocene crystalline sheet thrusts (Flysch from the Autapie and the Parpaillon) that overlay the black marls (Flageollet *et al.* 1999). The black

marls and the weathered flysch are mostly covered by moraines and/or slope deposits. The predominant land cover is forest (60%), agricultural lands which are progressively abandoned and bare lands. The Barcelonnette Basin has a dry and mountainous Mediterranean climate with strong inter-annual rainfall variability (733 ± 412 mm over the period 1928-2002), strong storm intensities (over 50 mm.h⁻¹) and 130 days of freezing per year (Remaître *et al.*, 2005). Due to this predisposing geological structure, the hillslopes are affected by severe gullying, shallow landslides, and deep-seated large landslides, some of which directly affecting the local population (Malet *et al.*, 2003).

The Barcelonnette Basin hillslopes are characterized by very steep slopes (slope gradient ranging between 30° and 70°) and more gentle slopes (slope gradient ranging between 10° and 20°) (Thiery *et al.*, 2007). The relief is irregular, and associates alternating steep convex slopes, regular planar slopes and hummocky slopes. The steepest convex slopes (> 35°) are carved in the black marl outcrops and are very often gullied in badlands or affected by rock-block slides or complex slides. The regular planar slopes (10°-20°) are made of thick morainic deposits (between 10 and 20 m), are very often cultivated and affected by rotational or translational slides. The hummocky slopes are generally covered by forests and/or by natural grasslands. Consequently, the main landforms are characterized by large relict landslides in moraine, badlands in black marls, deep-seated mudslides in black marls, and shallow slumps or debris slides in the moraine or in the colluvial cover (Malet *et al.*, 2004).

The collection of historical data in catalogues, newspapers, monographs, technical reports, bulletins and scientific papers for the period between 1850 and 2004 provides evidence of 561 torrential events. The type and quality of information collected, and the methodologies used to analyse the data are detailed in Flageollet *et al.* (1999) and Remaître (2006). The analysis indicates a dominance of flash floods with 461 recorded events while only 100 debris-flows (slope and gully) have been registered (Kappes *et al.*, 2011). Besides the historical information, the Barcelonnette basin has a considerable data information catalog which has been made open to the public and is accessible since 2010 (Malet, 2010). The information and data used in this study is described in Table 2.1 and displayed graphically in Figure 2.2.

The Barcelonnette area is one of the best studied mountain areas in Europe, and already for several decades many types of research have been carried out related to mass movements, in a series of EU and other projects. The most recent projects that have taken this area as test site are Mountain Risk,

SafeLand, CHANGES and ChangingRisk. Table 2.1 provides an overview of the key references for the study area.

Table 2.1: Overview of the available catalog used in this research as input data in the Barcelonnette Basin. Most of the data can be obtained from the following website: http://eost.u-strasbg.fr/omiv/data_access_Barcelonnette.html.

	Description
High resolution image	Orthorectified image derived from Google Earth with a 1.5 meter pixel size (van Westen <i>et al.</i> , 2010).
Contours	Map of 5 meter contour lines.
DEM	Digital Terrain Model of the terrain with 5 meter resolution.
Catchments borders	Map representing the catchments as units within the area.
Buildings	Building footprint map of the cities with information on building types, uses, number of floors and population in different periods.
Roads and power lines	Map of the roads and power lines with respective information.
Land use maps	Land use maps of the several periods.
Lithological map and Materials map	Map of the lithologies and surface material of the area.
Landslide inventory map 2007	Landslide map with information of 634 cases and description of the area, type of movement and level of activity.
Susceptibility map for shallow translational landslides	Susceptibility map for shallow translational landslides for the eastern part of the area, made through statistical analysis. This work was carried out by Thierry <i>et al.</i> , 2007.
PPR hazard map	Official hazard map
Key references	Flageollet <i>et al.</i> , 1999 ; Malet <i>et al.</i> , 2003; Malet <i>et al.</i> , 2004; Remaitre <i>et al.</i> , 2005; Remaitre, 2006; Thiery <i>et al.</i> , 2007; Remaitre <i>et al.</i> , 2008; Begueria <i>et al.</i> , 2009; Remaitre <i>et al.</i> , 2009, Malet, 2010; Kappes <i>et al.</i> , 2011; Quan Luna <i>et al.</i> , 2011.

Although the Barcelonnette area has a large amount of data available, there are also some types of data lacking, which make it difficult to carry out mass movement hazard and risk maps. The landslide inventory lacks substantial information on occurrence dates; there is no soil thickness map available, and also limited geotechnical data for the whole basin. For this reason regional scale landslide initiation modelling is difficult. Although the frequency of debris flows is well known, there is limited information available on individual events, such as deposit thicknesses, debris flow extent, release volumes and amount of entrainment. This makes back calibration complicated even in such a well studied area.

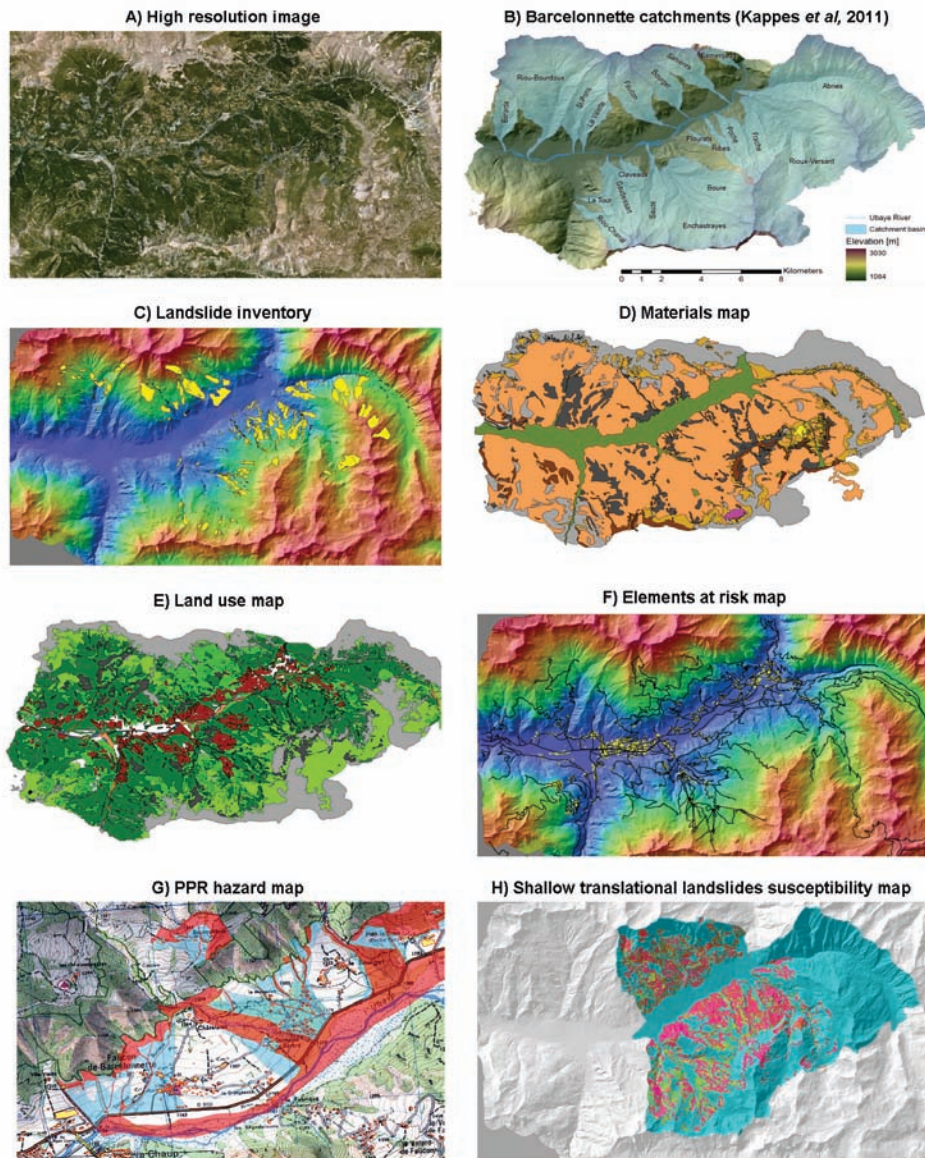


Fig. 2.2: Some key data (in form of maps) of the Barcelonnette area used in this research. A: High resolution image downloaded from Google Earth; B: catchment map (Kappes *et al.*, 2011); C: Landslide inventory map (Thierry *et al.*, 2007); D: Surface materials with black marls, morainic cover, bare rocks, and alluvial as main units; E: Land cover map from 2000; F: Elements at risk map; G: Multi-hazard map; H: Landslide susceptibility map (Thierry *et al.*, 2007).

2.1.1 Faucon torrent

Inside the Barcelonnette Basin, the Faucon torrent was selected as a test site. The Faucon catchment is a steep forested watershed with an area of approximately 10.5 km² which rises to 2984 m.a.s.l. (Figure 2.3). Most slopes are steeper than 25°, reaching 80° at the highest elevations. Most slopes in the Faucon catchment are covered by various Quaternary deposits: thick taluses of poorly sorted debris; morainic deposits; screes and landslide debris. These deposits have a sandy-silty matrix, may include boulders up to 1–2 m in size and are between 3 and 15 m thick (Remaître, 2006). The incised channel has an average slope of about 20°, ranging from 80° in the headwater basin to 4° on the alluvial fan, and is approximately 5500 m in length. Channel morphology is characterized by a V-shaped profile with a steep channel in the upper part, and a flat-floored cross-profile between steep slopes in the downslope section. The Faucon torrent has formed a 2 km² debris-fan that spreads across the Ubaye valley floor (Figure 2.3). It has a slope gradient ranging from 4 to 9°. The fan consists mostly of cohesionless and highly permeable debris (debris-flows strata and/or torrent deposits) (Remaître *et al.*, 2005).

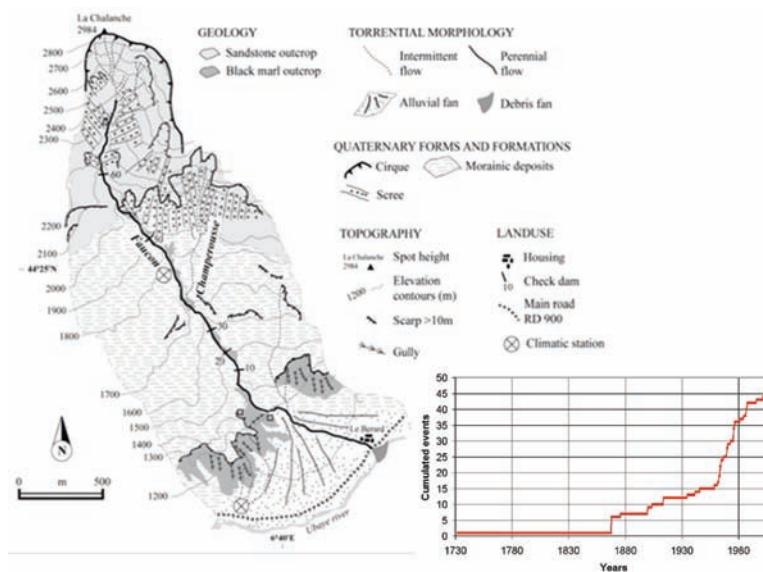


Fig. 2.3: Morphological map of the Faucon watershed, and cumulative debris flow occurrences from 1730 to now (Remaître, 2006).

The Faucon stream has a torrential flow regime with peak discharges in spring (snowmelt) and autumn (high precipitation) and a high variability in summer according to the occurrence of storms. Since 1850, at least 14 debris flows and 31 torrential floods have occurred in the Faucon torrent (Remaître *et al.*, 2005) (Fig. 2.3). However, for most of these events no

information is available on the initiation volumes, the run-out areas and depths required for the calibration of the numerical run-out models. In the following sections a description is given of the two events for which this information was available.

Faucon debris flow 19 August 1996

On 19 August 1996, a debris flow was triggered by an intense and local thunderstorm. According to eye-witnesses the total duration of the event was about 2.5 hours. The debris flow caused moderate damage and the main road across the alluvial fan was cut for several hours. The source area of the debris flow (above 2100 m.a.s.l.) consisted of several shallow landslides of moderate size ($<100 \text{ m}^3$) on slopes ranging from 30° to 50° . In this section the channel width ranged from 5 to 8 m. The headwater basin has a rocky sandstone substrate, which has been exposed over several square meters by stripping of the surface gravel. This suggests removal of this loose, cohesionless material by the flow (Remaître, 2006).

A release volume approximately $11,000 \text{ m}^3$ of debris-flow material was estimated and the total length of the transport zone is 3000 m with a slope gradient of about 25° . The scour depth of the surficial cover ranged between 0.5 and 2.0 m. Mapping of the debris-flow deposits in the path allowed us to estimate the volume at approximately. The final calculated volume was approximately $50\,000 \text{ m}^3$ (Remaître *et al.*, 2005).

Faucon debris flow 5 August 2003

The debris flow has been triggered on two specific spots on the east flank of the Faucon catchment: the Trois Hommes area, and the upper part of the Champerousse torrent (a tributary of the Faucon stream) (Fig. 2.4). For both cases, the morphology of the source area corresponds to a strong incision in scree slopes. The volume of the Trois Hommes debris flow ranged approximately from $4,000$ to $5,000 \text{ m}^3$. In the Champerousse torrent, the volume of the material in the source area ranged from $6,000$ to $7,500 \text{ m}^3$. The observations at the Trois Hommes slope and the Champerousse torrent indicate that the source volume ranges from $7,500$ to $9,500 \text{ m}^3$. A debris flow height of the 5 to 6 m. was reported (Remaître *et al.*, 2005; Remaître *et al.*, 2009). Figure 2.5 gives an overview of the 2003 debris flow event.

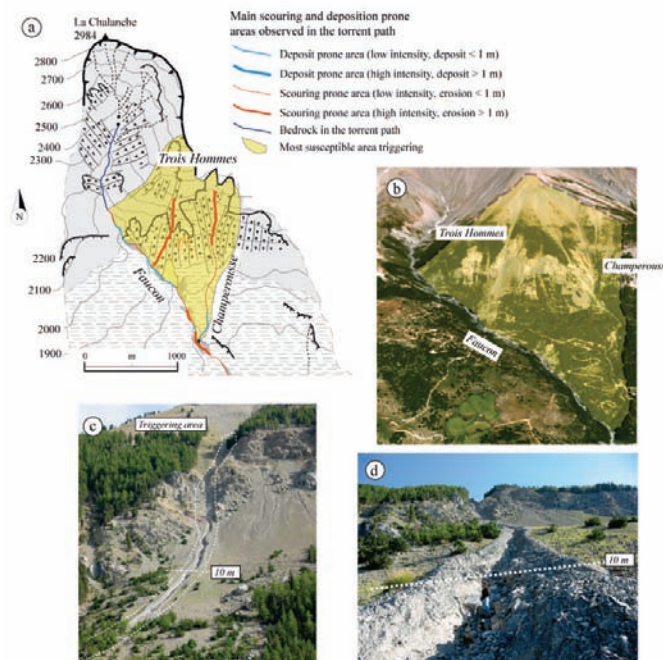


Fig. 2.4: (a) The Trois Hommes and Champerousse area; (b) 3D visual representation of the Trois Hommes and Champerousse slope; (c) Photograph of the channel created by the 2003 debris flow event in the Trois Hommes and Champerousse scree deposits; (d) Details of the debris flow path at the Trois Hommes and Champerousse slopes with the lateral levees clearly visible. (Source of figures and maps: Remaître, 2006).

According to the measured area and the depth of the deposits both in the channel and on the fan the total volume of the debris flow deposit was estimated to be $45,000 \text{ m}^3$ on the debris fan and $15,000 \text{ m}^3$ in the upper channel. Channel scouring was responsible for the great difference of $7,500\text{--}9,500 \text{ m}^3$ of the two source areas and the $60,000 \text{ m}^3$ of the total volume of the debris flow solid material. The total length of the flow track is about $3,500 \text{ m}$. The channel scour rate amounts to $15 \text{ m}^3 \cdot \text{m}^{-1}$. Observations indicate that the scour rate depth ranges between 0.5 and 4 m (Remaître *et al.*, 2009).

Two points of interest were selected in this research for the Faucon test site: the fan apex and the V.C. 3 Bridge. The fan apex was assessed as it is the start of the deposition zone on the fan and the location of RD 900 Bridge (main road). The second location assessed was the V.C. 3 Bridge located at the upstream part of the Domaine de Bérard village. It is the first bridge near the village that could come into contact with a future debris flow (Fig 2.5). Besides this, information and measurements of past events have been carried out at these points by Remaître (2006).

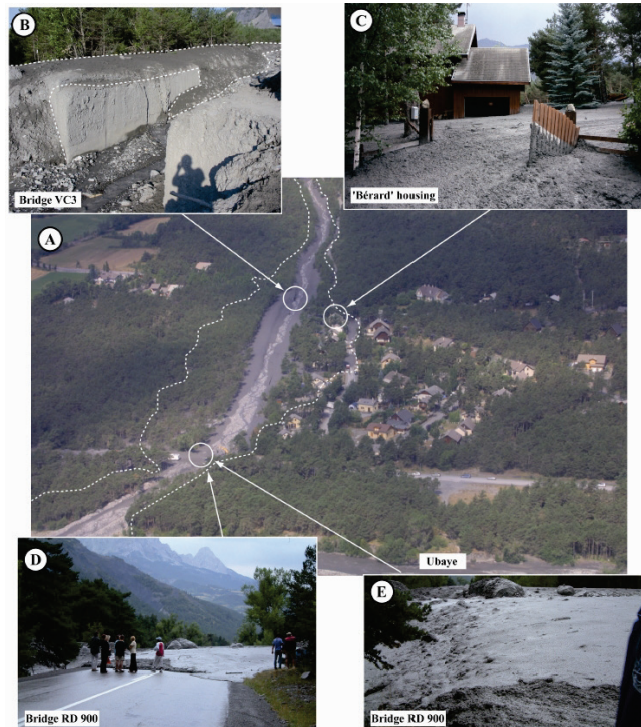


Fig. 2.5: Spreading of the 2003 debris flow on the Faucon torrential fan. (A) Aerial view of the Faucon fan (courtesy of Michel Peyron). (B) The VC3 Bridge completely destroyed. (C) A house overflowed. (D) The end of the debris-flow event at the RD 900 Bridge. (E) View of the 'fresh' debris-flow deposit at the RD 900 Bridge (Source: Remaitre, 2006).

2.2 Valtellina di Tirano, Italy

Valtellina is an important Italian alpine valley located in Central Italian Alps (Northern Italy, Sondrio Province). The valley starts near Bormio (1,225 m.a.s.l.) and it runs for about 100 km to Colico (218 m.a.s.l.) near Como Lake. The axis of the valley is formed by the Adda River, originating from small lakes in the Rhaetian Alps at 2,335 m.a.s.l. Adda River flows through the entire valley in a flat alluvial plain up to 3 km wide and it joins the Po River in the Lombardy Plain. The valley is aligned on a regional fault that sharply separates the properly-called Alps (Austroalpine, Penninic and Helvetic nappes) to the north from the Variscan basement of the Southern Alps to the south. The Periadriatic Fault, commonly known in Lombardy also as Insubric Line or Tonale Fault, has a mostly E-W trend in Lombardy, running on the northern slopes of Valtellina, some 500 m above the Adda River floodplain. The bedrock (the pre-Alpine metamorphic basement) is mainly composed of metamorphic rocks (gneiss, micaschist, phyllite and quartzite) and intrusive rocks, with subordinate sedimentary rocks. Due to the proximity of this tectonic lineament, cataclastic and mylonitic zones are

abundant (Crosta, 1990). Alluvial fans at the outlet of tributary valleys can reach a considerable size; with a longitudinal length up to 3 km. Valtellina has a U-shaped valley profile derived from Quaternary glacial activity. The lower part of the valley flanks are covered with glacial, fluvio-glacial, and colluvial deposits of variable thickness (Crosta *et al.*, 2003)

Valtellina has a history of intense landsliding. Landslides are among the most significant natural damaging events; they are one of the primary causes of life injury and property damages, resulting in enormous casualties and huge economic losses in that mountainous region. A large number of landslides affected Valtellina on 14 - 17 November 2000. A prolonged and intense rainfall event triggered 260 shallow landslides in an area of 270 km², most of them occurring on terraced slopes. This area suffered other intense landsliding phenomena on 1983 (200 shallow landslides) and 1987 (260 reported landslides) (Guzzetti *et al.*, 1992). Landslides are common in areas of run-off where the superficial flow is converging. In other cases they are associated with the reactivation of older debris flow scars (Cancelli and Nova 1985). A detailed database of debris flows past events and diverse spatial information of this area has been collected by Blahut *et al.*, (2010a). The data applied in this research is summarized in Table 2.2 and the resulting maps are shown in Figure 2.6.

Even though several major triggering events have taken place in the past decades, there are no complete debris flow inventory maps available for these events. Also it was not possible to obtain aerial photographs or satellite images that could be used for the reconstruction of these historical events. As indicated by Blahut *et al.* (2010a) the existing landslide databases in Italy, such as the GEOIFFI (2006) did not contain coherent information on the landslide occurrences. The database uses points instead of polygons, which were sometimes located in the scarp area and in some occasions in the accumulation area. Most of the landslides points in the database did not have information on the date of occurrence. In order to harmonize the landslide information, Blahut *et al.* (2010a) mapped all debris flow initiation areas using high resolution satellite images obtained from Google Earth, and used these in a debris flow initiation susceptibility assessment.

Within Valtellina there is a consortium of 12 municipalities (Mountain Consortium of Communes of Valtellina di Tirano). The total study area is about 300 km² with a population of about 30,000 inhabitants (Blahut *et al.*, 2010a).

Within the Valtellina area two specific test sites were selected for this research: the villages of Tresenda and Selvetta (See Fig. 2.7). Both sites have experienced recent debris flow events, which have been well

Test areas

documented, and which can be used in back analysis. The Selvetta case study is used for the generation of vulnerability curves (See Chapter 8). The Tresenda area is used for the quantitative risk assessment (See Chapter 9).

Table 2.2 Data catalog used in this research for the Valtellina Valley.

	Description
Contour map	Map which contains contour lines of 5 meter interval.
DEM	Digital Terrain Model with a 5 meter resolution. In some areas it was possible to have a LIDAR based DEM with a 2 m resolution.
Building map	Building footprint map with information on building types and uses.
Roads	A map with the locations of the streets and roads in the area.
Land use map	A land use map, derived from the 1:10,000 scale map of the DUSAF Project (2003), made by Lombardy Region using orthophotos from the year 2001. The map contains 23 classes of which the largest ones are coniferous trees and scarce vegetation.
Landslide inventory map DF2001	Landslide inventory map generated by Blahut et al. (2010a) map. The inventory database contains 458 records covering the period from 1600 till 2008. Half of them are dated with 64% occurring during the 20th century, mostly during its last quarter. Event magnitude, expressed as length, width and area, is reported in 27% of the records.
Susceptibility map for debris flow	Susceptibility map for debris flows made through statistical analysis by Blahut <i>et al.</i> (2010a)
Debris flow hazard map	Debris flow hazard maps created by Blahut <i>et al.</i> (2010b).
Lithology map	A geological surface material map, rasterized from a 1:10,000 scale geological map of Lombardy Region generated by the CARG Project (1992). The map contains 51 classes of lithological as well as soil cover units mapped directly in the field and by photo interpretation. Morainic deposits and gneiss rocks represent the most frequent classes.
Key references	Azzola and Tuia, 1983; Cancelli and Nova, 1985; Giacomelli, 1987; Crosta, 1990; Ceriani <i>et al.</i> , 1992; Guzzetti <i>et al.</i> , 1992 ; Agostoni <i>et al.</i> , 1997; Crosta <i>et al.</i> , 2003 ; Aleotti <i>et al.</i> , 2004; Luino, 2005; Blahut <i>et al.</i> , 2010a; Blahut <i>et al.</i> , 2010b; Blahut <i>et al.</i> , 2011; Quan Luna <i>et al.</i> , 2011.

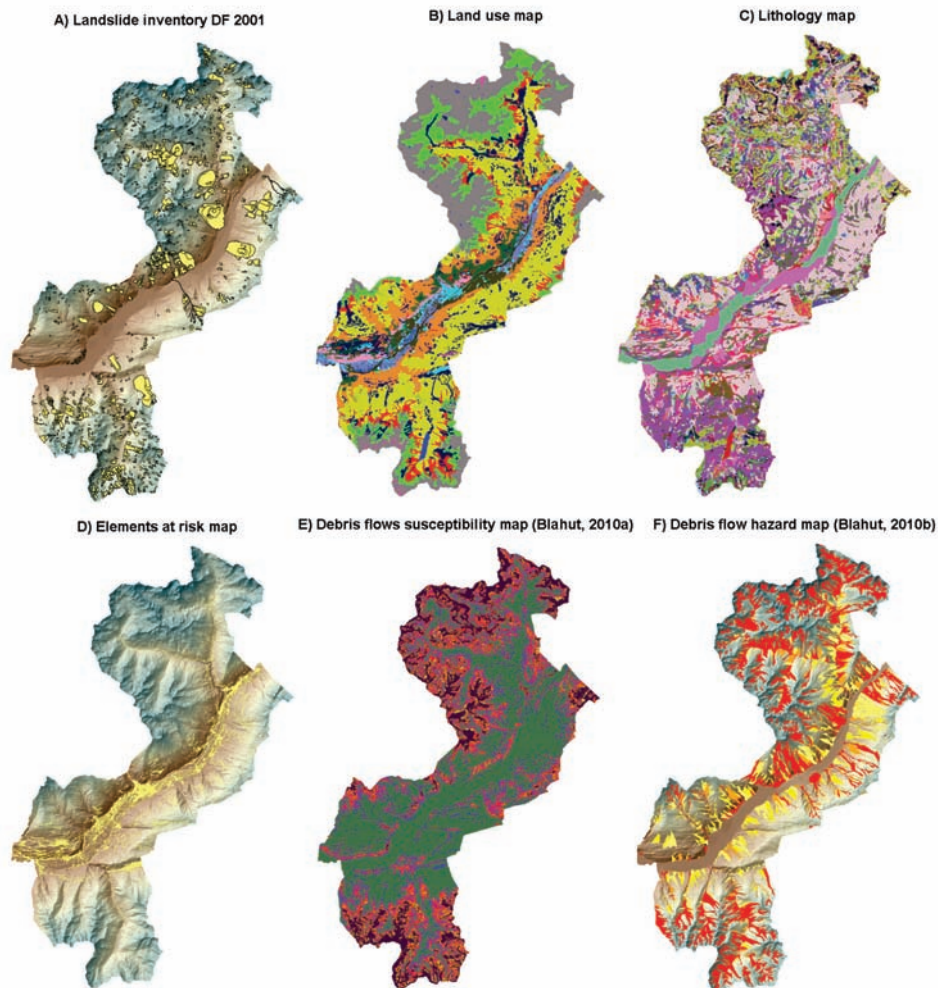


Fig. 2.6: Various thematic maps for the Valtellina Valley used in this research. A: Landslide inventory map (Blahut *et al.*, 2010a); B: Land use map from 2001 (DUSAF project, 2003); C: Lithological map (CARG project, 1992); D: Elements at risk map; E: Debris flow susceptibility map (Blahut *et al.*, 2010a) F: Debris flow hazard map (Blahut *et al.*, 2010b).

2.2.1 Selvetta debris flow event

The Selvetta test site is situated in Valtellina Valley, on the border between CM Valtellina di Morbegno and CM Valtellina di Sondrio. Selvetta village administratively belongs to two municipalities – Forcola and Colorina. The area affected by the debris flow lies, however, inside the Colorina municipality. On Sunday morning of 13th July 2008, after more than two days of intense rainfall, several debris and mud flows were released in the central part of Valtellina valley between Bormio and Forcola (Figure 2.7).

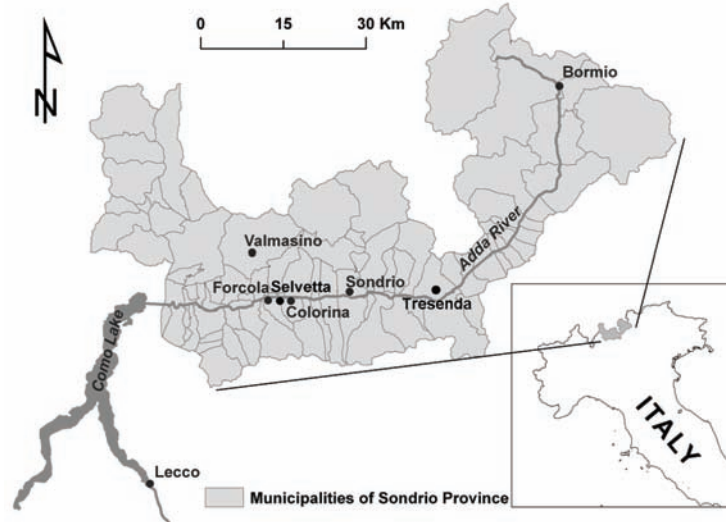


Fig. 2.7: Location of the Selvetta and Tresenda test sites.

The debris flow event was reconstructed after extensive field work and interviews with local inhabitants and civil protection teams. The main objective of the fieldwork was to collect information to describe the behaviour of the flow during its course. Flow depths were measured along the path and sedimentation features that hinted out when the flow evolved were carried out. Channel profiles were made in locations where the velocities and discharge of the flow could be deduced (Fig. 2.8). The evolution of the flow in terms of velocity was reconstructed by the use of empirical formulas. To derive the mean flow velocity in each channel cross-section, the superelevation formula (Eq. 2.1) proposed by McClung (2001) and Prochaska *et al.* (2008) was applied:

$$v = \sqrt{\frac{R_c g \Delta h}{k b}} \quad (2.1)$$

where, v is the mean velocity of the flow (m/s), R_c is the channel's radius curvature (m), g is the gravity acceleration (m/s^2), Δh is the superelevation height (m), k is a correction factor for the viscosity and b is the flow width (m). Prochaska *et al.* (2008) indicated that the value of the correction factor can be "1" with the exception of cases with sharp bends where some shock waves develop.

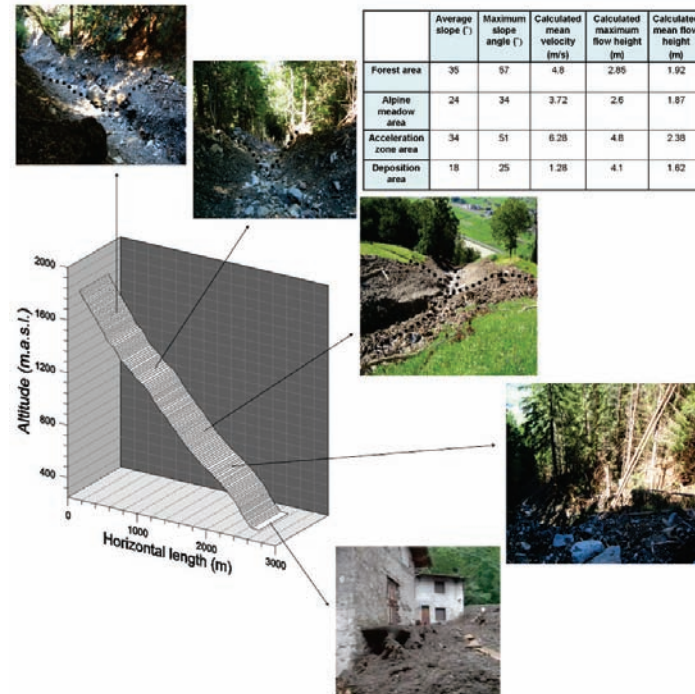


Fig. 2.8: Selvetta debris flow path including the calculated mean velocity, maximum flow height, and mean flow height for each morphologic section.

Geomorphologic investigations allowed distinguishing the following five main sections of the flow: 1) the proper scarp; 2) path in forested area; 3) path on alpine meadows; 4) accelerating section; and 5) accumulation area (Fig. 2.9). The initiation area of the flow was situated approximately at 1760 m.a.s.l. in a coniferous forest. The proper scarp was very small with an area of about 20 m² and a height about 0.5 m. The debris flow originated as a soil-slip in thin colluvial cover on a very steep (>45°) forested slope. This suggests that the flow started as a small failure and gained momentum with additional entrained material from the channel bed and walls. After some tens of meters the flow became larger and started to erode the channel to the bedrock. The channel erosion was associated with the acceleration of the flow on steeper parts of the slope and on rock steps. The average inclination of the path in the forested area is 35° but there are several steps steeper than 60°.

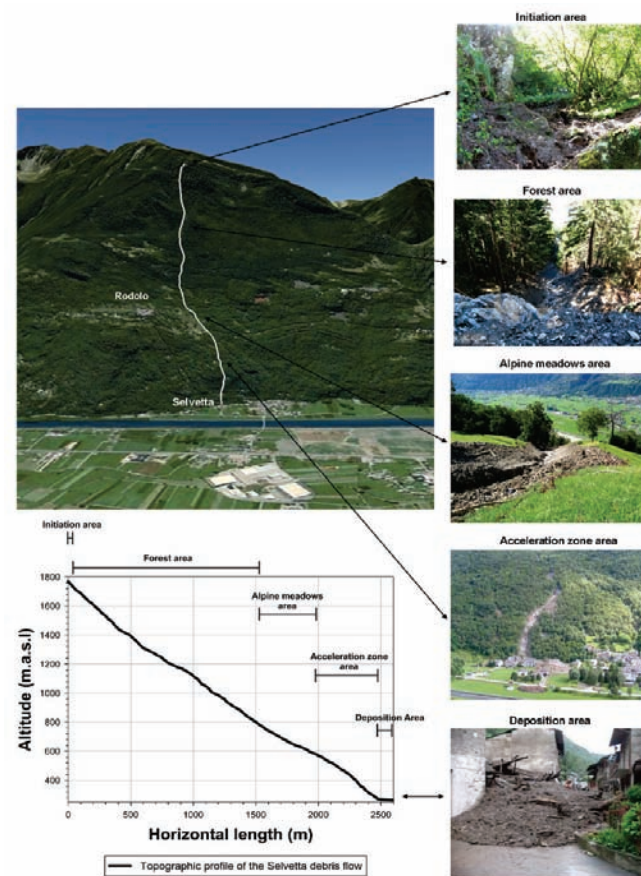


Fig. 2.9: Google image and profile of the Selvetta debris flow path with the five main morphological sections determined on the field.

At 760 m.a.s.l. the flow decreased its velocity when it reached another less steep part of alpine meadows on morainic sediments near Rodolo village. The flow channel in this section of the flow was not eroded to the bedrock and the flow itself accumulated a lot of material from the upper section. On a flat glacial terrace, at the height of 640 m.a.s.l., the flow diverged to the right side where it joined a small ravine and entered an acceleration zone area. In this section, the flow reached the highest velocity and heights. The apex of the accumulation zone starts at 310 m.a.s.l. The accumulation zone has an area of about 9,500 m² and the volume of the deposited debris was estimated by field mapping, to be around 15,000 m³.

Precipitation records showed that the flow did not occur immediately after the peak precipitation which was recorded at 7 A.M., but with more than three hour delay. The closest one ran gauge was in Morbegno (about 8 km from the scarp) and shows hourly peak rainfall of 22 mm/hour between 6 and 7

A.M. The cumulated rainfall during 48 hours before the event reached 92 mm. Although this record did not precisely describe the situation in the initiation area, it could be used for a rough estimation of precipitation and for measuring the delay of initiation after peak precipitation because records from other gauges in the vicinity show also the rainfall peak between 6 and 7 A.M.

2.2.2 Tresenda debris flow events

The second case study area in the Valtellina area is the Tresenda village, located in the municipality of Teglio (Fig. 2.7) in the Valtellina Valley. Spatial information of past damage derived from historical records, local chronicles, and interviews with local people confirmed that the village of Tresenda was affected by debris flows events which caused significant losses in 1983, 2000 and 2002 (See Fig. 2.10). Soil slips, resulting in debris flows were triggered on the steep slopes above Tresenda, where the soil thickness varies between 70 to 250 cm. The documented past events crossed minor roads and impacted buildings in the Tresenda village, while running along main drainage lines (Cancelli and Nova, 1985; Guzzetti *et al.*, 1992). If a major event occurs in future, casualties and serious property damages can be expected as well as the obstruction of a main road (S.S. 38) leading to high indirect losses. The area is located in a very narrow part of the Valtellina Valley, and the main road is the only connection with the upstream area which contains major tourist resorts.

In May 1983, severe precipitation triggered more than 200 shallow landslides and debris flows in the Valtellina valley. The rainfall station in Aprica measured a cumulated precipitation of 453 mm during this month, which corresponds to 34% of the total annual precipitation (Guzzetti *et al.*, 1992). In Teglio, three soil-slips evolved into debris flows with lengths varying between 300 to 460 m and areas reaching 60,000 m² (Fig. 2.11). Two of them occurred on 23rd May on the slopes above the village of Valgella and Tresenda (Fig. 2.10), causing 14 casualties in Tresenda and 4 in the neighbouring village of Valgella (Cancelli and Nova, 1985), and destruction of several buildings. The national road S.S. 38 was blocked, and this made impossible to reach the upper part of the valley for few days.

Apart from heavy precipitation, Crosta *et al.* (2003) mentioned as causes of failure the maintenance of the stone walls supporting the terraces. From interviews with local inhabitants, also the construction of paved paths and roads in the vineyard area was mentioned as possible causal factor, leading to rapid run-off and causing a rapid increase of the water table which leads to the failure of the stone walls and the consequent development of soil slips-debris flows.

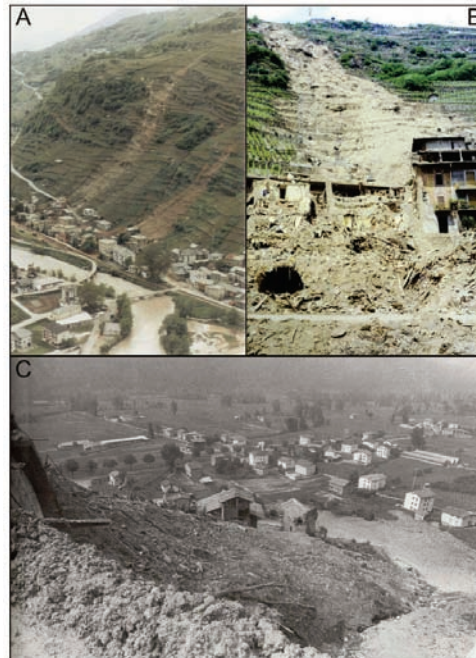


Fig. 2.10: A and B) Photographs of two debris flow from 22nd and 23rd May 1983 in Tresenda. Photo: Archive of CNR-IRPI, Torino. C) Photograph of debris flow from 23rd May 1983 in Valgella. Photo source: Giacomelli (1987).

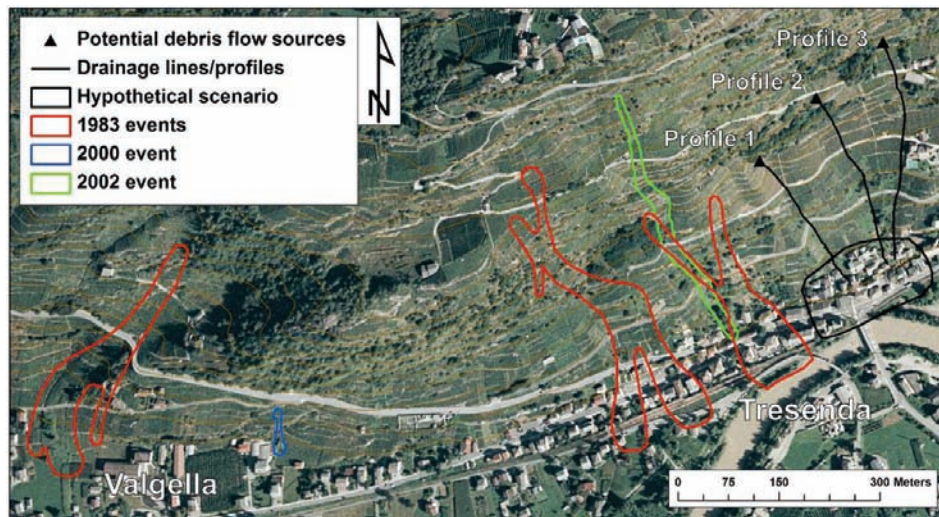


Fig. 2.11: Delimitation of the 1983 and 2002 debris flow according to GeoIFFI database (2006) and Blahut et al. (2010a). Possible sources and drainage lines/profiles of new debris flows are shown and area of a hypothetical risk scenario is delimited (See Chapter 9).

Another event took place in the area in 2000, causing only one minor debris flow. A similar event as in 1983 happened on the same slope on 26th of

November 2002 (Fig. 2.11), although producing less damage and no casualties. The flow remained confined and caused a minor flooding of the area close to the village due to an obstruction in the drainage channel. (Di Trapani 2009, personal communication).

2.3 Peringalam, Kerala, India

A third study area used in this research is the Peringalam test site, located near a small village in the upper catchment basin of the Meenachil river in the Kottayam district in the state of Kerala, India. The reason for including this test site was the joint research carried out with Kuriakose (2010) on dynamic modelling of landslide initiation areas, and subsequent run-out modelling. This region has experienced various types of landslides of which the debris flows are the most common. The Meenachil catchment is surrounded on its eastern and north parts by escarpments. The area is composed of hard crystalline rocks with charnokite (93% of the area), and smaller outcrops of quartzite, biotite gneiss, pink/grey granite and dolerite (Kuriakose, 2010).

The Peringalam debris flow event occurred in a topographic depression upstream of a first order non perennial stream on 14th of October of 2004 at 5:00 p.m. (Fig. 2.12). The event caused considerable damage to cultivated land and blocking the road that connects the village of Peringalam to the nearest major town, Poonjar. The landslide originated at an altitude of 500 m.a.s.l. and had a total run-out distance of 290.5 m. Measurements of the landslide were carefully done via fieldwork and aerial imagery. The calculated initial volume of the debris flow was 437 m³ with a deposited final volume of 1533 m³. The area of the landslide body at the initiation zone is 784 m², the run-out zone is 2336 m² and the area of the deposition zone is 2680 m².

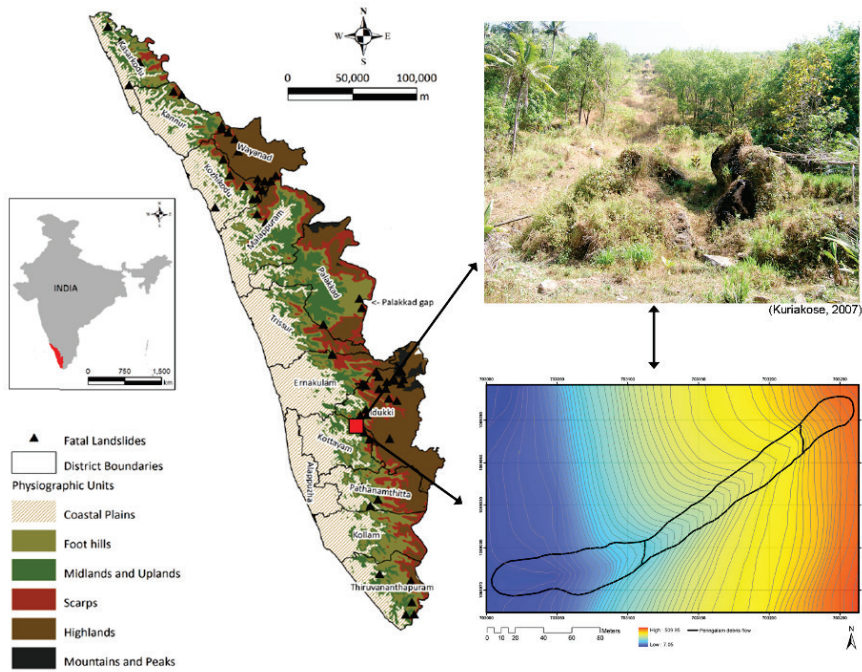


Fig. 2.12: Location of the Peringalam debris flow, in the upper Meenachil river basin, Kerala. (Kuriakose, 2010).

2.4 Summary

This chapter presented in general terms an overall description of the characteristics of the selected test areas which are relevant for this research. Table 2.3 presents a short summary of the test areas and the past events that were included and used for further investigation.

Table 2.3: Summary of the test areas and test sites characteristics used in this research.

Test sites and past events	Test area	Type of analysis done in the test site	Characteristics of the events	References
Faucon debris flow event, 1996	Barcelonnette Basin, France	-Back-analysis: used to calibrate the RAMMS model for the sensitivity analysis in Chapter 3. - Values used for validation in Chapter 6 and 7.	- Initiation volume : 5,000m ³ - Entrainment volume : 95,000 m ³ - Total deposited volume: 100,000 m ³ - Run-out distance: 3,000 m - Maximum debris flow height : 4.60m - Velocity: 4.9 - 5.1 m.s ⁻¹	Remaitre <i>et al.</i> , 2003; Remaitre, 2006.
Faucon debris flow event, 2003	Barcelonnette Basin, France	-Back-analysis: used to calibrate the RAMMS models for sensitivity analysis in Chapter 3. - Back-analysis.: used to calibrate the 1-D entrainment model. - Reported values used for validation in Chapter 6 and 7	- Initiation volume: 7,500 – 9,500 m ³ - Total deposited volume: 60,000 m ³ - Run-out distance: 4700 m - Maximum debris flow height near the bridge: 3.9 m - Max velocity near the bridge: 7.8 m.s ⁻¹ - Maximum debris flow height at the fan apex: 2.6 m - Max velocity near the fan apex: 6.4 m.s ⁻¹ - Mean max velocity : 6.4 – 8.9 m.s ⁻¹	Remaitre <i>et al.</i> , 2005; Remaitre <i>et al.</i> , 2008; Begueria <i>et al.</i> , 2009; Remaitre <i>et al.</i> , 2009 ; Quan Luna <i>et al.</i> , 2011.
Peringalam debris flow event, 2005	Kerala, India	-Back-analysis: used to calibrate the DAN3D model and MassMov2D model for the sensitivity analysis in Chapter 3	- Initiation volume: 1,435m ³ - Entrained volume: 593 m ³ - Max velocity: 20 m.s ⁻¹ - Mean deposit thickness: 1.6 m - Max deposit thickness: 4.1 m	Kuriakose <i>et al.</i> , 2009; Kuriakose, 2010.
Riou-Bourdoux, St. Pons, La Valette, Faucon, Bourget, Sanieres catchments	Barcelonnette Basin, France	- Forward analysis of run-out in Chapter 7	- Number of events since 1850: Riou-Bourdoux: 27; St. Pons :1; La Valette:1 ; Faucon: 14 ; Bourget:6 ; Sanieres:18. - Footprints of some past events.	Malet <i>et al.</i> , 2003; Malet <i>et al.</i> , 2004; Thiery <i>et al.</i> , 2007; Malet, 2010;
Eastern part of the Valtellina Valley	Valtellina Valley	- Forward analysis of run-out in Chapter 7	- Inventory and footprints of past events	Blahut et al., 2010a

Test areas

Cont. Table 2.3: Summary of the test areas and test sites characteristics used in this research.

Test sites and past events	Test area	Type of analysis done in the test site	Characteristics of the events	References
Selvetta debris flow 2008	Valtellina Valley	<ul style="list-style-type: none"> - Back analysis: used to calibrate the Flo-2D model in Chapter 8 - Generation of vulnerability curves in Chapter 8. 	<ul style="list-style-type: none"> - Initiation volume: 15 – 20 m³ - Entrainment volume: 14,500m³ - Total deposited volume: 14,500 – 15,000 m³ - Run-out distance: 2,500 m - Maximum debris flow height: 4.1 – 4.8 m - Mean velocity: 4.8 – 6.3 m.s⁻¹ 	Blahut <i>et al.</i> , 2010a, Quan Luna <i>et al</i> , 2011.
Tresenda village	Valtellina Valley	<ul style="list-style-type: none"> - Forward analysis of run-out in Chapter 6. - Quantitative risk assessment in Chapter 9. 	<ul style="list-style-type: none"> - Inventory and footprints of past events of the area. - Debris flow heights of 1983 event: 2.50 -4.50 m - Debris flow heights of event 2002: 2 – 3.75 m. 	Crosta, 1990 ; Crosta et al., 2003; Blahut <i>et al.</i> , 2010a.

Chapter 3: Dynamic run-out models: an overview

3.1 Introduction

Several approaches have been developed to model fast gravitational geomorphologic movements, in order to assess their characteristics, intensities and run-out. These approaches vary with respect to the required scope of the assessment, the scale of analysis, the available input data and the extent of the outputs required. A very important part of any debris flow risk assessment is a quantitative estimate of post-failure motion defining distance, material spreading and velocity. The main aspect of run-out modelling is to reproduce as accurately as possible the dynamics of the geomorphologic processes and to forecast the potential extension, height and velocity of future debris flows. It should be understood that the movement of a flow is complex and more than one phenomenon may be operating at the same time, and different phenomena may prevail at different locations of a given event. For this reason, no universal run-out model exists, this means that no single model can adequately describe all the movement types. However, the developed methods give a good systematic approach to assess the spreading, extension and impact that a landslide can generate. These methods can be divided in: *empirical methods*, *analytical methods* and *numerical methods*. A good overview of run-out methods is given by Hungry *et al.* (2005). The main characteristics of the various methods are summarized in Table 3.1.

Chapter 3 is based on:

Quan Luna, B., Kuriakose, S., Begueria, S., van Westen, C.J., van Asch, T.W.J., 2012. Comparison of two dimensional physically-based landslides run-out models that include the entrainment process. A case study in the Western Ghats of Kerala, India. (Under preparation).

Hussin, H.Y., **Quan Luna, B.**, van Westen, C.J., Christen, M., Malet, J.-P., van Asch, T.W.J., 2011.

Spatial frequency assessment of debris flow run-out using the RAMMS model. A parameterization analysis on a reference event in the French Alps. (Under review in Natural Hazards and Earth System Sciences)

Table 3.1 Scheme of the run-out methods type and their calculation dimensions.

Dimension of calculations	Type of methods	Inputs	Outputs
1-D	Empirical methods: - Heuristic - Angle of reach - Mass-change	- Volume estimation - Topographic profiles - Image interpretation - Geomorphologic studies	- Maximum run-out - Area of deposit - Flow depth
	Analytical methods (point mass models)	- Rheological parameters - Topographic profile	- Maximum run-out - Velocity
	Numerical methods	- Rheological parameters - Topographic profile - Volume	- Maximum run-out - Velocity - Impact pressures - Flow depth
2-D	Flow routing methods	- DEM (Digital elevation model)	- Pxy= probability of each cell to be affected by a flow - Flow trajectories and extension of deposits
	Numerical methods	- DEM - Rheological parameters - Volume	- Extension of deposits - Velocity - Flow depth - Impact pressures

3.1.1 Empirical methods

Empirical methods for assessing landslide run-out are usually based on extensive amounts of field observations and on the analysis of the relationships between the run-out distance and different landslide mechanisms, their morphometric parameters, the volume of the landslide mass, and the characteristics of the terrain. Empirical approaches are based on simplified assumptions, and although they lead to generalized results they are relatively easy to apply over larger areas. Empirical methods can be subdivided into: i) *heuristic methods*, ii) *the mass-change method* and iii) *the angle of reach method*.

Heuristic methods involve the identification and mapping of landslide deposits that provides a direct measurement of the distance travelled in the past. The extent of both ancient and recent landslide deposits is the basis for defining future travel distances. Field work and photo interpretation are classical procedures used to define the spatial distribution and extent of past landslides. The margin of the landslide deposits give an indication of the maximum reach that a landslide is able to reach in the present landscape (Hungry *et al.*, 2005).

The *mass-change method* is based on the phenomenon that as the landslide debris moves down slope, the initial volume/mass of the landslide is being modified through loss or deposition of materials, and that the landslide debris halts when the volume of the actively moving debris becomes negligible (Cannon and Savage, 1988). The average mass/volume-change rate of landslide debris was established by dividing the volume of mobilized material from the landslide by the length of the debris trail.

The *angle of reach method* is based on the angle of the line connecting the crest of the landslide source to the distal margin of the displaced mass also called the *fahrböschung* angle (Heim, 1932). This angle is also used as an index of efficiency for the dissipation of energy. Once the release source, volume and direction of the flow are known, these methods can estimate the length of the run-out. It is the most commonly used method in assessing the run-out of landslides due to its simplicity and straightforward results. One of the most well-known examples of the application of this method is done by Corominas (1996) who conducted a detailed study on the influence of various factors that affect the angle of reach using landslide records. He showed a linear correlation between volume and angle of reach for all types of failures. Regression equations for calculating the angle of reach of each landslide type were developed by Corominas (1996), Rickenmann (1999) and Devoli *et al.* (2008).

The spreading pattern of flow, entrainment and deposition can also be estimated. This requires more detailed morphological parameters accounting exclusively for site-specific conditions. Similar to the volume-angle of reach approach, statistical correlations between volume and deposit area have also been proposed by Iverson *et al.* (1998). These methods provide estimates of aerial extent for accumulation zones. Other correlations have been developed for estimating certain intensity parameters, including debris flow velocity and discharge (e.g., Rickenmann, 1999).

A common problem with the empirical methods is that the scatter of the data is too large for anything but very preliminary predictions of the travel distance. The flexibility of the empirical methods allows them to be applied in local to medium-scale landslide susceptibility and hazard maps but as they do not provide kinematic parameters (velocity, kinetic energy) of the landslides these approaches can be hardly applied to site specific analyses, and in quantitative risk assessment.

3.1.2 Analytical methods

Analytical methods include different formulations based on lumped mass approaches in which the debris mass is assumed as a single point. The simplest type of analytical methods is the sled model (Sassa, 1988), which

assumes that all energy loss during debris movement is due to friction and he describes the landslide as a dimensionless body moving down the profile of the path. The movement is controlled by a single force resultant, representing the gravity driving force as well as all movement resistance. The ratio of the vertical to horizontal displacement of the center of gravity of the block equals the friction coefficient used in the analysis. This method can provide an effective means for the calculation of run-out distance, velocity and acceleration of debris movement. Sassa (2000) improved the sled model by considering the effect of pore fluid pressures at the sliding plane. He considered the frictional resistance along the sliding plane to be a function of the internal friction angle and the pore pressure coefficient. The apparent friction angle in the improved sled model can be expressed as the combined effects of the internal friction angle of debris material, and the motion-induced pore pressure. Hutchinson (1986) developed a model for the prediction of run-out distances of flows in loose, cohesionless materials by assuming that the shape of a debris flow is a uniformly spread-out sheet. In the model, the basal resistance of the debris mass is assumed to be purely frictional, and the excessive fluid pressure in the debris mass is assumed to be dissipating according to the one-dimensional consolidation theory. As debris moves downslope, the shear resistance on the sliding plane increases due to a dissipation of excessive pore pressure. The debris mass halts when the resultant force along the sliding plane becomes zero. Many of the analytical approaches can also be extended to provide an estimate of the velocity profile and acceleration of the landslide, in the case of real time solution techniques (travel time of the flow) (Hunggr, 1995).

3.1.3 Numerical methods

Numerical methods for modelling run-out behaviour of landslide debris mainly include fluid mechanical models and distinct element methods. The most common and used approach for this methods is based on continuum mechanics. Continuum fluid mechanics models utilize the conservation equations of mass, momentum and energy that describe the dynamic motion of debris, and a rheological model to describe the material behaviour of the debris. By solving a set of governing equations with a selected rheological model describing the flow properties of the debris, the velocity, acceleration and run-out distance of debris can be predicted (Chen and Lee, 2000). Most continuum models are simplified by integrating the internal stresses in either vertical or bed-normal directions to obtain a form of the Saint-Venant or Navier-Stokes equations (shallow water assumption) (Iverson, 2005). Derivations of the constitutive relationships using the theory of frictional grain flow (Savage and Hutter, 1991) or the theory of mixture flow (Denlinger and Iverson, 2004; Iverson *et al.*, 2004) have also been investigated. Under the shallow water assumption, different types of solutions (1D and 2D) for fast gravitational flows can be derived from the

momentum equation for unsteady fluid flow, evaluating the dynamic equilibrium for a single column (or discretized unit) isolated from the flowing mass (Eq. 3.1 and 3.2):

$$\frac{\partial h}{\partial t} + \frac{\partial(hu)}{\partial x} + \frac{\partial(hv)}{\partial y} = 0 \quad (3.1)$$

$$\frac{\partial u}{\partial t} + u \frac{\partial u}{\partial x} + v \frac{\partial u}{\partial y} = -g \left(S_x + k \frac{\partial h}{\partial x} + S_f q_x \right) \quad (3.2)$$

$$\frac{\partial v}{\partial t} + v \frac{\partial v}{\partial x} + u \frac{\partial v}{\partial y} = -g \left(S_y + k \frac{\partial h}{\partial y} + S_f q_y \right) \quad (3.3)$$

where h is the flow thickness; (u, v) are the x and y components of the depth average velocities (m/s). Equation 3.1 is the mass balance equation. The momentum equations (Eq. 3.2 and 3.3) are expressed in terms of acceleration (m/s^2), where g is the acceleration due to gravity. The first term on the left side of the equation represents the local acceleration, expressing the time rate of change at a fixed position. The second and third terms on the left side of the equation represents the convective acceleration, i.e. the time rate of change due to change in position in the spatial field. The first term between the brackets represents the acceleration due to gravity, and $S_x = \tan \alpha_x$ and $S_y = \tan \alpha_y$ are the bed slope gradient in the x and y directions, respectively. The spatial derivative in the second term is the pressure acceleration, i.e. the time rate of change due to pressure differences within the flow. S_f is the flow resistance gradient, which accounts for momentum dissipation within the flow due to frictional stress with the bed (Begueria *et al.*, 2009). The terms q_x and q_y are coefficients (Eq. 3.4 and 3.5):

$$q_x = \frac{-u}{\sqrt{u^2 + v^2}} \quad (3.4)$$

$$q_y = \frac{-v}{\sqrt{u^2 + v^2}} \quad (3.5)$$

where the minus sign before u and v ensures that S_f opposes the direction of the velocity.

Eulerian and Lagrangian solutions of these equations have been developed by (Hung, 1995) and non-hydrostatic internal tangential stress has been introduced by Savage and Hutter (1991) assuming that the moving mass is frictional and undergoes plastic deformation according to the Rankine theory (Eq.3.6 and Eq.3.7):

$$K_a = \frac{1 - \sin\varphi}{1 + \sin\varphi} \quad (3.6)$$

$$K_p = \frac{1 + \sin\varphi}{1 - \sin\varphi} \quad (3.7)$$

The term k in Eq 3.2 and Eq.3.3 is the earth pressure coefficient. It ranges between two extreme values corresponding to the active and passive states in the Rankine theory, i.e. $k_a \leq 1 \leq k_p$. These values depend on the internal friction angle of the mixture defined by φ (Begueria *et al.*, 2009).

One of the advantages of the numerical methods is that they have the ability of computing (with a good compromise between computing effort time and accuracy) the movement of the flow over irregular topographic terrains. Besides this, the computed outputs of the models give directly the intensity factors of the landslides; which can be coupled directly to vulnerability or damage-stage functions for a quantitative risk assessment. Numerical models also provide the opportunity to investigate run-out frequencies and magnitudes of landslides in the absence of documentation of former events (volume involved, landslide travel distances).

3.2 Classification of dynamic run-out models

Dynamic run-out models that have a numerical methodology as a background can be classified in many ways but the most common classification groups them in the following types: - *models based on the solution dimension in 1D or 2D*; - *models based on the solution reference frame that can be formulated in Eulerian vs. Lagrangian frames*; and - *models based on the basal rheology*.

- *Models based on the solution dimension (1D or 2D)*: Dynamic models use an approach known as depth-averaging, in which the governing mass and momentum balance equations are integrated with respect to the flow depth. Stresses are assumed to increase linearly with depth below the top surface of the flow, which is assumed to be stress free, and shear stresses in the depth-wise direction are neglected (Savage and Hutter, 1991). This is based on the assumption that the depth varies gradually and is small relative to the length and width of the landslide. Depth-averaging combined with the shallow flow assumption essentially eliminates one dimension, the depth-wise dimension, from the governing mass and momentum balances. One dimensional models analyze the movement considering the topography as a cross-section of a single pre-defined width while two dimensional models makes the analysis considering the topography in plan and cross section.

- *Models based on the solution reference frame (Eulerian or Lagrangian)*: The equations of motion can be formulated in two different frames of reference: Eulerian or Lagrangian. A Eulerian reference frame is fixed in space, analogous to an observer standing still as a landslide passes. Models formulated in an Eulerian framework require the solution of a more complex form of the governing equations using a dense, fixed computational grid. The Eulerian approach is the conventional method in computational fluid dynamics. A Lagrangian reference frame moves with the local velocity, analogous to an observer riding on top of a landslide. This method simplifies the governing equations and does not sacrifice computational resources in void zones. When using the Lagrangian reference (also called material reference), the material velocity and acceleration are expressed in the form of (Eq. 3.8 and Eq. 3.9 respectively):

$$V(X, t) = \frac{D\zeta(X, t)}{Dt} \quad (3.8)$$

and

$$A(X, t) = \frac{DV(X, t)}{Dt} = \frac{D^2\zeta(X, t)}{Dt^2} \quad (3.9)$$

where V is the velocity; A is the acceleration; X the referential position; ζ is the motion that can be viewed as a transport of points from the reference configuration to the current configuration during a specific time interval $[0, t]$. Then, the displacement of a particle located at " X " is expressed as (Eq. 3.10):

$$U(X, t) = \zeta(X, t) - X \quad (3.10)$$

It is cumbersome to pinpoint the particle reference position X at $t = 0$ and recognize its exact trajectory. For this reason, the Eulerian reference (also known as spatial reference) is commonly applied. In the Eulerian reference the attention is given to a certain region in space and the material motion is observed within this region as time proceeds. The quantities of interest are expressed in terms of the current position x (or spatial coordinates) and time t . The spatial velocity and acceleration can be described as follows (Eq. 3.11 and Eq. 3.12 respectively):

$$v = v(x, t) \quad (3.11)$$

and

$$a = a(x, t) \quad (3.12)$$

The displacement can be expressed as (Eq. 3.13):

$$u(x, t) = x - \zeta^{-1}(x, t) \quad (3.13)$$

- *Models based on the basal rheology*: The rheology of the flow is expressed as the resistance forces (S_f in Eq. 3.2 and Eq.3.3) that interact inside the flow and at the interface between the flow and the bed path. The most common rheologies used in the dynamic models are: - "Frictional" (or "Coulomb") resistance (Hung and McDougall, 2009); - the frictional-turbulent "Voellmy" resistance (Voellmy, 1955); - the visco-plastic "Bingham" (or "Herschel-Bulkey") resistance (Coussot, 1997; Malet *et al.*, 2004); - and the "Quadratic" resistance (O'Brien *et al.*, 1993). (Table 3.2) A thorough description of rheologies can be found in Naef *et al.*, (2006).

Table 3.2: Most common flow resistance terms (See Eq. 3.2 and 3.3) used in dynamic run-out models.

Rheology (basal)	Description	Flow resistance term "Sf"
Frictional (Coulomb)	Resistance based on the relation of the effective bed and normal stress at the base and the pore fluid pressure (Hung and McDougall, 2009)	$Sf = \tan\phi'$ $\tan\phi' = (1 - r_u)\tan\phi$ <ul style="list-style-type: none"> - Sf is the unit base resistance; - r_u is the pore-pressure ratio; - ϕ is the dynamic basal friction angle.
Voellmy	Resistance that features a velocity-squared resistance term (turbulent coefficient ξ) similar to the square value of the Chezy resistance for turbulent water flow in open channels and a Coulomb-like friction (apparent friction coefficient μ). (Voellmy, 1955)	$Sf = \left[\tan\phi' + \frac{u^2}{\xi h} \right]$ <ul style="list-style-type: none"> - Sf is the unit base resistance; - $\tan\phi' = \mu$ is the apparent friction coefficient; - u is the flow velocity (m/s); - ξ is the turbulent coefficient (m/s²).
Bingham	Resistance that is a function of flow depth, velocity, constant yield strength (τ_c) and dynamic viscosity (η) (Coussot 1997).	$Sf = \frac{1}{\rho gh} \left(\frac{3}{2} \tau_c + \frac{3\eta}{h} u \right)$ <ul style="list-style-type: none"> - Sf is the unit base resistance; - τ_c is a constant yield strength due to cohesion; - ρ is the density of the flow; - η is the viscosity parameter.
Quadratic	Resistance that incorporates a turbulent contribution to the yield and the viscous term already defined in the Bingham equation (O'Brien <i>et al.</i> , 1993).	$Sf = \frac{\tau_c}{\rho gh} + \frac{K\eta}{8\rho g(h)^2} u + \frac{n^2(u)^2}{(h)^{4/3}}$ <ul style="list-style-type: none"> - Sf is the unit base resistance; - τ_c is the resisting shear stress; - u is the depth-averaged velocity; - h is the flow depth; - η is the viscosity of the fluid, - K is a resistance parameter that equals 24 for laminar flow in smooth, wide, rectangular channels, but increases with roughness and irregular cross sections; - n is the Manning coefficient value that takes into account the turbulent and dispersive components of flow.

3.3 An overview of several dynamic run-out models

Several dynamic run-out models have been developed in the past and the approaches for landslide modelling have been improved. These models have evolved from simple hydrodynamic models to more complex models that include various methods accounting for internal strength, entrainment and rheology variations. Table 3.3 gives an overview of some well-known commonly used 2D run-out dynamic models and were classified based on their implementation and scheme of their entrainment rates. In the “defined entrainment rate” the amount of entrained material is specified by the user while in the “process-based entrainment rate” the amount is calculated by a prescribed algorithm that considers the material properties. Other characteristics of the models are also summarized: basal rheology, solution approach, reference frame of solution and variation of rheology along the flow path.

Table 3.3: An overview of several 2D dynamic numerical run-out models.

Model	Rheology	Solution approach	Reference Frame	Variation of rheology	Entrainment rate
MADFLOW (Chen and Lee, 2007)	Frictional, Voellmy and Bingham	Continuum Integrated	Lagrangian with mesh	no	Defined
TOCHNOG (Crosta <i>et al.</i> , 2003)	Frictional (elastoplastic model)	Continuum Differential	Differential (adaptive mesh)	yes	Process based
RAMMS (Christen <i>et al.</i> , 2010)	Voellmy	Continuum Integrated	Eularian	yes	Process based and defined
DAN3D (Hungri and McDougall, 2009)	Frictional, Voellmy and Bingham	Continuum Integrated	Lagrangian meshless	yes	Defined
FLATMODEL (Medina <i>et al.</i> , 2008)	Frictional and Voellmy	Continuum Integrated	Eulerian	no	Process based
SCIDDICA S3-hex (D'Ambrosio <i>et al.</i> , 2003)	Energy based	Cellular Automata	Eulerian	no	Process based
3dDMM (Kwan and Sun, 2006)	Frictional and Voellmy	Continuum Integrated	Eulerian	yes	Defined
PASTOR model , (Pastor <i>et al.</i> , 2009)	Frictional, Voellmy and Bingham	Continuum Integrated	Lagrangian meshless	yes	Defined
MassMov2D (Begueria <i>et al.</i> , 2009)	Voellmy and Bingham	Continuum Integrated	Eulerian	yes	Defined
RASH3D (Pirulli and Mangeney, 2008)	Frictional, Voellmy, Quadratic	Continuum Integrated	Eularian	no	No entrainment rate is used
FLO-2D (O'Brien <i>et al.</i> , 1993)	Quadratic	Continuum Integrated	Eularian	no	No entrainment rate is used
TITAN2D (Pitman and Le, 2005)	Frictional	Continuum Integrated	Lagrangian with mesh	no	No entrainment rate is used

Cont. Table 3.3: An overview of several 2D dynamic numerical run-out models.

Model	Rheology	Solution approach	Reference Frame	Variation of rheology	Entrainment rate
PFC (Poisel and Preh, 2007)	Inter-particle and particle wall interaction	Solution of motion of particles by a distinct element method	Distinct element method	no	No entrainment rate is used
VolcFlow (Kelfoun and Druitt, 2005)	Frictional and Voellmy	Continuum Integrated	Eulerian	no	No entrainment rate is used

Most of the above mentioned models were applied in an important benchmarking exercise on landslide debris run-out and mobility modelling that was carried out in 2007 at the International Forum on Landslide Disaster Management. The main goal of this exercise was to assess whether the field of run-out modelling was on its way towards establishing some degree of commonality among different methods used by various parties and to highlight the main progresses in that topic (Hungry *et al.*, 2007). In that exercise, 13 research groups that work on the topic of run-out analysis participated by performing simulations of twelve different case studies. The participants were able to select which model and case study was most convenient based on their resources. The main results were presented in the forum and also discussed in a round table. The main key points during that discussion were:

- Run-out modelling is very sensitive to the topography and the resolution of the computational domain. Mesh refinements methods will help to improve the modelling results.
- Run-out models should be computationally efficient.
- The momentum-based formulation in continuum models is still the most reliable approach for run-out modelling.
- The presented models are consistent in the use of Eulerian and Lagrangian approaches. Although both methods have their advantages and disadvantages, they are viable to use and promising.
- Run-out models can be accurate when used for a back calibration of a well documented event but inconsistencies are evident when performing a forward analysis.
- More data from real landslides is needed to refine the models and their parameterization.
- It is needed to gain more confidence in the selection of suitable rheological models and their parameters for different types of landslides.

3.4 Dynamic run-out models used in this research

In this research a combination of a qualitative and quantitative suitability assessment for back-analyzing past events was performed using different run-out models: -MassMov2D; DAN3D; RAMMS; FLO-2D, and FLOW-R. Two other models have been used which were originally developed by Th.W.J. van Asch and they were optimized in the framework of this research: a 1-D model described in chapter 4, and a 2-D regional model described in chapter 7. Table 3.4 gives an overview of the models used and the reasons for selecting these specific ones. The selection of the assessment was based on the amount and quality of information disposed and the type of accuracy needed. To evaluate the influence of the variations in the rheological input parameters to the final results, a sensitivity analysis of the models was carried out. This was achieved by evaluating how the percentage of the variation in the output of a model can be apportioned among percentage of variation of the model inputs. In the case of the FLO-2D model, no sensitivity evaluation was carried out in this research because the yield strength and the viscosity parameters are usually selected from the set of materials presented by O'Brien and Julien (1988), where empirical coefficients defined by laboratory experiments (O'Brien and Julien, 1988) are included in empirical relationships as a function of the sediment concentration. These values and the sets of materials are suggested in the user manual of FLO-2D and a parametric analysis of them was carried out earlier by Cepeda *et al.* (2007).

Table 3.4: The models used in this research and the reasons for selecting them. Also the test sites are indicated where the models have been applied (see chapter 2).

Model	Reasons for selecting this particular model	Test area	Chapter/Section
MassMov2D	<ul style="list-style-type: none"> - Open source model implemented in a dynamic GIS (PCRaster). - Possibility to use different rheologies. - Models entrainment. - Outputs of the results can be obtained in forms of maps, graphs or text files. - User friendly. - Code can be modified to the user needs. - Can run batch files - Computationally efficient 	<ul style="list-style-type: none"> - Peringalam, India - Faucon, France - Tresenda, Italy 	<ul style="list-style-type: none"> - Section 3.4.1; 3.4.3. - Chapter 6
DAN3D	<ul style="list-style-type: none"> - Different rheologies can be selected. - Models entrainment - Uses SPH (Smooth Particle Hydrodynamics) method. - It is a commonly used and well-known model for run-out assessments. 	<ul style="list-style-type: none"> - Peringalam, India 	<ul style="list-style-type: none"> - Section 3.4.2; 3.4.3.
RAMMS	<ul style="list-style-type: none"> - User friendly - Have a comprehensive Graphical User Interface - Models entrainment - Use the Voellmy rheology - Results are displayed in maps and graphs. - Results can be exported easily to other platforms (e.g. ESRI and Google Earth). 	<ul style="list-style-type: none"> - Faucon, France 	<ul style="list-style-type: none"> - Chapter 3.4.4
FLO-2D	<ul style="list-style-type: none"> - Input as a hydrograph which is routed with a quadratic rheology. - Allows the modelling of water (run-off) and sediments (run-out). - Outputs and results nicely displayed and can be easily exported as ESRI files. - Several results can be obtained such as: impact forces and pressures. 	<ul style="list-style-type: none"> - Selvetta, Italy - Tresenda, Italy 	<ul style="list-style-type: none"> - Chapter 8 - Chapter 9
FLOW-R (*)	<ul style="list-style-type: none"> - Simple regional model for run-out assessment. - Use the energy-line approach. 	<ul style="list-style-type: none"> - Barcelonnette, France - Valtellina, Italy 	<ul style="list-style-type: none"> - Chapter 7
1-D entrainment model (*)	<ul style="list-style-type: none"> - Models entrainment with a concept based on limit equilibrium and the generation of excess pore water pressure through undrained loading of the bed material. 	<ul style="list-style-type: none"> - Faucon, France 	<ul style="list-style-type: none"> - Chapter 4
AschFlow (*)	<ul style="list-style-type: none"> - Simplified regional run-out model. - Based on rheological parameters. - Different rheologies can be selected. - Models debris flow velocity and thickness. 	<ul style="list-style-type: none"> - Barcelonnette, France - Valtellina, Italy 	<ul style="list-style-type: none"> - Chapter 7

(*) These models will be described in further chapters.

In all the back-analysis cases, the input parameters of the rheological models were modified by trial and error using a qualitative assessment until the characteristics of the modelled debris flows were approximately close to the real event debris flows. The criteria that were chosen to compare the simulation results with the real event were deposit depth, velocity, deposited volume, area of the deposits and entrained volume.

3.4.1 MassMov2D model

MassMov2D is a two-dimensional model of mud and debris flow dynamics over complex topography, based on a numerical integration of the depth-averaged motion equations using a shallow water approximation. The core part of the model is implemented using the GIS scripting language PCRaster. The MassMov2D model is based on a 2-D finite difference solution of a depth-averaged form of the fluid dynamics equations. The flow is treated as a one-phase material, whose behavior is controlled by rheology (i.e. by a functional relationship between strain and stress). The Bingham and Voellmy rheological models are implemented within a common numerical scheme inside the model. MassMov2D can accept a detailed description of a complex topography through a digital elevation model (DEM). The model is implemented in a geographical information system (GIS) package, which is beneficial for the preparation of input data and evaluation of the results. The core equations of the model (mass balance, equation of motion, rheology) are accessible to the user in an easy-to-learn scripting language which enables the modification of the original code. A detailed description of the MassMov2D model can be found in Begueria *et al.* (2009) and in Appendix 2.

3.4.1.1 MassMov2D model setup

A back-analysis of the Peringalam, India event (described in Section 2.3) was performed with the MassMov2D model. Based on the characteristics of the flow, the Voellmy rheology module was chosen for this case. The selected time step was one second to register the outputs, although internally the model used fractional time steps which vary depending on the flow characteristics, based on the Courant-Friedrichs-Levy condition (CFL) (Begueria *et al.*, 2009). In order to control the numerical stability the CFL upper limit was set to 0.5 and the lower limit was 0.3. Five different maps in raster form were used to describe the computational domain. The first map contained information before the debris flow event (pre-event) about elevation and topographical features of the terrain. This map also defines the mesh size where the computations take place. The second map was produced to define the initiation thickness, shape and area of the released mass. A third binary map was created to display an outlet cell for the flow (open boundary). A fourth map was used to define the distance of the whole domain to the toe of the initiation area. And a fifth map was created with the soil depths to identify the amount of entrained material that the flow can entrain. MassMov2D has also implemented a fluidization term which describes the pace of the transition between the solid release mass and how it fluidizes once the mass is set into motion. This fluidization rate is described as a velocity and it only takes place during the initiation of the movement. In both simulated cases, the fluidization rate chosen was 10 m/s.

3.4.1.2 MassMov2D results of back-analysis

The combinations of model parameters that produced the best predictions for the Peringalam debris flow event were: an apparent friction angle of 34° ; a turbulent coefficient of 250 m s^{-2} ; and an entrainment rate (McDougall and Hungr, 2005) of 0.035 m^{-1} . In terms of the internal pressures, the models was adjusted to the assumption that the flow was hydrostatic ($k=1$ in Eq 3.2). A simulation time of 100 s was selected. In all the simulations the density of the flow was considered at 2000 kg m^{-3} . The simulations of the Peringalam debris flow are presented in Figure 3.1, which shows selective images of the calculated sequences at time steps 0, 10, 20, 35, 50 and 100 seconds.

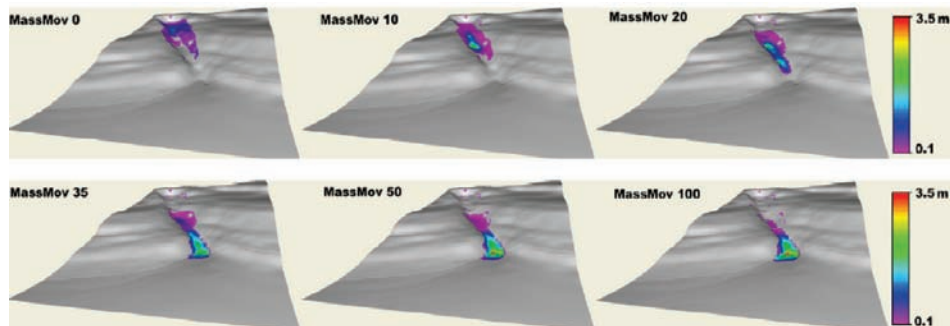


Fig. 3.1 Temporal evolution of debris flow height as modelled by MassMov2D for the Peringalam event, India (see chapter 2).

The simulations done with MassMov2D displayed a lower eroded soil depth than with DAN 3D (see next section) close to the release area and the modelled erosion is more evenly spread in the whole channel. A simple model of material entrainment was incorporated in MassMov2D which was originally proposed in the DAN3D model in its original version (Hungr, 1995). The erosion rate increases in proportion to the flow depth, resulting in a depth proportional distribution of entrained material and natural exponential growth of the landslide with displacement. The erosion amount is limited by a user-defined, spatially distributed “erosion depth” (McDougal and Hungr, 2005) (See Appendix 3). Fig. 3.2 shows the eroded materials modelled with MassMov2D for the same event. The resulting values for the entrained soil and the thickness and spreading of the flow materials corresponds well with field observations.

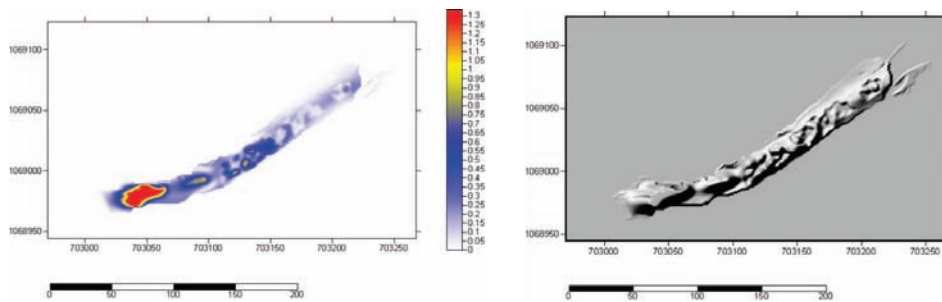


Fig. 3.2: Maps of the eroded thickness in MassMov2D. Left: the distribution of debris flow thickness along the path of the Peringalam debris flow (values are in meters). Right: Hillshading image of the material thicknesses.

3.4.2 DAN3D model

The DAN3D model (developed at the University of British Columbia) uses a semi-empirical approach based on the concept of equivalent fluid defined by Hungr (1995). In this framework, the heterogeneous and complex landslide material is modelled as a hypothetical material governed by simple rheological relationships. Internal and basal rheologies are different from each other. This is based on the assumption that internal and basal friction mechanisms has its roots in the depth-integrated solutions of classical fluid dynamics, where a variety of viscous or turbulent relationships can be used to determine basal friction forces of a flowing sheet of fluid, while the internal stress distribution is assumed to be hydrostatic (McDougall and Hungr, 2004). The DAN3D model allows for frictional (Frictional model), viscous (Bingham model) or turbulent (Voellmy model) resistance acting on the base of an internally frictional flow. The DAN3D model is based on a Lagrangian formulation that discretises the flow in a number of particles representing bed-normal columns of flow. The values of the field variables for each particle are calculated at each time step using an interpolation technique based on Smoothed Particle Hydrodynamics (SPH). The internal stresses are functions of the internal shear strains and are bounded by active and passive states. The model features include: - the ability to simulate flow across complex three-dimensional terrain; - the ability to allow non-hydrostatic and anisotropic internal stress distributions, coupled with strain changes through frictional relationships; -the ability to simulate material entrainment; - a choice of different rheological models; and - a meshless solution, which eliminates problems with mesh distortion during long displacements. A detailed description of the model and its numerical scheme can be found in Hungr and McDougall (2009) and Appendix 3.

3.4.2.1 DAN3D model setup

A back-analysis of the Peringalam event (See Section 2.3) was also performed with the DAN3D model. Besides the information of the release

volume and the rheology model parameters, the numerical parameters for DAN3D are: the number of particles, the time step, the particle smoothing coefficient, the velocity smoothing coefficient, and the stiffness coefficient. The values of the parameters of the particle smoothing coefficient and the stiffness coefficient were set equal to 4 and 200, respectively as suggested in the applications presented by McDougall (2006). The initial release volume is discretised by the model in particles with equal initial volumes. The number of particles should be large enough to ensure the accurate simulation with respect to flow spreading, junctioning and branching (McDougall and Hungr, 2004). The volumes to be simulated in the back-analysis with the number of particles were set to 2000 for all the simulations. A time step of 0.05 s was selected for all simulations. The velocity smoothing coefficient (See Appendix 3) increases the numerical stability and improves the behaviour of the model in channelized reaches by reducing the tendency for particles to line up. McDougall (2006) suggests a value up to about $C = 0.01$ to be appropriate.

3.4.2.2 DAN3D results of back-analysis

The DAN3D model was applied using the same combinations of model parameters used with the MassMov2D model that produced the best results for the Peringalam debris flow event. This was done in order to compare the sensitivity to the friction parameters of both models and to observe the outputs of both models in comparison to each other. The parameters used were: an apparent friction angle of 34° ; a turbulent coefficient of 250 m s^{-2} ; and an entrainment rate of 0.035 m^{-1} . The flow was assumed to be hydrostatic. A time step of 100 s was selected and a density of the flow was considered as 2000 kg m^{-3} . Some results of the simulations of the Peringalam debris flow are presented in Figure 3.3, showing images of the calculated sequences at time steps 0, 10, 20, 35, 50 and 100 seconds. The DAN3D model reproduced similarly the thickness of the final deposits and the spreading of flow. Even though the constraint of not having a more detailed field measurements, the DAN3D model provided a good approximation of the observed behaviour of the past event. The models provided similar results in terms of total run-out distances as well as flow heights and velocities.

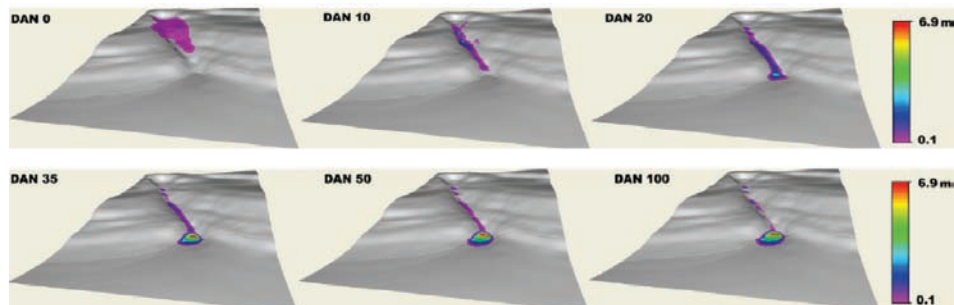


Fig. 3.3: Temporal evolution of debris flow height as modelled by DAN3D for the Peringalam event, India (see chapter 2).

The results with DAN3D showed that the process of entrainment starts almost instantaneously from the start of the simulation. The entrainment process in the model is mostly affecting the channelled zone (Fig. 3.4).

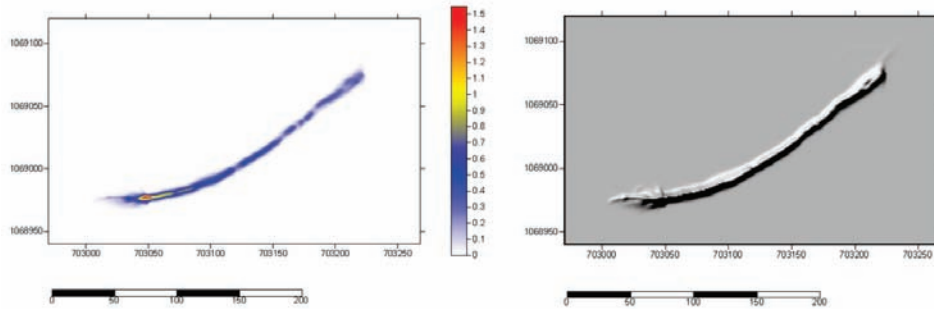


Fig. 3.4: Maps of the simulated erosion in DAN3D. Left: the distribution of debris flow thickness along the path of the Peringalam debris flow (values are in meters). Right: Hillshading image of the material thicknesses.

3.4.3 MassMov2D and DAN3D sensitivity of the resistance parameters

After obtaining the results of the back-calibration (Table 3.5), a sensitivity analysis was carried out for the rheological parameters of the Voellmy rheology in both models: MassMov2D and DAN3D. This was done using the same methodology in both models to assess the influence of the parameters in the models and the differences between them. The apparent friction angle was varied with 10% increments of the calibrated value of 34° in the range between 3.4° and 53.2° . The turbulent coefficient was varied in steps of 25 units, from values of 25 m/s^2 to 1000 m/s^2 . In order to compare the results of the sensitivity analysis, the back calibrated simulation was used as a reference. For all the simulations (a total of 47 runs), all the starting parameters were kept constant except the parameter selected for the sensitivity.

Table 3.5 Observed and simulated properties of the Peringalam debris flow. The initial volume was 1435 m^3 .

	Observed	MassMov2D	DAN3D model
Entrained volume (m^3)	593	614	619
Max velocity (m/s)	20	24	21
Mean deposit thickness (m)	1.6	1.7	2.2
Max deposit thickness (m)	4.1	3.5	6.9

The requirements needed regarding both parameters in this analysis were: - the apparent friction angle must be less than the starting-zone slope; - the apparent friction angle cannot be zero; otherwise the flow would not come to rest on a horizontal plane within a finite time; and - both apparent friction angle and turbulent coefficient must be positive or else the friction would not

be dissipative. Two different locations inside the flow path were used to measure the variation of flow depth and velocity according to the variation of the parameters: point "D" that is located in the depositional zone at the fan apex and point "R" located at the exact middle length of the run-out path (Fig. 3.5 and Fig. 3.6)

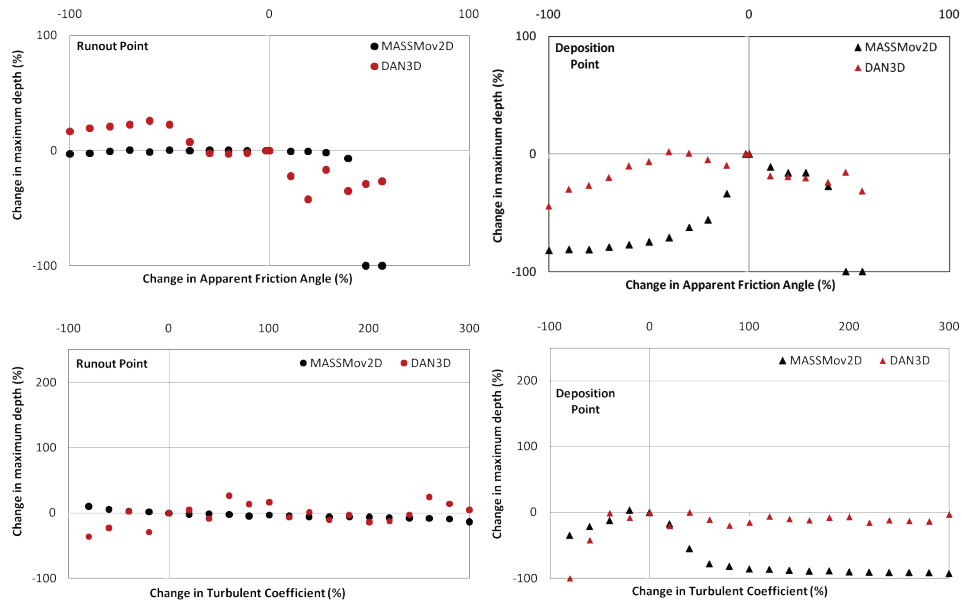


Fig. 3.5: Percentage of change in the flow depth in accordance to the percentage of change in the input parameters of the Voellmy model using the MassMov2D and DAN3D run-out models. The left graph present the values at a point in the run-out area and the right graphs a point in the depositional area.

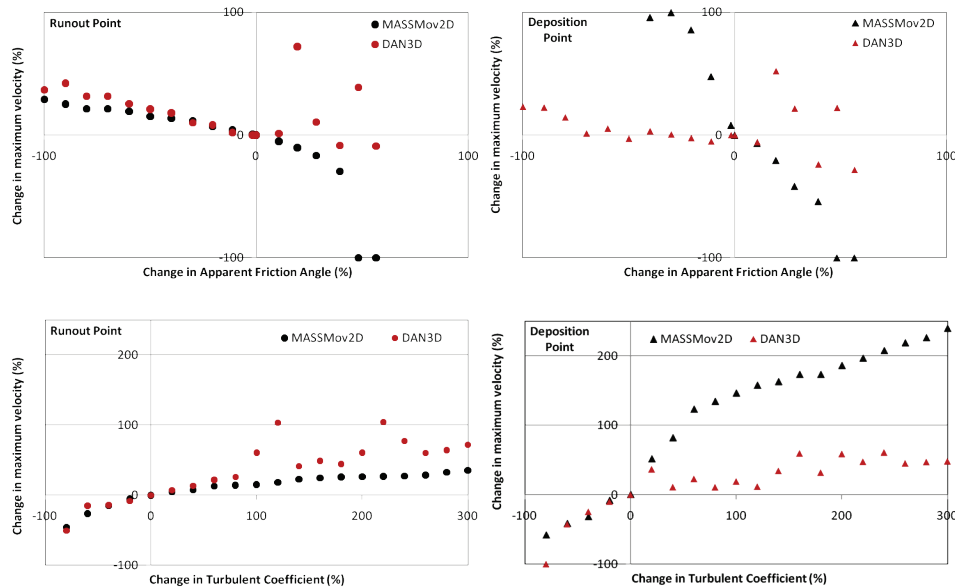


Fig. 3.6 Percentage of change in the flow velocity in accordance to the percentage of change in the input parameters of the Voellmy model using the MassMov2D and DAN3D run-out models. The left graph present the values at a point in the run-out area and the right graphs a point in the depositional area.

3.4.4 RAMMS model

The RAMMS model has been developed in Switzerland by a team of experts at the WSL Institute for Snow and Avalanche Research SLF and the Swiss Federal Institute for Forest, Snow and Landscape Research WSL. The RAMMS model is a generalization of the quasi one-dimensional model as discussed by Bartlet *et al.* (1999). RAMMS uses the Voellmy-Salm fluid flow continuum model (Salm, 1993) based on the Voellmy-fluid flow law and describes the debris flow as a hydraulic-based depth-average continuum model. The flow resistance is divided into a dry-Coulomb friction and a viscous resistance turbulent friction. RAMMS further contains an entrainment model that is a rate-controlled entrainment method which regulates the mass being up taken by the incoming debris flow and adjust the time delay to accelerate this mass to the debris flow velocity discussed by Sovilla *et al.* (2006). The model solves the governing mass and momentum equations using a finite volume scheme. (Christen *et al.*, 2010). Flow heights and velocities are calculated on three-dimensional digital terrain models with the possibility of choosing single or multiple release areas. A detailed description on the RAMMS model and its equations can be found in Christen *et al.* (2010) and Appendix 4.

3.4.4.1 RAMMS model setup

A back-analysis of the Faucon 2003 debris flow event (See Section 2.1.1) was performed with the RAMMS model. In the RAMMS model the terrain is represented by a DEM and the besides of selection of the friction parameters, a geometrical description of the release area has to be clearly defined. The definition of the release area and the possible initiation volume was carried out based on the reported historical event combined with an image interpretation. A thickness of the failed mass at the initiation zone was defined at 1.5 m. This resulted in an initiation volume of 8,750 m³. Two points in the channel (at the V.C. 3 Bridge and apex of the alluvial fan) were selected to measure the flow velocities and heights as mentioned in Section 2.1.1. These points were also used in further analysis (sensitivity analysis in Section 3.4.4.3 and in Chapter 6).

3.4.4.2 RAMMS results of back-analysis

The calibrated values that were found the most appropriate for the Faucon event were: $\mu = 0.06$, $\xi = 500 \text{ m/s}^2$ and the RAMMS entrainment coefficient $K = 1$. The volume outputs of the model and their deviation from the observed volumes of the 2003 debris flow are shown in Table 3.6. As the intensity parameters of the 2003 event are defined in terms of specific ranges, the suitability of the model is calculated in percentage difference from the lowest or highest values of this range depending on whether the calibrated values are underestimated or overestimated in comparison to the 2003 debris flow parameters. The model underestimates the debris flow heights at both the apex and the bridge when compared with the 2003 event. The average maximum flow heights ranged between 1.5 to 3 m and increased rapidly just before the fan apex. The initiation volume used for modelling was 8,750 m³, and the entrainment volume was 55,150 m³ resulting in a final deposition of 61,800 m³.

Table 3.6: The 2003 debris flow intensity parameters compared with the model results.

	Faucon 2003 debris flow event	Model results	Suitability (%)
Initiation volume	7,500 – 9,500 m ³	8,750 m ³	0 %
Entrainment volume	52,500 – 55,000 m ³	55,150 m ³	0 %
Total deposited volume	60,000 – 65,500 m ³	61,800 m ³	0 %
Run-out distance	4,700 m	4,760 m	+ 1.4 %
Maximum height near fan apex	5.0 – 6.0 m	3.44 m	- 32.4 %
Maximum height at the bridge	5.0 – 6.0 m	2.75 m	- 44.8%
Velocity near fan apex	6.4 – 8.9 m/s	7.25 m/s ²	0 %
Velocity at the bridge	2.0 – 5.0 m/s	2.60 m/s	0 %

3.4.4.3 RAMMS sensitivity analysis

Three input parameters were used in the analysis: the friction coefficient μ , the turbulent coefficient ξ and the RAMMS entrainment coefficient K (see Appendix 4). Each input parameter was increased or decreased by a certain percentage from its original calibrated value while the other two input parameters were kept constant at their calibrated values. The value ranges for the friction coefficient μ were between 0.01 and 0.7, the turbulent coefficient ξ between 100 and 3000 m/s^2 and the entrainment coefficient K between 0 and 5. A total of 120 debris flow run-outs were simulated with these parameter ranges. Three different outputs were assessed in the sensitivity analysis: the total run-out distance, the maximum debris flow height at the apex and at the bridge; and the maximum debris flow velocity at both locations (Fig 3.7 and Fig 3.8)

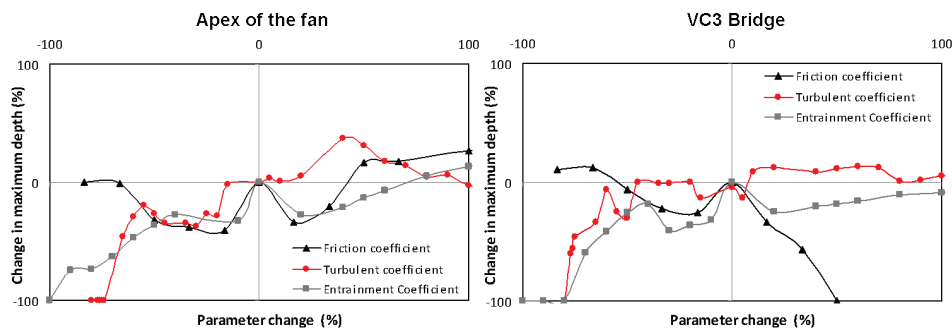


Fig. 3.7: Sensitivity of the flow height at the apex of the fan (left) and the bridge (right) to the Voellmy rheological parameters and the entrainment parameter.

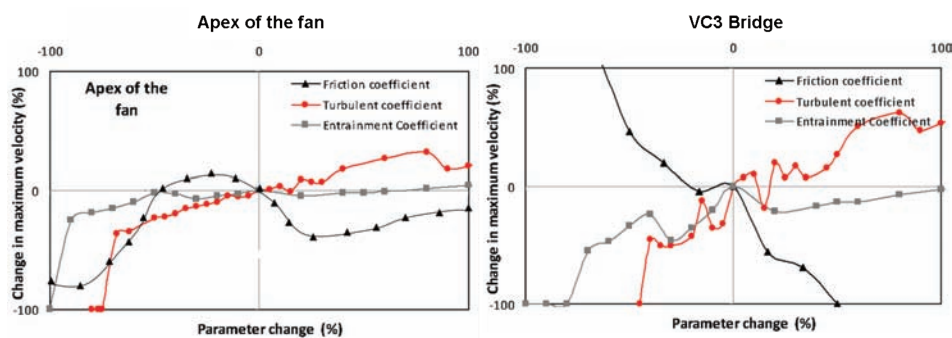


Fig. 3.8: Sensitivity of the flow velocities at the apex (left) and the bridge (right) to the Voellmy rheological parameters and the entrainment parameter.

3.4.4 FLO-2D model

FLO-2D is a Eulerian two-dimensional finite difference model that is able to route non-Newtonian flows in a complex topography based on a volume conservation model. The flow volume is routed through a series of tiles that simulates overland flow (2D flow), or through line segments for channel

routing (1D flow). Flow in two dimensions is accomplished through a numerical integration of the equations of motion and the conservation of fluid volume. The differential equations of motion are solved using a central difference scheme. The boundary conditions are specified as follows: the inflow condition is defined in one or more upstream grid elements with a hydrograph (water discharge vs. time) and values of C_v for each point in the hydrograph; the outflow condition is specified in one or more downstream grid elements. Time steps vary according to the Courant-Friedrich-Lewy stability condition (O'Brien et al., 1993). The model requires the specification of the terrain surface as a uniformly spaced grid. Within the terrain surface grid, a computational grid, i.e. a domain for the calculations, must be specified. The Manning n values should be assigned to each grid element to account for the hydraulic roughness of the terrain surface. The values can be spatially variable to account for differences in surface coverage. The internal stresses are isotropic. The basal shear stresses are calculated using a quadratic model. A detailed description of the FLO-2D model can be found in the O'Brien et al. (1993), FLO-2D manual (2009) and Appendix 5.

The FLO-2D model was used to back-analyze the Selvetta debris flow event of 2008 and the Tresenda case, which were described in Section 2.2.1 and Section 2.2.2. The FLO-2D model requires a calculation of an input hydrograph that can be defined using variable and constant sediment concentrations. The model parameters for the yield strength and the viscosity were selected from the set of materials described by O'Brien and Julien (1988). A Manning n -value that characterizes the roughness of the terrain needs also to be defined. The FLO-2D manual (2009) suggest the use of ranges according to three values: 0.04, 0.1, and 0.2. These values correspond to the lower bound for open ground with no debris (0.04), the limit between open ground with debris and without debris (0.1), and the upper bound for open ground with debris (0.2).

The results obtained with the FLO-2D are described in detailed in Chapter 8 and 9, where the model was used to compute vulnerability curves based on a back-analysis of the Selvetta debris flow and a quantification of risk in the Tresenda village.

3.5 Discussion and conclusions

An important aspect in a debris flow hazard assessment is the delineation of endangered areas and the likelihood to know the intensity characteristics of the event. In this chapter an overview of methods for run-out assessment of debris flows was given. Run-out methods can be divided into empirical (statistical) and dynamic (analytical or numerical) methods. Empirical methods are often easy to use and can be applied where the conditions are similar to those on which their development is based. Empirical methods can

compute the total travel distance and the run-out distance on the fan, while some more sophisticated empirical methods can also estimate peak discharge and flow velocity. On the other hand, dynamic models are physically based and consider the momentum conservation of the flow. Dynamic run-out models which are able to compute the velocity and run-out of the failed mass have been developed either for mass point or lumped mass models, or for continuum based models which also simulate the deformation of the moving mass along the flow path.

Continuum based dynamic run-out models can be classified according to the dimension of their calculations and the reference frame of the formulated solution. Another type of classification, and the most common one, is based on the basal rheology (which takes into account the resistance characteristics of the flow). In this Chapter, a number of the available models are listed based on their solution approach, their reference frame, the ability to have changes in rheology during the course of the flow and the capacity to model entrainment and the rate at which the entrainment is computed (defined by the user or based on the physical characteristics of the flow process).

This Chapter gives also a short summary of the models used in this research to back analyze past events. The model set-up and the resistance parameters used to simulate past events are described. The results of the model simulations when compared with the observations of natural debris flows, some general debris-flow characteristics needed for hazard assessment can be reasonably well simulated with dynamic models if prior calibration of the model parameters is possible.

A major difficulty in the application of dynamic models for debris-flow run-out assessment is the choice of appropriate resistance parameters or material rheologies. For this reason, a sensitivity of the frictional parameters of these models using the Voellmy rheology was performed in order to observe the influence of the input parameters in the final results. For three models (MassMov2D, DAN3D and RAMMS) results are presented of a sensitivity analysis. Table 3.7 gives a summary of the main results classified in: high sensitivity, moderate sensitivity and low sensitivity.

Table 3.7 Summary of the sensitivity analysis of the used models in their results.

	MassMov2d		Dan3D		RAMMS	
	Flow height	Velocity	Flow height	Velocity	Flow height	Velocity
Apparent Friction angle	Moderate sensitivity	High sensitivity	High sensitivity	High sensitivity	High sensitivity	High sensitivity
Turbulent coefficient	Moderate sensitivity	High sensitivity	Low sensitivity	High sensitivity	Moderate sensitivity	High sensitivity
Entrainment coefficient	No measured sensitivity	No measured sensitivity	No measured sensitivity	No measured sensitivity	High sensitivity	Moderate sensitivity

It was noted during the process of calibration and sensitivity, that the apparent friction angle was the parameter that have a greater impact in the extent of the deposits and the length of the run-out. It was also observed that a lower apparent friction coefficient generates lower deposit heights in the run-out zone and thinner deposits (although with a higher spreading) in the depositional zone. The apparent friction angle is in general terms the parameter that controls the extension of the run-out. The turbulent coefficient was the parameter that influenced mostly the velocity of the flow. This parameter controls the drag forces of the flow in the topography and influence the speed of the run-out. When using lower values of the turbulent coefficient, the deposits are spreading more evenly during the whole simulations and during the deposition at the fan. When the turbulent coefficient reaches very high values, the Voellmy model becomes close to pure frictional behaviour and the only parameter that influences in that case the flow is the apparent friction angle. This makes the velocities of the flow to reach high values during the down slope movement. An increase in the entrainment coefficient K of the RAMMS model significantly increases the debris flow height when compared to the other frictional parameters. A 200% increase in the entrainment coefficient K causes a 60% increase in the flow height at the apex.

Chapter 4: A run-out model with an entrainment module

4.1 Introduction

Most dynamic run-out models assume a constant volume during the motion of the flow, ignoring the important role of material entrained along its path. Consequently, they neglect that the increase of volume can enhance or reduce the mobility of the flow and can significantly influence the size of the potential impact area. Limited work has been done to quantify the entrainment process and only a few have proposed physical explanations for it. One of the reasons is that material entrainment is a complex process and an adequate understanding of the phenomenon is needed to facilitate the development of appropriate dynamic models. A proper erosion mechanism needs to be established in the analyses of debris flows that will improve the results of dynamic modelling and consequently the quantitative evaluation of risk.

Entrainment of channel path and torrent flanks material, and sediment deposition during run-out are key features of many debris flows. Such entrainment mechanisms are able to change significantly the mobility of the flow, through rapid changes of the flow volume and its rheological behaviour (Iverson *et al.*, 1997; McDougall and Hungr, 2005; Takahashi, 2009). The entrainment process is frequently observed on debris flows during the run-out phase (Chen *et al.*, 2006; Remaitre, 2006). After failure at the source zone, the entrained materials may increase several times in volume with respect to the initially mobilized mass (Vandine and Bovis, 2002). Entrainment occurs when a flow moves along an erodible layer applying a shear stress that surpasses the strength of the erodible layer material. This process can occur during short intervals or semi-continuously over large areas. Single particles or larger pieces of the bed material will be detached and accelerated by the flow and frequently added into it (Gauer and Issler, 2004). Entrainment can either accelerate or decelerate the moving mass depending on the characteristics of the erodible material as well as on the topography and on the dynamics of the flow (Mangeney *et al.*, 2010).

Chapter 4 is based on:

Quan Luna, B., Remaitre, A., van Asch, Th.W.J., Malet, J.-P., van Westen, C.J., 2011. Analysis of debris flow behavior with a one dimensional run - out model incorporating entrainment. In: Engineering geology, in press 13 p.

Models using a constant volume cannot yield an accurate forecast of debris flows characteristics. This especially applies for debris flows occurring in heterogeneous torrential watersheds characterized by various geological settings and superficial surface deposits (Crosta *et al.*, 2009). Erosion processes affect the motion in two different ways: firstly the addition of mass to the flow causes a decrease in the bed friction force per unit mass and in the potential energy of the flow, and secondly generates a resistive force on the moving mass, because of the momentum transfer between the flow in motion and the soil cover that has to be mobilized and accelerated to the flow velocity. For this reason, the entrainment mechanisms have to be included in the depth-averaged flow models through erosion and deposition rate formulas, and the addition of an entrainment force term in the momentum balance equation (Issler and Johannesson, 2011). However, its parameterization can become a cumbersome task because of an actual poor understanding and limiting assumptions of the physics and mechanics behind the involved processes (Bouchut *et al.*, 2008). This adds to the lack of consistency of depth-averaged models that includes entrainment laws.

This chapter presents and evaluates the performance of a 1D debris flow model with a material entrainment concept based on limit equilibrium considerations and the generation of excess pore water pressure through undrained loading of the in-situ bed material. The debris flow propagation model is based on a one dimensional continuum mechanics approach using a depth-integrated approximation based on the shallow water assumption (Saint-Venant equations). The flow is treated as a laminar one-phase material, in which behaviour is controlled by a visco-plastic Coulomb-Bingham rheology. The model parameters are evaluated and the model performance is tested on a debris flow event that occurred in 2003 in the Faucon torrent. The purpose of developing a 1-D debris flow model that takes into account an entrainment concept was to identify and state the advantages of including entrainment in the calculation of practical debris flow dynamics for hazard analysis. This was done by performing a sensitivity evaluation of the reliability of the model and back-calibrating the model with observational data of a past debris flow event.

4.2 *Entrainment mechanism analysis - brief summary of previous work*

In Chapter 3 an overview was given of the various approaches for run-out modelling. In this section we will review these methods, with specific emphasis on the analysis of entrainment. Some efforts have already been made to quantify the erosion processes and entrained volumes, trying to propose a physical explanations for the extreme bulking rates (e.g. Takahashi, 1978; McDougall and Hungr, 2005; Crosta *et al.*, 2009; Mangeney

et al., 2010). This previous work can be divided in: experimental investigations, empirical and numerical analyses.

4.2.1 Experimental investigations

Experiments to understand the physics and to construct mathematical models for entrainment rates have been performed at laboratory and full scale. In the past, most of the full scale experiments have been carried out with snow avalanches. Sovilla *et al.* (2006) based on observations in the Monte Pizzac (Italy) and Vallée de la Sionne (Switzerland) test sites concluded that in spite of the differences of the snow characteristics and released mass, the maximum erosion took place where the slope is 35° or more. The erosion process decreased where the slopes became gentler. The initial mass, the amount of erodible snow and the avalanche velocity were found to be correlated to the erosion per unit area. They recognized three different mechanisms of snow entrainment: ploughing, step entrainment and basal erosion or abrasion. Ploughing or front entrainment rates measurements where as high as $350 \text{ kg m}^{-2} \text{ s}^{-1}$ (in the Vallée de la Sionne test site) and the entire snow cover can be entrained in a very short time. The step entrainment can also lead to high entrainment rates but is less common. It depends on the layered structure of the snow cover. In step entrainment, the abrasive stresses the avalanche applies to the running layer can cause a crust layer to collapse. However, the entrainment location is no longer directly at the front. Basal erosion is the third possible mechanism but entrainment rates due to this process are low. Recently, Iverson *et al.* (2011) conducted entrainment experiments in a large 95-m-long and 2-m-wide flume in which water saturated debris flows (containing a mixture of 56% of gravel, 37% of sand and 7% mud sized grains) were discharged abruptly across a partially saturated bed. The key variable that was manipulated during the experiments was the bed sediment volumetric water content. Iverson *et al.* (2011) findings were that entrainment is accompanied by an increased flow momentum and velocity only if large positive pore pressures develop in wet bed sediments as the sediments are overridden by the flows. The increased pore pressures facilitates progressive scour of the bed, reduces basal friction and instigates positive feedback that causes flow velocity, mass and momentum to increase.

Laboratory scale experiments attempts to replicate the entrainment process in a controlled environment. The most common setup is a defined granular mass that flows over an inclined plane that is covered by an erodible layer. Flume tests and a dimensional analysis were conducted to investigate the characteristics of bed erosion by Egashira *et al.* (2001) and Papa *et al.* (2004) proposing a formula for erosion-deposition rate. They observed that bed slope is always adjusted to its equilibrium value in case of debris flows running over an erodible bed. A debris flow either erodes bed material or

leaves sediment on the bed from the body so as to form an equilibrium bed slope. The rate is a product of the depth averaged velocity of the debris flow, the sediment concentration in the non-flowing layer by volume, the bed slope and the equilibrium bed slope corresponding to sediment concentration of the debris flow body (mass density of sediment particles, the mass density of water, the depth averaged sediment concentration of debris flow by volume and the inter-particle friction angle of sediment particles). Sediment deposition takes place when the bed slope is less than the equilibrium bed slope resulting in a negative value of erosion rate. Takahashi (2001) performed flume experiments to obtain the erosion and deposition characteristics of flows. The flume bed was set to a longitudinal slope of 35°. The experimental flow compressed and eroded the bed layer. From such an experimental result a model of erosion velocity was proposed relating the thickness of the bed layer, the velocity of the avalanche and the length of the front part of the avalanche. As for the deposition velocity, an experiment was carried out setting the flume gradient to 30°. The velocity near the bed decreased at first; the slip velocity, however, was still high, and the velocity decreased gradually showing the characteristic movement of a rigid body. Therefore, it is possible to assume that the whole flow stops in a short time as soon as the velocity becomes smaller than a threshold value. This was also in agreement with the observations made by Barbolini *et al.* (2005) in their laboratory experiments. They also observed and agreed with the observations made by Sovilla *et al.* (2007) that ploughing was the main mechanism responsible for the erosion of the bed material. Abrasion at the surface of separation between the incoming flow and the erodible layer was also observed, but this mechanism was mainly responsible for the inclusion of already detached particles into the moving material. The experiments performed by Mangeney *et al.* (2010) confirm that the front zone of the flow, the inclination of the slope and the thickness of the bed layer play a key role in the erosion process. They propose a function for granular collapse deposits between the inclination angle of the plane and the friction angle of the material involved. Their findings are in accordance to the observations of Crosta *et al.* (2009) and the experiments of Rickenmann *et al.* (2003), where erosion efficiency increases as the slope increases; and where for gentler slopes the flow is insensitive to the presence of an erodible layer or can even reduce the run-out of the flow.

4.2.2 Empirical analyses

McDougall and Hungr (2005) proposed an empirical rule of erosion velocity related to the growth rate. They defined the growth rate as the bed-normal depth eroded per unit flow and unit displacement. The volume of entrained material grows with the volume of the initial mass and velocity. In this approach the growth rate is already specified and is exponential with travel length of the flow. Chen *et al.* (2006) proposed a new concept of yield rate

based on the assumption that the volume eroded is proportional to the surface area to be affected and the travelled distance of the centre of mass. A correction coefficient is applied to account for the system nonlinearity. In a similar way, Christen *et al.* (2009) defined an entrainment rate for a unit flow velocity based on the heights and densities of the different bed layers (maximum of three layers); referring to this entrainment procedure as a mass-controlled model since the entrainment rate can be controlled directly by the user. They found stress controlled procedures (i.e. velocity thresholds) to be somewhat artificial because the limit stress is arbitrarily chosen such that the measured entrainment rates are reached.

4.2.3 Numerical analyses

Some efforts have been made in the past to describe the entrainment process numerically and incorporate basal entrainment taking into account the shear stress of the erodible layer. In this research, the focus was mainly on the numerical analyses that define the process as entrainment rates and are embedded inside run-out models. Sassa (1988) proposed a model that takes into account the shearing at the bed channel induced by pore water pressure development. The pore water pressure is produced by undrained loading and if the undrained shear in the bed material is higher than the pore water pressure in the mixture a shear takes place. Therefore, a shear is dependant on the degree of saturation. De Joode and van Steijn (2003) used a similar approach based on water pore pressures development where the shear is dependent on the apparent friction angle of the bed material. One step further in this direction was done by Medina *et al.* (2008) who proposed a static and a dynamic approximation. In the static approximation the flow shear stress and the basal shear stress (based on the Mohr–Coulomb failure criterion) are calculated and the condition of equilibrium is calculated at each time step. If there is no equilibrium, the model calculates the magnitude of entrainment necessary to achieve equilibrium related to the erosion depth. This translates in a reduction of velocity because of the low quantity of momentum of the new mass. The dynamic approximation has the same principle of the flow and basal shear stress with the difference that the new mass is accelerated to the mean velocity of the flow, depending on the availability of momentum. Sovilla *et al.* (2006) following up the approach proposed by Grigorian and Ostroumov (1977) and based in her work on entrainment of snow avalanches, proposed a numerical model where the entrainment is localized at the head of the avalanche and step entrainment is not considered. The flux rate of the mass is governed by mass and momentum conservation at the avalanche front but limited by mass availability. The model volumetric entrainment rate is given by an entrainment velocity that specifies the velocity at which the snow cover height is decreasing. This velocity is related to the applied pressure of the avalanche and the resisting strength of the snow cover. In an attempt to

improve the mechanical and physical description of the process, Issler and Johannesson (2011) proposed the addition of an “entrainment force” term (equal to minus the entrainment rate times the mean flow velocity) in the momentum balance equations of the depth-averaged gravity mass flow models. They found a relationship in the idealized setting of a quasi-stationary, entraining flow of a Bingham fluid, between the acceleration of the particles, entrainment rate and the velocity profile. It allows the velocity and stress profiles to be found in terms of entrainment rate. The latter can be determined by requiring that the bed shear stress be equal to the erosion threshold of the bed material. The deposition rate is limited by the difference between internal and bed shear stresses and by the inverse of the flow velocity. Mangeney *et al.* (2007b) described a partial fluidization model that takes into account the transition among sliding–flowing (Landau theory of phase transitions). The shear stress in a partially fluidized mass is composed of a dynamic part proportional to the shear strain rate and a static part independent of the strain. The magnitude of the static shear stress is controlled by the order parameter (liquid and solid phase) and the phase transition is controlled by the dynamic stresses and flow density. A fluidized layer may then develop at the bottom of a mass flow, and the flow sinks in the erodible bed and entrains the material. The model provides insights into the static/flowing transition within the granular mass and allows reproducing qualitatively granular flows over an erodible bed when conventional depth-averaged models without entrainment fail. Iverson *et al.* (2011) stressed the importance of initial moisture content on entrainment and change in momentum and velocity of the flow. Based on measurements and mechanical considerations it was shown that entrainment of wet material results into an increase in velocity and flow momentum, while relative dry material show much less entrainment of mass and even a decrease in velocity. The main mechanism behind the scouring process is the generation of high pore pressures in the wetter material, resulting in a decrease in friction, which produces an increase in scouring of the bed surface. In their presented model, pore pressure generation plays also a critical role in the entrainment process and they estimated the evolving local forces affecting momentum change during entrainment obtaining an expression for the net normalized force per unit basal area.

The work done in the past regarding the entrainment mechanism hints that the entrainment process plays an important role in the debris flow run-out evolution that leads to a better understanding of the flow behaviour. Currently, few dynamic run-out models include entrainment rates in their calculations. These rates can be classified based on the scheme used to estimate the amount of entrained material and the approach that defines and incorporates these rates into the dynamic models as: where the rate of entrained volume is defined or controlled directly by the user (mass

controlled); and where the rate of entrained volume is estimated by the model by some particular stress limit (stress controlled). Difficulties still arise in trying to characterize the physics behind the entrainment phenomenon within dynamic models. A reason for this is that the introduction of entrainment in the models requires additional parameters, such as bed stratigraphy, bed material and substrate strength which complicate practical calculations by introducing further uncertainties (Sovilla *et al.*, 2007).

4.3 Model description

The model proposed here is based on earlier work of van Asch *et al.* (2004). It is a dynamic one dimensional debris flow model that takes into account the entrainment concept based on the generation of excess pore water pressure through undrained loading of the in-situ material. The flow is treated as a laminar one phase, incompressible continuum material. Based on the Savage–Hutter model, the flow can be simulated by numerically solving the system of depth-averaged one-dimensional governing equations composed of the mass balance, momentum conservation equation, and the friction resistance based on the constitutive Coulomb–Bingham rheological equation (Coussot, 1997). The flow is modelled by a Saint–Venant type system derived in a reference frame linked to an inclined plane (Fig. 4.1) (Begueria *et al.*, 2009). In a 1D version of this model described the mass (Eq. 4.1) and momentum (Eq. 4.2) can be described as follows:

$$\frac{\partial h}{\partial t} + c_x \frac{\partial(hu)}{\partial x} - \frac{\partial d_{sc}}{\partial t} = 0 \quad (4.1)$$

$$\frac{\partial u}{\partial t} + c_x u \frac{\partial u}{\partial x} = g \left[c_x S_x - c_x K \frac{\partial h}{\partial x} - c_x S_f - \frac{\partial u}{\partial t} \frac{\rho_s d_{sc}}{\rho h} \right] \quad (4.2)$$

where, h is the flow height (m) in the direction normal to the bed; u is the x component of the velocity ($m s^{-1}$), d_{sc} the scour depth (m) ; the coefficient $c_x = \cos \alpha_x$ is the direction cosine of the bed and α_x is the slope bed angle (degrees) , which is taken positive when it dips downward in the (positive) x -direction. $S_x = \tan \alpha_x$; K is the earth pressure coefficient and g the acceleration of gravity ($m s^{-2}$) (See Section 3.1.3).

A Coulomb-Bingham rheology model (Eq. 4.3) is applied to determine a solution to the resisting force S_f in Eq. 4.2. The model assumes a linear stress-strain rate relationship once the yield strength is exceeded. Other types of rheologies can be integrated inside the model giving the possibility to simulate other types of flows and mass movements. For the purpose of this paper and the calibration of the 2003 Faucon event (clay-shale lithology

properties from the bulk of the moving material (Sassa, 1988; McDougall and Hungr, 2005).

In the here proposed model a loading of the bed deposits is generated when the moving mass flows on top. The model calculates this applied loading of the in-situ soil (Fig. 4.1) through the changes in normal stress (Eq. 4.6) and the shear stress (Eq. 4.7) caused by the flow:

$$\Delta\sigma = \rho_{fl}gh \quad (4.6)$$

$$\Delta\tau = \rho_{fl}gh \tan\alpha \quad (4.7)$$

where, ρ_{fl} is the density of the flow material, g is the gravity force, h the height of the flow and α the angle of the slope. Because of this loading, volume reduction and an increase in pore water pressure takes place. The calculation of the increase in pore water pressure (Eq.4.8) is based on the Skempton (1954) equation that expresses pore water pressures in an undrained triaxial test and modified by Sassa (1988) for an undrained direct shear test. Assuming that the soils along the shear zone inside the channel deposits are subjected to an undrained direct shear:

$$\Delta p = B_D(\Delta\sigma + A_D\Delta\tau) \quad (4.8)$$

where, A_D and B_D are the pore pressure parameters in the direct shear state. Based on the laboratory tests of compressibility of the soils and assuming that the soils are not anisotropic, Sassa *et al.* (1985) proposed that the pore pressure parameter B_D is approximately the same with the B pore pressure parameter proposed by Skempton. B_D value is affected by the loaded stress level and its values are very sensitive to the degree of saturation. In "saturated soil" the compressibility of the soil skeleton is almost infinitely greater than that of the pore water and essentially all of a stress increment applied to a saturated soil is carried by the pore fluid; $B_D=1$. In "dry soil" the compressibility of the pore air is almost infinitely greater than the compressibility of the soil skeleton, and thus essentially all of the increment in total stress applied to the dry soil element is carried by the soil skeleton; $B_D = 0$. The transition of B_D values from a "saturated soil" to a "dry soil" is very drastic (e.g. values for a complete saturated state that ranges from 1 to 0.8 can quickly drop down to values of 0.1 or 0.2 for a slightly saturated soil). The pore pressure parameter A_D value changes with strain and probably the A_D value may increase after failure due to the crushing of grains, but dissipation of pore pressure may take place because shear zone is not as great as the compressed zone by the loaded normal stress. A value of A_D at failure can be assumed for the pore pressure parameter during motion. In

general soft, loose soils have high values of A_D and the higher the shear strain the higher the value of A_D .

It is assumed that during an intense rain event, a ground water table may be formed in the surface bed layer. When there is ground water flowing parallel to the slope pore pressure (Eq. 4.9) is calculated by:

$$p_{ini} = \rho_w g d_w \cos \alpha \quad (4.9)$$

where d_w is the height of groundwater in the in situ soil measured perpendicular to the slope

The total pore water pressure is then (Eq. 4.10):

$$p_{tot} = p_{ini} + \Delta p \quad (4.10)$$

New stresses on the bottom of the in-situ soil are then computed by (Eq. 4.11 and 4.12):

$$\sigma_{tot} = (\rho_{fl} g h + \rho_{bot} g d) \quad (4.11)$$

$$\tau_{tot} = (\rho_{fl} g h + \rho_{bot} g d) \tan \alpha \quad (4.12)$$

where, ρ_{bot} is the density of the in-situ soil and d is the depth of the erodible layer. The factor of safety on bottom (Eq. 4.13) and top (Eq. 4.14) of the in-situ soil is calculated as follows:

$$F_{bot} = \frac{c_{bot} + (\sigma_{tot} - p_{tot}) \tan \delta_{bot}}{\tau_{tot}} \quad (4.13)$$

$$F_{top} = \frac{c_{bot} + (\Delta \sigma - \Delta p) \tan \delta_{bot}}{\Delta \tau} \quad (4.14)$$

where, c_{bot} (kPa) is the cohesion and δ_{bot} the friction angle (degrees) of the in-situ soil. In the case where F_{top} and $F_{bot} < 1$ then d_{sc} which is the thickness of the failed layer equals the total thickness of the in-situ material (d). In the case where $F_{bot} < 1$ and $F_{top} > 1$ then d_{sc} is again total thickness of in-situ material (d) and in the case where $F_{bot} > 1$ and $F_{top} < 1$ we have a portion of d which will fail and it is calculated as follows (Eq. 4.15):

$$d_{sc} = \frac{1 - F_{top}}{F_{bot} - F_{top}} d \quad (4.15)$$

This computed failed mass is then incorporated to the flow enlarging its volume and changing its momentum.

High pore pressures in the presented model are generated by undrained loading and not by contraction of loose material during deformation of the bed by shearing (Iverson *et al.*, 2011). Effective rise in pore pressure by loading occurs only, according to Skempton's law, when the material is at a degree of saturation of around 80% or more (Sassa, 1988), while in loose material as presented and measured by Iverson *et al.* (2011), an effective rise in pore pressure due to compaction occurs already when the soil is about halfway saturated.

4.4 Sensitivity analysis

As presented in Chapter 3, a sensitivity analysis was carried out: 1) to recognize which input parameters contribute the most to output variability; 2) which parameters are insignificant and can be held constant; and 3) to determine the optimal range within the parameter space for use in calibration studies. In this section we concentrate specifically on the effect of entrainment and the Coulomb Bingham rheology. The analysis was performed using the Bingham rheology on a synthetic profile (Fig. 4.2) and was divided in two parts based on the model structure: 1) sensitivity to the rheological parameters; and 2) sensitivity to the in-situ soil parameters that influences the scouring. The inputs of interest identified in the rheological model were: dynamic viscosity (η), earth pressure coefficient (K) and yield strength (τ strength). The input parameters selected for the in-situ soil were: friction angle (δ_{bot}), cohesion (c'_{bot}), density of the in-situ soil (ρ_{bot}), pore pressure parameter A_D , pore pressure parameter B_D and soil depth (hsoil).

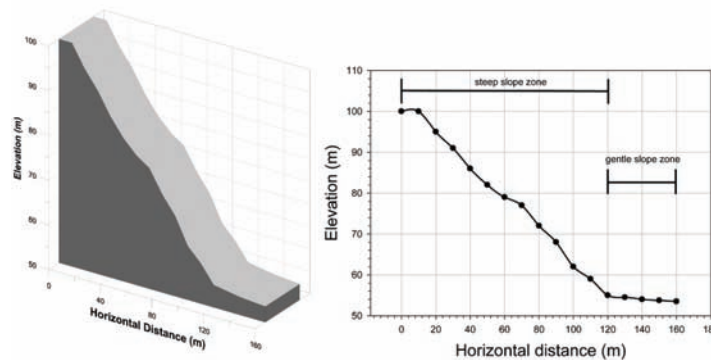


Fig. 4.2: Synthetic longitudinal profile used for the sensitivity analysis. The profile was divided into a steep slope zone and a gentle slope zone to assess the behaviour of the flow with changing topography.

All initial parameters were kept constant except the parameter chosen for the sensitivity (Table 4.1). All the inputs parameters except the pore pressure parameter B_D (in-situ soil) and the pressure parameter K (rheological model) were used with a variation of 10% from the initial simulation. For the pore

pressure parameter BD values ranging from 0 to 1 were chosen (saturation degree). The Rankine's active or passive pressure coefficient K (which depends on the velocity gradient downwards) was selected in this sensitivity analysis. The values are related to the internal friction angle, which were ranged from 1 to 0.10. The selected outputs to be measured were: 1) the velocity of the flow considered in relation with the time needed by the flow to reach the 120 m and 160 m cell (called "Time R"). These cells were selected in order to distinguish the velocity in the upper part and on the lower part of the profile; 2) the height of the flow for the cells 80 m, 100 m, 120 m, 140 m and 160 m at the time "Time R"; and 3) the mass balance measured at the "Time R".

Table 4.1: Initial parameters used in the sensitivity analysis

Debris flow material (rheology)			In situ material (soil)					
T	K	V (viscosity)	δ bot	Cbot	ρ bot	A_D	B_D	h
strength (Kpa)	pressure	(kPa/s)	($^{\circ}$)	(kPa)	(kg/m ³)			(soil) (m)
0.20	0.60	10.00	12	1	1600	0.6	0.1	0.3

The sensitivity was quantified as the percentage of change in the outputs subjected to a constant variation (percentage of change, in case of BD: degree of saturation and in case of K: degree angle) in the input parameters. It was found out that the most sensitive rheological parameter was the dynamic viscosity (η). This parameter influences significantly the run-out distance and velocity of the flow however it does not play an important role in the entrainment process. Inside the model, increasing the dynamic viscosity decelerates the flow considerably. Confirming the retarding effect on the motion of the flow, an increase of 20% in the dynamic viscosity made the flow stop completely when the flow reached the gentler slope (Figs. 4.3 and 4.4). The most sensitive in-situ soil parameters were the soil friction angle, the soil depth and the in-situ soil cohesion. They affect directly the amount of entrained material but do not have a substantial effect in the velocity of the flow. As the soil friction angle parameter increases, the entrained material by the flow in the steeper part of the slope augments until it reaches a threshold where the entrainment becomes continuous. But when the flow reaches the gentler slope, the increase of the friction angle had an opposite effect in the variation of mass (decreasing the entrained material). In contrast, the increase in the cohesion parameter enlarges the mass entrained until reaching a threshold of continuous entrainment both in the steep and gentle slope zones. The soil depth has a direct effect on the entrained material, an increment in the soil depth results in a growth of mass and entrainment (Figs. 4.3 and 4.4). This is in good agreement with the experimental observation made by Mangeney *et al.* (2010). The pore pressure parameter

BD has an influence on the variation of mass only when the in-situ soil starts to reach a complete degree of saturation of the soil with values between 0.8 and 1.

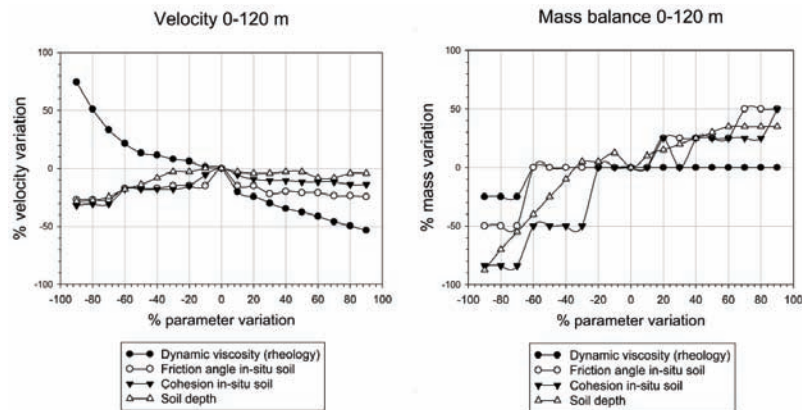


Fig. 4.3: Variation percentage of the velocity and the mass with regard to the percentage of change of the most sensitive parameters in the model during the steep slope section of the terrain path (0–120 m).

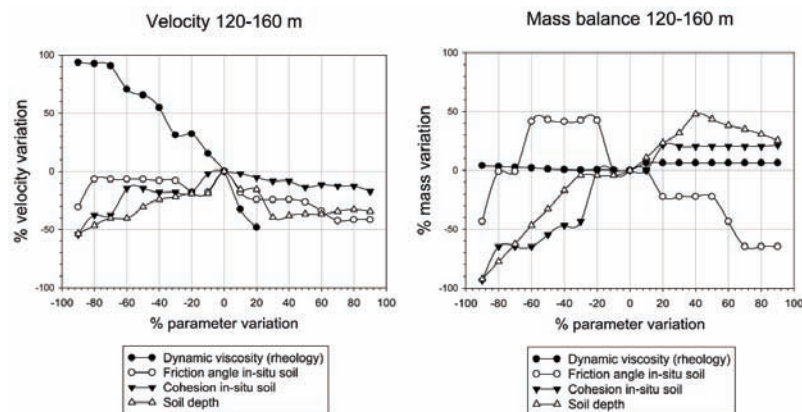


Fig. 4.4: Variation percentage of the velocity and the mass in regard to the percentage of change of the most sensitive parameters in the model during the gentler slope section of the terrain path (120–160 m).

4.5 Testing the model in the Faucon test area

The Faucon 2003 event (See Section 2.1.1) was modelled because of its significant overflowing in the alluvial fan area. Remaître *et al.* (2008) carried out a detailed post-event mapping of the erosion and deposits. His observations of the channel indicate that the scour depth ranges between 0.5 and 4 m. The channel scour rate per meter length is calculated to $15 \text{ m}^3\text{m}^{-1}$. The velocities that were back calculated ranged from 6.4 to 8.9 m/s (Remaître, 2006).

The criteria chosen to compare the simulation results with the 2003 Faucon debris flow event were flow velocity, deposit heights and run-out distance. The Faucon debris flow of 2003 has already been modelled by Remaître *et al.* (2005) with a Bingham rheology with the BING 1D code (Imran *et al.*, 2001). The parameters for the best simulation were $\tau_y = 404$ Pa and $\eta = 122$ Pa s. The event has also been modelled based on Janbu's equilibrium method to calculate the yield strength and the shear stress which are then used in a simplified 2-parameters Bingham plastic rheology (Remaître *et al.*, 2008). Other efforts to model the event in two dimensions and accounting for deposition in the fan were done by Begueria *et al.* (2009). They found that the best calibrated parameter sets were $\tau_y = 400$ Pa and $\eta = 67$ Pa s. with a Bingham rheology and $\tau_y = 200$ Pa, $\phi' = 3.8^\circ$ and $\eta = 10$ Pa s. with a Coulomb-viscous rheology. However, these attempts have not considered the dynamic entrainment process that plays an important role in the development and behaviour of the flow.

In the present study, the calibration was completed through back analysis and was based on a trial and error adjustment of the input parameters defining the flow resistance and entrainment process. The inputs were adjusted until the computed criteria patterns matched as close as possible the real event. A profile of the torrent was created and the channel width of the torrent was considered for the volume estimation. The initiation area was distributed in uniform slices of 10 m and the total released volume was 8443 m³. A Bingham rheology was used to model the event. The parameters that best fitted the 2003 Faucon event were $\tau_y = 210$ Pa and $\eta = 63$ Pa s., which matches with a 52-53% of solids concentration by volume measured for the event (Remaître *et al.*, 2008). A constant Rankine's earth pressure parameter of 1 assuming hydrostatic pressure and a density of the flow of 1850 kg.m⁻³ were used for the simulation. The in-situ soil parameters found to match the entrainment amount of the event were $\phi = 15^\circ$ and cohesion = 0.1 kPa. The density of the in-situ soil used was 1600 kg.m⁻³. The pore pressure parameter used were $A_D = 0.6$ and $B_D = 0.9$. These values correspond to an in-situ soil that has a high degree of saturation. The surface flow occurs in standard time and no air is entrapped under the water table. A homogeneous erodible in-situ soil depth of 3.5 m was found to be the value that agrees best with the quantity of entrained material by the original event. A calculation time step of 0.05 s was set up and the simulation had a time elapsed of 453.60 s. The model predicted high velocities and higher amounts of entrainment when the slope is predominantly inclined and lower velocities and entrainment when it reaches the gentler slope in the lower section of the torrent. Figure 4.5 shows the plots for maximum heights and velocities during the course of the flow. The final deposition volume is around 58338.91 m³ (553 % of increase in mass balance) with an average velocity during the whole event of 8.77 m s⁻¹.

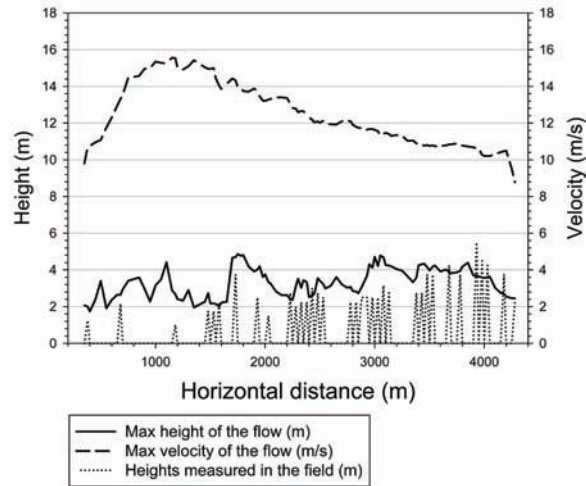


Fig. 4.5: Max velocity and max height of the flow during the flow course. The velocity distribution shows that the maximum velocity takes place when the debris is pushing down in the steepest part of the slope.

The application to the Faucon 2003 debris flow event give reasonable results in comparison to the field observations mainly based on the geometry of the deposits. Figure 4.6 shows the relation between the flow height that the model predicts and the flow heights that were observed in the field. Relative higher deposits were simulated with an average height of approximately 3.23 m an m and a maximum height of 4.95 m.

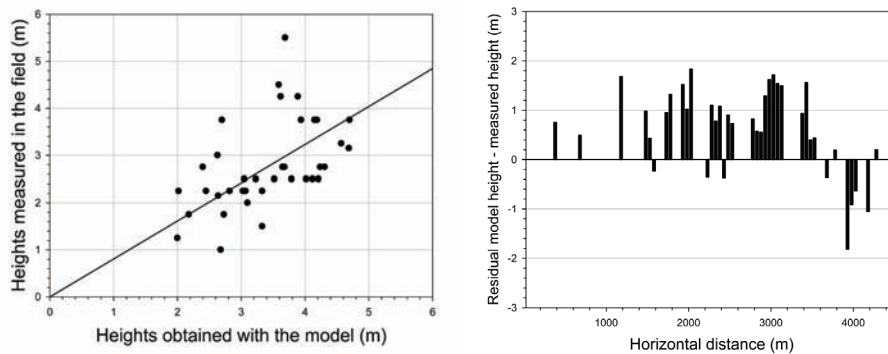


Fig. 4.6: Scatter plot between observed heights in the field and the computed heights (left). Residuals values between the simulated and observed heights (right)

The difference between the heights and velocities calculated with the model and the real event measured in the field, can be explained by the fact that other processes are involved in the entrainment processes (i.e. abrasion) and due to the application of a 1D-model to a 3D-phenomenon. Figure 4.7 shows

the distribution of the entrained volume during the course of the flow and the accumulated final volume.

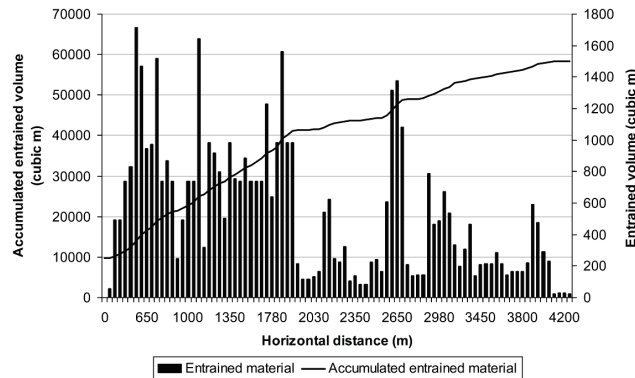


Fig. 4.7: Cumulative volumes of the deposits during the entrainment process and the entrained volume during the course of the flow.

The model calculates the stability as a factor of safety of the in-situ soil based on the normal stresses, shear strength and increase of the pore pressure caused by the rapid loading of the flow in each time step. Once the stability threshold is exceeded, the entrainment process is dominated by the amount of soil capable to erode in the in-situ soil bed and the increasing variations of pore water pressures caused by the loading. The increase of the pore water pressures is influenced by the loaded stress levels and its value changes with the degree of saturation. As a result and in accordance to the experimental results and theoretical predictions of Iverson *et al.* (2011); the in-situ soil becomes unstable and entrainment occurs (Fig. 4.8). Another important factor affecting the entrainment is the transition in the slope angle. The slope influences the variation of stresses on the in-situ soil and the behaviour of the flow during its course, explaining why entrainment is prominent on the steeper part of the track. The pore water pressures response is linked to the variation in the slope playing an important role in the entrainment process (Fig. 4.8). This is in agreement with the experimental results obtained from Mangeney *et al.* (2010) and Crosta *et al.*, (2009) where they emphasize the importance of the slope inclination angle effect on the increase or decrease of the run-out distance.

To show the effects of the entrainment process, a simulation was performed using the numerical model without entrainment. The maximum flow height along the flow path with and without entrainment is shown in Figure 4.9. Entrainment has a significant influence on the flow depths, the run-out and the maximum flow heights. By taking into account the entrainment process he calculated maximum height of the flow can increase with a factor 2 and even 3 while the length of the run-out distance is nearly doubled (Fig.

4.9). This confirms the results obtained by Sovilla *et al.* (2007). Since the entrainment scheme presented here is influenced by the flow height, the addition of entrained material that results in bigger heights has a large effect on the overall behaviour of the flow.

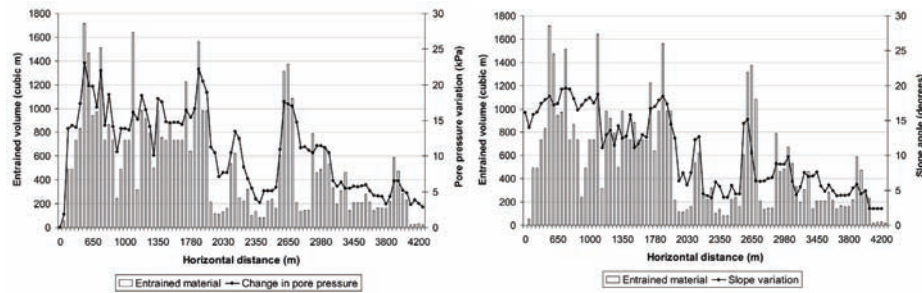


Fig. 4.8: The increase of the pore pressures produced by the undrained loading causing a rise in undrained shear in the ground which led to failure and entrainment of the in-situ soil (left). The effect of slope angle and stress variation on the amount of entrainment of the in situ soil by the flow during its course (right).

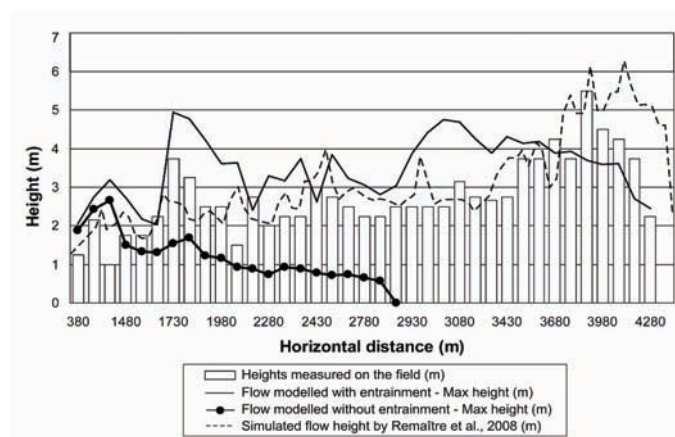


Fig. 4.9 Maximum heights along the flow path. Comparison between a simulation with and without entrainment. The modelled heights are compared with the heights measured in the field.

4.6 Discussion and conclusions

The model presented in this chapter accounts for the entrainment process based on the generation of excess pore water pressure through undrained loading of the in-situ soil. The model highlights only one physical principle of entrainment which can be dominant during an event, especially on steeper slopes, but other principles (as described before in this paper) might also be valid and may have large effects on the overall behaviour of the flow. A typical case where the model can be applied is when a soil mass has already failed because of a rainfall event (i.e. rise of groundwater table). At the same

time, a high degree of saturation exists in some parts of the in-situ soil of the torrent or the channel. The failed mass moves progressively downstream, loading the saturated in-situ soil causing it to fail and enlarging of the flow volume. Further research is needed to assess other dominant principles of entrainment under various conditions.

Based on a sensitivity test that was performed for the model, the rheological parameters and in particular the dynamic viscosity (η) influences the run-out distance and velocity but do not have a significant effect on the entrainment process. This is inherent to the static entrainment concept which was developed here, and which is based on the equilibrium condition of the in situ soil. Therefore the in-situ soil parameters such as the soil friction angle, the soil depth and cohesion affect directly the amount of entrained material. The model calculates the stability of the in-situ soil based on a safety factor which is influenced by the fluctuations of the pore pressures caused by undrained loading. Once it is reached, the entrainment process is dominated by the amount of soil capable to erode.

A back-analysis of the Faucon 2003 debris flow and calibration of the model was carried out. The model estimates reasonably the flow characteristics measured in the field (heights and velocity). The results show the advantage of including entrainment in a model because much better estimates of run-out and deposited volumes are obtained. However, a disadvantage is that no longer the resistance parameters (rheological parameters) are the only source of uncertainty but also soils depths and pore pressure parameters.

Based on the importance of the entrainment process and its outcomes, research on debris flows and rapid mass movement dynamics can no longer disregard this phenomenon. Although, the process is not completely understood, the aforementioned simple model uses measurable geotechnical parameters in an attempt to describe the bulking phenomena of a real event. The model makes an effort to improve the application of numerical models that defines the dynamic behaviour of debris flows which entrains large amounts of material. More and vast information of the process and an increase of the knowledge of the model parameters behaviour are still needed to calibrate entrainment models in order to reduce the output uncertainty.

Chapter 5: Parameterization of dynamic run-out models

5.1 Introduction

The run-out behaviour of a landslide is controlled by a complex interaction between mechanical and hydraulic properties, and solid and fluid phases; and reflects spatio-temporal trends in the effective strength and rheological properties of the material. Due to these complex interactions, the parameterization of hydrological and geomechanical factors by field and laboratory tests is not sufficient to describe the post-failure movement patterns of landslides and not all the processes can be included in detail inside the models (van Asch *et al.*, 2007). Because of the complexity and the difficulty to model all the phenomena that take place inside a flow, the use of simplified rheological models that represent the flow behaviour is a common approach. Models based on the rheological characteristics of the flow with three or less adjustable parameters have been used extensively and calibrated as precisely as possible based on back analysis of past events. The calibration of these parameters makes it possible to use the same model for different types of events in different locations. One example of this is the Voellmy model which was originally developed for snow avalanches, and which is widely used for modelling the run-out of lahars, debris flows and rock avalanches (e.g. Revellino *et al.*, 2004; McDougall, 2006; Quan Luna, 2007; Christen *et al.*, 2009). There is a large range of these rheological parameters reported in the literature, and some of them do not have a precise physical meaning which makes a forward analysis very difficult to assess. Often there is not enough information available about the range of rheological parameters for the estimation of hazard at a specific location. To indicate the uncertainty of these input parameters and thus the uncertainty of the run-out hazard analysis (which will be dealt with in Chapter 6) it might be useful to combine the scarce local information with the range in values obtained by many case studies over similar areas. Therefore, in this research an extensive literature study was carried out regarding run-out modelling publications and a database of past back-analyzed events was created in order to define the range of values used for the various parameters of the different models that has been applied. The data were used to determine Probability Density Functions (PDFs) for rheological parameters for different movement types, initiation volumes and environmental settings.

Chapter 5 is based on:

Quan Luna, B. et al. 2010. A preliminary compilation of calibrated rheological parameters used in dynamic simulations of landslide run - out. In: Mountain Risks: bringing science to society : proceedings of the Mountain Risks International Conference, Firenze, Italy, 24-26 November 2010 / ed. by J.-P. Malet, T. Glade and N. Casagli.- Strasbourg : CERIG, 2010. ISBN 2-95183317-1-5. pp. 255-260.

5.2 Parameters used in run-out modelling – a brief summary

The flow behaviour, sediment concentration and velocity during the occurrence of a debris flow event may vary in space and in time. The complexity of the flow processes and its activity are characterized by a rheological model and a numerical model of the equations of conservation of mass and momentum (discussed in Section 3.1.3). A usual assumption is that the flow behaves as a single phase mixture with representative bulk parameters. The following three different approaches are used for estimating the rheological parameters of a solid-fluid mixture:

1) *Laboratory and rheometer experiments*: Samples are collected in the field after a recent event and the rheological parameters are derived directly through laboratory tests and/or empirical laws. Such direct derivation of the rheological parameters might be the most desirable option. However, measuring for instance pore-pressure and viscosity remains extremely difficult for full-scale events and point-wise determined parameters may not be representative of the actual event. Despite this, significant work has been done regarding the use of rheometers and other laboratory equipment in order to obtain values that describe the characteristics of the flow behaviour. To mention a few examples of this approach and their methodology: Phillips and Davies (1991) designed and constructed an inverted cone-and-plate viscometer/rheometer to determine the rheological parameters of debris flow materials and clay slurries such as apparent viscosities and shear rates from two sites in New Zealand. Kaitna *et al.* (2007) used a ball rheometer to obtain values of shear stress and shear rate from fresh debris flow deposits in Eastern Switzerland. Sosio *et al.* (2007) also used a ball rheometer in order to assess the behaviour of the finer matrix of a debris flow that occurred in the Central Alps of Italy obtaining values for yield strength and viscosity. Scotto di Santolo *et al.* (2010) evaluate the behaviour of a pyroclastic-derived soil during the flow in the Campania region, Italy. Using a rotational rheometer and two rheometrical systems (parallel plates and vane rotor system) they observed the influence of solid concentration and grain size distribution obtaining a simple relation between the solid concentration and the yield stress. Boniello *et al.* (2010) analyzed deposits of a debris flow that occurred in the Northeastern part of Italy, using a rheometer equipped with a serrated parallel plate; obtaining values of viscosity and the shear dependent behaviour was examined at different concentrations. Other work using different types of rheometers are described by Major and Pierson (1992), Coussot and Piau (1995), O'Brien and Julien (1988), Contreras and Davies (2000), Schatzmann *et al.* (2003), Bisantino *et al.* (2010).

2) *Flume tests*: Physical experiments in flume tests are usually carried out because it offers the possibility to obtain direct measurements of an event resembling the actual debris flow event. Small-scale flume tests are very valuable for investigating scale independent effects but are limited by the difficulty of accounting for scaling the rheology changes and flow heterogeneity. For example, Coussot *et al.* (1996) used an inclined plane to provide an approach that describes the form of the deposits remaining after free surface flow stoppage as a function of fluid characteristics. Hubl and Steinwendtner (2000) used a belt conveyor (conveyor channel) to measure flow behaviour and rheological properties of natural debris flow material. This set-up enabled to study behaviour of viscous debris flow material with maximum grain diameters up to 20 mm. where velocities and rheological parameters (shear stresses and viscosity) were measured with varying solid concentration and slope of the channel. McDougall and Hungr (2004) tested the DAN3D model (described in Section 3.4.2) frictional rheology by analyzing a series of laboratory flume experiments with granular materials, both on straight and curved paths. Kaitna *et al.* (2007) carried out experiments in a vertically rotating flume, in order to determine rheological parameters of debris flow material mixtures containing grain sizes larger than to be measured in standard viscometers. From the measured flow parameters total boundary shear stress and corresponding shear rate of the flowing mixture were derived. De Blasio *et al.* (2011) replicated small-scale artificial debris flows in a flume with variable percentages of clay and sand, and measure separately the rheological properties of sand–clay mixtures which were used to develop modifications of an existing numerical code that uses the Bingham rheology. Parsons *et al.* (2001) carried out a series of experiments to explain the nature of the transition between fluid-mud and grain-flow behaviour. Measurements were performed with several cameras and visual tracers, while the mass flow rate was recorded using a load cell at the exit chamber. Other rheological tests were used to calculate independently the yield strength and matrix viscosity of the debris-flow mixture. Remaître *et al.* (2011) used a flume test with a combination of other approaches (rheometer and slump tests) to investigate the sedimentological and rheological properties of the debris-flow deposits (grain-size distribution, petrography, yield strength, viscosity) of the Faucon 2003 debris flow event (described in Section 2.1.1). Large-scale experiments have been conducted during the past decade at the USGS debris-flow flume (e.g., Iverson *et al.*, 1997; Iverson and Denlinger, 2001; Denlinger and Iverson, 2001, Iverson *et al.*, 2004) where the experiments provided high-resolution data that helped to constrain interpretation of field observations (e.g. rheological behaviour, entrainment). More work using flume tests that describe the behaviour of debris flows are described by Takahashi (2001), Pudasaini and Hutter, (2007), Mangeney *et al.* (2007a).

Generally, laboratory experiments are combined with mathematical modelling to calibrate rheological models. Then, the laboratory-calibrated numerical model is used to predict debris flow behaviour at field scales. Nevertheless, this extrapolation of results from laboratory experiments to field scales may lead to inaccurate predictions. A rheological model that provides good results in the laboratory, does not necessarily replicate a field event.

3) *Back calibration*: The model parameters are back-calibrated so that the model outcome fits with observations of a past-event. Observations may thereby include run-out estimated from historical records, vegetation damage and/or statistical models having as results useful estimates of velocity and impact pressures along the path and run-out zone (e.g. Chen and Lee, 2003; Malet *et al.*, 2004; Pitman and Lee, 2005; Hürlimann *et al.*, 2007; Pirulli and Sorbino, 2008). Back calibration of well-documented events is also used to evaluate the applicability and limitations of a model and to facilitate a better understanding of the relative significance of the input parameters. In general, the back analysis results show broad agreement with the field observations of signs of debris velocity (e.g. from the superelevation of the mud-lines in bends of the channel), debris thickness and travel distance, indicating that the basic physical equations of motion and relatively simple rheological models can approximate the behaviour of real landslide events in a reasonable manner (e.g. Revellino *et al.*, 2004; Remaitre *et al.*, 2005; Quan Luna, 2007; Crosta *et al.*, 2009). In a back analysis, the key parameters are varied in order to achieve a close match with the field indicators. There can be reasonable confidence in the results of the back analysis where: - the field data are comprehensive and of good quality, - the computer programs which are used provide a good match with the field data, and - the different back analyses results in similar basic rheological parameters (McDougall and Hungr, 2004; Medina *et al.*, 2008; Pirulli and Mangeney, 2008; Pastor *et al.*, 2009 ; Quan Luna *et al.*, 2011).

5.3 Database compilation and description

Models are conceptual representations of a phenomenon and are limited by the assumptions made in constructing them – as the number of assumptions increases, the accuracy and relevance of the model for exploring the phenomenon decreases. Models are also limited by the extent and quality of the input data. As a result of the involved uncertainties regarding the factors of scaling and the relative high expenses for field collection, laboratory analyses and flume tests of numerous samples; the approach based on back analyses of past-events is the most common in practice. Major variations of the back-calibration results are associated with the fitted observations and establishing probability-density functions may provide a starting point to better estimate ranges where the data situation is poor (Brunetti *et al.* 2009).

As a first step towards a stochastic analysis of ranges and uncertainties of parameters and their effects on run-out modelling, a database was compiled from past-analyzed events reported in the literature. The database includes the rheological parameters (Voellmy and Bingham rheologies) and volumes from many previously back-calibrated events that have been described by many authors. The database is presented in Appendix 1 and it includes information of 301 run-out events, characterized by the type of landslide, volume, run-out behaviour and rheological parameters derived from model back-calibration (Table 5.1).

Table 5.1 Example of a case analyzed inside the database created showing the different fields of classification.

Case	Panabaj, Guatemala (2005)
Movement type	Debris flow
Volume (m³)	65,000
Length run-out (m)	4,900
Angle of reach (°)	16.3
Max velocity (m/s)	15
Rheology	Voellmy
Apparent friction coefficient	0.04
Turbulent coefficient (m/s²)	450
Viscosity (Pa.s)	---
Yield stress (Pa)	---
Author and year	Quan Luna, 2007
Method	Back-calibration
Post-failure behaviour	Channeled
Environment	Volcanic
Source sediment	Pyroclastic material

The database was compiled from peer-reviewed literature and unpublished reports. In total 75% of the cases in the database are debris flows and landslides and 25% are rock avalanches. The Voellmy rheology is used in 169 events and 132 events use the Bingham rheology. Table 5.2 shows some examples of the references used to create the database.

In the case of the Bingham rheology, the majority of the database contained information of debris flows in mountainous environments which was gathered by Malet (2010). This is due to the fact that this type of rheology is commonly used for these types of cases. For this reason, the Bingham rheology divisions were done based only on the ranges of volumes of the events (0-50,000 m³, > 50,000). On the other hand, the Voellmy rheology (according to the information gathered) is used in different types of settings and with different types of movements. In an earlier studies, Rickenmann and Koch (1997) and Naef *et al.* (2006), compared several flow rheologies embedded in dynamic run-out models. They tested different simple rheological models, such as the Bingham fluid, a Newtonian laminar fluid, a dilatant grain shearing model, a Newtonian turbulent fluid, and a Voellmy

fluid. They found the best agreement of the observed global flow behaviour using the Voellmy fluid. Recently, the Voellmy model is one of the most common type of rheology frequently used in the dynamic models and has been used extensively and with reasonable results by Hungr (1995); Revellino *et al.* (2004); McDougall and Hungr (2005); Quan Luna (2007); Hurlimann *et al.* (2008); Pirulli and Sorbino (2008); among others. For the Voellmy model, the division of the database properties was made based on:

- ranges of volume (0-50,000 m³, > 50,000);
- - type of movement (debris flows, rock avalanches);
- - type of environment (alpine/mountainous, volcanic/tropical, glacial).

Each of the cases was analyzed according to this classification making it possible to cluster the parameters for each specific condition.

Table 5.2 Examples of the references used in the collection of the database

Type of movement	Rheology	References
Debris flows and landslides	Voellmy	Hungr and Evans, 1996; Koch, 1998; Jakob <i>et al.</i> , 2000; Hurlimann <i>et al.</i> , 2003; McArdell <i>et al.</i> , 2003; Sun <i>et al.</i> , 2003; Revellino <i>et al.</i> , 2004; Zanuttigh and Lamberti, 2004; Bertolo and Weiczorek, 2005; McDougall <i>et al.</i> , 2006; McDougall and Hungr 2006; Hurlimann <i>et al.</i> , 2006; Muir <i>et al.</i> , 2006; Cepeda, 2007; Chen and Lee, 2007; Galas <i>et al.</i> , 2007; Hungr <i>et al.</i> , 2007; Kwan and Sun, 2007; Lucas <i>et al.</i> , 2007; Pastor <i>et al.</i> , 2007; Quan Luna, 2007; Wang and Sassa, 2007; Armento <i>et al.</i> , 2008; Bertolo and Botino, 2008; Cesca, 2008; McKinnon <i>et al.</i> , 2008; Blanc, 2008; Kowalski, 2008; Medina <i>et al.</i> , 2008; Mergili, 2008; Paudel and Law, 2008; Pirulli and Sorbino, 2008; Cepeda, 2009; Kuriakose <i>et al.</i> , 2009; Hungr and McDougall, 2009.
	Bingham	Koch, 1998; Malet <i>et al.</i> , 2004; Zannutigh and Lamberti, 2007; Bertolo and Weiczorek, 2005; Remaitre <i>et al.</i> , 2005; Naef <i>et al.</i> , 2006; Cetina <i>et al.</i> , 2006; Remaitre, 2006; Haddad, 2007; Pastor <i>et al.</i> , 2007; Armento <i>et al.</i> , 2008; Bertolo and Botino, 2008, Medina <i>et al.</i> , 2008; Remaitre <i>et al.</i> , 2008; Begueria <i>et al.</i> , 2009.
Rockfalls	Voellmy	Evans, 1989; Evans <i>et al.</i> , 1994; Hungr, 1995; Hungr and Evans, 1996; Jakob <i>et al.</i> , 2000; Hungr and Evans, 2004; McDougall and Hungr, 2006; Quan Luna, 2007; Haddad, 2007; Guthrie <i>et al.</i> , 2007; Hungr <i>et al.</i> , 2007; Kwan and Sun, 2007; Pastor <i>et al.</i> , 2007, Chen and Lee, 2007, Lucas <i>et al.</i> , 2007; Galas <i>et al.</i> , 2007; Sosio <i>et al.</i> , 2007; McKinnon <i>et al.</i> , 2008; Deline, 2009; Allen <i>et al.</i> , 2009; Froese <i>et al.</i> , 2009

5.4 Design of probability density functions

Uncertainty could be the result of measurement errors, sampling errors, model uncertainty (uncertainty due to simplification of real-world processes, incorrect model structure, misuse of models, and use of inappropriate assumptions), descriptive errors, aggregation errors, errors in professional judgment and uncertainty of the variability. Variability, usually measured as standard deviation or variance, represents natural random processes. The variability for a parameter can be represented as a probability density function (PDF), also referred as a probability function, frequency function, or frequency distribution. For a continuous variable (a variable that can assume any value within some defined range) the probability density function expresses the likelihood that the value for a random sample will fall within a particular very small interval.

Within the database, the variability for a parameter was represented as a probability density function (PDF). Fig. 5.1 and 5.2 show different types of curves that were used to fit the distributions of the parameters for the Voellmy and Bingham models, using the values derived from the whole database. A curve fit of the parameters was done using different types of distributions: *normal distribution*; *a kernel distribution*, and *a Lognormal distribution*. A kernel distribution is a non-parametric way of estimating the probability density function of a random variable. The kernel density estimation is a fundamental data smoothing problem where inferences about the population are made, based on a finite data sample. In the case of the resistance parameters, a Lognormal distribution was found as the one that best fitted the data. The proper selection of the PDF's is essential for a good assessment of the uncertainties associated with the choice of rheological parameters.

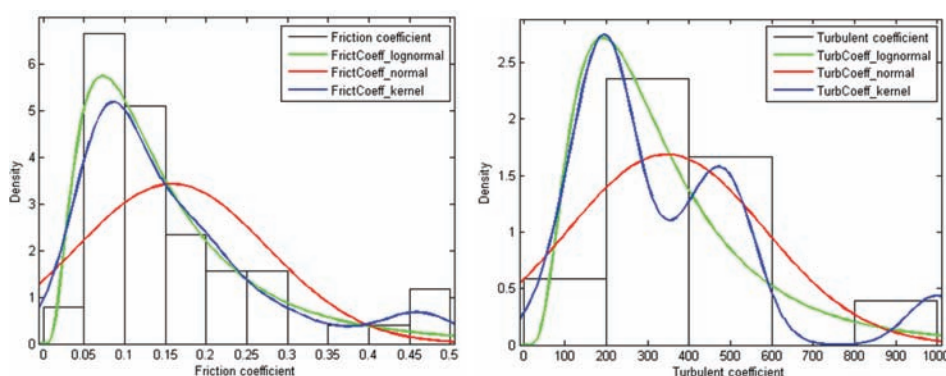


Fig. 5.1: Curves used to fit the probability density function of the apparent friction coefficient (μ) and the turbulent coefficient (ξ) (m/s^2) inside the Voellmy model.

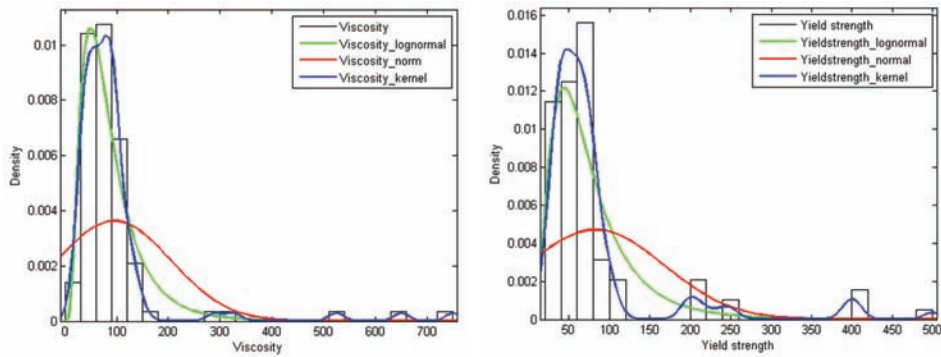


Fig. 5.2: Curves used to fit the probability density function of the viscosity (η) (Pa.s) and the yield stress (τ) (Pa) inside Bingham model.

The arithmetic and geometric moments for the Lognormal distribution of the Voellmy and Bingham rheology can be seen in Table 5.3. These values can indicate a parameter range for forward modelling using the analyzed rheologies (e.g. Chapter 7).

Table 5.3 Moments for the fitted Lognormal distributions to the resistance parameters

	Lognormal parameters		Arithmetic moments		Geometric moments	
	Mu	Sigma	Mean	Standard deviation	Mean	Standard deviation
Bingham model Viscosity	4.2882	0.6240	88.4970	61.0690	72.8378	1.8665
Bingham model Yield strength	4.1577	0.6204	77.4994	53.1063	63.9294	1.8597
Voellmy model Friction coefficient	-2.0882	0.7310	0.1618	0.1360	0.1239	2.0773
Voellmy model Turbulent coefficient	5.6486	0.6302	346.2624	241.7950	283.8959	1.8780

The database contained large discrepancies and a large range of displaced volumes of the analyzed events. Fig. 5.3 shows the distribution of run-out volumes reported in the literature for both debris flows and rock avalanches. The mass movements events in the database were categorized according to their physical characteristics and type of movement to obtain true statistical populations.

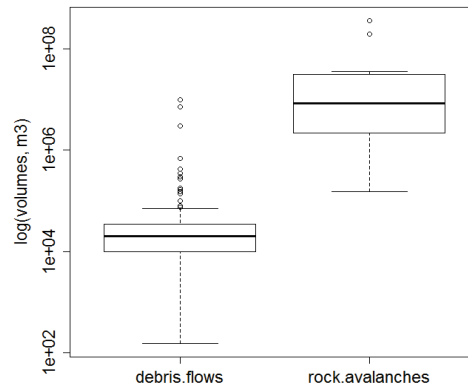


Fig. 5.3 Boxplot representation of the volumes of debris flows and rock avalanches of the events in the database. Inside the database a large range of displaced volumes was reported.

Numerous studies on the statistical properties of landslide inventories have demonstrated that the probability distribution of landslide areas and volumes can be approximated by heavily-tailed PDFs (e.g. Hovius *et al.*, 1997; Malamud *et al.*, 2004; Guzzetti *et al.*, 2002; Antiano and Gosse, 2009; Stark and Guzzetti, 2009; Brunetti *et al.*, 2010). Power law distributions of those parameters can be observed for historical inventories as well as for event-based inventories. Assuming that power-law scaling may determine the probability distribution of other physical factors in a similar fashion it was investigated if the turbulent coefficient and the friction coefficient can be approximated with heavily-tailed PDFs. Thirty three different functions including Weibul, Frechet, Levy, Pareto, Burr and Gamma and other commonly used PDFs were tested to approximate probability distributions of the coefficients. The underlying physical model constrains the coefficients to positive values and suggests sharply decreasing probabilities for very small friction values and turbulent coefficients approaching zero. All PDFs which were not fulfilling those criteria were disregarded and the remaining solution where compared according to their goodness of fit. Fig. 5.4, 5.5., 5.6 show a family of Gamma functions which consistently provided a good fit to the probability distributions. In most cases the generalized form of the gamma function demonstrated better fit than the closely related Inverse Gamma function, whereas the Inverse Gamma function can be adopted if the generalized form returns non-zero probability densities for coefficient values equal zero.

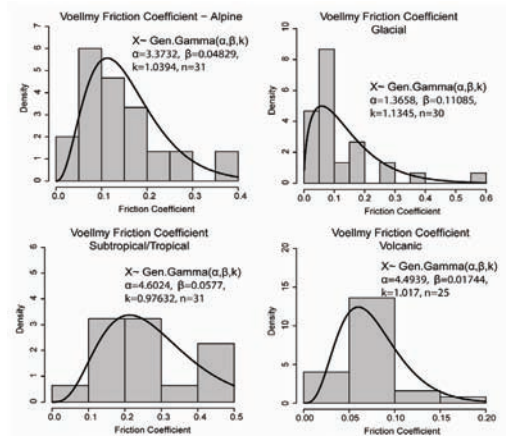


Fig 5.4: Best-fitting gamma functions for the apparent friction coefficient of events in the four environmental classes (Alpine, Glacial, Subtropical/tropical and Volcanic).

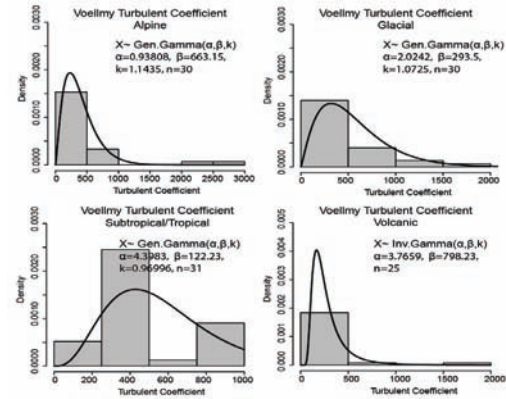


Fig 5.5: Best-fitting gamma functions for the turbulent coefficient of events in four environmental settings (Alpine, Glacial, Subtropical/tropical and Volcanic).

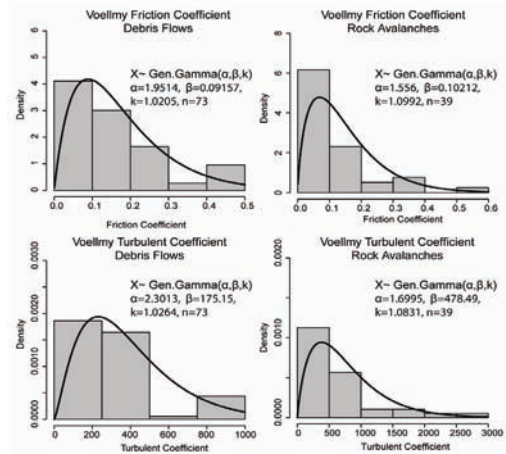


Fig. 5.6: Comparison between the best-fitting gamma functions for the turbulent coefficient and friction coefficients of debris flows and rock avalanches.

5.4.1 Coupled distribution functions

As in the previous section the distribution of single parameters was investigated, the aim of this section is to evaluate the relationships between the parameters in the Voellmy and Bingham models, in order to see whether they are independent and be fitted in coupled distribution functions. The relationships between the parameters of the the Voellmy and Bingham rheologies were plotted (Fig. 5.7) and after analyzing several options a “Gaussian Copula” was determined to be the best choice to define the probability density function for both rheological models.

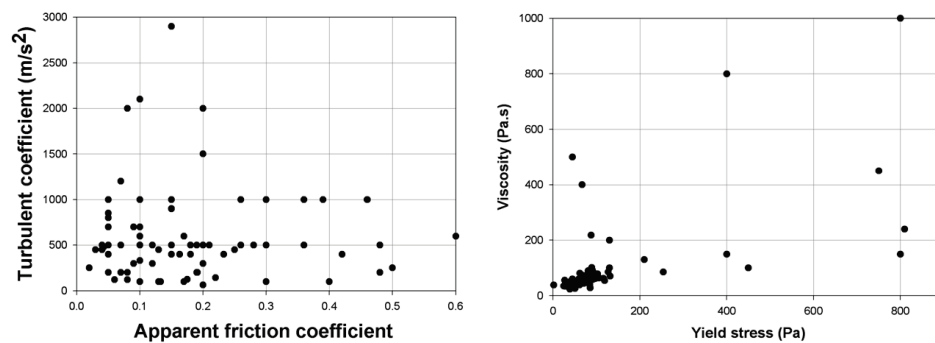


Fig. 5.7 Data dispersion between the Voellmy model parameters: turbulent coefficient (ξ) and friction coefficient (μ) (right). Data dispersion between the Bingham model parameters: viscosity (η) and yield stress (τ) (left).

The Gaussian copula provides a way to create distributions to model correlated multivariate data. A bivariate copula is simply a probability distribution of two random variables, each of whose marginal distributions is uniform. These two variables may be completely independent, deterministically related, or anything in between.

As an example probability density distributions were generated for debris flows based on the range of volume from 0-50,000 m³ in an alpine/mountainous environment. The results are presented in Fig. 5.8 and 5.9. This characterization includes also uncertainties related to the extension procedure between different sites.

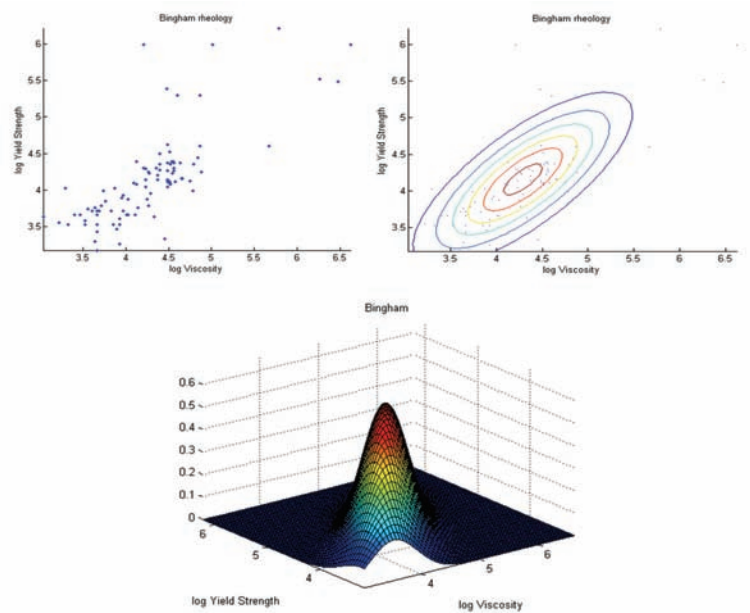


Fig 5.8: Fitted “Gaussian copula” distribution function to the Bingham rheology parameters using data from well documented and back calibrated events from the database presented in this chapter. Dispersion of the data in the x and y axis (top left). “Gaussian copula” fitted distribution in two dimensions (top right). Three dimension view of the fitted distribution (bottom)

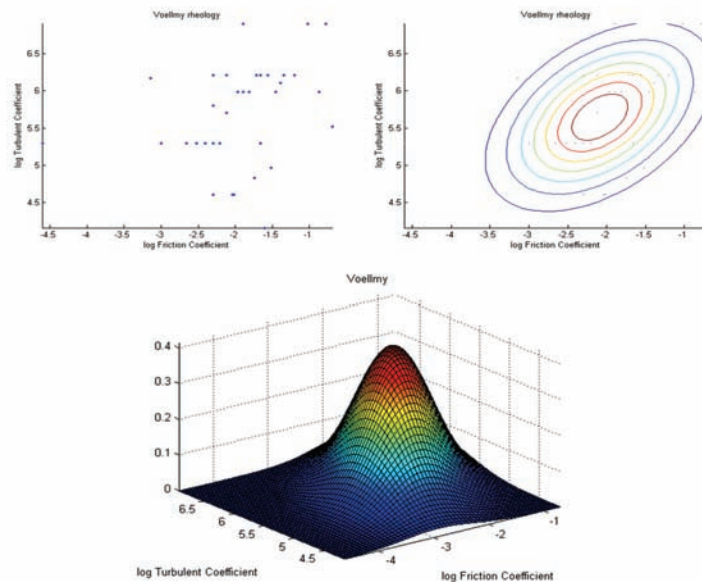


Fig 5.9: Fitted “Gaussian copula” distribution function to the Voellmy rheology parameters. Data dispersion in the x and y axis (top left). “Gaussian copula” fitted distribution in two dimensions (top right). Three dimension view of the fitted distribution (bottom).

The resulting probability density functions obtained are used as an input for a probabilistic methodology where the uncertainties in the unit base resistances (rheological parameters) inside the dynamic models can be addressed (See Chapter 6). Defining the statistical distributions (PDFs) that will be used for the model's input parameters is probably the most important aspect of a stochastic analysis.

5.5 Discussion and conclusions

One of the main objectives of this research is to have the possibility to perform a forward modelling of hazard scenarios. This can be approached by having enough and detailed information of past events that have been back analyzed with run-out analyses of modelled past events. Forward modelling uses the same technique on an event that has yet to occur, trying to estimate the hazard extent and intensity. In the past, forward modelling needed experts investing significant time to constrain model parameters through back analyzing similar historical events. For this reason, a characterization that can hint a parameter space and its uncertainties is a step forward, not only for an experienced modeller but for any user.

Although some efforts have been done in the past via laboratory analysis and flume tests, the rheological resistance parameters used in dynamic run-out models can not be directly related to well define physical processes and their measurement is very dubious. For this reason the estimation of these parameters is done most of the time empirically based. It is not possible to determine all these parameters, and a run-out hazard assessment must therefore be based on "conceptual" physical models and expert judgment. Inevitably, the resulting hazard estimates are subject to large uncertainties. To ensure a rational approach, it is essential that these uncertainties are explicitly addressed by the models within a single framework to ensure consistency. The alternative and most common procedure is to perform a back calibration of the model on the basis of suitably recorded historical events which requires an extensive amount of reliable information. The above mentioned problems may be solved by collecting a database of back calibrated events that allowed to express the resistance coefficients for a given range of volume, type of movement and environment in terms of a proper probability distribution function. This may help in assessing the confidence of the dynamic run-out model outputs such as the distribution of deposits in the run-out area, velocities and impact pressures.

It is not possible to provide guidelines to determine the specific parameter ranges for different types of mass movements. The only possibility is to provide a realistic range of parameters given probable conditions for a future event, in the case where insufficient information is available to obtain the range of values from back calibration. Once a landslide is categorized by its

physical characteristics, the presented probability functions can be used for forward modelling by using the recommended rheologies and parameters with statistically justified expectations.

The proposed functions in this chapter are highly dependent on the accuracy of the reported observations and the information collected in the database. No attempt was made to verify or reinterpret reported observations; minor errors are presumably compensated for by the large quantity of landslides analyzed. Some subsets of events are underrepresented in the analyzed sample although this may be rectified in future research. One of the drawbacks regarding the information contained in the database is that the back calibration methods and procedures are not fully known, and neither their accuracy. In most of the cases, each practitioner individually back analyzed historic events using different approaches (qualitative or quantitative manner) to select the best fit rheologies and parameters without having a standard selection criterion regarding the modelling outputs. Another drawback is that different types of models with different types of solutions were used to simulate the past events. An additional point to consider is that neither the quality and resolution of the terrain profiles are known nor the topography and the quality of the input data (e.g. release areas, soil depths). This might lead to different outcomes in the parameterization of the same event which is back analyzed by two different practitioners.

However, the recommended functions of the resistance parameters can also provide a context for the resistance parameters arrangement and can contribute to the fine tuning of the usual iterative process for parameter selection in the construction of a more detailed back analysis. Besides this, the creation of a probability density function is a first step for a stochastic approach to be implemented for dynamic run-out models in order to assess hazard and risk at a specific locality.

Chapter 6: Application of a Monte Carlo method to debris flow run-out modeling

6.1 Introduction

Dynamic run-out models are able to simulate the distribution of the material, and its intensity, which allows defining the exposure and vulnerability of the elements at risk, and are therefore essential tools to evaluate quantitatively the hazard and risk at a specific site. Another advantage of the application of dynamic models is that they can simulate the effect of variations in the release volume as well as friction coefficients for different scenarios including ones that have no historical evidences.

Usually, outputs of a model characterized as single values of intensities are used to describe a run-out analysis (i.e. depth in meters, velocities in m/s) implying that the determined values is an adequate representation of an event. However, these models are based on rheological parameters which cannot be measured directly. As a consequence, these models are associated with large uncertainties, which must be addressed in risk assessments. In practice, deciding which value or range of input values that can best describe an event turns out to be a cumbersome and arduous task. This can be added to the assumptions done by the individual user who is modelling the process. The lack of consistency obliges to re-analyze each event by a new modeller because of the personal differences in techniques and judgment. An example of this, can be illustrated by well known events that has been modelled several times (e.g.. the Frank Slide by Pastor *et al.*, 2007; Galas *et al.*, 2007; Lucas *et al.*, 2007; Hungr *et al.*, 2007) with different parameters (in some cases even the same rheological model has been applied).

Chapter 6 is based on:

Quan Luna, B., et al., 2011. Analysis and uncertainty quantification of dynamic run - out model parameters for landslides. Proceedings of the Second World Landslide Forum, 3-9 October 2011, Rome, Italy. 4 p.

Quan Luna, B., et al., 2011. A Monte Carlo method for debris flow run-out modeling (under preparation)

In practice, a substantial degree of uncertainty still characterizes the definition of the deterministic model parameters. This is due to the lack of experimental data and the poor knowledge of the mechanical behaviour of the moving flows. Consequently all models, either those widely used in practical applications or those more recently developed, are based on simplified theoretical descriptions of mass motion which tries to capture the complex rheology of the flow phenomenon. This results in a generalization of all models to attempt to reproduce the general features of the failed mass motion through the use of parameters (restricted to friction coefficients) which account for aspects not explicitly described or oversimplified. The outcome is that the model parameters cannot be related to a specific physical process, and therefore directly measured, but need to be calibrated. At the moment, a relatively complete and well-established calibration for most of the run-out models is still lacking or not enough reliable to be applied in practical applications. This represents one of the basic limitations with the use of dynamic run-out models, since they turns out to be remarkably sensitive to the frictional coefficients (Revellino *et al.*, 2004; Hurlimann *et al.*, 2007; Hungr and McDougall, 2009). Inherent uncertainties in models input-data specification are well acknowledge but usually not explicitly incorporated into the analysis and considered mapping results. They are normally addressed through conservative estimate of parameters, or in some cases, by a sensitivity analysis. However, each of these approaches has limitation in assessing the statistical implication of uncertainties, and may lead to conservative, impractical and dangerously underestimations of actual hazard levels.

In order to analyze the effect of the uncertainty of input parameters a probabilistic framework based on a Monte Carlo simulation for run-out modelling is considered a useful approach. Monte Carlo analysis is a method that uses statistical sampling techniques to derive the probabilities of possible solutions for mathematical equations or models. Monte Carlo analysis was initially developed in the 1940's and it has been applied to all sorts of problems dealing with the uncertainty of data and models (Metropolis and Ulam, 1949; Metropolis, 2007).

The application of stochastic techniques for run-out modelling has received quite some attention in the area of snow avalanches, as there are more options to observe, measure and describe them (natural or artificial triggered). A good example is the work carried out by Gauer *et al.* (2009) who describe the measurements and observations of dry-snow avalanches at the Ryggfonn test-site (Norway) with respect to their behaviour in the run-out area. The measurements of front velocities and retarding accelerations were used to create probability distributions. Those distributions were used in Monte-Carlo simulations with a run-out model to supplement measurements

of the run-out distances and to evaluate the effectiveness of a catching dam in the run-out area. Other relevant examples of the application of Monte Carlo analysis for snow avalanche run-out modelling are presented by Ancey *et al.* (2004) and Bozhinskiy (2004). Meunier and Ancey (2004) used a dynamic numerical model and fitted the model parameters (friction coefficients and the volume of snow involved in the avalanches) to field measurement data. Then, using those parameters as random variables, they adjusted appropriate statistical distributions and simulated a large number of (fictitious) avalanches using the Monte Carlo approach. The cumulative distribution function of the run-out distance was computed over a much broader range than was initially possible with the historical data. Ancey (2005) performed a Monte Carlo calibration of avalanches described as Coulomb fluid flows. A Bayesian inference technique was applied to specify the model uncertainty relative to data uncertainty and to solve the inverse problem. Barbolini *et al.* (2004) estimated snow avalanche hazard by means of a Monte Carlo procedure involving a regional statistical analysis to evaluate the PDF of the avalanche release depth and the simulation of the avalanche propagation by means of a dynamic, 1D mathematical model. They also took into account the uncertainty in the choice of rheological parameters of this model by assigning their PDF estimated on the basis of a regional analysis. In this way, they estimated the PDF of the avalanche impact pressure in each point of the computational domain and computed the specific risk.

Monte Carlo simulations for landslide and debris flow run-out modelling have been carried out by Revellino *et al.* (2004). They back calibrated the run-out of 17 debris flows that occurred in the Campania region of Italy. Using a Voellmy model embedded in the DAN model (Hungar, 1995), they found that after the back calibration, that the flow resistance parameters varied within a relatively narrow range. A histogram of the friction angles coefficient used for their analyses was created and an approximate normal distribution fit was superimposed. Calvo and Savi (2008) applied a Monte Carlo procedure for debris flow hazard assessment that randomly selected the input variables of the FLO-2D software to model the triggering, propagation and stoppage of debris flows. They used a Monte Carlo approach in which a stochastic model of rainfall was used to generate synthetic input series to the FLO-2D model. The magnitude–frequency relationship was then estimated from the derived synthetic output series. They estimated the probability density function of the output variables characterizing the intensity of a debris flow (i.e. impact forces) at a point of the alluvial fan.

The framework presented in this chapter is based on a dynamic model, which is combined with an explicit representation of the different parameter uncertainties. The probability distributions of these parameters were

determined from the analyzed database described in Chapter 5. The uncertainty in these inputs can be simulated and used to quantify the probability of run-out distances and intensities. In a Monte Carlo procedure the input parameters of the numerical model are randomly selected. Many model runs are performed using the randomly generated input values. This allows estimating the probability of the output variables characterizing the intensity of debris flows (for instance depth, velocities and impact pressures) at any point along the path. To demonstrate the implementation of this method, the MassMov2D model was used (See Section 3.4.1 for a description of the model). The main goal with this proposed methodology is to present a framework to obtain potentially expected run-out extents and intensities of debris flows in areas where it is not possible to determine the rheological parameters on the basis of back-analysis. In many situations past events have not been well documented, and information is lacking on the exact distribution of the debris flow. Even if this is available it is also difficult to reconstruct information on the released volume, and the height and velocity distribution of the debris flow materials.

6.2 Methodology

One of the reasons to use a Monte Carlo analysis is to examine the effect of uncertainty regarding the variability of the rheological parameters on the estimation of debris flow run-out. This statistical sampling-analysis method allows evaluating the probability distribution of the relevant parameters (intensity parameters) for a hazards assessment once the proper probability distributions for the friction coefficients have been defined. By this way it is possible to account explicitly and objectively for uncertainties in the model inputs definition and in the mapping results. To conduct probabilistic modelling using Monte Carlo analysis each of the input parameters is assigned a distribution. The output from the model is calculated many times, randomly selecting a new value from the probability distributions for each of the input parameters each time. The outputs from each run of the model are saved and a probability distribution for the output values is generated. This allows the probability of the occurrence of any particular value or range of values for the output to be calculated. Figure 6.1 presents a representation of how Monte Carlo analysis is conducted.

The shape of the probability distribution can greatly affect the outcome of the Monte Carlo analysis and it is extremely important that an appropriate distribution is selected. It should be mentioned that a Monte Carlo analysis does not require PDFs for all input parameters. In multiple-parameter models where there is no basis for assigning a PDF to particular parameters, it is acceptable to keep a fixed value for those parameters while assigning PDFs to parameters where sufficient information is available. In this study, the released volume is considered to be independent from the frictional

coefficient terms and was taken constant. The reason for this was that when analyzing the database, similar released volumes in different setting conditions produced significantly different flow dynamics and behaviour (run-out and intensities). Another reason for this is that the variation in volumes is defined by a specific return period which is beyond the scope of this study. The uncertainty resulting from the physical process that is difficult to describe (variability inherent to the phenomenon) is expressed inside the probability density functions of the frictional parameters.

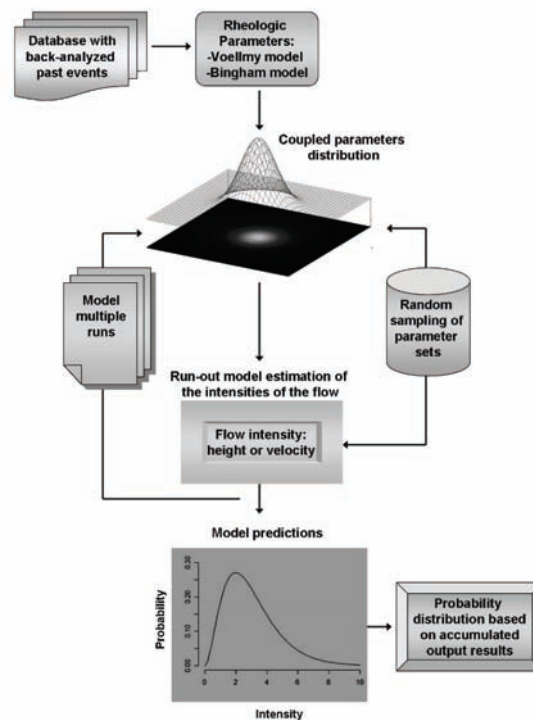


Fig. 6.1: Flow chart of the application of a Monte Carlo method for a hazard assessment

The Monte Carlo method involves deliberate use of random numbers in a calculation that has the structure of a stochastic process. Monte Carlo works by using random numbers to sample the “solution space” of the problem to be solved. In our case, we sample randomly with a “random number generator” each distribution (Voellmy and Bingham rheologies) with a number of 5000 values. Once the PDFs of the input parameters have been defined and used to generate random sets of parameters, a routine was used to repeatedly run the run-out model as many times as the generated sets (5000 times). After each run of the model was completed, the output values were saved for specific points on the accumulation area. After all the simulations were completed, the frequency of particular output values at

these points was analyzed. The resulting set of output values was evaluated to determine descriptive statistics such as the mean, range, standard deviation, etc. In addition, the probability that the outcome will exceed a particular value or will fall within a certain range of values was calculated.

The dynamic run-out model MassMov2D (Begueria *et al.*, 2009) was selected because it allows the use of scripts which can be modified to include output reports in forms of maps or text files. A batch file was built-in and incorporated inside MassMov2D which selects the randomly generated numbers of the PDFs to produce continuous multiple runs. The results of each simulation regarding the maximum flow depth and maximum velocity at each control point were reported in a text file form (to be statistically analyzed with MATLAB).

In this study, we selected two locations described in Chapter 2 to apply the Monte Carlo method (The Faucon catchment in Barcelonnette and The Tresenda Village in Valtellina). In each location two points (which can represent an element at risk) were selected on the accumulation area to represent the maximum flow height and the maximum velocity at each location. In each of the points 5000 values for flow height and velocity were statistically analyzed. Two different rheological models were applied to two different locations (the Bingham model to Faucon and the Voellmy model to Tresenda) in order to take into account the characteristics of the flow and the flow behaviour displayed in the past.

6.3 Results

6.3.1 The Faucon catchment in the Barcelonnette Basin

A description of the Faucon catchment, located in the Barcelonnette area in the French Alps, was presented in Chapter 2. Extensive work on debris flow run-out modelling in this area has been done by Remaitre *et al.* (2005). The release volume chosen in the Faucon study was 50,000 m³ and was used as constant inside the simulation. As explained in Chapter 5, several classes were selected for the release volume in order to represent the PDFs. The value of 50.000 m³ was used as a margin between the first two classes. Past events in the Faucon area have had smaller volumes (6,500 – 10,000 m³) and entrainment has increased the final volume around 6 - 7 times as compared to the initial release volume (55,000 m³ – 80,000 m³). In the collected database, all the examples include the parameterization of the rheological coefficients no entrainment was modelled dynamically or included inside the modelling. However, the mobility caused and altered by the entrainment process is already considered and taken into account inside the rheological parameters when performing the calibration. As mentioned

before, the frictional parameters inside the models are more conceptual than physical; this leads to a generalization of back calibrating the parameters of past events including the entrainment process without even modelling it. Then, the calibrated parameters inside the database have been fine tuned in order to make the modelled flow match the real event which has been influenced by the entrainment and other processes. In the Faucon case, the main purpose of the study was to observe the behaviour of the frictional parameters that includes the entrainment process and if this is a valid conceptualization. Past events in the Faucon catchment have recurrently a channelized behaviour; based on this, the two control points chosen to measure the flow intensities were included inside the channel. This two control points were used in the same location to measure the sensitivity of the RAMMS model in Chapter 3 (Fig.6.2).

The values of the simulation that were kept constant were:

- Gravity acceleration of 9.8 m/s^2 ;
- Unit weight of debris flow of 19 kN/m^3 ;
- Release volume: 50.000 m^3

The flow was assumed to be hydrostatic. The time step was set at 1 s and the total duration of each simulation was 500 s. The Monte Carlo method applied in the Faucon catchment was modelled with the Bingham model. This model was selected because of the geo-environmental setting of the area where past events are described to have a viscoplastic behaviour (Remaitre *et al.*, 2006). In the past, other authors have modelled the run-out in Faucon using the same rheology (Malet *et al.*, 2004; Remaitre *et al.*, 2005; Begueria *et al.*, 2009).

An amount of 5,000 runs were completed and the input parameters used were taken from the random sampling of the Gaussian copula fitted to the Bingham data. For each of the 5,000 runs, the maximum flow heights and maximum velocities were reported for each of the two points. The results of each point were used to populate a probability density function of each intensity parameters. A Gamma distribution was the distribution that best fitted the maximum flow height measured in Point A (Fig. 6.3). The distribution mean is: 5.31 m with a variance of 11.79 and a Log likelihood of -12,142. The estimate for the shape parameter is 2.39 and a standard error of 0.045 and the estimate for the scale parameter is 2.21 with a standard error of 0.046. The percentage of model runs that did not reach the point A was 2.82 %.

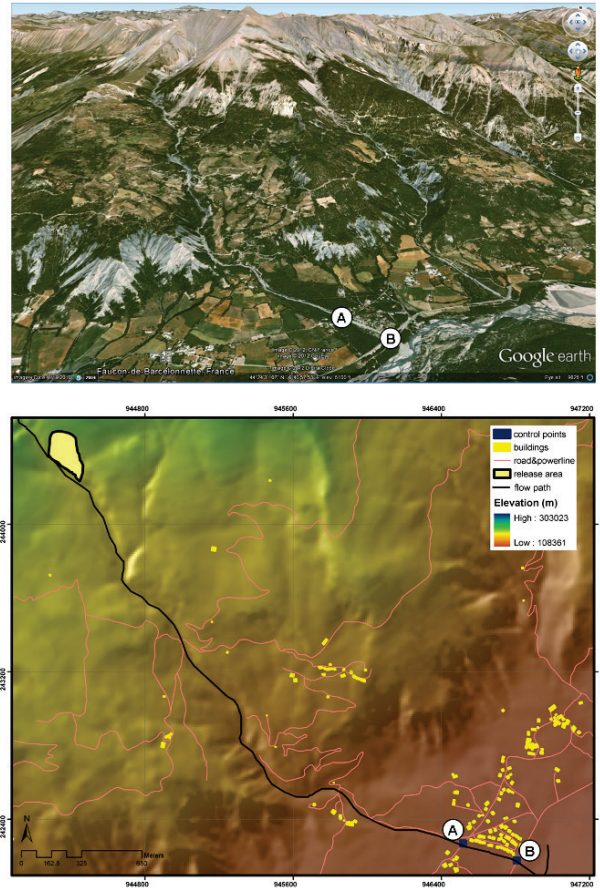


Fig. 6.2: Google map image of the Faucon catchment with the location of the two points used for reporting the results (A and B) (top). Digital elevation model used for the simulation showing the location of the release area and the two control points used for obtaining maximum flow heights and maximum velocities (bottom).

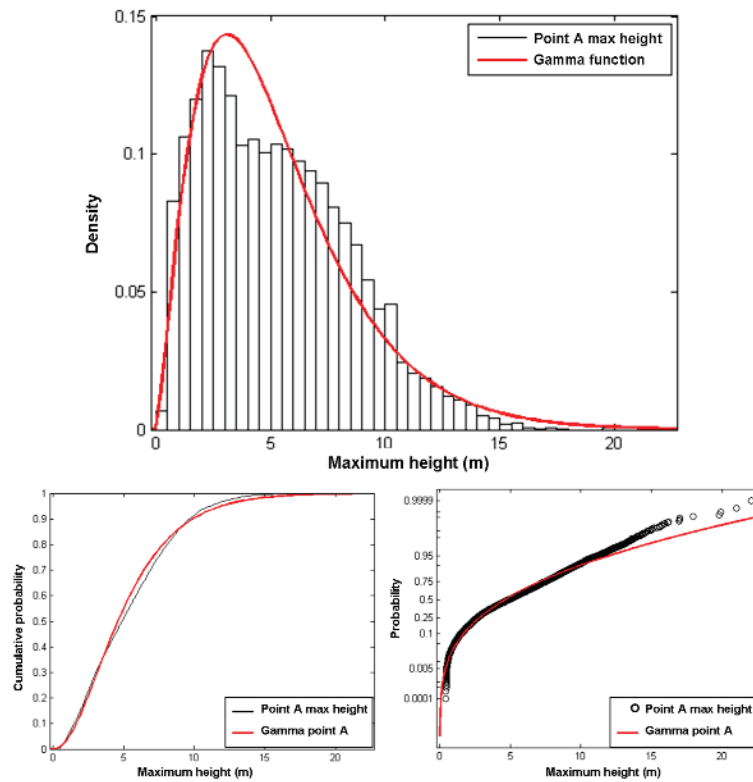


Fig. 6.3: Gamma distribution fitted to the maximum height values reported in point A (top). Cumulative probability plot (bottom left) and Q-Q plot (bottom right) of the Gamma distribution as a function of the maximum depth.

The maximum flow velocity measured in Point A was also fitted best with a Gamma distribution (Fig. 6.4). The distribution mean is: 11.75 m/s with a variance of 48.11 and a Log likelihood of -15,693. The estimate for the shape parameter is 2.86 and a standard error of 0.055 and the estimate for the scale parameter is 4.09 with a standard error of 0.086.

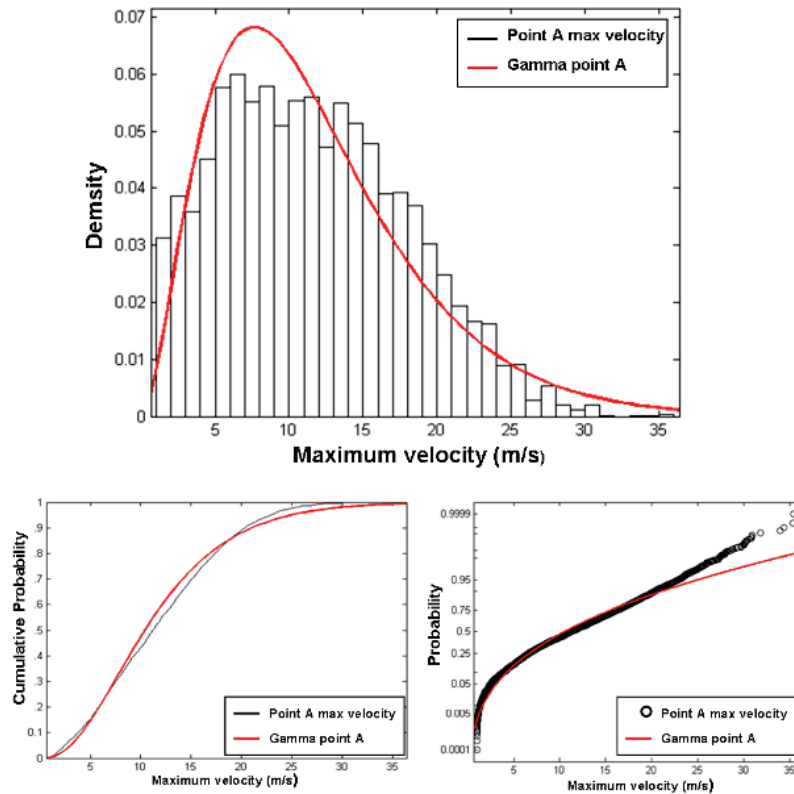


Fig. 6.4: Gamma distribution fitted to the maximum velocity values reported in point A (top). Cumulative probability plot (bottom left) and Q-Q plot (bottom right) of the Gamma distribution as a function of the maximum velocity.

The results for point B are shown in Fig 6.5 (height) and Fig 6.6 (velocity). The distribution mean of the height is: 4.74 m with a variance of 8.23 and a Log likelihood of -11,345. The estimate for the shape parameter is 2.73 and a standard error of 0.052 and the estimate for the scale parameter is 1.73 with a standard error of 0.036. The percentage of model runs that did not reach the point B was 3.02 %.

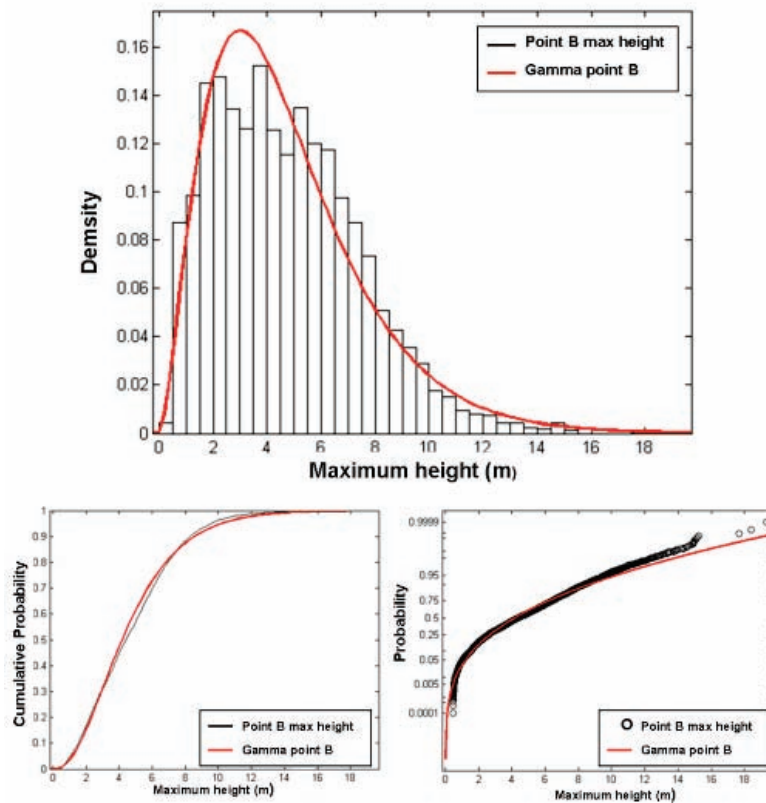


Fig. 6.5: Gamma distribution fitted to the maximum height values reported in point B (top). Cumulative probability plot (bottom left) and Q-Q plot (bottom right) of the Gamma distribution as a function of the maximum height.

The distribution mean of flow velocity at point b is: 9.20 m/s with a variance of 25.21 and a Log likelihood of -14,191. The estimate for the shape parameter is 3.36 and a standard error of 0.065 and the estimate for the scale parameter is 2.73 with a standard error of 0.057.

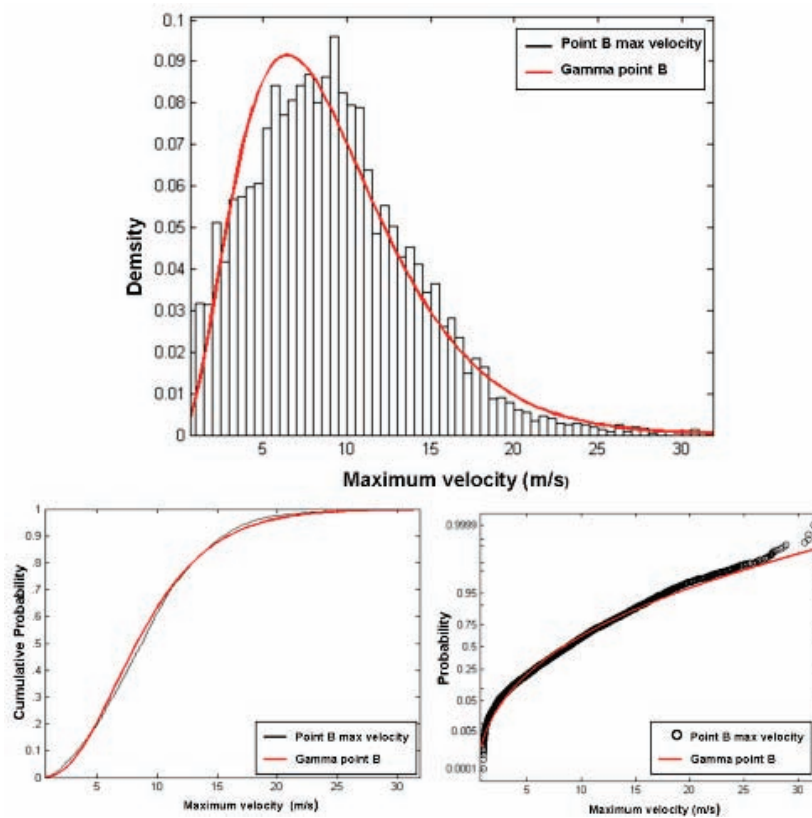


Fig. 6.6 Gamma distribution fitted to the maximum velocity values reported in point B (top). Cumulative probability plot (bottom left) and Q-Q plot (bottom right) of the Gamma distribution as a function of the maximum velocities.

The obtained results of the mean values of height and velocity computed with the Monte Carlo method were compared with the events that took place in 1996 and 2003 (Remaitre *et al.*, 2003; Remaitre *et al.*, 2005). In both cases, the model overestimates the flow height and the flow velocities (Table 6.1). In the modelling results, Point A which is located higher up in the catchment than Point B (apex of the fan) displays higher values in terms of both intensity factors (height and velocity). Based on the computed results with the Monte Carlo approach, the probabilities of the 1996 and 2003 events in terms of intensity factors with a volume of 50,000 m³ were obtained and reported in Table 6.1.

Table 6.1 Summary of the results of the Monte Carlo simulation for the Faucon test site and comparison with values observed or inferred from the last two historical debris flow events.

	Point A	Point B
Mean debris flow maximum height obtained with the model (m)	5.31	4.74
Debris height observed in 1996 event (only reported at one point) (m)	No value reported	4.6
Debris height observed in 2003 event (m)	3.9	2.6
Probability of debris height of the 1996 event	----	0.53
Probability of debris height of the 2003 event	0.42	0.31
Mean max velocity obtained with the model (m/s)	11.75	9.20
Velocity observed in 1996 event (only reported at one point) (m/s)	No value reported	4.9 – 5.1
Velocity observed in 2003 events (m/s)	7.8	6.4
Probability of velocity of the 1996 events	----	0.27
Probability of velocity of the 2003 event	0.40	0.39

6.3.2 Tresenda village in the Valtellina Valley

The Monte Carlo method was also applied in the Tresenda village in the Valtellina Valley (See Section 2.2 for a description of this study site). In the Tresenda case, the main purpose of the study was to observe the response of the model when using more than one release area. In the Tresenda case three simultaneous release areas with different volumes were considered (Table 6.2). Another aim of applying this method in Tresenda was to observe the response to flow convergence from two different failed masses. Based on the past events in the area that had a similar behaviour, the converging flows from different release areas make this an interesting scenario to analyze.

Table 6.2: Release volume used for the Monte Carlo simulation for the three different release areas in the Tresenda village

	Release Volume (m³)
Release area 1	1424
Release area 2	1410
Release area 3	1518
Total released volume	4352

The initiation of the debris flow is caused by soil slips and the flows are unchanneled in a large part of their path. For this reason and because of the flow converging, two reporting points were selected to analyze the flow intensities. One point was selected at the convergence point and the other where there is only one flow travelling down slope (Fig. 6.7). The same values were used for the gravity acceleration and the unit weight of debris flow as in the case of Faucon. Regarding the internal friction angle, the flow was

assumed to be hydrostatic. The time steps for each simulation used were 500 s. The Voellmy model was used in the run-out analysis in order to apply this methodology in this rheology.

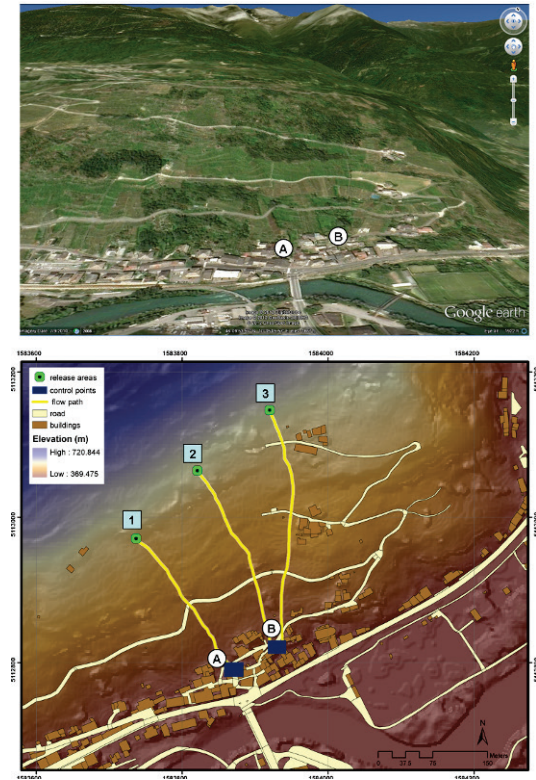


Fig. 6.7: Google map image of the Tresenda village with the location of the two points (A and B) for which the results for the run-out modelling are presented (top). Digital elevation model used for the simulation showing the location of the three release areas and the two points used for obtaining maximum flow heights and maximum velocities (bottom).

An amount of 5,000 runs were completed and the input parameters used were taken from the random sampling of the Gaussian copula fitted to the Voellmy data. For each of the 5,000 runs, the maximum flow heights and maximum velocities were reported for each point. The results of each point were used to populate a probability density function of each intensity parameters. Also here a gamma distribution had the best fit regarding the obtained data.

Fig. 6.8 shows the results for the maximum flow height measured in Point A. The distribution mean is: 4.73 m with a variance of 6.56 and a Log likelihood of -10,913. The estimate for the shape parameter is 3.41 and a standard error of 0.066 and the estimate for the scale parameter is 1.38 with a

standard error of 0.029. The percentage of model runs that did not reach the point A was 3.22 %.

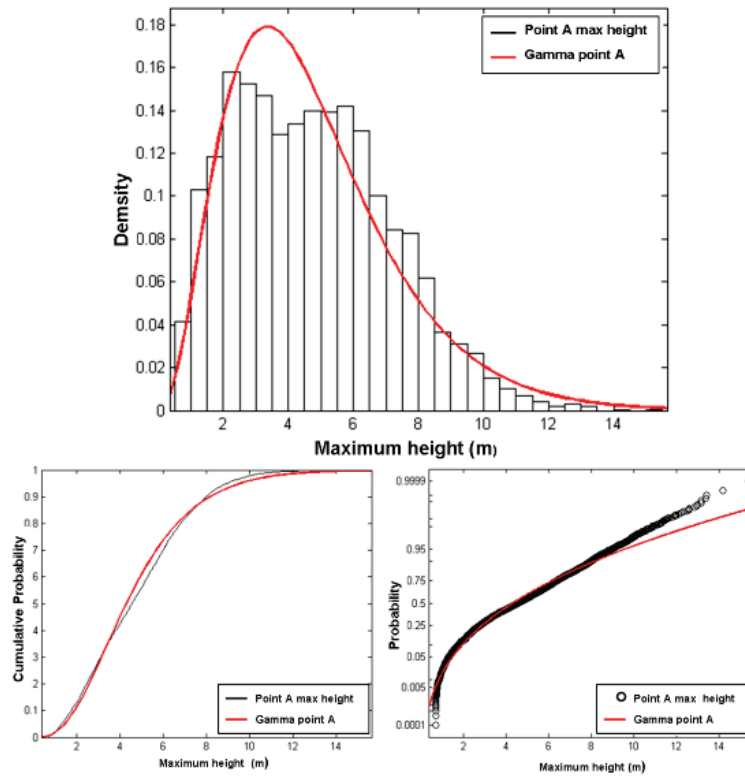


Fig. 6.8: Gamma distribution fitted to the maximum height values reported in point A (top). Cumulative probability plot (bottom left) and Q-Q plot (bottom right) of the Gamma distribution as a function of the maximum depth.

The results for the flow velocity measured in Point A are shown in Fig. 6.9. The distribution mean is: 7.74 m/s with a variance of 19.65 and a Log likelihood of -13,501. The estimate for the shape parameter is 3.05 and a standard error of 0.058 and the estimate for the scale parameter is 2.53 with a standard error of 0.053.

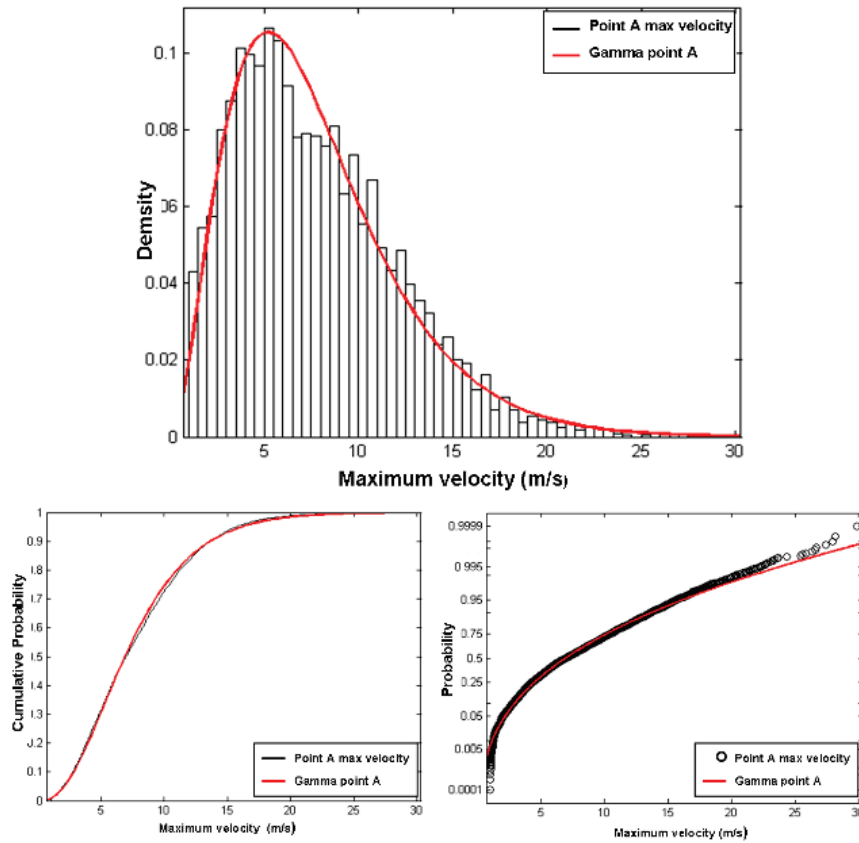


Fig. 6.9 Gamma distribution fitted to the maximum velocity values reported in point A (top). Cumulative probability plot (bottom left) and Q-Q plot (bottom right) of the Gamma distribution as a function of the maximum velocity.

The results for the maximum flow height measured in Point B are shown in Fig. 6.10. The distribution mean is: 4.11 m with a variance of 4.60 and a Log likelihood of -10,226. The estimate for the shape parameter is 3.68 and a standard error of 0.071 and the estimate for the scale parameter is 1.11 with a standard error of 0.023. The percentage of model runs that did not reach the point B was 1.94 %.

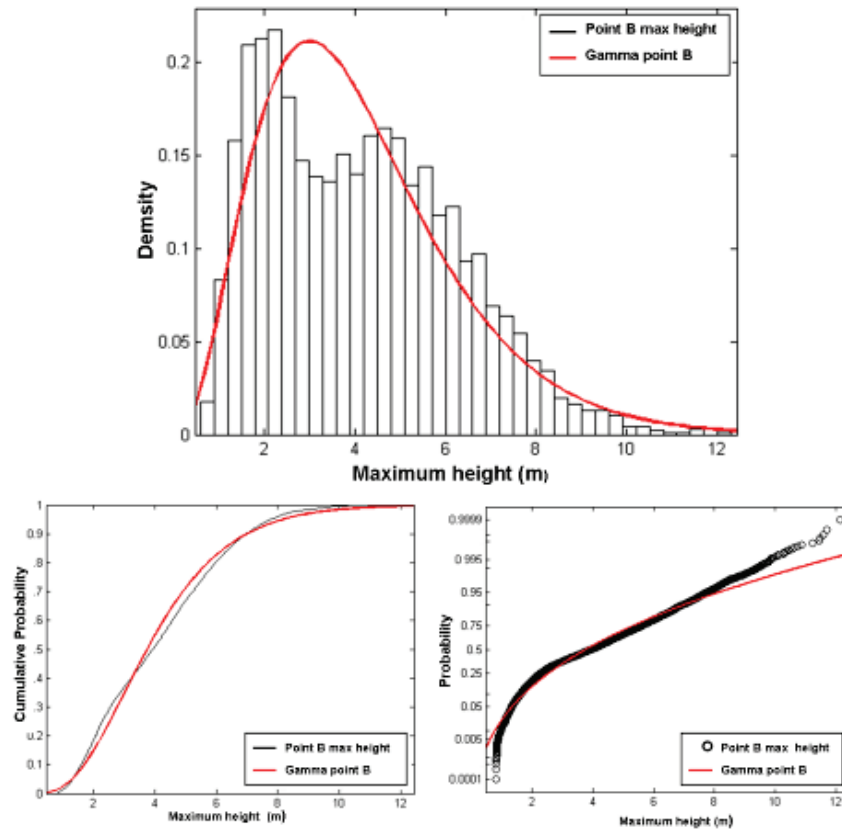


Fig. 6.10: Gamma distribution fitted to the maximum height values reported in point B (top). Cumulative probability plot (bottom left) and Q-Q plot (bottom right) of the Gamma distribution as a function of the maximum height.

Finally the results of the maximum flow velocity measured in Point B are shown in Fig. 6.11. The distribution mean is: 9.40 m/s with a variance of 27.21 and a Log likelihood of -14,516. The estimate for the shape parameter is 3.24 and a standard error of 0.062 and the estimate for the scale parameter is 2.89 with a standard error of 0.060.

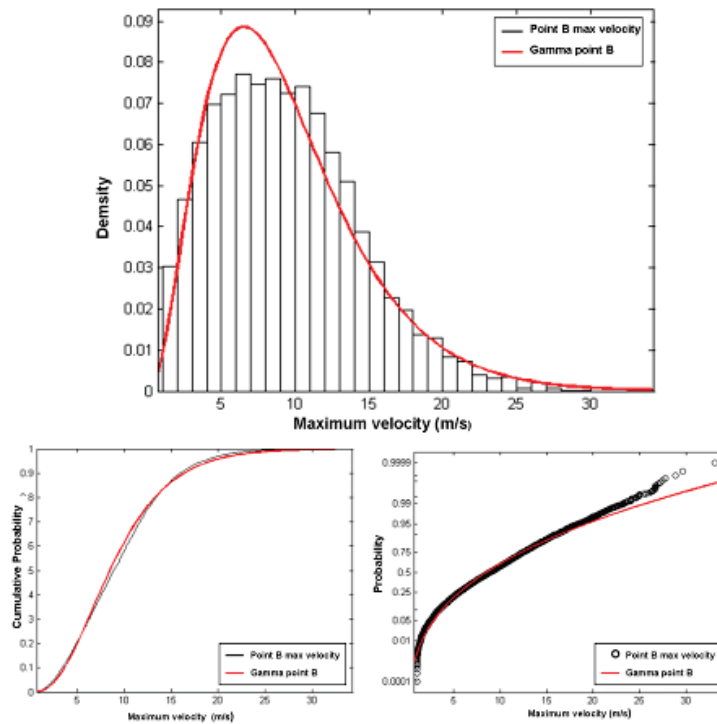


Fig. 6.11 Gamma distribution fitted to the maximum velocity values reported in point B (top). Cumulative probability plot (bottom left) and Q-Q plot (bottom right) of the Gamma distribution as a function of the maximum velocities.

The results for the Tresenda case study are summarized in Table 6.3. The mean values obtained of the maximum height and velocity probability density function were compared with the event of 1983 and 2002 (Table 6.3). In these events, only information regarding the flow heights was available (no velocities are reported for these events). In the Tresenda case, the mean value of the flow height in Point A is overestimated compared to the real event while Point B has a lower mean value than the observed event. In the Tresenda case the values are closer to the real events than in the Faucon case. This can be possibly attributed to the potential of the Voellmy rheology to model consistently these types of events. The probability of a flow with a release volume of $4,352 \text{ m}^3$ and the same behavioural characteristics reaching the point A and B with the same intensity values of the 1983 and 2002 events was computed and reported in Table 6.3.

Table 6.3 Summary of the results of the Monte Carlo simulation for the Tresenda test site and comparison with values observed or inferred from historical debris flow events.

	Point A	Point B
Mean debris flow maximum height obtained with the model (m)	4.73	4.11
Max debris height observed in 1983 event (only reported at one point) (m)	No reported value	4.50 m
Max debris height observed in 2002 event (only reported at one point) (m)	3.75	No reported value
Probability of debris height 1983 event	---	0.67
Probability of debris height 2002 event	0.39	
Mean max velocity obtained with the model (m/s)	7.74	9.40

6.4 Discussion

The main objective of this chapter was to perform a Monte Carlo simulation for debris flow modelling, using ranges of rheological parameters that are taken from debris flow past events from the literature. In both study cases there have been historical debris flows and the results of the Monte Carlo simulations were compared with the reported values of these events. When comparing the results, a tendency was observed of the Monte Carlo results to moderately overestimate the maximum flow height and velocity. This can be contributed to:

- The application to a specific location of possible unlikely combinations of rheological factors resulting from the sampling of the probability density functions;
- The large diversity of debris flow events that have been reported in literature with a variety of specific characteristics. Even though selection criteria were used for debris flow events with a given volume and occurring in an Alpine region, there is still a very large variation in the rheological parameters, related to large differences in material compositions, flow behaviour and type of failure (erosive or failed mass);
- The released volume used was kept constant and chosen subjectively while the spatial location was determined based on past events in the site. A Monte Carlo approach to determine the factors of safety, the release volumes and the spatial location is recommended for future work.
- The entrainment and other types of processes that take place once the flow is moving downslope were considered to be included inside the probability functions by other authors. However, these processes can be very event specific in terms of the flow behaviour, sediment availability and the type mechanism.
- Local factors not taken into account in the database but might influence directly the flow like type of material (geological setting), the geomorphologic characteristics and the topography of the terrain. .

The results in this study were presented for two single points along the debris flow track, because the objective of this research was to measure the probability of impact of an element at risk in a specific location by a debris flow with a specific height and velocity. This was achieved by computing PDFs of maximum heights and velocities for two selected points. The goal of this methodology is that the results (in terms of intensity) can be linked directly to vulnerability curves which are usually very specific for the element at risk characteristics. Nevertheless, another way to display the results of the application of a Monte Carlo method for a run-out assessment is by generating intensity maps. These maps should be created with the results of the PDFs at each point of the flow track and the deposition zone, having as an output a confidence probability map for the intensity factors. This was not done in this study because it was too computationally intensive. It implicated the creation of 5000 maps of flow height and 500 maps of flow velocity. For each pixel the 5000 values for each of the two factor should then be sampled, a PDF generated and the probability for given intensities calculated. However, the creation of confidence maps and the spatial display of the presented Monte Carlo method are highly recommended for future work.

In the analysis presented in this research only the effect of the variability of the rheological parameters was considered. The uncertainty of the release volume has not been taken into account. A special attention should be given to the selection and establishment of release areas and their volume. The application of a Monte Carlo approach in order to assess the probability of failure in terms of release volumes is recommended for future analysis. This assessment should include the temporal aspect in terms of return periods and the spatial aspect in terms of the susceptibility of failure. If this can be achieved, the results can be linked to the presented study (in this chapter) and will allow having a full analysis of initiation probability coupled with run-out probability.

One important consideration in this type of very computationally intensive modelling, is the minimum number of models runs that would still allow us to be able to represent the resulting debris flow intensities in an acceptable manner. The number of samples in the Monte Carlo simulation should be selected such that a balance is attained between the computational expenses and the convergence in the parameters of the probability distribution. The computational expense can be measured in terms of duration of computations. In order to obtain an approximation to the minimum number of simulations to reach convergence, the following procedure was followed:

- The output of the 5000 simulations was randomly sampled 4951 times in order to obtain subsets having 50, 51, ..., 5000 samples (i.e., increasing each subset with 1 sample).

- Each one of the 4951 subsets was fitted to a gamma distribution and the corresponding mean and standard deviation were calculated.
- In every subset, the mean and standard deviation for each output parameter (maximum velocity and maximum depth) were plotted against the number of samples.
- In the previous plots, the minimum number of simulations to reach convergence in the variance can be visually estimated as the minimum abscissa above which the dispersion appears to be constant and independent of the number of samples. The results of the above procedure are shown in Figures 6.12 and 6.13. The red lines are trend lines, which yield a horizontal slope in all plots.

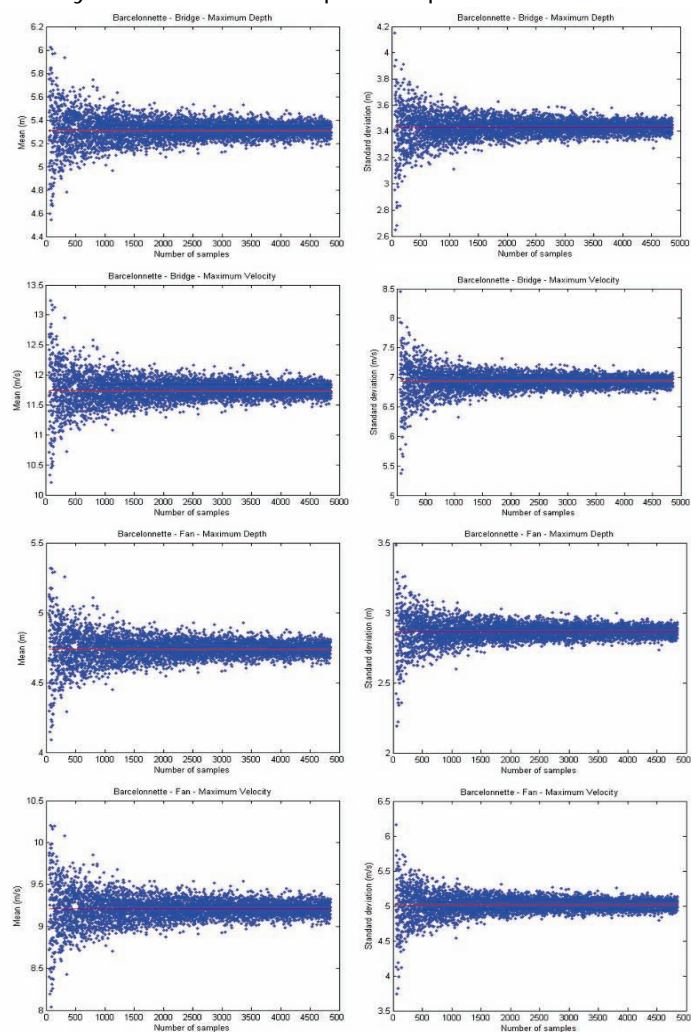


Fig. 6.12: Mean and standard deviation vs. number of samples for the randomly sampled subsets for the Point A –Bridge (top four figures) and Point B- Fan (bottom four figures) in the Barcelonnette test site.

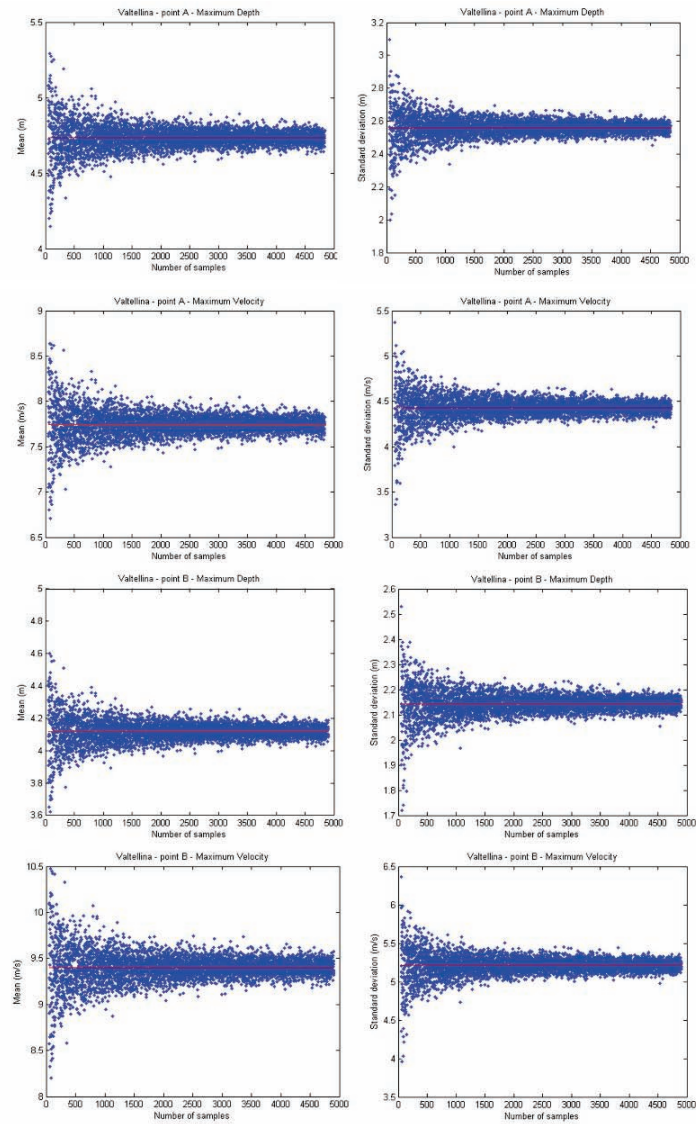


Fig. 6.13: Mean and standard deviation vs. number of samples for the randomly sampled subsets for the Point A (top four figures) and Point B (bottom four figures) in the Valtellina test site.

An examination of Figure 6.12 and 6.13 indicates that the minimum number of samples to assure an accurate estimation of results is approximately in the range of 2000-2500 simulations.

6.5 Conclusions

In this chapter, the uncertainty in the inputs parameters inside the rheological models was simulated and used to estimate the probability of

certain run-out intensities. As a result, velocities and flow heights and hence the impact pressure can be calculated at any point along the path with a degree of probability. In this study a method was applied to compute the variation in run-out intensities of debris flows by using a dynamics run-out model (MassMov2D) and a Monte Carlo simulation. This methodology has been exemplified by using two study sites: the Faucon catchment in the Barcelonnette Basin and the Tresenda Village in the Valtellina Valley using both the Bingham and Voellmy rheologies. In the application of the Monte Carlo method, 5,000 values were randomly sampled from the input probability distributions that fitted a Gaussian copula distribution. Each set of samples was an iteration of the model, and the resulting outcome from the samples was recorded. The result was a Gamma probability distribution of possible intensities in the selected control points.

The Monte Carlo method provides a number of advantages over deterministic analyses; one of them is the potential to obtain the results in a probabilistic manner (how likely each outcome is) and that different probable scenarios can be analyzed. However, one of the limitations regarding the use of the Monte Carlo method is that the generated probability density functions for the friction parameters are highly dependent on the accuracy of back analyzed events by other authors. These uncertainties are presumably compensated for by the large quantity of events analyzed. Another limitation of this study is that the estimated probabilities are basically spatial and not temporal.

It is recommended in the future, that it should be a common practice to apply the run-out models with stochastic approaches in order to produce adequate future hazard scenarios and reduce the uncertainty in the process. This will result in more accurate hazard maps while making the outcomes of run-out modelling more accessible to end users.

Chapter 7: A dynamic run-out model for medium scale hazard analysis

7.1 Introduction

Landslides and debris flow hazard assessments require a scale-dependent analysis in order to mitigate damage and other negative consequences at the respective scales of occurrence (Glade, 2005). Medium or large scale landslide run-out modelling for many possible landslide initiation areas has been a difficult task in the past. This arises from the difficulty to precisely define the location and volume of the released mass and from the inability of the run-out models to compute the displacement with a large amount of individual initiation areas (computational exhaustive). In the past, several methods have been applied for the regional assessment of the susceptibility of landslides and debris flows. At such scales the initiation areas are normally determined with statistical or simple deterministic models. These result in susceptibility zones which can be characterized according to records of past landslide events. Most of the existing physically based run-out models have difficulties in handling such situations. Therefore empirical methods have been used as a practical mean to predict landslides mobility at a medium scale (1:10,000 to 1:50,000). They are the most widely used techniques to estimate the maximum run-out distance and affected zones not only locally but also regionally (Castellanos, 2008). In 2005, Glade *et al.*, made a comprehensive review of spatial hazard investigations where debris flows have been investigated at catchment, regional and national scales. Such investigations have been focused on general inventories of spatial debris flow occurrence or on distributions following distinct triggering events.

Chapter 7 is based on:

van Westen, C.J., **Quan Luna, B.**, Vargas Franco, R.D., Malet, J.-P., Jaboyedoff, M., Horton, P., Kappes, M., 2010. Development of training materials on the use of geo - information for multi - hazard risk assessment in a mountainous environment. In: Mountain risks: bringing science to society : proceedings of the Mountain Risks International Conference, Firenze, Italy, 24-26 November 2010 / ed. by J.-P. Malet, T. Glade and N. Casagli. - Strasbourg : CERG, 2010. ISBN 2-95183317-1-5. pp. 469-475.

van Asch, Th.W.J., Daehne, A., Spickermann, A., Travelletti, J., Remaitre, A., Malet, J.-P., **Quan Luna, B.**, 2010. A comparison of two run - out models and a preliminary evaluation of their potentials for regional hazard and risk assessment. In: Mountain risks : bringing science to society : proceedings of the Mountain Risks International Conference, Firenze, Italy, 24-26 November 2010 / ed. by J.-P. Malet, T. Glade and N. Casagli. - Strasbourg: CERG, 2010. ISBN 2-95183317-1-5. pp. 129-133.

7.1.1 Brief summary of regional run-out modelling and past work

Medium scale analysis which include scales in the range from 1:10 000 to 1:50 000 can provide an initial overview of the hazard in a specific area. The goal of a medium scale analysis is to identify all the potentially unstable areas as accurate as possible and the down-slope regions probably affected by the flow. This analysis should be used as a first assessment for the potential impact zones and to give an indication where further local studies should be carried out with more detail (van Westen *et al.*, 2006). The past work can be divided by: - *methods using empirical approaches*, - *methods using flow routing models*; and - *method using dynamic run-out models*.

Methods using empirical approaches: In the past, several efforts to model rapid mass movements and debris flows in mountainous environment at medium scale has been carried out successfully despite the differences between the approaches used. Miller and Burnett in 2008, analyzed the regional susceptibility of debris flow using low resolution digital elevation and land-cover data (10-m DEMs and 25-m satellite imagery) and an empirical model to determine flow paths. They calculated empirical probabilities for debris-flow run-out over DEM-determined flow paths and show how these probabilities can be combined over all sources to estimate the potential for debris-flow delivery to stream reaches throughout entire channel networks. The model was calibrated and model predictions were compared to field-mapped debris-flow travel paths from study sites in the Coast Range of Oregon, USA. Their model predicts debris-flow probability over channel-reach scales that can be aggregated to basin-scale measures of debris-flow potential. Strimbu (2011) presented a travel distance model for debris flows based on information collected in southeast British Columbia, Canada. The model incorporates a variable that represents terrain morphology by a single number. The terrain morphology was defined by a site-specific character, providing a process-based representation of local conditions. A multiple regression analysis was used to assess the dependency of even travel distance on terrain morphology, slope, stand height, terrain curvature and canopy closure. Following a similar approach, Tang *et al.* (2011) proposed an empirical regression model for preliminary estimates of the maximum run-out length and lateral width of debris flow on fans for the Wenchuan earthquake-affected region (12 May 2008). From a rainfall triggering event on September 24th of 2008, 46 debris-flow catchments with well-defined debris-flow deposits on alluvial fans were selected for the analysis. . To determine the variables needed for the prediction of debris flow run-out characteristics on alluvial fans, a multiple regression analysis was used to establish a statistical model for the prediction of the characteristics of debris-flow run-out zones. Their model was able to estimate debris-flow run-out zones from easily

measurable topographic parameters and the availability of loose sediments in the drainage basin. From the terrain parameters used for the prediction of the characteristics of debris flow run-out zones, the volume of removable sediment was the most important factor for establishing an applicable prediction model. Conway *et al.* (2010) used iso-maps and associated field observations, to found a relationship between ground slope and patterns in deposition volume in the Westfjords of Iceland. They used their finding as a basis for an empirical model that enables to make an estimate of the total travel distance and final thickness of future debris flows. Toyos *et al.* (2007), based on the debris flow events that occurred in May 1998 in the area of Sarno, Southern Italy, presented an approach to simulate debris flow maximum run-out. Flow mobility ratios (H/L) were derived from the x,y,z coordinates of the lower-most limit of the source areas (i.e. apex of the alluvial fan) and the distal limit of the flows. They performed a regression analyses that showed a correlation between the estimated flow volumes and mobility ratios. As mentioned before, for its simplicity, statistical and empirical models are often the preferred and a well established approach when trying to assess the hazard at a medium scale (e.g. Liu *et al.*, 2002; Castellanos, 2008).

The disadvantage of using these types of empirical methods is the requirement of comprehensive and relevant datasets with the identification of both source points and end points (geometrical characteristics). Another drawback of these methods is that they are not able to provide an estimate of the flow velocities or pressures, which is important in any type of quantitative risk assessment. Besides this, if the data is taken from one single triggering event (e.g. heavy rainstorms, high magnitude earthquake) in a specific area, they are usually not representative for other areas (Tang *et al.*, 2011). Hürlimann *et al.* in 2008, points out that there are several potential shortcomings when using empirical models for a risk assessment:

- They do not take into account the specific catchment characteristics that may influence dynamic behavior of the flow (e.g. topography);
- The correct selection of the future flow trajectory on the fan may be difficult to determine;
- Finding a location for the initiation point in a longitudinal profile is a cumbersome task if no other information is available;
- There is a lack of the intensity information which can only be determined indirectly, requiring additional use of other empirical relationships.

Methods using flow routing models: To avoid the shortcomings of the empirical models in terms of dimensions simplicity and in order to take the terrain topography into consideration, two dimensional routing models (- *single flow direction models*, which direct flow from a starting cell to one of the eight neighboring cells based on slope gradient; and - *multiple flow*

direction models, where the flow can invade several neighboring cells) have been developed and used in regional studies in the past. Scheidl and Rickenmann (2010) proposed a new method to predict the run-out of debris flows which was determined with a data base of documented sediment-transporting events in torrent catchments of Austria, Switzerland and northern Italy. They evaluated an empirical approach by correlating the planimetric deposition area with the event volume, and compared it with results from other studies. They introduce a new empirical relation to determine the mobility coefficient as a function of geomorphologic catchment parameters (reflecting some of the flow properties during the depositional part of an event). The empirical equations are implemented in a GIS-based simulation program and combined with a simple flow routing algorithm, to determine the potential run-out area covered by debris flow deposits. For a given volume and starting point of the deposits, a Monte-Carlo technique is used to produce flow paths that simulate the spreading effect of a debris flow. The run-out zone is delineated by confining the simulated potential spreading area in the down slope direction with the empirically determined planimetric deposition area. The debris flow volume is then distributed over the predicted area according to the calculated outflow probability of each cell. Scheidel and Rickenmann (2010) results confirm the semi-empirical relationship between planimetric deposition area and event volume, first proposed by Iverson *et al.* (1998) and applied in subsequent studies as the LAHARZ model. The LAHARZ software was developed by the United States Geological Survey (Schilling, 1998). LAHARZ is a GIS code and is based on a semi-empirical model proposed by Iverson *et al.* (1998), which delineates lahars inundation hazard zones on a Digital Elevation Model (DEM). The program uses two semi-empirical equations calibrated by statistical analysis of the cross-sectional area inundated and the planimetric area inundated by a lahar measured for 27 lahars deposits located at 9 volcanoes in the USA, Mexico, Colombia, Canada and Philippines (Iverson *et al.*, 1998). Using also flow routing algorithms, Huggel *et al.* (2003) proposed a modeling approach for a first-order assessment of hazards from glacier-lake outbursts for two lake outburst events in the southern Swiss Alps. Flow routing routines were used to simulate the debris flow resulting from the lake outburst. A multiple and a single flow direction approach were applied and the propagation was given in probability related values indicating the hazard potential of a certain location. The debris flow run-out distance was calculated on the basis of empirical data on an average slope trajectory.

One of the most recent efforts to embark upon a delineation of debris flows susceptibility maps in two dimensions for a medium scale is the software Flow-R (van Westen *et al.*, 2010) developed by Horton *et al.* in 2008 at the University of Lausanne, Switzerland. This software uses a GIS-based approach that couples an automatic detection of the source areas and a

simple assessment of the debris flow spreading (Kappes *et al.* 2011). Flow-R attempts to give an insight of existing or potential new susceptibility zones without any notion of intensity or occurrence probability in a regionally scale with limited data. Horton *et al.* (2008) applied the model Flow-R using a digital elevation model for the Canton de Vaud territory (Switzerland), a lithological map and a land use map to identify the potential source areas. The spreading and run-out estimates were based on basic probabilistic and energy calculations that allow them to define the maximal run-out distance of a debris flow. Blahut *et al.* (2010b) used also Flow-R for a debris flow hazard assessment at medium scale in Valtellina di Tirano, Italy. Maximum probable run-out zones were calibrated using documented past events and aerial photographs. As a result, they proposed two debris flow hazard maps: the first map delimits five hazard zones, while the second one incorporates the information about debris flow direction probabilities, showing areas more likely to be affected by future debris flows. Kappes *et al.* (2011) applied the Flow-R model to the Barcelonnette Basin in France using the model for source areas identification and the empirical angle of reach concept to define a worst-case scenario in the area. They also generated scenarios for high, medium and low frequency events, based on a varying angle of reach. The results were compared with the footprints of a few mapped events, showing a high dependency on the quality of the digital elevation model. Ma (2011) applied a method for multi-hazard mass movement susceptibility assessment with run-out, using Flow-R, in a mountainous area with limited information on past events at a regional scale in Mtsekheta-Mtianeti, Georgia. Maps with cells containing significant values of susceptibility for initiation areas were created using SMCE (Spatial Multi-Criteria Evaluation). These cells were used as initiation points and the run-out assessment was performed with the Flow-R model. Based on the level of susceptibility, three different triggering scenarios were produced heuristically.

The main advantage of using flow routing models is that they are linked directly via a DEM, to the topographic characteristics of the terrain and the flow is distributed depending on the attributes of the terrain features. Flow routing models can simulate the course of the flow without a time consuming back-analysis, as no physical or pseudo-physical parameters have to be selected or defined. The disadvantages of using flow routing models are that they are highly dependent on the DEM quality and their results reflects the dependency on the accuracy of the topographical data. Flow routing models do not include the released mass volume of the flow; and for this reason, the intensity of the flow can not be obtained directly.

Method using dynamic run-out models: Past efforts working at regional scales has taken into account the flow behavior, their resistance and the possibility to entrain material during its course by analyzing each individual

event (and its behavioral characteristics) and then imposing those characteristics for a whole region. This task can become very cumbersome for a very large area or for a single triggering event that has caused many flow events in a same area. To name some examples of this methodology, Revellino *et al.* (2004) used the one dimensional DAN model (Hungar, 1995) to simulate the velocity and duration of debris avalanches and the distribution of the deposits in the areas of Sarno/Quindici and Cervinara, (Italy). Using a large amount of available data (i.e. material properties and geomorphological settings), 17 cases were selected. Individual back-analysis of each case was carried out using a trial-and-error procedure and a combination of rheological parameters was found, that provided the best correspondence for each individual event in terms of run-out distance, velocity and distribution of deposits. The majority of the cases at the two sites were simulated with only one specific pair of rheological parameters (Voellmy rheology). Based on their successful simulation with closely constrained selection of input parameters, they propose to use the model to produce quite realistic first-order predictions of run-out of potential slides and to outline potential hazard areas. Another example of using physical models at medium scale is depicted by Hurlimann *et al.* (2006) who carried out a detailed debris flow hazard assessment in five torrent catchments in the Principality of Andorra. Using a magnitude–frequency relationship and a geomorphologic–geologic map, they were able to determine the potential initiation zones and volumes of future debris flows for each catchment. Having this information, they applied a one-dimensional physically based numerical code to analyze the defined scenarios. This was done by evaluating the critical channel sections in the fan area and the maximum run-out on the fan, resulting in intensity maps for each defined scenario and for each modeled event.

As shown before, medium scale analyses are important to pinpoint susceptible areas where a landslides and debris flows can or might occur. This can give a spatial hint where more detailed studies and assessments are required in the future. At the moment, there is a lack of physically based models at the regional scale. For this, reason it was considered important to develop a medium scale numerical model for rapid mass movements in mountainous and volcanic areas. The deterministic nature of the approach should make it possible to apply it to other sites since it considers the rheological resistance and erosive characteristics of the process. Another requirement is that model can be used in an open source environment geographical information system (GIS) and should be transparent (understandable and comprehensible) to the end user.

7.2 Description of the model

The developed and implemented model ("AschFlow") is a 2-D one-phase continuum model that simulates the spreading, entrainment and deposition process of a landslide or debris flow at a medium scale. "AschFlow" is based on an infinite slope model without any lateral or active-passive forces assuming that the forces are hydrostatic. The flow is thus treated as a single phase material, whose behavior is controlled by rheology (e.g. Voellmy or Bingham). Different types of rheology are implemented within a common numerical routing scheme in the model, which will be computed from a digital elevation model (DEM). The model uses a flexible time step based on a CFL (Courant-Friedrichs-Levy) condition in order to maintain the stability of the solution throughout the simulation (Begueria *et al.*, 2009). The model aims to create a user-friendly and practical environment while modeling by making its implementation in the open source GIS PCRaster (Karszenberg *et al.* (2001).

Raster maps are generated as output results after a simulation run. Three different types of maps containing information regarding the velocity of the flow, the height of the flow and the depth of the entrained material are displayed separately. Also, a raster map can be created for each time step selected in the simulation. The model also reports time series of the mass balance, time series of entrainment expressed as volume and time series of the total mobilized volume.

7.2.1 Dynamic routines inside the model

The model "AschFlow" distributes the flow in two dimensions (x,y) with respect to the terrain topography. The flow distribution is a routing routine that is encompassed inside the near raster cells based on the gradient and the aspect of the topography. The model takes into account the change of gradient due to the change of the flow height. The bed surface gradient is calculated based on the slope of the terrain and the estimated new gradient. The aspect direction of the free surface is computed from the aspect of the new gradient. The fraction of the total material that is to be routed towards the x and y direction is determined by the computed aspect direction of the free surface.

The model is implemented in an explicit finite difference (Eulerian) mesh (i.e. the flow was described by variation in the conservative variables at points of fixed coordinates as a function of time (n)). The mesh is defined as a regular grid with size $s = \Delta x = \Delta y$. The motion of the flow is determined in each time step based on the volume displaced in accordance to the height and the velocity of the flow. This displaced volume is then routed depending by the estimated fraction of the material linked to the aspect of the terrain. This

routing process is highly dependent on the CFL condition for stability due to the effect of the topography in the displacement of the volume and the over- and underestimation of the flow resistance term, which typically happens in accelerating and decelerating flows. The value of the Courant-Levy-Friedrichs condition (Appendix 2) is applied to the areas of the flow that are experiencing sudden changes and have the limit values of the CFL that are specified as input parameters.

7.2.2 Rheologies and entrainment mechanisms

Two different rheologies are embedded as different modules inside the model representing the bed shear stress of the flow which is responsible for energy dissipation: –Bingham (See Section 3.2) and -Voellmy (See Section 3.2). For both rheology modules, the model calculates the driving stresses, the resistance stresses and the excess stresses according to the infinite slope equilibrium conditions

Regarding the entrainment processes, the “AschFlow” model includes two different options to be considered depending on the type of process. These options are: - Entrainment rate in terms of a change of flow height per time step (Rickenmann *et al.*, 2003); and - Entrainment rate in terms of velocity and height: based on the entrainment model proposed by McDougall and Hungr (2005) (See Appendix 3).

Once the entrainment rate has been computed, the model calculates a new flow height due to the scouring by adding in a cumulative manner the entrained material. The model also calculates a new soil depth based on the entrainment caused by the flow. The entrainment stops when the soil depth is zero. The model has the possibility to change the rheological parameters of the flow depending on the entrained material and the travel distance. If the flow overpasses a critical distance (defined by the user) and if entrainment occurs, the model uses the new values defined as input parameters.

7.2.3 Model setup and initial conditions

For the initial setup of the “AschFlow” model, three raster maps are required:

- The first raster map defines the topography of the terrain in a DEM form. This map defines not only the basal boundary of the flow, but also the spatial computation domain and the mesh size. No flow is allowed outside the spatial limits of the DEM.
- The second map defines the released mass. This map delineates the spatial location, the area and the depth (thickness) of the failed material. The thickness of the failed mass can be variable or constant.

- The third map defines the soil depth domain throughout the whole terrain topography. This map is relevant to delimit the amount of material that the flow can entrain.

In addition to these maps, the model requires specification of other inputs that are defined by constants; these are depending on the selected rheology. For the Voellmy rheology the inputs needed are: the turbulent coefficient, apparent friction angle, gravity acceleration, unit weight of the flow. For the Bingham rheology the model requires the following inputs: viscosity, yield strength, gravity acceleration, and unit weight of the flow. If the entrainment module is selected for a simulation, the required inputs are: the velocity scour rate coefficient or the height scour rate coefficient.

The number of time steps of each simulation has to be defined. The reporting time interval for the creation of maps must be stated, if this is not selected an end time raster map is reported automatically. In terms of the numerical stability control, the higher and lower values of the Courant-Friedrichs-Levy condition must be defined, as well as the maximum and minimum number of internal loops.

7.3 Case studies

The developed regional model "AschFlow" was applied and evaluated in well documented areas with known past events. This was done in order to test its use for medium scale debris flow susceptibility assessment. As mentioned in the introduction, two of the most recent studies in regional modeling of hazard have been done by Blahut *et al.* (2010b) and Kappes *et al.* (2011) with the Flow-R model. The results of the "AschFlow" model are compared with their results in order to evaluate the advantages and disadvantages of the two modeling approaches and to make an assessment of the obtained modeling outputs.

7.3.1 Barcelonnette Basin, France.

A debris flow spatial susceptibility assessment that takes into account the intensities of impact at medium scale in the northern part of the Barcelonnette basin was performed with the "AschFlow" model. The northern part of the basin was selected because there are the most active catchments with regarding debris flows and where past events have been mapped (recorded) in six major streams (Riou-Bourdoux, St. Pons, La Valette, Faucon, Bourget, Sanieres). The run-out of the susceptible initiation areas was estimated and evaluated according to past events and studies (Kappes *et al.*, (2011). Control points were located at the beginning of each alluvial fan where the flow spreading starts and the maximum flow intensities were

registered at each control point (flow height, flow velocities and flow volume with entrained material) (Fig. 7.1).

Most of the input data was derived from Malet (2010) and van Westen *et al.* (2010), which is an extensive database that contains topographic data (satellite images, a DEM with 10 m resolution, slope angle, aspect, plan curvature and flow accumulation), environmental factors (soil types, land use, rainfall data, lithology) and inventory data (past events information, map of catchments with frequency data of debris flows).

Initiation area characterization

The information contained in the database was used in analyzing initiation areas of events. As most of the elements at risk are located in the flood plain, on alluvial fans, and on lower slopes, the largest hazard is due to run-out of the flow, rather than to initiation (van Westen *et al.*, 2010). For the run-out analysis source maps are required indicating areas where debris flows might occur. In this case study, a heuristic method was applied to assess the sources of the areas of initiation. The most relevant factor maps (land use, slope angle, plan curvature, flow accumulation and lithology) were used to

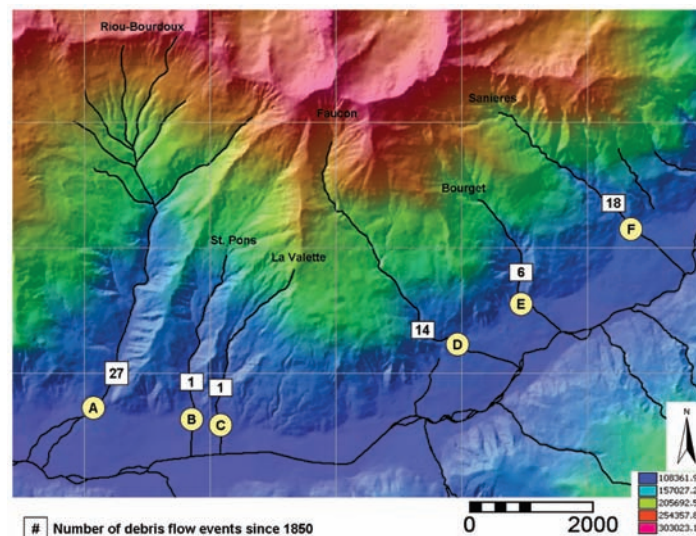


Fig. 7.1: Selected active debris flow streams in the north part of the Barcelonnette Basin with their respective control point at the fan.

generate joint-frequency tables, in which an expert can directly indicate the expected susceptibility class (high, moderate, low or not susceptible). In order to link the initiation susceptibility to a triggering process and to be able to include this in the run-out maps, it is assumed that during a major triggering event mass movements might initiate in the high, moderate and

low susceptible areas, and that a minor triggering event will trigger only landslides in the high susceptible zones. Table 7.1 indicates the assumptions that during a major triggering event, mass movements might initiate in all three zones (high, moderate and low susceptible areas). During a moderate triggering event, only mass movements are expected to be initiated in the moderate and high susceptible zone, and during a minor triggering event only in the high susceptible zones (van Westen *et al.*, 2010).

Table 7.1: Relation between the susceptibility classes for source areas and the triggering events. The value of 1 indicates that a debris flow may occur.

Source area susceptibility class	Triggering event		
	Major event	Moderate event	Minor event
High	1	1	1
Moderate	1	1	0
Low	1	0	0

This results in a series of 3 maps, indicating the presence or absence of source areas for major, moderate and minor debris flow events (Figure 7.2). This susceptibility maps indicates the relative likelihood for the initiation of debris flows to be generated. The resulting maps were tested using existing data and the factors were improved using an iterative procedure until a good agreement was reached. However, there is no comprehensive landslide inventory that will allow characterizing this in detail, so it is highly based on expert opinion.

Run-out characterization

The source areas defined in the previous section were subsequently used for run-out modelling on a medium (1:25.000) scale, using the "AschFlow" model. As discussed in Chapter 2 and according to lithological settings of the Barcelonnette Basin (clay-shale lithology), the Bingham rheology was selected. Mud and debris flows have often been modeled as viscoplastic materials with the Bingham rheology (Remaître, 2006). In clay-shale basins, the debris flow matrix is characterized by a high fines content and the grain-size distribution analyses of the debris-flow deposits demonstrate the muddy character of the flow (more than 20 per cent clay and silt). Moreover, in clay-shale basins, during the debris flow run-out, the coarse particles may be crushed. Hence the fraction of fine elements may increase during the run out. In such a case the presence of colloidal fractions may increase yield stresses (Remaître *et al.*, 2005).

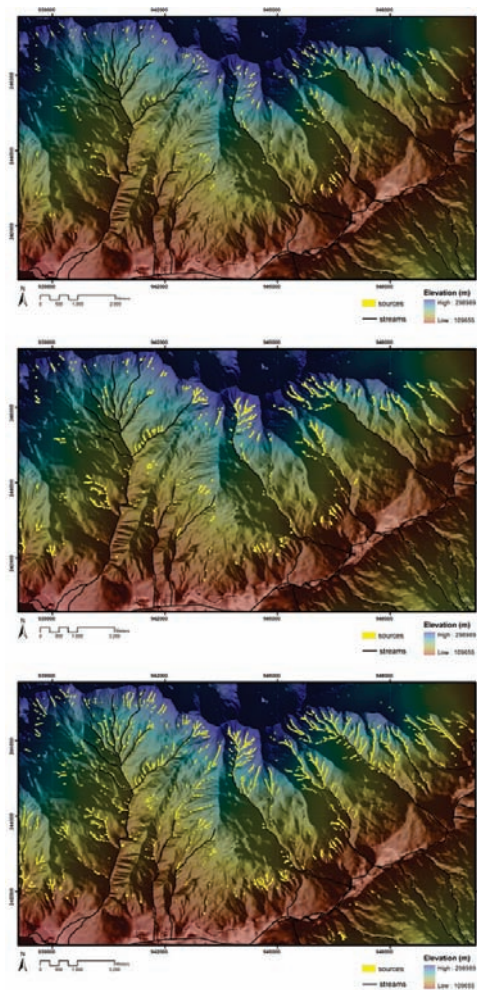


Fig. 7.2: Susceptible areas for debris flow initiation in the northern part of the Barcelonnette basin. The release areas are depicted for a minor event (top), a moderate event (middle) and a major event (bottom) (van Westen *et al.*, 2010; Kappes *et al.*, 2011)

Because of the lack of information regarding the behavior, the footprints and velocity distributions of past events, it was not possible to parameterize the area regarding the Bingham model with back analyses. For this reason the moments of the Lognormal frequency distribution described in Chapter 5 has been used to obtain the range of parameters for input in the model (Table 7.2). From the obtained Log-Normal distribution, the mean and standard deviation of each parameter were used to run the model for each type of event and the intensity parameters were recorded at each control point (Table 7.3). A homogeneous erodible soil depth of 2.5 m was selected since there was a lack of information about this or a soil depth map (this depth was

also assumed to quantify the release volume). Based on the geological, lithological and morphological description of the area and based on the account of historical data, a soil depth of 2 – 3.5 m was found to be the value that agrees best with the quantity of entrained material in past events (Remaître *et al.*, 2008; Quan Luna *et al.*, 2010). This was also done to assess the performance of the model when no values of soil depth can be obtained and an assumption regarding the unknown soil depth has to be done.

Table 7.2: The geometric moments of Log-normal distribution of the Bingham model were used as input parameters inside the "AschFlow" model.

	Lognormal parameters		Geometric moments			
	Mu	Sigma	Mean	Standard deviation	Mean + 1SD	Mean - 1SD
Viscosity Pa s	4.2882	0.6240	72.8378	1.8665	135.9529	39.0233
Yield strength Pa	4.1577	0.6204	63.9299	1.8597	118.8954	34.3750

Regarding the computational time parameters, a time step of 1 s was selected and the simulations had a total time elapsed of 500 s. For the simulation numerical stability control the values for the CFL superior limit used was 0.6 and lower limit was 0.3 with a maximum of 124 loops. Other selected parameters were: gravity acceleration of 9.8 m/s²; unit weight of debris flow of 19 kN/m³; unit weight of the soil bed of 16 kN/m³. The distance selected from the initiation point to the point where the flow starts to entrain material was 50 m. The cut-off threshold to assume a zero velocity was 0.02. The entrainment rate selected was computed based on the velocity of the flow and height; because of the average length of the streams and the released volumes, the entrainment rate used was 0.0065.

Table 7.3: Intensity parameters obtained with the model (Bingham rheology). Measurements were done at each control point for each simulation. Zero values mean that the flow does not reach the control point.

	Type of event	Max height (m)			Max velocity (m/s)			Max volume + entrainment (m ³)		
		-1 σ	\bar{X}	+1 σ	-1 σ	\bar{X}	+1 σ	-1 σ	\bar{X}	+1 σ
Riou-Bordoux Point A	Minor	0	0	0	0	0	0	0	0	0
	Moderate	1.83	2.38	3.06	12.92	14.17	17.30	18,518	26,712	38,326
	Major	4.18	5.71	6.63	19.10	21.15	23.73	36,881	44,553	51,615
St.Pons Point B	Minor	0	0	0	0	0	0	0	0	0
	Moderate	0	0	0	0	0	0	0	0	0
	Major	0.85	2.33	3.79	7.44	14.22	18.55	8,523	16,211	19,274
La Valette Point C	Minor	0	0	0	0	0	0	0	0	0
	Moderate	0	1.22	1.93	0	12.47	17.94	0	12,572	15,494
	Major	1.85	3.88	5.16	8.21	19.77	23.55	11,893	16,759	23,322
Faucon Point D	Minor	0	0	0	0	0	0	0	0	0
	Moderate	0	1.16	3.26	0	11.75	18.48	0	22,363	34,846
	Major	3.12	4.98	7.92	19.44	22.21	24.55	55,377	83,013	127,362
Bourget Point E	Minor	0	0	0	0	0	0	0	0	0
	Moderate	0	0.66	1.15	0	12.12	17.41	0	9,539	15,253
	Major	1.88	4.12	7.17	16.66	21.83	24.83	23,365	74,746	104,682
Sanieres Point F	Minor	0	0	0	0	0	0	0	0	0
	Moderate	0	0.74	1.39	0	13.42	17.77	0	11,772	18,829
	Major	2.13	4.64	7.36	18.48	22.17	24.15	27,503	79,452	108,774

The spatial distributed modeled outputs of the “AschFlow” model that simulated a major event using the mean values of the distribution were compared directly with the work of Kappes *et al.* (2011), where the worst case modeled scenario was analyzed in the same area. Kappes *et al.* (2011) assessed the Flow-R model performance by means of a comparison of the potentially affected areas with the footprints of the past events. For the worst-case scenario an enclosure of all past events into the modeled area was assumed and checked by an overlay of the area susceptible according to the model and the footprints of recorded debris flows. According to Kappes *et al.* (2011), their results are matching nearly completely past events for the slopes and the torrential fans. Minor differences are observable only for the further run-out in the flood plain of the Ubaye river. The “AschFlow” model results show agreement regarding the susceptible areas where a debris flow can occur in terms of run-out length (Fig. 7.3). The main difference between the two models regards the spreading of the flow. The “AschFlow” model uses a yield strength and a viscous resistance, these values can stop the flow at a critical thickness and slope angle preventing it for further spreading, which is not the case with Flow-R using probable frictional reach lines over the DTM.

Because of these differences, “AschFlow” models the flow in a more confined manner than the Flow-R model.

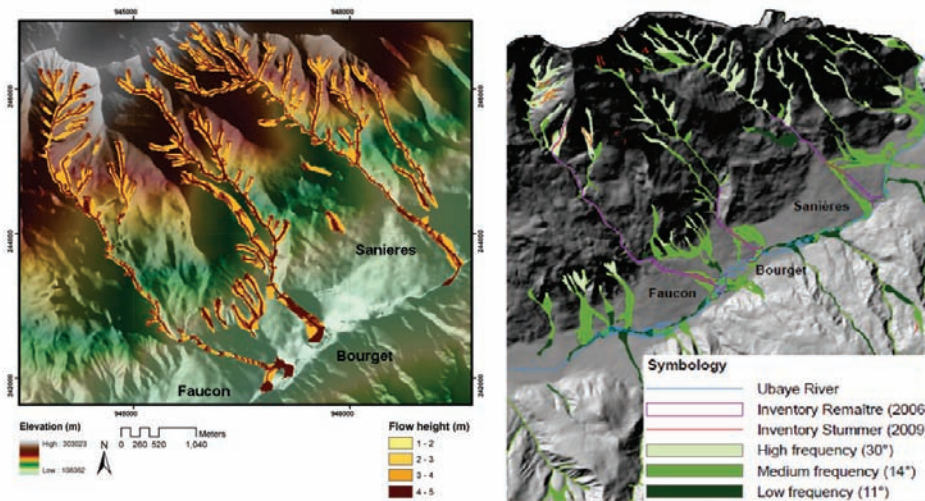


Fig. 7.3: Debris flow height map generated with the “AschFlow” model for the Barcelonnette basin (left). Spreading reach map generated with the Flow-R model (figure taken from Kappes *et al.*, 2011) (right). When comparing both maps, similarities in terms of run-out length are observable. However, the Flow-R model simulates a considerable spreading when the flow reaches the fan and goes into the valley while the “AschFlow” model simulates these cases in a moderate manner because it is governed by a frictional regime.

Besides the differences in geometry of the flow, the “AschFlow” model generates, on the basis of calculated velocities and flow heights, intensity parameters which are important additional indicators to assess priorities for more detailed research (Fig. 7.4). In the case of the Flow-R model, the debris flow source has a certain unit potential energy (the volume is defined as a unit and can not be specified otherwise) regarding its adjacent cells downhill. During propagation, part of this energy is lost in friction. If the kinetic energy increases reaching a maximum threshold, the energy line will have the same shape as the topography. The debris flow stops when the friction line reaches the topographical surface (Horton *et al.*, 2008). In the “AschFlow” model the velocities are based on the slope friction of the rheological model, this means that the velocity is controlled not only by the topography but by the frictional coefficients that are parameterized inside the model. Although it is evident that also with the AschFlow model like the Flow-R model, the determination of the source areas and the run-out assessment at a medium scale may lead to an overestimation of the areas potentially affected.

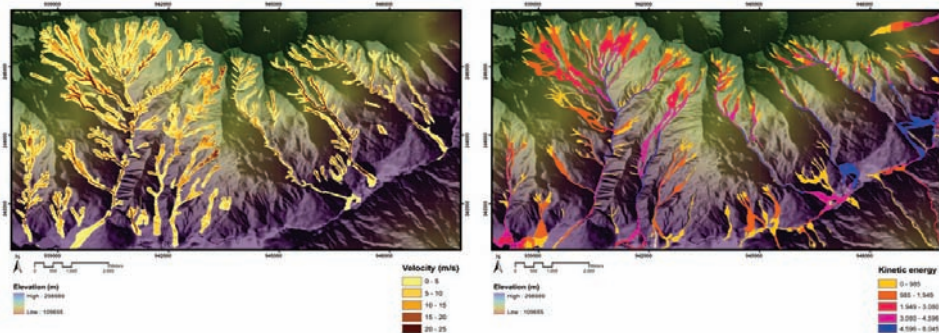


Fig. 7.4: Velocity map generated with the “AschFlow” model for the Barcelonnette basin (left). Kinetic energy map generated with the Flow-R model (Kappes *et al.*, 2011) (right).

7.3.2 The Valtellina Valley in Italy

A similar susceptibility assessment that was performed in the Barcelonnette area was carried out in the Valtellina Valley in Italy. To evaluate the other modules embedded in the “AschFlow” model, the Voellmy rheology and the entrainment rate based on the height of the flow (Rickenmann *et al.*, 2003) was selected for the Valtellina Valley case study. The western part of the valley was chosen for a case study because a DEM with a resolution of 5 meters was available. Another reason to select that area was the availability of an inventory of past events and a susceptibility map of initiation areas (Blahut *et al.*, 2010a, Blahut *et al.*, 2010b) (Fig. 7.5). Control points were located at the beginning of the alluvial fans where the debris flows are assumed to be most active and where the flow spreading starts. Maximum flow intensities were registered at each control point (flow height, flow velocities and flow volume including entrained material). Most of the input data was derived from Blahut *et al.* 2010a and analyzed to compute the initiation areas.

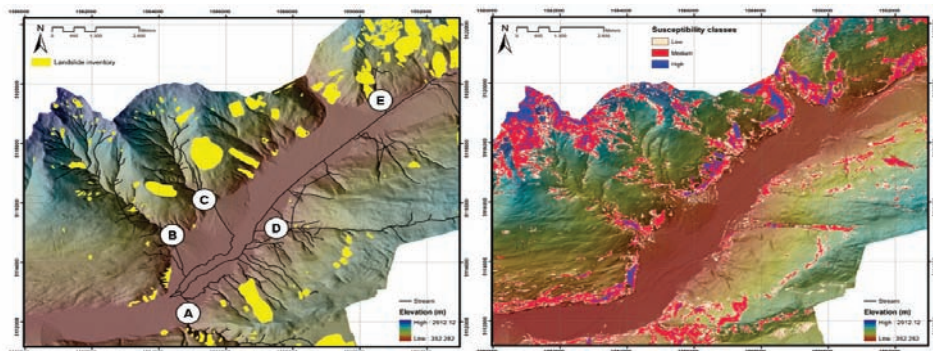


Fig. 7.5: Selected active debris flow streams in the southern part of the Valtellina Valley with their respective debris control point at the fans. The yellow polygons are landslides past events in the area that were registered in the DF2001 database (left). Susceptibility map of the area proposed by Blahut *et al.* (2010a) (right).

Initiation area characterization

In the Valtellina Valley case study, relevant topographic factors were overlaid in order to get a first approach to susceptible initiation areas. Three topographic parameters slope, flow accumulation and planar curvature and were complemented by lithology and a land use map. Each factor map was implemented as a raster map and thresholds for each one of them were created. A susceptible raster was considered when all the thresholds were exceeded. The threshold used for the planar curvature was: $-2/100\text{m}-1$ and for the slope angle: $>15^\circ$. All lithological units were included except limestones, alluvial sediments, dolomite, quartzite, or peat materials. Urbanized areas, water, quarries and orchards were excluded from the land use map. Thresholds values for the terrain factors and the exclusion of units from the land use and lithological maps were chosen based on the values used by Blahut *et al.* (2010b) and Kappes *et al.* (2011). A buffer zone linked to the flow accumulation of 50 meters was created in order to include only the susceptible points inside these areas. To assign classes to the susceptible areas, they were crossed with the susceptibility map created by Blahut *et al.* (2010a) (Fig. 7.5). This gave an indication of expected susceptibility classes: - high, - moderate, - low. This results in a series of 3 maps, indicating the presence or absence of source areas for major, moderate and minor debris flow events (Figure 7.6). This susceptibility maps indicates the relative likelihood for the initiation of debris flows to be generated. The resulting maps were tested using the existing inventory.

Run-out characterization

The initiation areas divided in classes that were computed in the previous section were used for run-out modelling on a medium scale using the "AschFlow" model. The Voellmy rheology was chosen in this study case to observe the model performance and its ability of another rheological model. A homogeneous erodible soil depth of 2 m was selected since there was no detailed soil depth map available (this depth was also assumed to quantify the released initial volume). This assumption was done after analyzing the descriptions of the geological and morphological characteristics of the area and past events by Cancelli and Nova (1985), Crosta (1990) and Crosta *et al.* (2003). In terms of the computational time parameters, as used in the Barcelonnette study case, a calculation time step of 1 s was selected and the simulations had a total time elapsed of 500 s. For the simulation numerical stability control the values for the CFL superior limit used was 0.6 and lower limit was 0.3 with a maximum of 124 loops. Other selected parameters were: gravity acceleration of 9.8 m/s^2 ; unit weight of debris flow: 19 kN/m^3 ; unit weight of the soil bed: 16 kN/m^3 . The distance selected from the initiation point to the point where the flow starts to entrain material was 50 m. The threshold to assume a zero velocity was 0.02. The entrainment rate selected

was computed based on the height of the flow, the entrainment rate used was 0.001 (Rickenmann *et al.*, 2003).

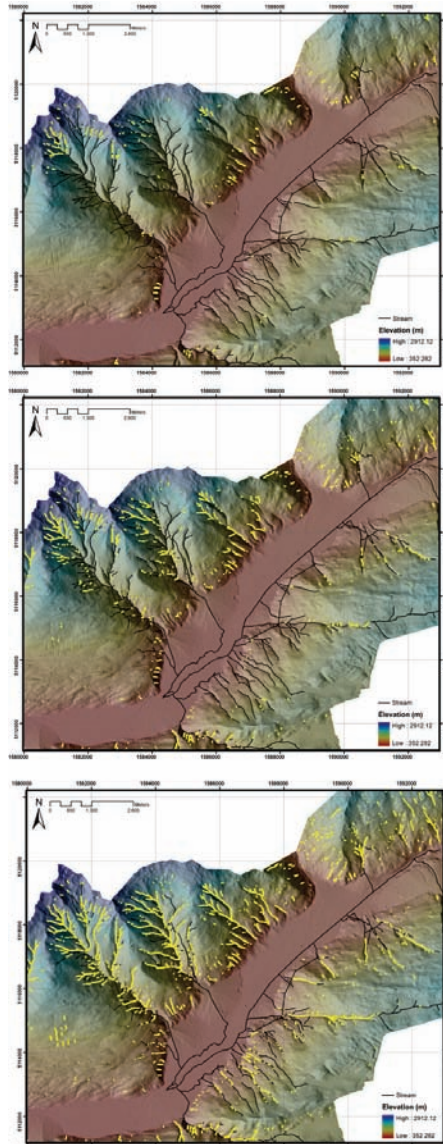


Fig. 7.6: Susceptible areas for debris flow initiation in the western part of the Valtellina Valley. The release areas are depicted for a minor event (top), a moderate event (middle) and a major event (bottom)

The moments of the Lognormal frequency distribution of the Voellmy rheology described in Chapter 5 were used to obtain the values of the parameters for input in the model (Table 7.4).

Table 7.4: Log-normal distribution of the Voellmy model parameters. The geometric moments of each distribution were used as input parameters inside the "AschFlow" model.

	Lognormal parameters		Geometric moments			
	Mu	Sigma	Mean	Standard deviation	Mean + 1SD	Mean - 1SD
Friction coefficient	-2.088	0.7310	0.1239	2.0773	0.2573	0.0596
Turbulent coefficient	5.6486	0.6302	283.89	1.8780	533.1640	151.1670

From the obtained Log-Normal distribution, the mean and standard deviation of each parameter were used to run the model for each type of event and the intensity parameters were recorded at each control point (Table 7.5).

Table 7.5: Intensity parameters obtained with the model (Voellmy rheology). Measurements were done at each control point for each simulation. Zero value represents that the flow does not reach the control point.

	Type of event	Max height (m)			Max velocity (m/s)			Max volume + entrainment (m ³)		
		-1 σ	\bar{X}	+1 σ	-1 σ	\bar{X}	+1 σ	-1 σ	\bar{X}	+1 σ
		Point "A"	Minor	0	0	0	0	0	0	0
	Moderate	1.58	2.33	2.74	6.15	7.89	9.31	11,357	23,145	26,388
	Major	2.76	4.42	5.82	6.23	11.55	13.55	27,495	39,290	48,673
Point "B"	Minor	0	1.05	1.59	0	5.22	5.86	0	9,050	11,308
	Moderate	1.22	3.58	4.82	5.47	8.69	11.04	12,892	34,885	40,566
	Major	3.18	4.74	5.66	7.17	10.34	12.28	36,735	43,932	56,332
Point "C"	Minor	0	1.15	2.37	0	5.66	8.15	0	12,680	26,085
	Moderate	2.05	4.12	4.78	8.05	10.17	11.29	25,460	39,075	42,536
	Major	3.38	6.15	7.84	9.83	14.25	14.85	39,322	53,481	61,265
Point "D"	Minor	0	1.80	2.07	0	6.10	8.32	0	13,045	19,538
	Moderate	3.90	5.55	7.79	10.00	12.94	14.26	35,857	44,465	57,330
	Major	4.69	6.96	9.12	11.16	14.04	14.90	42,935	58,027	74,844
Point "E"	Minor	0	0	1.85	0	0	6.25	0	0	18,633
	Moderate	2.31	3.15	4.22	6.34	7.57	9.94	18,755	23,534	27,700
	Major	1.17	4.14	5.26	5.20	9.18	10.07	16,280	26,376	31,121

Intensity parameters at each control point were recorded and also displayed in the form of maps (Fig. 7.7).

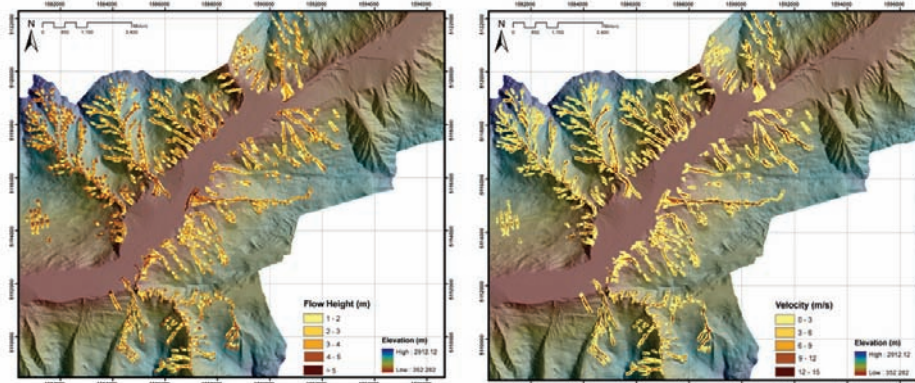


Fig. 7.7: Results of a simulation with the “AschFlow” model for a hypothetical major event using the mean values of the back calculated Voellmy parameter distribution (see also Table 6.3). Flow height map (left) and velocity map (right) of the Valtellina valley.

The results of the “AschFlow” model in the Valtellina Valley simulating a major event using the mean values of the distribution were compared to the geometric results of Blahut *et al.* 2010b where they calibrate the maximum probable debris flow run-out with the 19th July 1987 event and aerial photographs from 2001 (using the edge of alluvial fans where previous debris flows were observed). The modeled footprints obtained with “AschFlow” were compared with the modeled classes in the Flow-R model. As seen in the Barcelonnette case study, there is less spreading of the flow in the simulated results of the “AschFlow” model (Fig.7.8)

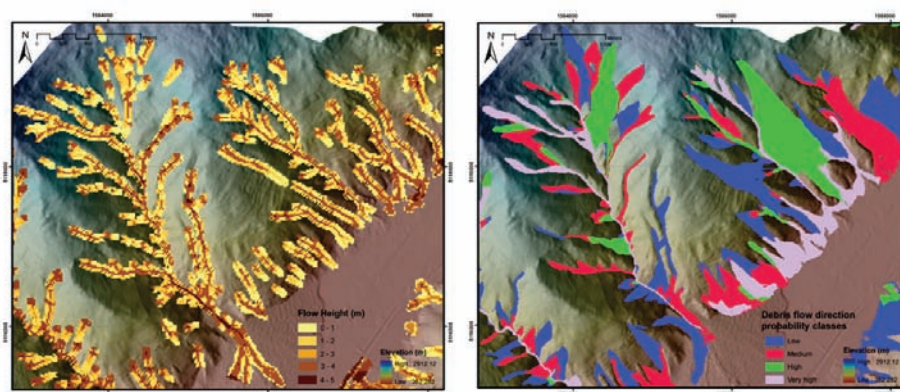


Fig. 7.8: Debris flow height map generated with the “AschFlow” model for a major event for the Valtellina Valley (left). Debris flow direction probability classes map generated with the Flow-R model (Blahut *et al.*, 2010b) (right). Even though some spatial similarities arise when comparing both results, the “AschFlow” model can generate directly quantitative intensity outputs such as velocity and heights of the flow.

7.4 Discussion and Conclusions

One of the main purposes of a medium-scale debris-flow susceptibility analysis with the "AschFlow" model is to have a fast assessment with limited spatial information and few historical data of past events. The development of a model containing different modules for simulating flows and landslides within the framework of an open source GIS environment presents a straightforward and flexible approach. The run-out modeling process can be accomplished within a single GIS environment (PCRaster) or selected modeling steps might be accomplished outside the provided framework (i.e. initiation susceptibility maps) and then imported to the model. The "AschFlow" model is simple and fast to set up a simulation and the input parameters are easy to define. The model can serve as a tool and platform within which various modeling concepts can be tested. Because of its design it is flexible enough to work with different configurations of the initial and boundary conditions; this will allow end-users to adjust the settings of the model to a variety of situations. The inclusion of several rheological models allows easy comparison of various flow types, to choose between different types of events (e.g. hyperconcentrated or granular) and to simulate a real event as close as possible.

The result of the "AschFlow" model can be considered as an indication of areas possibly affected with a certain amount of impact by a debris flow event rather than an actual hazard map because of the level of detail and the number of assumptions made regarding the initiation areas. From a user perspective the "AschFlow" model can be seen as a stand alone model which can be utilized for a first assessment of potentially impact areas.

The comparison between the results of the "AschFlow" model and the Flow-R model results proved to be helpful for an evaluation of this kind of regional models. The modeled initiation areas as well as the run-out modeling resulted in reasonable outcomes when enough site specific information is available, although there are still a lot of assumptions to be done. Table 7.6 mentions some advantages and shortcomings of both models regarding its use for a hazard analysis.

A direct calibration of the scenarios on the basis of mapped deposition areas and frequency estimates is also possible, although not done in this study. Future work with the model should consider the use of the model for various settings and compare the parameterization in relation to the environmental conditions. Information on the parameter ranges especially in regions with detailed information on volumes of past events would provide support for the calibration of the model to unknown zones. The information obtained from areas where there is sufficient information on volumes and run-out of past events can facilitate extrapolations to areas with high scarcity of data. Other

versions of the model will be developed in the future which debris flow solids are generated by run-off and erosion of available loose materials accumulated in steep gullies. In these versions the severity of an event is controlled by the meteorological input, which will give information about the frequency magnitude of these events.

Table 7.6. "AschFlow" model and Flow-R model characteristics for hazard assessment.

		"AschFlow" model	Flow-R model
Initiation zones	Advantages	- The model considers as an input the initiation areas and released volumes.	- The model is able to estimate and identify the initiation areas or sources. - Site topographic and geomorphologic factors are used to analyze the source areas.
	Disadvantages	- Initiation zones can not be modeled directly by "AschFlow". - Initiation areas have to be imported as volumes from other models or defined by the user.	- No release volume is considered. Only the areal extent. - Each raster has a unit value.
Parameterization for the run-out calculation	Advantages	- The input parameters used by the "AschFlow" are the rheological resistance parameters and the entrainment rates. This represents in a more physical way the resistance of the flow and the terrain taking into account the entrainment process.	- The input parameters used by Flow-R are: - an average slope angle (constant friction loss corresponding to that angle) and a choice of direction algorithm.
	Disadvantages	- Uncertainty in the rheological parameters (which can be approached in a stochastic manner). - The more parameters, the more difficult is to calibrate a model.	- No physical meaning of the input parameters. - The choice of direction algorithms has a big influence in the spreading.
	Advantages	- The model is based on time steps calculations. Outputs results can be obtained at each time step.	- The model takes less effort computationally. - Results can be seen faster.
	Disadvantages	- Depending on the size of the area a big effort is done by computing which can be time consuming.	- Output results can not be displayed until the last computation is done.
	Advantages	- The model depends on the topographical and rheological characteristics for the spreading and extent of the flow.	- The model has several direction algorithms that can be selected. This can influence the spreading in the results.
	Disadvantages	- Uncertainty regarding the selection of the right rheology.	- Uncertainty regarding which direction algorithm to select for different cases or scenarios.

Cont. Table 7.6: "AschFlow" model and Flow-R model characteristics for hazard assessment.

		"AschFlow" model	Flow-R model
Spreading	Advantages	- The model depends on the topographical and rheological characteristics for the spreading and extent of the flow.	- The model has several direction algorithms that can be selected. This can influence the spreading in the results.
	Disadvantages	- Uncertainty regarding the selection of the right rheology.	- Uncertainty regarding which direction algorithm to select for different cases or scenarios.
Outputs (modeling results)	Advantages	- The model outputs are intensity values: flow height, flow velocity and entrained volume. This can be used directly for a preliminary hazard assessment and opens the way for a quantitative risk assessment.	- The model outputs are: probability of a cell being reached by the flow and kinetic energy.
	Disadvantages		- No direct intensity values - No volume is taken into account when modeling. - Can not be used directly for quantitative assessment.
Entrainment	Advantages	- The model takes into account entrainment of the flow during its course. - The model has two different entrainment models.	
	Disadvantages	- Entrainment parameters can introduce another source of uncertainty.	- Does not take into account the entrainment process.
Model platform		- Open source GIS (PCRaster)	- MATLAB environment

Chapter 8: Local scale run-out modelling for vulnerability assessment

8.1 Introduction

The increase in population and resulting demand for resources has given rise to a continuous pressure to settle in places where the interaction between humans and continuous land processes becomes a potential risk (Nadim and Kjekstad, 2009). For this reason, it is essential to analyze the possible damage that the hazard process can yield in the affected sectors. A quantifiable integrated approach of both hazard and risk is becoming a required practice in risk reduction management (Fell and Hartford, 1997; Duzgun and Lacasse, 2005). This quantitative assessment should include the expected losses as the product of the hazard with a given magnitude, the costs of the elements at risk, and their vulnerability (Uzielli *et al.*, 2008). In the past, several authors have proposed different methods to quantify the risk by estimating the hazard in a heuristic-empirical or statistical manner; while assessing the vulnerability of the affected elements in a qualitative method (Liu and Lei, 2003; Remondo *et al.*, 2008; Zezere *et al.*, 2008).

In order to improve the results of a debris flow risk assessment, it is necessary to analyze the hazard event using quantitative information in every step of the process (van Asch *et al.*, 2007) and the vulnerability of the elements exposed. The contribution of the dynamic run-out models inside a quantitative assessment is to reproduce the distribution of the material along the course, its intensity, and the zone where the elements will experience an impact. For this reason, dynamic run-out models have been used in recent years as a tool that links the outputs of a debris flow hazard initiation/susceptibility modelling (released volumes) with physical vulnerability curves.

This chapter presents a method to use dynamic run-out modelling for the reconstruction of the debris flow intensities caused by a recent event in the study site of Selvetta (Italy, described in Section 2.2.1) and to use this information in combination with damage data for the construction of physical vulnerability curves for buildings.

Chapter 8 is based on:

Quan Luna, B., Blahut, J., van Westen, C.J., Sterlacchini, S., van Asch, T.W.J., Akbas, S.O.. 2011. The application of numerical debris flow modelling for the generation of physical vulnerability curves. *Nat. Hazards Earth Syst. Sci.*, 11, 2047-2060, doi:10.5194/nhess-11-2047-2011.

8.2 Numerical modelling for hazard analysis in a quantitative risk assessment (QRA)

Different approaches and methods have been developed in the past for a quantitative risk analysis using dynamic run-out models and incorporating the physical vulnerability of the elements at risk. For example, Bell and Glade (2004) performed a quantitative risk analysis for debris flows and rock falls (focusing on the risk to life) in NW Iceland. Their approach to the hazards is based on empirical and process modelling that resulted in specific run-out maps. The hazard zones were determined based on the recurrence interval of the respective processes. For the determination of the levels of vulnerability, a semi-quantitative approach defined by matrices was used based on available literature and the authors' past findings (Glade, 2003). Muir *et al.* (2008) presented a case study of quantitative risk assessment to a site-specific natural terrain in Hong Kong, where various scenarios were generated with different source volumes and sets of rheological parameters derived from the back analyses of natural terrain landslides in Hong Kong. Debris mobility modelling was performed using the Debris Mobility Model (DMM) software developed by the Geotechnical Engineering Office (Kwan and Sun, 2006), which is an extension of Hungr's (1995) DAN model. They derived probability distributions from past events run-outs and calculated the probability distribution of debris mobility for each volume class. Regarding the vulnerability, they used an "Overall Vulnerability Factor" (OVF) and the average number of vulnerable population in a given facility directly hit by a landslide. The OVF was derived from the landslide volume, location of the elements at risk, and the protection a facility can offer. Individual risk was calculated as the summation of the product of the frequency of a flow affecting the facility and the vulnerability of the most vulnerable individual for each of the scenarios. They also calculated the societal risk. Castellanos (2008) performed a local risk assessment based on the back-analysis of one historical landslide in Cuba. Based on the parameters obtained from the modelling of past events, run-out simulations were carried out with a beta version of the MassMov2D software (Beguiria *et al.*, 2009) for twelve potential zones. Vulnerability curves based on the depth of the flow and the conditions of the buildings were generated using detailed building typology characteristics and run-out results, and economic risk values were computed for three scenarios. Zimmerman (2005) described Switzerland's new approach of natural hazards and risk management using the Sorenberg debris flow as an example. For the Sorenberg event, hazard maps were prepared according to three probability classes scenarios. The scenarios were based on past events and field verification. Debris-flow run-out was simulated using a random walk approach (Gamma, 2000) by applying a simple model that assumes that the motion is mainly governed by two frictional components: a sliding friction coefficient and a turbulent friction

coefficient that is determined by a Chezy-type relation (Rickenmann, 1990). Results of the modelling were displayed as intensity maps. Federal recommendations provide definite criteria for the intensity classes based on the height and the velocity of the flow. Adjustment of the land-use plans and building codes were established regarding the intensity classes. Jakob and Weatherly (2005) quantified debris flow hazard and risk on the Jonas Creek fan in Washington, USA. They constructed frequency-magnitude graphs to build different return period scenarios as an input to a debris flow run-out model. The FLO-2D model was used to calculate maximum flow depths and velocities in order to assess the hazard. Intensity maps were developed based on the modelled outputs of each modelled scenario. Potential deaths were calculated assuming that in the high intensity areas the vulnerability is equal to 1, while the vulnerability is equal to 0 in the medium and low intensity zones. In terms of risk management, Crosta *et al.* (2005) carried out a cost-benefit analysis for the village of Bindo in the Valsassina valley (Central Pre-alps, Italy) where a part of an active slope is still a threat. They identified different mitigation plans such as a defensive structure, monitoring, and a combination of both. They built hazard scenarios with a method that coupled a stability analysis with a run-out assessment for different potential landslides. The stability analysis was modelled using a 2-D numerical code and the run-out was simulated with the quasi-three-dimensional finite element method of Chen and Lee (2000) in the Lagrangian frame of reference. The different scenarios were compared with a scenario where no mitigation action was introduced. A cost-benefit analysis of each scenario was performed considering the direct effect on human life, houses, and lifelines.

The recent work done by means of numerical physical modelling within a risk analysis suggests that dynamic run-out models (correctly used) can be of practical assistance when attempting to quantify the assessment. Together with a good understanding of the slope processes and their relationship with other conditional factors, run-out models results can be used in a hazard analysis to estimate the spatial probability of the flow affecting a certain place with detailed outputs as deposition patterns, travelled distance and path, and velocities and impact pressures. Results obtained from the run-out modelling are directly involved as factors that influence and affect the vulnerability of an exposed element. However, quantitative vulnerability information for landslides is difficult to obtain due to the large variability in landslides types, the difficulty in quantifying landslides magnitude, and the lack of substantial historical damage databases (van Westen *et al.*, 2006; Douglas, 2007).

8.3 Physical vulnerability assessment

Several efforts have been made in the past to define and assess the vulnerability of an element or group of elements exposed to a landslide

hazard. The vulnerability can be classified as: *physical*, *functional*, and *systemic* vulnerability. The *physical vulnerability* relates to the consequences or the results of an impact of a landslide on an element (Glade, 2003). *Functional vulnerability* depends on the damage level of the element at risk and its ability to keep functioning after an event (Leone *et al.*, 1996). *Systemic vulnerability* defines the level of damage between the interconnections and functionality of the elements exposed to a hazard (Pascale *et al.*, 2010). In this paper, a focus on the physical vulnerability will be highlighted with regard to a method which is commonly used in a quantitative risk assessment.

In a quantitative risk assessment, physical vulnerability is commonly expressed as the degree of loss or damage to a given element within the area affected by the hazard (van Westen *et al.*, 2006). It is a conditional probability, given that a landslide with a certain magnitude occurs and the element at risk is on or in the path of the landslide. Physical vulnerability is a representation of the expected level of damage and is quantified on a scale of 0 (no loss or damage) to 1 (total loss or damage) (Fell *et al.*, 2005). Thus, vulnerability assessment requires an understanding of the interaction between the hazard event and the exposed element. This interaction can be expressed by damage or vulnerability curves. Some progress has been made in developing vulnerability curves, matrices, and functions for several types of hazards including mass movements. Extensive work has been carried out by FEMA (US Federal Emergency Management Agency) on vulnerability functions for earthquakes, floods, and hurricanes. These functions are used in the HAZUS (Hazard US) software application to quantitatively estimate the losses in terms of direct costs (e.g. repair, loss of functionality), as well as regional economic impact and casualties (Hazus, 2006). In the case of snow avalanches, Wilhelm (1998) obtained a function by analyzing the damages caused in terms of impact pressure by dense snow avalanches on concrete buildings with reinforcement. The building vulnerability was defined as the ratio of the cost of repairing the damages and the value of the building. Based on the function proposed by Wilhelm (1998), Cappiabanca *et al.* (2006) developed a function for people inside the buildings. Using the same approach of relating the expected losses of a structure with the impact pressures of the avalanche, Barbolini *et al.* (2004) proposed vulnerability functions for buildings and persons for powder snow events. To overcome the scarcity of well documented events and their consequences, Bertrand *et al.* (2010) used numerical models to simulate the behaviour of structures under snow avalanche loading. The structures were modelled in three dimensions with a finite element method (FEM), and a damage index was defined on global and local parameters of the buildings (e.g. geometry of the structure, compressive strength of the concrete). The vulnerability was established as a function of the impact pressure and the structure features. For rock falls,

Heinimann (1999) estimated vulnerability curves as damage functions of six different categories (type) of buildings related to the intensity of the rock fall. The response of reinforced concrete buildings to rock fall impact was investigated by Mavrouli and Corominas (2010), considering a single hit on the basement columns. They calculated for a range of rock fall paths and intensities, a damage index (DI) defined as the ratio of structural elements that fail to the total number of structural elements.

Regarding vulnerability functions for landslide and debris flow hazards, Kaynia *et al.* (2008) applied to a real event the proposed probabilistic methodology of Uzielli *et al.* (2008) to estimate the physical vulnerability of building structures and the population to landslides. Vulnerability is defined quantitatively as the product of landslide intensity and the susceptibility of elements at risk. The uncertainties are considered by a First-Order Second Moment approach (FOSM). This work was complemented by Li *et al.* (2010) by proposing new functions for the vulnerability of structures and persons based on the landslide intensity and the resistance of the exposed elements. Using another type of procedure to assess the vulnerability, Galli and Guzzetti (2007) gathered information of past events in Umbria (Italy) that have damaged buildings and roads. They established functions between the area of the landslide and the vulnerability of buildings, major roads, and minor roads. To assess the vulnerability to a debris flow, Haugen and Kaynia (2008) proposed that the impact of a flow sets a structure in a vibratory motion. Structural vulnerability is defined by a damage state probability. This was approached using the principles of dynamic response of simple structures to earthquake excitation and fragility curves proposed in HAZUS. Fuchs *et al.* (2007) used a well-documented debris flow event in the Austrian Alps to derive a vulnerability function for brick masonry and concrete buildings. They defined a damage ratio that describes the amount of damage related to the overall damage potential of the structure. A vulnerability function was created from the calculated damage ratio and the debris flow intensity (flow height). A comprehensive review of several qualitative vulnerability methods used in landslide risk analysis was made by Glade (2003). Whereas the above mentioned examples analyze the hazard separately from the vulnerability of the elements at risk, our aim is to use the strength of the debris flow run-out models to quantify physical vulnerability by means of the impact pressure outputs.

This chapter presents an integrated approach of detailed rainfall data and dynamic modelling to calculate the intensity and run-out zone of the 2008 Selvetta debris flow that caused damage to thirteen buildings. The debris flow event was reconstructed and back-analyzed. Geomorphologic investigations were carried out to study the behaviour of the flow and intensity aspects such as run-out distances, velocities, and depths. Synthetic

physical vulnerability curves were prepared based on the flow depth, impact pressures, and kinematic viscosity. These curves relate the physical outputs of the modelling and the economic values of the elements at risk.

8.4 Modelling the Selvetta 2008 event for determining vulnerability curves

The field observations of the debris-flow event in Selvetta were taken into account and used for a back analysis using a dynamic run-out modelling approach. They were the basis to calibrate the model and simulate the debris flow process during its course. The modelling of the Selvetta debris flow was divided into two parts. The first part was a simulation of the rainfall in the area to calculate a discharge hydrograph and the effect of the rainfall intensity in the flow. The second part was a simulation of the debris flow that included the results of modelling of the rainfall and the entrained material. The DEM available and used for the Selvetta area was a 2m grid model obtained from a LIDAR survey. The FLO-2D software was used to simulate the rainfall and the debris flow event (FLO-2D, 2009). A damage analysis of the elements at risk in the Selvetta event led to a vulnerability assessment which was then later combined with the modelling outputs. This resulted in three proposed vulnerability functions: flow height, impact pressure, and kinematic viscosity curves (Fig. 8.1).

The mathematical model used to model the Selvetta debris flow event was FLO-2D (described in Chapter 3 and Appendix 1), which is an Eulerian two dimensional finite difference model that is able to route non-Newtonian flows in a complex topography based on a volume-conservation model. The model input is in the form of a flow hydrograph at the head of a depositional debris fan, distributing the debris over the fan surface, allowing for obstructions and pathways such as infrastructures (buildings, roads, channels, and bridges). These make the model relevant for the determination of flow patterns on the surface of a fan.

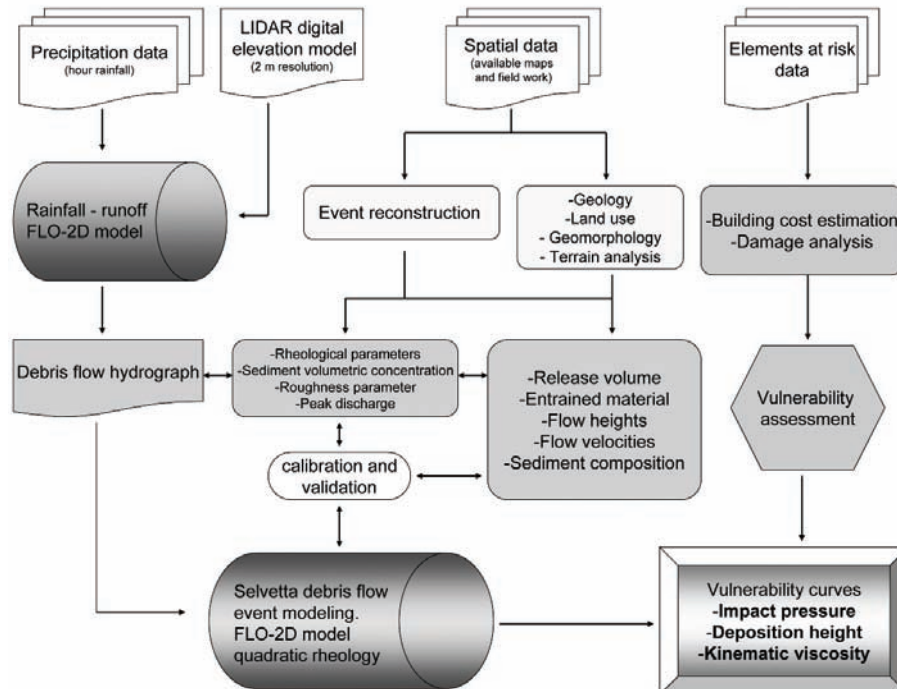


Fig. 8.1: Flowchart of the methodology applied in the Selvetta case study area to determine vulnerability curves.

8.4.1 Rainfall modelling

The hourly measured rainfall data for the period from 11 to 13 July 2008 were used for modelling the accumulated rainfall distributed over the area (hourly time steps). Outflow sections were selected where the run-off rain of the modelled area domain is discharged. The outflow sections are artificial sections whose purpose is to discharge flow off the area domain system. For the Selvetta event, two zones were selected as outflow sections: (1) the scarp, where the release area is located and the slope failure occurred; and (2) the debris flow path channel, where the amount of rain can be an influencing factor in the mobility and the sediment concentration of the flow. The result of the rainfall/runoff modelling was a water discharge hydrograph that is later added to the release volume of the failed mass in order to obtain a time stage debris flow release hydrograph.

8.4.2 Debris flow modelling

The estimation of the peak discharge inside the discharge hydrograph is of vital importance as it determines the maximum velocity and flow depth, momentum, impact forces, ability to overrun channel walls, as well as the run-out distance (Rickenmann, 1999; Whipple, 1992; Chen *et al.*, 2007). For

the estimation of the final debris flow hydrograph, the volumes of the entrained material estimated from measurements during the field work were introduced as an additional and variable sediment concentration into the hydrographs of the FLO-2D model with the use of an empirical formula proposed by Mizuyama *et al.* (1992), who established a relation between the magnitude of the debris flow (volume in m³) and the peak discharge for muddy-debris flows (Eq. 8.1):

$$Q_p = 0.0188M^{0.790} \tag{8.1}$$

where, Q_p is the peak discharge (in m³/s) and M is the debris flow volume magnitude (in m³). A time-stage of sediment concentration was produced based on the shape of the hydrograph (Fig. 8.2). This was done to agree with observations that the peaks in debris flow hydrographs correspond to high sediment concentrations, while the final part of the hydrograph has a more diluted composition. The procedure also reproduced the distribution of sediment concentration influenced by a dilution in the falling tail of the hydrograph. The maximum and minimum concentrations were 0.55 and 0.25, respectively.

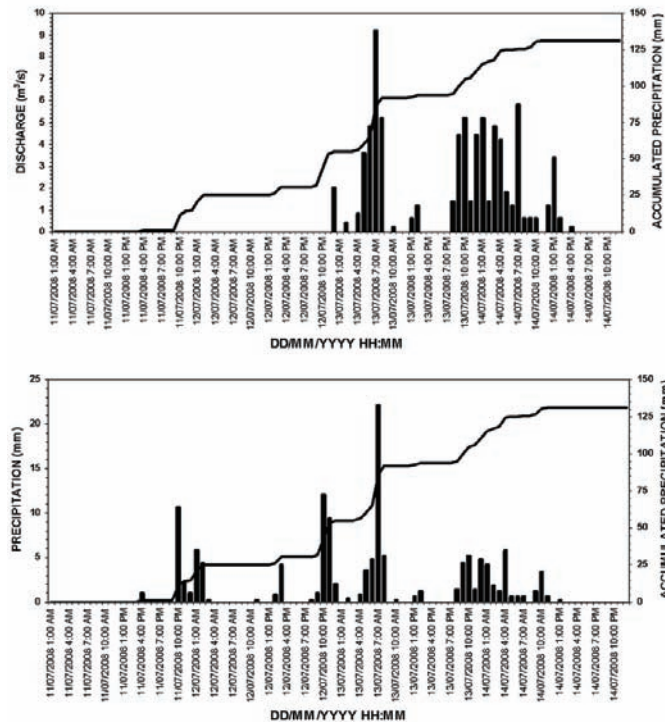


Fig. 8.2: Derived hydrograph of the debris flow, including the released volume and peak discharge (above) obtained from the hourly precipitation records from the Morbegno rain gauge (bottom).

Parameterization of the FLO-2D model was done by calibration, since no independent estimates of the model resistance parameters were available. The calibration of the model was based on a trial-and-error selection of rheological models and parameters, and the adjustment of the input parameters which define the flow resistance. The parameters that reasonably filled the calibration criteria and had the best results were $\tau_y = 950$ Pa and $\eta = 1500$ Pa. These rheological parameters were calculated according to the sediment concentration of the flow (taken into account inside the debris flow hydrograph) and the constant values of $\alpha = 0.0345$ for τ_y and 0.00283 for η ; and $\beta = 20.1$ for τ_y and 23.0 for η , were selected from O'Brien and Julien (1988). The chosen Manning n-values that characterize the roughness of the terrain were $= 0.04 \text{ sm}^{-1/3}$ where the flow was channelled and $0.15 \text{ sm}^{-1/3}$ in the deposition zone. The Manning n-values and the constant value along the channel of $K = 24$ were selected as suggested in the FLO-2D manual.

Figure 8.3 shows the maximum run-out and deposition modelled by FLO-2D and the field-measured extent of the event which underlines the good agreement of the simulation with what actually happened. The modelled accumulation heights show good agreement with the real situation measured in the field. The highest accumulations are reached upslope from the destroyed and heavily damaged buildings, decreasing to the edges of the deposition area. It should be noted that in some cases the flow did not reach some of the lightly damaged structures. This is caused by the fact that FLO-2D does not model the destruction of the building and thus it remains as an obstacle causing the "shadow" effect. Apparent increase of heights of accumulation in the distal parts of the flow is most probably caused by the imprecision in the interpolation of the LIDAR points in the used DEM. Highest values of impact pressure are reached immediately near the start of the apex. Afterwards, the pressures continuously decrease. This is caused by the progressive decrease of accumulation heights and velocities on the alluvial fan (See Section 2.2.1).

8.5 Generation of vulnerability curves

The Selvetta debris flow event represents an important case study due to the fact that both hazard information and damage information is available. The different damage degrees of the buildings make it possible to assess the vulnerability using a vulnerability function that relates the hazard intensity with the degree of damage.

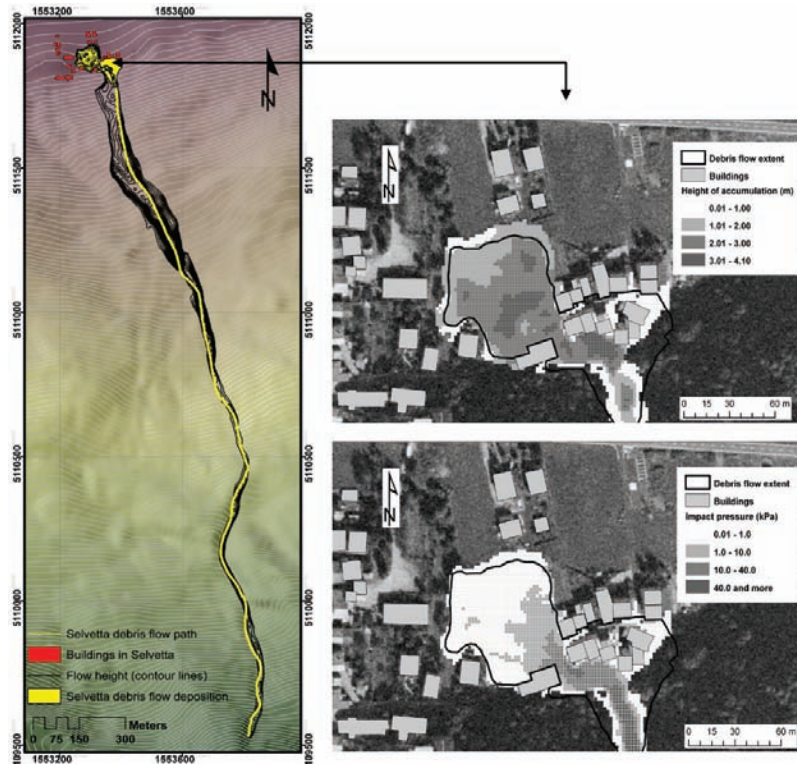


Fig. 8.3: Modelling results of the Selvetta debris flow (left). Comparison of the real and modelled debris flow run-out extent: The maximum heights of the accumulation and maximum impact pressures modelled by the FLO-2D model are shown (right).

8.5.1 Methodology

In this approach, the vulnerability functions were calculated using damage data obtained from the official documents of damage assessment coupled with the information from the modelling outputs. This allows calculation of vulnerability functions using the height of debris accumulation and also the impact pressure. The impact pressure information is widely used in snow avalanche risk assessment but it is not widely applied for debris flows risk calculations.

The damage data was analysed from the RASDA documents (RACcolta Scheda DAnni – Damage Assessment Form), which are mandatory to be drafted within 48 hours after a disaster for claiming compensation funding. For the Selvetta debris flow, these documents were prepared by the engineers of the General Directorate of Civil Protection of the Lombardy Region, and the local police. They estimated the approximate reconstruction value for each building according to building type and size, using the data given in the Housing Prices Index prepared by the Engineers and Architects

of Milan (DEI, 2006). All of the buildings are single to three storey brick masonry and concrete structures. The calculated reconstruction values of the buildings in the studied area range from € 66,000 to € 455,000, while the recorded damage ranges from about € 2,000 to € 290,000 (Table 8.1).

Vulnerability is defined by the fraction between the loss and the individual reconstruction value. This was calculated for each of the thirteen buildings that were affected by the debris flow event (Fig. 8.3). The obtained results were consequently coupled with the modelling results (height of accumulation, impact pressures). This allows developing vulnerability curves that relate the building vulnerability values with the process intensity. The generated physical vulnerability curves can be used as an approach for the estimation of the structural resistance of buildings affected by a debris flow events for similar buildings in other areas.

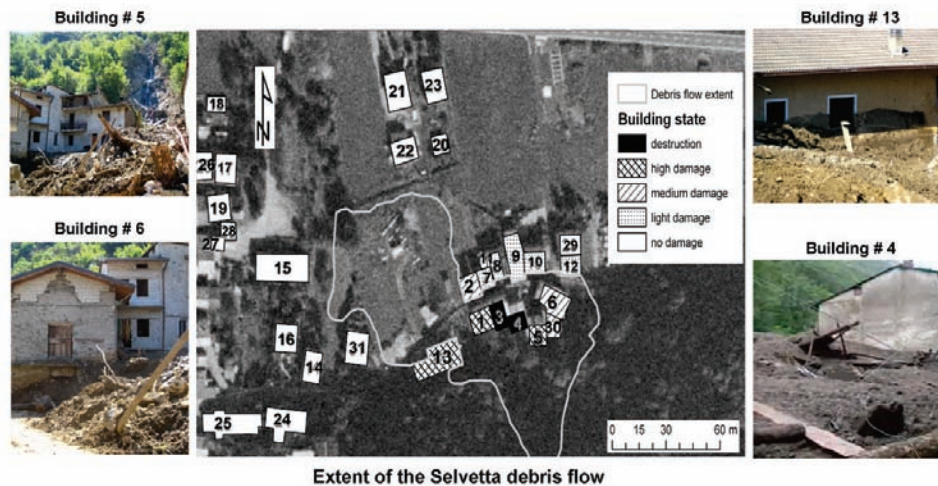


Fig. 8.3: Extent of the Selvetta debris flow damage to buildings. Destruction: $V = 1$; heavy damage: $V = 0.5-1$; medium damage: $V = 0.1-0.5$; light damage: $V = 0-0.1$.

Table 8.1: Values used for the vulnerability functions assessment.

Building No.	Building type	No. of floors	House price index €/m2	Building value (€)	Damage (€)	Vulnerability	Model flow height "H" (m)	Model Max velocity "V" (m/s)	Model Impact pressure "P" (kPa)
1	brick masonry	3	881	426,900	284,251	0.666	2.29	1.37	22.03
2	brick masonry	2	881	129,720	3,000	0.023	0.68	0.29	1.66
3	brick masonry	3	881	256,190	256,190	1.000	3.54	1.48	35.86
4	brick masonry	2	881	66,240	66,240	1.000	3.70	1.46	38.06
5	brick masonry	2	881	216,200	120,100	0.556	2.00	1.25	23.89
6	brick masonry	2	881	146,760	20,000	0.136	0.47	0.40	8.53
7	brick masonry	2	881	105,720	2,000	0.019	0.15	0.26	0.03
8	brick masonry	2	881	108,100	2,100	0.019	0.15	0.26	0.03
9	brick masonry	2	881	170,760	3,000	0.018	0.40	0.29	0.04
10	brick masonry	2	881	129,720	2,000	0.015	0.18	0.29	0.01
12	brick masonry	2	881	108,100	2,400	0.022	0.28	0.25	3.26
13	brick masonry	3	881	455,360	290,167	0.637	2.10	1.33	20.21
30	brick masonry	2	881	170,760	60,000	0.351	1.26	0.94	13.61

8.5.2 Generation of a vulnerability curve using accumulation heights

Values for the accumulation height were extracted for each affected building. For most buildings the maximum and minimum heights of accumulation vary a lot. As a consequence, an average height near building walls oriented towards the flow direction was considered. Figure 8.4 shows the relationship between the vulnerability and deposition height values. This figure indicates that the vulnerability increases with increasing deposition height. We propose to use a logistic function (Eq. 8.2). The calculated function has coefficient of determination (r^2) is 0.99, for intensities between 0 and 3.63 m:

$$v = \frac{1.49 * |h / 2.513|^{-1.938}}{1 + |h / 2.513|^{-1.938}} \quad \text{for } h \leq 3.63 \text{ m} \quad (8.2)$$

$$v = 1 \quad \text{for } h > 3.63 \text{ m}$$

where, v is vulnerability and h is the modelled height of accumulation. From its definition the vulnerability cannot exceed 1, thus for intensities higher than 3.63 m, the vulnerability is equal to 1.

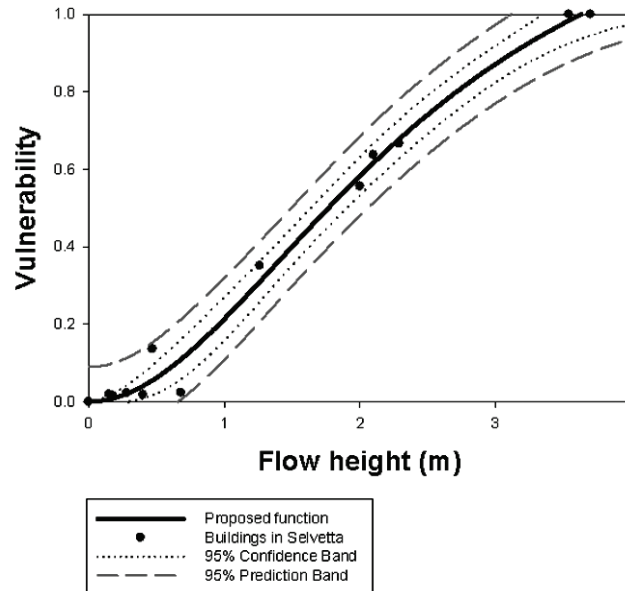


Fig. 8.4: Proposed vulnerability function for accumulation heights obtained from the modelling.

8.5.3 Generation of a vulnerability curve using impact pressures

Impact pressure values were extracted in the same way as accumulation heights considering the values near building walls oriented towards the flow direction. Maximum modelled impact pressures were used to calculate the vulnerability function (Fig. 8.5). A logistic function (Eq. 8.3) which fits the results has a high coefficient of determination (r^2) reaching 0.98 for impact pressures up to 37.49 kPa:

$$v = \frac{1.596 * |P/28.16|^{-1.808}}{1 + |P/28.16|^{-1.808}} \quad \text{for } P \leq 37.49 \text{ kPa} \quad (8.3)$$

$$v = 1 \quad \text{for } P > 37.49 \text{ KPa}$$

where, V is vulnerability and P is the modelled impact pressure. As vulnerability cannot exceed 1, for intensities higher than 37.49 kPa, the vulnerability is equal to 1.

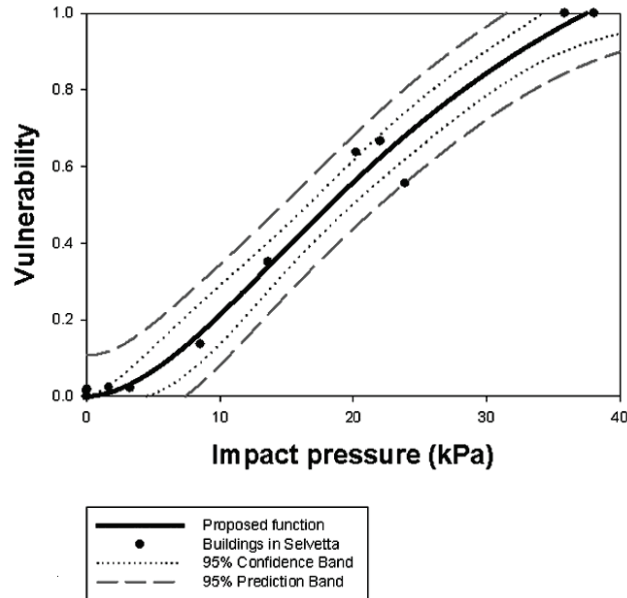


Fig. 8.5 Proposed vulnerability function for modelled impact pressures.

8.5.4 Generation of a vulnerability curve using kinematic viscosity

Using the same approach as described before, a vulnerability function where the momentum of the flow is taken into account is proposed. This function relates the maximum velocity of the flow and its height at the moment of impact with a structure (Fig. 8.6). A logistic function which fits the results has a high coefficient of determination (r^2) reaching 0.98 for the kinematic viscosity up to 5.32 m^2/s (Eq. 8.4):

$$v = \frac{5.38 * |kv / 29.26|^{-0.867}}{1 + |kv / 29.26|^{-0.867}} \quad \text{for } P \leq 5.32 \text{ m}^2/\text{s} \quad (8.4)$$

$$v = 1 \quad \text{for } P > 5.32 \text{ m}^2/\text{s}$$

where, V is vulnerability and kv is the modelled kinematic viscosity ($h*v$). As vulnerability cannot exceed 1, for intensities higher than 5.32 m^2/s , the vulnerability is equal to 1.

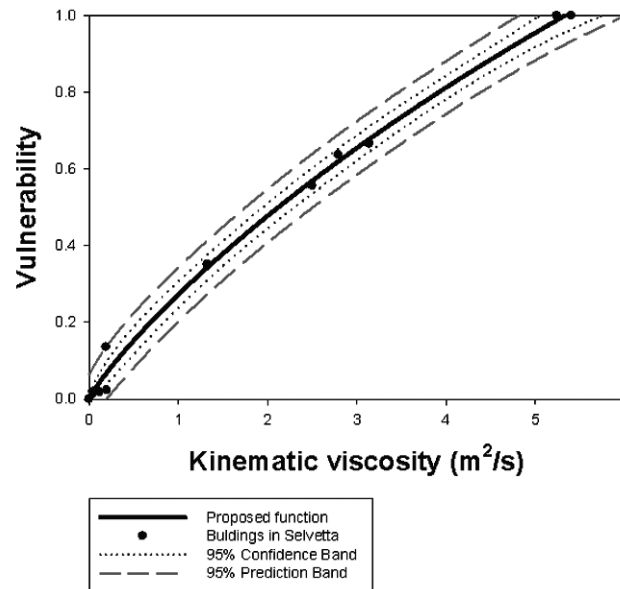


Fig. 8.6: Proposed vulnerability function for kinematic viscosity obtained from the modelling.

8.6 Discussion and conclusions

Three physical vulnerability curves that relate the intensity of debris flows and the economic losses were derived from the Selvetta debris flow event. The event was reconstructed using a numerical approach using a quadratic rheological model. Field geomorphologic investigations were directed towards evidences related to the behaviour of the flow and different sections of the flow path were identified regarding the activity and deposits of the flow during its course (see chapter 2). The FLO-2D model is applied for the back-calculation and the results coincide in a good manner with the real event. The most significant results obtained by the model are the maximum height, maximum velocities, and impact pressures reached by the flow in each cell throughout the entire simulation. These outputs were compared with the resulting damage to the affected buildings. The intensity parameters used for the generation of the vulnerability curves are based on the height of accumulation, maximum velocity, and impact pressures. However, more data is needed to increase the robustness of the curves.

The flow height vulnerability function obtained in this study suggests different vulnerabilities compared to those obtained using the equations given by Fuchs *et al.* (2007) and Akbas *et al.* (2009) (Fig. 8.7). Vulnerability 1.0 (total destruction) is reached at 3.63 m, which is considerably higher than 2.5 m of Akbas *et al.* (2009) and 3.0 m of Fuchs *et al.* (2007). However, the number

of data points in both studies is limited; therefore, it is not possible to reach a robust conclusion about whether the observed discrepancy is the result of the difference in modelling, construction techniques, or a combination of both. The difference may also be partly due to the estimation of the average accumulation height.

The calculated impact pressure vulnerability function was compared to two functions used in snow avalanche risk assessment (Fig. 8.8). Similar behaviour of the function can be noticed in comparison with the linear function of Barbolini *et al.* (2004) which was developed from avalanche data from West Tyrol, Austria. Wilhelm (1998) proposed two different relationships for vulnerabilities higher than 0.5 (Fig. 8.8). The former (a) continues its linear trend and reaches vulnerability 1.0 at 34 kPa. The latter (b) indicates that structures are considered beyond repair in case of impact pressures higher than 25 kPa. The functions of Wilhelm (1998) were calculated from data about reinforced structures impacted by avalanches in Switzerland. Compared to our equation, results from Wilhelm (1998) vary a lot in lower vulnerabilities (up to 0.6). At vulnerability of 0.9 (33 kPa) our function crosses the function of Wilhelm (a) and reaches $V = 1.0$ at 37.49 kPa. This is also different from Barbolini *et al.* (2004), who put vulnerability of 1.0 at impact pressure of 34 kPa similar as Wilhelm, (1998).

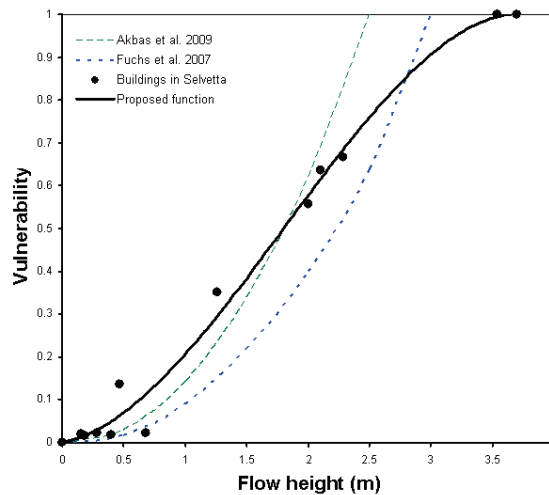


Fig. 8.7: Comparison of the proposed vulnerability functions proposed by Akbas *et al.* (2009), Fuchs *et al.* (2007) and the vulnerability curve calculated from the Selvetta debris flow event in 2008.

The use of numerical modelling for the simulation of the dynamics of debris flows in the generation of vulnerability curves can present an advantage because the intensity outputs (e.g. flow height and pressures) are

straightforward and can be spatially displayed. The results can be overlaid with the elements at risk and detailed physical information can be obtained in a specific area. The approach presented here can be assumed as an approximation of a building resistance to endure a debris flow which is information that is difficult to obtain directly in the field. Another important advantage in the employment of run-out models is that the intensity factors of the hazard can be analyzed in conjunction with the physical vulnerability of the elements at risk making it easier to quantify the suffered consequences. The aim to present different types of vulnerability curves in this analysis is to help the decision makers to decide which type of intensity description fits best to their needs and affected area. As it can be argued that the impact pressure vulnerability function can be used to measure the resistance of the structure itself whereas using a flow height vulnerability function can also take into account the contents inside the structure.

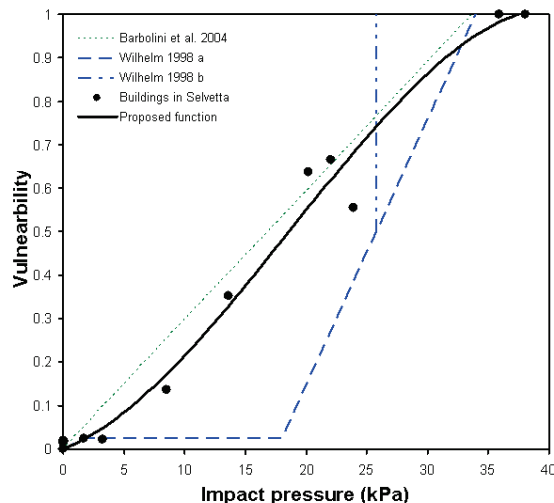


Fig. 8.8: Comparison of the proposed vulnerability functions proposed by Barbolini et al. (2004), Wilhelm (1998), and the vulnerability curve calculated from the Selvetta debris flow event.

However, still shortcomings in our analysis exist and further research needs to be done regarding this. One of the major shortcomings is the insufficient data points regarding the affected elements at risk and the variation in values due to the differences in building quality, state and structural characteristics. This should also be complemented by collecting more data of damaged buildings affected by debris flows, organizing them according to the type and use. This kind of description plays a very important role for the analysis, as in the case where damage to buildings contents will be higher than to the building structure itself (i.e. shops and warehouses). Hence, a better estimation of the reported damage should be assessed based on

structural and non-structural damage. A complete database with detailed information about building type, building use, building characteristics, building quality and state, and the amount of recorded damage (physical and economical) should lead to a better estimation of debris flow vulnerability curves.

There is also a high degree of uncertainty regarding the use of the model to simulate the different processes that played a key role in the evolution of the Selvetta debris flow event. Assumptions and empirical laws were used based on the input requirements of the FLO-2D model and the behaviour of the process (e.g. addition of sediment in the discharge hydrograph to model the entrained material and peak discharge). Uncertainty regarding each modelled process has to be quantified in the future and tried to be reduced. Although dynamic debris flow run-out models has been used frequently in the past to reconstruct past events by calibration of the input parameters, there are still some limitations in the physical description of the parameters defining the used rheology (quadratic).

Nevertheless, the presented approach attempts to propose a quantitative method to estimate the vulnerability of an exposed element to a debris flow that can be independent on the temporal occurrence of the hazard event.

Chapter 9: Use of run-out models for a quantitative risk assessment at a local scale

9.1 Introduction

The analysis of hazard scenarios and their consequences is slowly becoming an accepted and expected practice in landslide risk management (Glade *et al.*, 2005). For this reason, landslide risk investigations have been a major research focus for the international community in recent times (Cruden and Fell, 1997; Dai *et al.*, 2002; Leroi *et al.*, 2005). Several approaches have been applied in the past to analyze landslide risk depending on the scope of the analysis; the scale of the study; the physical context; and social environment (van Westen *et al.*, 2006). These approaches can be classified regarding the way they estimate the risk based on the level of quantification in: -qualitative-, semi-quantitative and quantitative methods (van Westen *et al.*, 2006). Significant attempts have been performed in the past in expressing the hazard frequency and the vulnerability of the elements at risk in numerical terms in order to derive a quantitative risk assessment that can provide a systematic analysis of tangible and intangible consequences of hazard scenarios. Complete examples of quantitative landslide risk assessment are still scarce due to the difficulties in expressing the temporal-spatial and intensity probability of hazard events, and the quantification of vulnerability (van Westen *et al.*, 2006).

Chapter 9 is based on:

Quan Luna, B., Blahut, J., Camera, C., van Westen, C.J., Apuani, T, Jetten, V., Sterlacchini, S., 2012 Quantitative risk assessment for debris flows based on physically-based dynamic run-out modelling. A case study in Tresenda, Northern Italy. (under review in Landslides)

Quan Luna, B., et al., 2010. From deterministic hazard modelling to risk and loss estimation. In: Mountain risks : bringing science to society : proceedings of the Mountain Risks International Conference, Firenze, Italy, 24-26 November 2010 / ed. by J.-P. Malet, T. Glade and N. Casagli. - Strasbourg : CERIG, 2010. ISBN 2-95183317-1-5. pp. 373-380.

The past attempts can also be classified in terms of the applied methodology used for the analysis and by the scale on which the assessment was performed. One example that best illustrates this was done by Castellanos (2008), where he used several methods for landslide risk assessment applicable at different scales. Castellanos (2008) carried out four case studies for landslide risk assessment in Cuba. A division was made based on the different scales and different types of methods used: national scale (1:1,000,000); provincial scale (1:100,000); municipal scale (1:50,000); and the local scale (1:25,000). A quantitative method was used in the local scale where the hazard was assessed with a dynamic run-out model (MassMove2D, explained in chapter 3) based on rheological parameters and the vulnerability values were adopted based on flow heights and the conditions of the buildings. Economic risk values were computed for three different scenarios.

At a regional scale and considering the initiation of the landslides only, Remondo *et al.* (2008) and Zezere *et al.* (2008) made a risk quantification using methods based on statistical analysis. Remondo *et al.*, (2008) carried out a quantitative landslide risk analysis in the Bajo Deba area (northern Spain) obtaining risk maps and tables of economic losses for a 50-year period. The spatial probability was assessed by a statistical landslide susceptibility model that related the past landslides and causal terrain factors. The temporal aspect of the hazard was based on the past landslide behaviour to calculate failure frequency for the coming 50 years. For the vulnerability of the elements at risk, a ratio was determined of the losses and the actual value of the elements affected. The risk was computed for each element considered and indirect losses from the disruption of economic activities were also assessed. Zezere *et al.*, (2008) performed a landslide risk analysis considering direct costs in the area north of Lisbon (Portugal). The hazard was assessed for three different types of slope movement based on statistical susceptibility analysis using past events information and rainfall return period analysis. This allowed the possibility to create different scenarios based on specific return periods. The vulnerability was classified for the three landslide groups based on magnitude, damage levels and literature. Direct costs for buildings and roads were calculated for each triggering scenario.

Focusing on a local scale and based on a comprehensive data base of landslides over several decades, Jaiswal *et al.* (2010) applied a quantitative approach for landslide risk assessment to a road and a railway alignment in the Nilgiri hills in southern India. Historical landslide events were catalogued initiating from cut slopes along the railway and road alignment and grouped into three classes based on the landslide type, volume, scar depth, and run-out distance. Landslide probability of occurrence was obtained using frequency-volume distributions. Hazard scenarios were generated using the

three magnitude classes and six return periods. The assessment of the vulnerability of the road and railway line was based on damage records. Direct specific loss for the alignments (railway line and road), vehicles (trains, buses, lorries, cars and motorbikes) was expressed in monetary value and direct specific loss of life was expressed in annual probability of death. Indirect specific loss derived from the traffic interruption was also evaluated.

Also at a local scale and applying other methods that incorporate the run-out of mass movements in a quantitative risk assessment, Michael-Leiba *et al.* (2003) used the general angle of reach approach for estimating the run-out extension. They carried out a quantitative landslide risk assessment of Cairns, Australia. After a detailed mapping and characterization of the study area, the slope processes (landslide types and modes of occurrence) were defined. They collected information on the process rate from which landslide hazard may be assessed and spatial occurrence relations were made. Rainfall intensity-frequency-duration (IFD) curves were used to assess the mean recurrence intervals of rainfall triggering events. The total volumes of landslides triggered by three rainfall events and their run-out was estimated using the angle of reach approach. The vulnerability was assessed with historical data from past events in the Cairns area and the Australian landslide database. A risk map was created for resident people and buildings and the total risk for roads on hill slopes, for a rainfall event with a 10-year return period was assessed. Bell and Glade in (2004) performed a quantitative risk analysis in NW-Iceland for debris flows and rock falls that focused on the risk posed to persons. They analyzed the hazards based on empirical and process modelling that resulted in specific run-out maps. The hazard zones were determined based on the recurrence interval of the respective processes. For the consequence analysis they defined and attributed vulnerability values to the elements at risk. The factors considered to define the elements at risk were: vulnerability of people and property; number of people; probability of temporal impact; probability of spatial impact; and probability of seasonal occurrence. The respective levels of vulnerability were defined by matrices based on available literature and the authors' past findings. Risk was calculated and portrayed in final risk maps as: object risk to people in buildings and individual risk to people in buildings.

Quantitative run-out modelling for landslide risk assessment is a relatively new research field. The problem in the application of such models is the difficulty in parameterization of the run-out models, and the link between the modelling of initiation susceptibility and the volumes information for the subsequent run-out analysis. Li *et al.* (2010) quantified the risk of cut-slope projects under construction using as example the Shuifu-Maliuwan Highway in the northeast of Yunnan Province in China. Finite element analyses

determined the most dangerous landslide scenario among all construction steps. The slope failure probability was estimated using a Monte Carlo method to simulate the uncertainty and variability of soil and rock parameters. After identifying the failure surface and estimating the volume of the sliding mass, the run-out behaviour of sliding mass were simulated with a dynamic run-out model. Vulnerabilities of the exposed elements at risk were identified by values obtained in the literature. The landslide risk was assessed for three types of consequences: casualties, economic loss and time overrun (extra time for clearing debris and reconstruction).

The above examples show the versatility and functionality of different approaches for quantitative landslide risk assessment. Depending on the availability and quality of the data, a QRA can be successfully applied to different scales, although it is most applicable to large scales (> 1:10,000). A QRA can be carried out for different types of processes, different triggering events, environmental settings, and for different objectives (e.g. cost-benefit analysis of risk reduction measures, emergency preparedness). One of the main advantages of a QRA is that it can be compared with other types of risk that can affect a community and because of its quantitative nature it can be communicated more comprehensibly to the policy and decision makers to be used for risk management strategies.

In this site-specific study which focus on the Tresenda Village in the Italian Alps (See Section 2.2.2), a forward prediction for a quantitative analysis was attempted with an integrated approach using general data and the commercial software FLO-2D. In this chapter, no application of a Monte Carlo method was performed because the choice of the model (FLO-2D) was an important aspect in this part of the research. To apply this methodology, new PDFs of the input parameters used in the quadratic rheology of FLO-2D were needed but was not possible to obtain since there was not a significant amount of cases back-analyzed with this model. However, the use and application of the quadratic rheology was very interesting in this scenario. Other important characteristics of FLO-2D that influenced its selection were: - possibility to model rainfall, water run-off and debris flows run-out in one single model; - it is a well-known, well-documented and established commercial software; - a hydrograph is defined as input; - allows modelling the impact of the flow within obstacles; and – straightforward handling of the outputs.

The presented methodology in this chapter, allowed modelling the hazard scenarios and quantifying the risk in economic terms. Risk curves of the potential monetary loss of buildings were generated for the flow height and the impact pressures of the synthetic debris flows. The hazard scenarios were validated using information about debris flow extent from past events. The

main purpose of this study besides doing a complete risk analysis was to compare the outputs obtained as risk curves, generated from the results of the flow height and the flow impact pressures. Results from both curves reveal a big range of values in the calculated economic losses.

9.2 Methodology

A quantitative risk assessment using run-out modelling was carried out for the Tresenda test site in Valtellina, Italy (See Section 2.2.2). Based on the historical events described in Chapter 2 it was assumed that potential debris flows in the study area will be triggered in areas with steep slopes and high flow accumulation (Blahut *et al.*, 2011). On the basis of the debris flow susceptibility map made by Blahut *et al.* (2010), three potential debris flow sources were selected which were modelled in a dynamic numerical approach to assess the run-out intensity. The methodology used in this analysis is schematically presented in Fig. 9.1. It consisted of several components, such as a detailed analysis of rainfall return periods, the modelling of rainfall-runoff, the analysis of soil samples in the laboratory, the analysis of terrain characteristics, the modelling of the run-out of the debris flows using the FLO-2D software, the application of vulnerability curves (presented in chapter 8) and the generation of risk curves.

9.2.1 Estimation of rainfall return periods

Hourly rainfall data for the period 1980 to 2009 from the range gauge at Castelvetro, located 3 km west from Tresenda, were analysed to calculate the return periods of rainfall events. To calculate the rainfall amounts for return periods of 10, 50, and 100-years a Gumbel Extreme Value Type I distribution was used (Gumbel, 2004). The results for the three return periods are summarized in Table 9.1.

Table 9.1 Calculated precipitation for different return periods and rainfall duration

Duration (h)	10 years return period	50 years return period	100 years return period
	Precipitation (mm)		
1	27	36	40
2	40	53	59
3	46	61	68
6	61	80	89
12	85	113	125
24	112	147	162
48	143	192	212

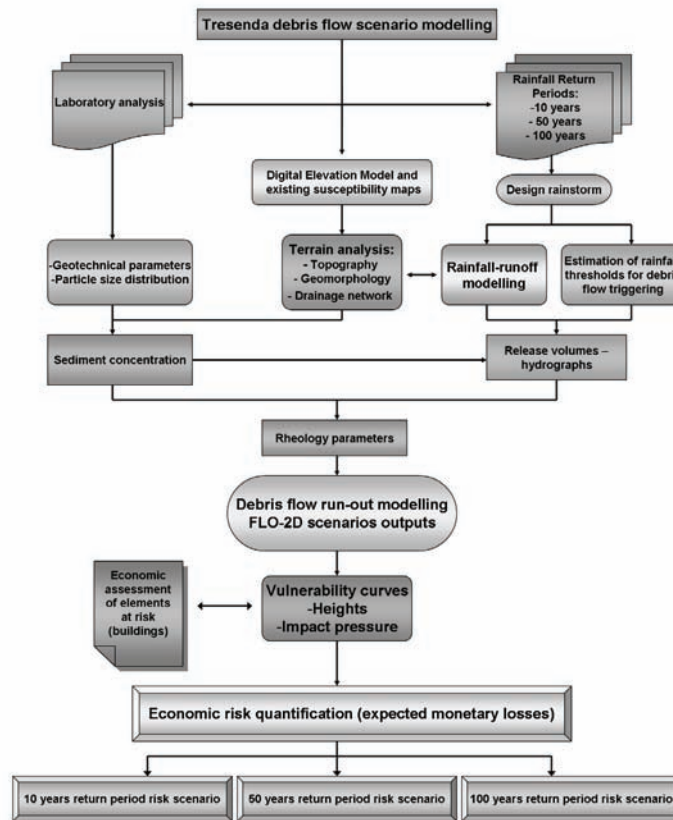


Fig. 9.1: Flowchart of the debris flow risk scenario modelling.

9.2.2 Rainfall-runoff simulation and threshold estimation

A 48-hour rainstorm was modelled using the FLO-2D model, because historical information (Guzzetti *et al.*, 1992; Crosta *et al.*, 2003; Di Trapani, personal communication) showed that past debris flow events in this area were usually caused by rainstorms with this duration. The rainfall during the 48-hour rainstorm was discretized as a cumulative percentage of the total, based on the 1983 rainfall event. The rainstorms were distributed spatially over a grid system and were calculated for all three rainfall return periods.

There are several rainfall thresholds for debris flow initiation available for the study area (Govi *et al.*, 1984; Cancelli and Nova, 1985; Ceriani *et al.*, 1992; Agostoni *et al.*, 1997; Luino *et al.*, 2008). These rainfall thresholds show very similar results, except for the threshold by Luino (2008), which shows much lower values than the others. Although it could be considered as being too conservative, it was used to recognize the minimum initiation time of the debris flows as a worst case scenario. For a 10-year return period this threshold was exceeded after 22.55 hours of modelled rainfall. For a 50-year

return period this threshold was reached after 18.18 hours of rainfall and for the 100-year return period after 17.45 hours (Fig. 9.2).

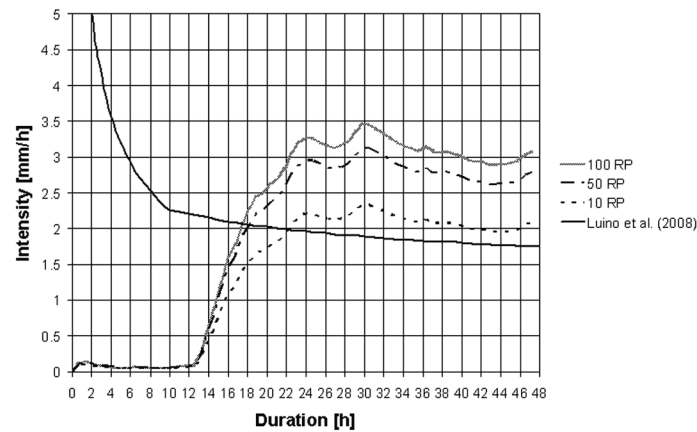


Fig. 9.2: Threshold exceedance according to Luino *et al* (2008) (worst case scenario) of rainfall intensities of 10, 50, and 100-year return periods for the 48-hour modelled rainfall

9.2.3 Laboratory analysis

Soil samples were collected between July 2009 and February 2010 along the slope uphill from Tresenda. Representative samples were selected based on the criteria of the proximity to the initiation and run-out zones. The materials are mixed loose deposits mostly composed of gravel (36%) and sand (44%) with a minor percentage of silt (19%) and less than 1% of clay. According to the ASTM Unified Soil Classification System (USCS), they are classified as GM (silty gravel with sand) or SM (silty sand with gravel), with a uniformity coefficient (CU) between 20 and 90. All samples were taken near the surface and they are relatively rich in organic matter (3.3-7.3%). The bulk unit weight (γ_0), was measured in place by the sand-cone method. The specific weight of the soil (G_s) equals to 27.2 kN/m^3 . Direct shear tests were performed to obtain the peak (c_p ; ϕ_p) and residual values (c_r ; ϕ_r) of the shear strength parameters. It was also possible to calculate porosity (n) and the sediment volumetric concentration (vc). A summary of the measured parameters is given in Table 9.2. These are in agreement with previous laboratory analysis of soils from nearby areas (Cancelli and Nova 1985; Crosta *et al.*, 2003).

Table 9.2: Summary of material characteristics obtained from in situ and laboratory tests

	c_p [kPa]	ϕ_p [°]	c_r [kPa]	ϕ_r [°]	n [m ³ /m ³]	vc [m ³ /m ³]	γ_0 [kN/m ³]	CU [-]
max	18.50	36.50	17.00	36.50	0.52	0.60	16.10	90
mean	10.70	33.80	12.95	30.45	0.46	0.54	14.95	45
min	3.40	27.50	6.60	26.30	0.40	0.48	13.80	20

9.2.4 Debris flow modelling

The debris flows scenarios were modelled with the 2-dimensional depth averaged FLO-2D software which was described in Chapter 3 and Appendix 5. The time when the rain storm exceeded the threshold was registered and discharge hydrographs with constant sediment concentration were produced using the rainfall-runoff component of the FLO-2D software. Release volumes were calculated from an infinite slope stability analysis and the peak discharge of the hydrographs (Table 9.3).

Table 9.3: Release volumes and peaks discharge for the three profiles and return periods

	10 years return period			50 years return period			100 years return period		
	Profile 1	Profile 2	Profile 3	Profile 1	Profile 2	Profile 3	Profile 1	Profile 2	Profile 3
Release volume (m ³)	390	330	425	1162	1142	1251	1424	1410	1518
Peak discharge (m ³ /s)	4.8	4.2	5.1	11.4	11.2	12.1	13.4	13.3	14.1

The same rheological parameters found by calibration for the Selvetta 2008 event (See Chapter 8.4.2) were also applied in the Tresenda scenarios ($\tau_y = 950$ Pa and $\eta = 1500$ Pa). The Manning n -value that characterises the roughness of the terrain was selected as $0.04 \text{ sm}^{1/3}$; this value corresponds to the lower boundary for open ground with no debris (FLO-2D, 2009).

To confirm the choice of the parameters and the results for the three modelled hazard scenarios (10, 50 and 100 years return period), in the three catchments a validation was performed using five historical events from the study area. Three debris flow events from 1983, one from 2000 and one from 2002 were modelled using available rainfall data from the Castelvetro rain gauge. Geotechnical parameters used for the modelling were similar to that used for the hazard scenario preparation. Azzola and Tuia (1983) gave a detailed description of the debris flow event in 1983, which permitted the validation. Figure 9.3 shows the model results together with the outline of the actually affected areas, which show a good agreement. A similar validation was performed for the 2000 and 2002 events.

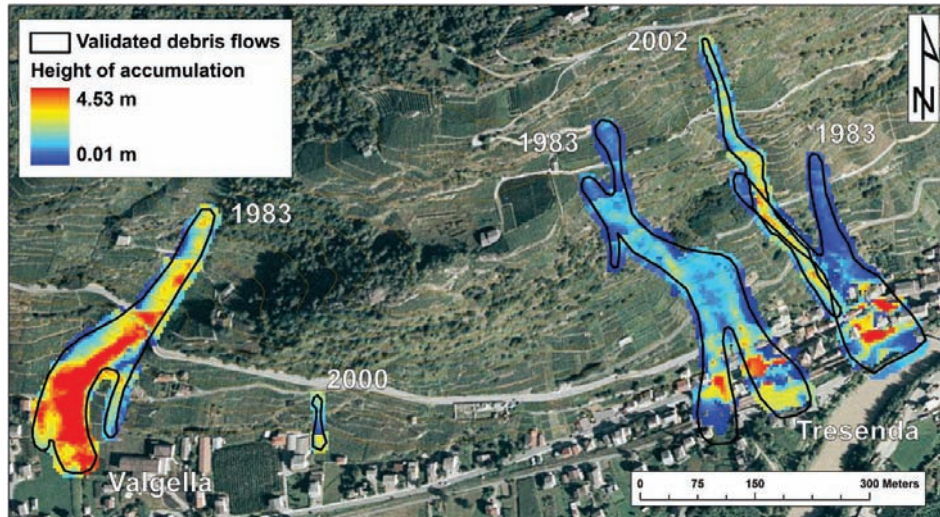


Fig. 9.3: Result from the validation of the 1983, 2000 and 2002 debris flows modelled with geotechnical parameters similar to that used in the hazard scenario preparation.

9.3 Quantitative risk analysis

After validating the results of the debris-flows models for the historical damage sites, the models were applied to the potential debris flow sites (See Fig. 2.11 in Section 2.2.2). The results were subsequently used in combination with building information for the quantification of potential damage to buildings for three return periods using two vulnerability curves (for heights and impact pressures, respectively) described in section 8.5. Direct losses to the buildings were calculated by multiplying the calculated vulnerability by the building value.

9.3.1 Elements at risk in the study area

A total of 111 buildings were mapped in the Tresenda area, of which 57 are located in the areas that might be affected by the potential debris flows. The majority consists of three storey reinforced concrete frame buildings with brick masonry walls. The value of each building was estimated using the construction prices provided by engineers and architects from Milan (DEI 2006). According to them, a construction cost of 801 €/m² corresponds to a single house with 2-3 storeys. The value of the buildings was calculated by multiplying their footprint area from the DB2000 (2003) database by the number of floors and by the reconstruction value per m². The total value of the potentially exposed buildings is almost 14,9 million Euro with values of individual buildings ranging between 0.034 to 1,1 million with an average value of 0.26 million.

Beside the buildings, the state road S.S.38 is located in the potentially affected area between the buildings and the Adda River and minor paved roads are also within the run-out zone. A principal railway line is running along the state road, connecting the provincial capital of Sondrio with Tirano and Switzerland upstream of the Adda River. According to the database of the Registry Office, 173 people are living in the houses within the delimited scenario. The analysis only focused on assessing the economic risk to buildings.

9.3.2 Loss estimation

A total of six hazard scenarios were prepared for each return period. Two maps were generated with accumulation heights and impact pressures, respectively. The results are presented in Figure 9.4 in which also the possible damage to the buildings is shown, resulting from the calculated vulnerability using two vulnerability functions: one for accumulation height and one for impact pressure (described in Chapter 8). Light damage means vulnerability between 0 and 0.1, medium damage represents vulnerability from 0.2-0.4 and heavy damage relates to vulnerabilities between 0.5 and 0.9. Destruction means that vulnerability of 1 was reached.

9.3.3 10-year return period

In the hazard scenario considering the 10-year return period (0.1 annual probability) of the debris flows, 35 buildings are likely to be impacted. After the application of the vulnerability function based on the height of accumulation, 30 buildings will suffer light damage and 5 buildings medium damage. None of the buildings will be destroyed or suffer heavy structural damage. After application of the impact pressure vulnerability function, very different risk pattern appears: 19 buildings will suffer light damage, 10 buildings will have medium damage and 2 buildings will be heavily damaged. Four buildings are likely to be destroyed in this scenario. These results are very different one from another and the question about the appropriate vulnerability function arises. The total direct damage to houses is considerably affected by the use of different vulnerability functions. Considering the height vulnerability function, the direct damage reaches € 561,010. In the case of impact pressure vulnerability function, the total direct monetary loss to the buildings is estimated to € 1,996,425 (355.86% of the first damage estimate). Risk levels span from 0 (no risk) to 8,586 €/year for a single building in case of the height of accumulation vulnerability function and from 0 to 27,780 €/year for a single building in case of the use of impact pressure vulnerability function (Fig. 9.5).

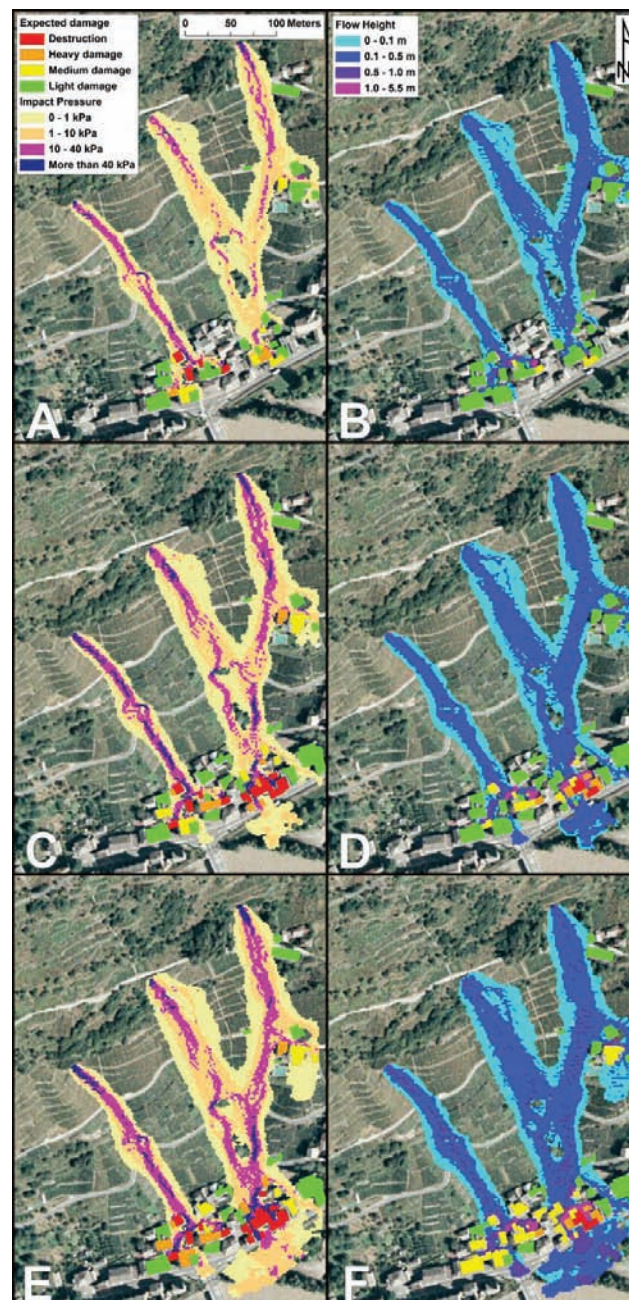


Fig. 9.4: Results of the hazard modelling for the 10, 50 and 100-year return period, showing the calculated degree of damage to the buildings. On the left of the figure the modelled impact pressures of the flow are shown (A= 10 years return period, C= 50 years return period, E= 100 years return period) and on the right of the figure the modelled flow height of flow are shown (B= 10 years return period, D= 50 years return period, F= 100 years return period)

9.3.4 50-year return period

In the 50-year return period hazard scenario (0.02 probability), 49 buildings are likely to be impacted. After the application of the vulnerability function using as an intensity parameter height of accumulation, 32 buildings will suffer light damage, 9 buildings medium damage, and 5 buildings high damage. Three buildings will be completely destroyed. After application of the impact pressure vulnerability function, different results were obtained: 21 buildings will suffer light damage, 7 buildings will have medium damage and 7 buildings will have heavy damage. Fourteen buildings will be probably destroyed. These results show the same pattern as in the case of 10-year return period. However, as this scenario considers much higher debris flow volume, higher accumulations of deposits are reached, resulting in higher expected damage. The total direct damage to houses is considerably affected by the used of the different vulnerability functions as in the case of the previous scenario. Considering the height of accumulation vulnerability function, the direct damage reaches € 2,241,051. In the case of impact pressure vulnerability function, it reaches € 5,044,630. This is 225.10 % of the first damage estimate, which is lower than the previous case. Risk reaches 7,644 €/year for a single building in both cases of risk calculation (Fig. 9.5).

9.3.5 100-year return period

In the 100-year return period hazard scenario (0.01 probability), 49 buildings are likely to be impacted as in the case of the 50-year scenario. After the application of the vulnerability function using as an intensity parameter height of accumulation, 19 buildings will suffer light damage, 22 buildings medium damage, and 4 buildings high damage. Four buildings will be completely destroyed. After application of the impact pressure vulnerability function, higher damage pattern was obtained: 17 buildings will suffer light damage, 6 buildings will have medium damage and 8 buildings will have heavy damage. Eighteen buildings will be probably destroyed. These results shows the same pattern as in the case of 10 and 50-year return periods. The number of affected houses is similar to the previous scenario. Expected damage is, however, much higher. The total direct damage to houses is considerably affected by the use of the different vulnerability functions as in the case of the previous scenarios. Considering the height of accumulation vulnerability function, the direct damage reaches € 3,105,773. In the case of impact pressure vulnerability function application, the total direct monetary loss to the buildings is estimated to € 6,367,743 (205.03%). This estimate is only two times higher than in the case of height of accumulation vulnerability function (much lower than in previous 10 and 50-year return period scenarios). Risk reaches 3,822 €/year for a single building in case of the

accumulation heights vulnerability calculation and 6,003 €/year for a single building in case of the impact pressure use (Fig. 9.5).

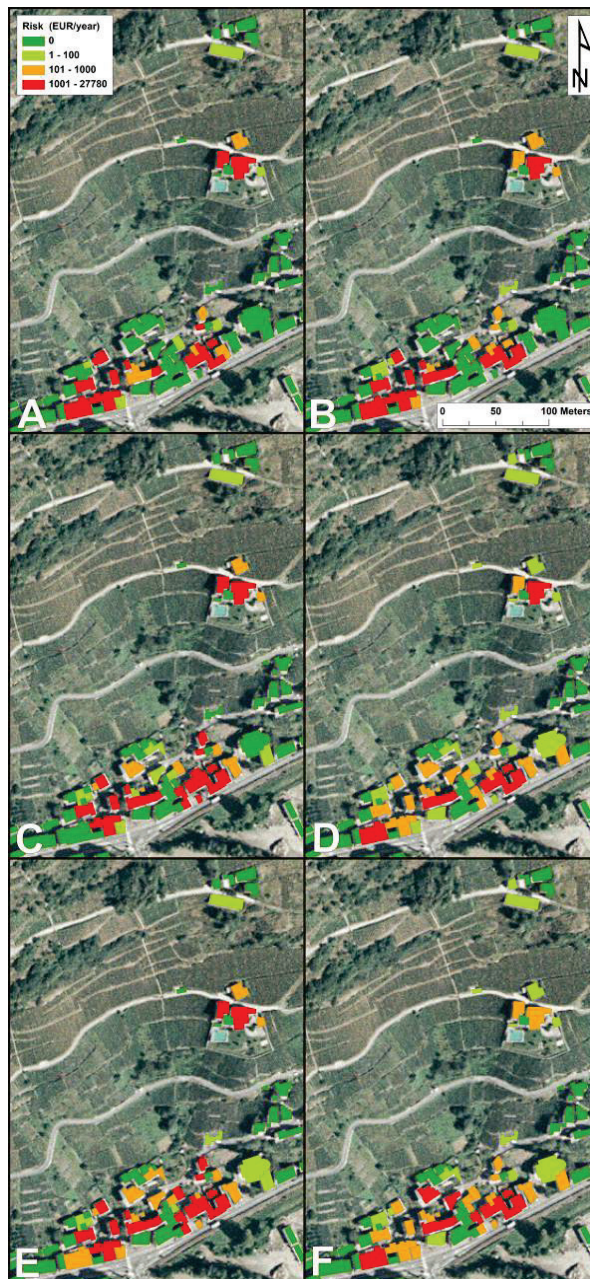


Fig. 9.5: Risk maps for a 10, 50 and 100-year return period debris flows. On the left of the figure the modelled impact pressures of the flow are shown (A= 10 years return period, C= 50 years return period, E= 100 years return period) and on the right of the figure the modelled flow height of flow are shown (B= 10 years return period, D= 50 years return period, F= 100 years return period)

9.4 Results

Six risk scenarios were compared (for the three return periods and for the two vulnerability functions each). The results are summarized in Table 9.4. It can be noted that the total damage estimate is increasing with the debris flows magnitude. There are, however, considerable differences between the estimates for the same return periods. Usage of the impact pressure vulnerability curve gives substantially higher estimates than the application of height of accumulation vulnerability function. This difference is, however, decreasing with the magnitude of the debris flows. The results show that high difference between the two vulnerability curves applied arises when they are used for the prospective damage estimation. The comparison of the results is shown in Figure 9.6. In an ideal case, the comparison between the curves would make a straight line going from 0 to 1. However, the scatter cloud shows the differences for each potentially affected building.

Table 9.4 Summary of the economic losses and the differences between the application of the different types of vulnerability curves

Damage	Vulnerability	10 year Return period		50 year Return period		100 year Return period	
		Nr_B (A.H)	NR_B (I.P.)	Nr_B (A.H)	NR_B (I.P.)	Nr_B (A.H)	NR_B (I.P.)
Light	0-0.1	30	19	32	21	19	17
Medium	0.2-0.5	5	10	9	7	22	6
Heavy	0.6-0.9	0	2	5	7	4	8
Destruction	1	0	4	3	14	4	18
Losses (million €)		0.561	1.996	2.241	5.045	3.106	6.368

Nr_B: number of buildings affected; **F.H.:** Accumulation height; **I.P.:** Impact pressure

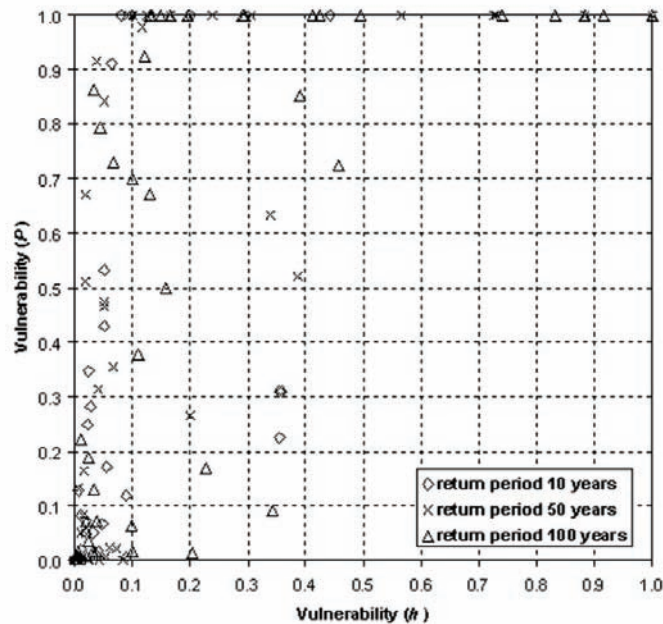


Figure 9.6: Comparison of vulnerability estimates for three return periods using two vulnerability curves -impact pressure (p) and accumulation height (h)

Maximum and minimum values of the laboratory analysis were used and varied as inputs inside the run-out assessment of the hazard (Table 9.2). This variation influenced the peak discharge of the hydrograph and the spatial distribution of the flow as well as the accumulations heights and the impact pressures outputs. The resulting values of the modelled run-out were applied to the 95% confidence intervals of the vulnerability curves to compute the economic risk of each variation. Moreover 95% confidence interval was applied also to the construction unit price of the buildings. As a result, three curves of expected losses were obtained for each flow vulnerability attribute: maximum, average and minimum risk curve for the accumulation of the flow and maximum, average and minimum risk curve for the estimated impact pressure (Fig. 9.7).

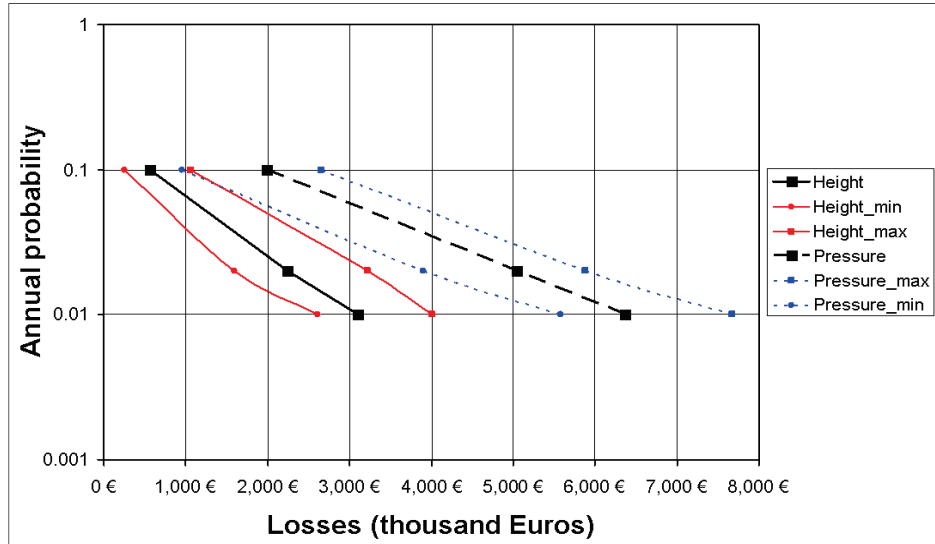


Figure 9.7: Risk curves calculated for the two different vulnerability curves with their maximum and minimum ranges. The range variation accounts for the uncertainty in the run-out modelling parameters and the vulnerability curves.

9.6 Discussion and conclusions

The modelling itself as well as the results allowed expressing the economic risk to exposed buildings in a quantitative way. However, there are still some limitations and uncertainties which need to be addressed. Firstly, it is assumed that the return period of a rainfall, potentially causing a debris flow, is the same as the return period of the resulting debris flow. Other assumptions arise from the modelling itself: DEM resolution, rheological properties acquired in the laboratory and volume estimates are upscaled to the entire area. Other implications arise from the application of vulnerability curves applied to the Tresenda scenario which might seriously affect the resulting damage and risk estimates. It turned out, that the use of impact pressure-based vulnerability curve is giving much higher damage estimates than the accumulation height-based vulnerability curve. In our opinion, the use of impact pressures is more reliable as the direct effects on the stability conditions of the buildings can be assessed on a case-by-case basis considering the particular conditions of each building. The estimated economic value of the building has also important effect on the results, as a similar unit value of buildings, is assumed neglecting its particular conditions and current state. Finally, estimates about the value of the furniture and expenses needed to remove and re-deposit the debris material, or damage to the roads and lifelines are not taken into account.

A quantitative risk assessment should always take these uncertainties into account and it should be possible to express them as a range of risk values.

These estimations should also be included inside the analysis and be well defined. Considering the impact of the uncertainties in this analysis, an evaluation for each scenario proposed (10-50-100 years return period) was implemented. This evaluation incorporated the variation of the laboratory analysis results and the application of the 95% confidence intervals of the proposed vulnerability curves.

Besides the presented limitations, we believe that the approach applied in this analysis is generally applicable to other areas and may give important information to the local stakeholders. Moreover, this allows to assess debris flow hazard and risk in a quantitative way and to calculate prospective direct damage to buildings in the case study area. Direct economic losses to the buildings were estimated, reaching € 561,010 to 6,368,000, depending on the hazard scenario and vulnerability curve used. With the 95% variation of the input parameters the values varies between € 249,339 and 7,672,500 respectively.

The approach proposed in this study may assist local decision makers in determining the nature and magnitude of the expected losses due to a dangerous event. Besides, a preventive knowledge of the prospective physical effects and economic consequences may help to properly allocate financial resources for disaster prevention and for mitigation measures. It is obvious that the approach still has some weak points (e.g. assessment of people's vulnerability). However, beside its limitations, it increases the knowledge about prospective outcomes of future hazards and thus contributes to the protection of the people and their assets.

Chapter 10: Conclusions

This research analyzed different approaches, developments and difficulties regarding the application of dynamic run-out modelling of debris flows, mud flows and landslide hazard at a local and medium scale with a focus on physically-based approaches. Emphasis was given to the problems involved in parameterization of such models, focusing on rheological parameters and entrainment. The main objective of this research was to apply, improve and optimize the use of dynamic run-out models in quantitative risk assessment. The deterministic characteristics of these models and the possibility to obtain direct intensity values make the run-out models an interesting tool to be used in these types of analyses.

The current practice of landslide risk assessments procedures are still performed with a great deal of empiricism and personal judgment needs to be introduced in the definition of important inputs. Consequently, the results are strongly sensitive and influenced by the “knowledge” of the individual that produces the assessment. This work addresses the urgent demand for methods in quantifying the uncertainties in the definition of the various input variables and the resulting effect in a hazard assessment. Applying, evaluating and introducing a probabilistic method to dynamic run-out models were regarded in this research as the main point to address these problems.

Chapter 3 in this research gives a brief overview of the existing methodologies used for a run-out assessment. A special attention in terms of the numerical scheme and input set-up is given to the models used in this research to back calibrate past event and a description of their embedded rheologies are mentioned (MassMov2D, DAN3D, FLO-2D and RAMMS). Except for the FLO-2D model (that uses a quadratic rheology and does not takes into account the entrainment mechanism), all the models used in this research included an entrainment module and the Voellmy rheology which is the resistance law that is the most commonly used for debris flow run-out assessment. For this reason a sensitivity analysis of the Voellmy rheological parameters was performed. During the back analysis and sensitivity tests it was clearly found that the two main parameters used in the Voellmy rheology (“apparent friction” coefficient μ and the “turbulent friction” (drag) coefficient ξ) should be considered conceptual parameters since they do not account for any well-defined physical processes inside the flow regime. The “apparent friction” coefficient μ parameter has a stronger influence on the run-out distance than the “turbulent friction” parameter ξ , but ξ is important for controlling the avalanche speed and thus the pressure exerted on obstacles. The choice and resolution of the initial conditions (e.g. release volume and the terrain topography) plays a decisive role in all the models. Besides this,

all the models used in this research showed consistent results if all parameters were chosen reasonably.

While evaluating the application of dynamic run-out models to past events and back calibrating the rheological parameters, it was observed that the inclusion of the entrainment process in the simulations improved their quality, Entrainment is a key feature mechanism that is able to change significantly the mobility of the flow, the flow volume and its rheology.

In chapter 4 of this research, a 1-D dynamic run-out model that includes entrainment was proposed. This model accounted for the entrainment process based on the generation of excess pore water pressure through undrained loading of the in-situ soil. The model calculates the stability of the in-situ soil based on a safety threshold. Once it is reached, the entrainment process is dominated by the amount of soil capable to erode and the fluctuations of the pore pressures caused by the loading. A back-analysis of the Faucon 2003 debris flow and calibration of the model was carried out and it was observed that the model estimates resemble the flow characteristics measured in the field (heights and velocity) showing the necessity of including entrainment in a run-out model. Based on the importance of the entrainment process and its outcomes, research on debris flows and rapid mass movement dynamics can no longer disregard this phenomenon. However, new uncertainties are added in terms of depths and pore pressure parameters. Although, the entrainment process is not completely yet understood, the proposed model uses measurable geotechnical parameters in an attempt to describe the bulking phenomena of a real event. It is to be noted that the proposed model accounts for one possible entrainment mechanism but other concepts of entrainment have been proposed by other authors, which can be valid under different circumstances. Future works needs to be done to test all these concepts in experiments and possible field circumstances.

It is important to bear in mind that run-out models are conceptual representations of a complex phenomenon. Good models explain the past, make predictions about the future, are cost effective, and easy to use. All models are limited by the assumptions made in constructing them, as the number of assumptions increases, the accuracy and relevance of the model for exploring the phenomenon decreases. Models are also limited by the extent and quality of the input data: with poor quality input, the predictions will be equally unreliable. For this reason it is relevant to assess the uncertainties involved in the parameters used in the run-out models.

In chapter 5, the above mentioned problems were attempted to be approached by collecting a database of back-calibrated run-out modelling

events that allowed expressing the rheological coefficients for a given range of volume, type of movement and environment in terms of a proper probability distribution function. The data was used to determine Probability Density Functions (PDFs) for the rheological parameters of the Voellmy and Bingham models. When using the entirety of values inside the database, a Lognormal distribution was found to be the best description of the samples. In contrast, when the data was classified (into different movement types, initiation volumes and environmental settings) the sampled data followed a Gamma distribution. When both parameters were analyzed together, a Gaussian copula was determined to be the best choice to define the probability density function for both rheological models.

In chapter 6, a random sampling of the Gaussian copula allowed to model 5000 events using a Monte Carlo method. This methodology has been proposed to explicitly incorporate the uncertainties into the analysis and allows an evaluation of the resulting probability distributions of the relevant variables for a debris flow and landslide hazard assessment (intensity values of height and velocity at a well defined point in the terrain or an element at risk). The proposed approach intends to reduce the overall degree of subjectivity which at present is involved in a forward analysis of run-out modelling when no past events or historical data is available. Most limitations in assessing the statistical implication of uncertainties that are usually adopted to address this problem, like conservative estimates of the parameters or sensitivity analysis, might be overcome. It has to be remarked that, regardless of the use of a probabilistic method like the Monte Carlo approach, the probability density function of the rheological parameters can be considered as a useful stand-alone tool that gives insight in the parameter range used to back analyze past events. The use of these distributions can potentially increase the accuracy in the definition of the design of input conditions that have to be introduced in the current modelling applications.

Although run-out models have been successfully applied in local-scale back-analysis studies of historical events, their application in forward modelling is much more complicated. Even more so in smaller scales, and in situations where there are no historical events that can be used in a back-analysis to calibrate the rheological parameters. In Chapter 7 of this research, a medium scale routing model based on the physical description of the rheological properties of the flow was developed, which was provisionally named "AschFlow". The model can be used in a medium-scale debris-flow susceptibility analysis to have a fast assessment with limited spatial information and few historical data of past events. The development of a model containing different modules for simulating flows and landslides processes within the framework of an open source GIS environment, presents a straightforward and flexible approach. The medium scale model is simple

and relatively fast; and the input parameters are relatively easy to define. The model results can be considered as an indicator of areas possibly affected by debris flow events rather than an actual hazard map because of the level of detail. One of the main advantages of this model is the possibility to obtain intensity values as results. From a user perspective the model can be seen as a standalone model which can be utilized for a first assessment of potentially impact areas. The modelled initiation areas as well as the run-out modelling resulted in reasonable outcomes when compared to results from other models.

In chapter 8, physical vulnerability curves (based on impact pressure, height and kinematic viscosity) were generated with an application of a dynamic run-out model where the modelling outcomes and damage data of elements at risk were analyzed. The methodology was implemented using a numerical model (FLO-2D) for the simulation of the impacts of debris flows in the well documented Selvetta test site. The advantage of this method is that the intensity outputs (e.g. flow height and pressures) are straightforward and can be spatially displayed. The calculated impacts were overlaid with the degree of damage of the elements at risk and a detailed damage curve was obtained for a specific area. The benefit of applying run-out models in this type of assessments is that the intensity factors of the hazard can be analyzed in conjunction with the available physical vulnerability curves of the elements at risk, making it easier to quantify the suffered consequences. Risk modellers can decide which type of intensity description best fits their needs in a specific area. The values determined by the vulnerability functions can be used directly in a quantitative risk assessment. However, shortcomings in the methodology still exist and further research needs to be done. A complete database with detailed information about building type, building use, building characteristics, building quality and state, and the amount of recorded damage (physical and economic), should lead to a better estimation of debris flow vulnerability curves. Nevertheless, the presented approach attempted to propose a quantitative method to estimate the vulnerability of an exposed element to a debris flow that can be independent of the temporal occurrence of the hazard event.

In chapter 9, a direct application of a dynamic run-out model to a quantitative risk assessment was also demonstrated in this thesis. Using the proposed vulnerability curves, six risk scenarios were prepared for the Tresenda test site (for three different return periods and for two vulnerability functions). The modelling itself as well as the results allowed expressing the economic risk to exposed buildings in a quantitative way. However, there are still some limitations that are needed to be addressed and future work has to be done regarding this. Uncertainties arise from the modelling itself such as: estimates of released volumes and the run-out modelling. These should be

analyzed using Monte Carlo or a FOSM method. In the case of the run-out model, given the large duration of the simulation runs using the FLO-2D software and problems involved in automating the modelling procedure using batch processing this would be very complicated. Other implications arise from the application of vulnerability curves developed in another test area and applied to the Tresenda scenario which might seriously affect the resulting damage and risk estimates. The use of an impact pressure-based vulnerability curve gives much higher damage estimates than the accumulation height-based vulnerability curve. Estimated economic values of the buildings had also important effect on the results, as similar unit values of buildings, are assumed, neglecting its particular conditions and current state. Finally, estimates about the value of the non-structural elements (building contents) and expenses needed to remove and re-deposit the debris material, or damage to the roads and lifelines are not taken into account. Considering the impact of the uncertainties in this analysis, an evaluation for each scenario proposed (10-50-100 years return period) was implemented. Maximum and minimum values of the laboratory analysis were used and varied as inputs inside the run-out assessment of the hazard. This variation influenced the peak discharge of the hydrograph and the spatial distribution of the flow as well as the accumulations heights and the impact pressures outputs. The resulting values of the modelled run-out were applied to the 95% confidence intervals of the vulnerability curves to compute the economic risk of each variation. As a result, three curves of expected losses were obtained for each flow vulnerability attribute: maximum, average and minimum risk curve for the accumulation of the flow and maximum, average and minimum risk curve for the estimated impact pressure. The presented approach allowed to assess debris flow hazard and risk in a quantitative way and to calculate prospective direct damage to buildings in the case study area. Beside its limitations, it increases the knowledge about prospective outcomes of future hazards and thus contributes to the protection of the people and their assets.

The aim of run-out modelling in practice is to determine the hazard at a given location in order to take protective measures. It has to be noted that nowadays there is not a single model that is able to assess all the aspects of the hazard. Determination of realistic conditions is a serious problem in practical applications that has not received sufficient attention in the past. A practical implementation of the different elements of this research was done to support the validity of the described methodologies and to give encouraging hints for further work.

10.1 Future scope of research and practical needs of dynamic run-out models

Based on the limitations encountered in this research, future work regarding dynamic run-out models and their application to quantitative risk assessment is recommended in the following topics:

- A more accurate and straightforward way to determine realistic and precise initial conditions of the released mass (in a spatial and temporal manner) is needed. Both the initial release volume which is dependant on return periods are usually not well described by many models resulting in imprecise and inaccurate outcomes. The determination of the effect of uncertainties in the initial condition on the results should be assessed in a stochastic way.
- It is evident that at the moment, there is not a model that is able to address all the issues and processes that a landslide and debris flows in movement involves. However special features should be considered such flow regime transitions and the entrainment. These processes should be described appropriately inside the models.
- It is of utmost importance that organizations responsible for mountain hazard assessment and mitigation make extensive analysis of historical events, and try to obtain information on spatial extend, height, velocity, initiation mechanism, initial volume, entrainment and damage. This historical information is crucial in order to be able to better estimate run-out hazards and risk in future.
- The database of rheological parameters should be made publicly available and other authors should be able to add new data. It is recommended to expand and increase the amount of back analyzed past events inside the database collected during this research. This will increase the amount of data inside the selected characteristics constraints (environment, volume and type of movement) which will improve the generation of new probability density functions or give a higher confidence in the created one.
- In this research based on the Monte Carlo method, the probability density functions of intensities outputs were obtained at several points in the flow track. This enables to estimate the probability of a certain height or a certain velocity to be reached at a certain location where an element at risk might be or is located. This work should be expanded in future in order that the results can be displayed spatially as maps. A spatial

distribution of the intensities probabilities should be linked later to the temporality of the event for a hazard assessment.

- From the dynamic models evaluated in this research, either simple or complex, all of them had important features that can describe the movement of the flow with different types of solutions and approaches. Some processes are better described in some models while lacking others processes. This research encourages the development of simple, understandable and user friendly models which can be validated and easy to parameterize (with well known rheological models). These models can play an important role in a quantitative risk assessment as they allow rapid scanning of the relevant potential hazard locations which later on can be introduced into more advanced models for detailed simulations of selected scenarios.
- In this research the interaction between different types of hazards (e.g. landslides blocking valleys leading to lake break out flooding) was not taken into account. More research is needed to understand the interaction between hazards, and how to properly make a multi-hazard risk assessment
- Based on the proposed methodology in this research, the generation of a diversity of vulnerability functions established for the different characteristics of the elements at risk and their uncertainties is recommended. Data collection should include enough data points regarding the affected elements at risk and the variation in values due to the differences in building quality, state, and structural characteristics. This should also be complimented by collecting more data of damaged buildings affected by debris flows, organizing them according to the type and use. This kind of description plays a very important role, as in the case where damage to buildings contents will be higher than to the building structure itself (i.e. shops and warehouses). Hence, a better estimation of the reported damage should be assessed based on structural and non-structural damage.

This research aimed at contributing to an improvement of the existing methodologies for assessing and quantifying risk in landslide- and debris flow-prone areas with the application of dynamic run-out models. This contribution is hopefully translated to a reduction of the loss of lives due to natural disasters in mountainous areas.

Conclusions

References

- Agostoni, S., Laffi, R., Sciesa, E., 1997. Centri abitati instabili della provincia di Sondrio. CNR-GNDCI, Milano, 59 pp. + annexes.
- Akbas, S.O., Blahut, J., Sterlacchini, S., 2009. Critical assessment of existing physical vulnerability estimation approaches for debris flows. In: Malet, J.-P., Remaitre, A., Bogaard, T. (Eds.): Proceedings of the International Conference "Landslide Processes", Strasbourg, France, 229-233.
- Alcantara-Ayala, I., 2002. Geomorphology, natural hazards, vulnerability and prevention of natural disasters in developing countries. *Geomorphology*, 47(2-4): 107-124.
- Aleotti, P., Ceriani, M., Fossati, D., Polloni, G., Pozza, F. 2004. I fenomeni franosi connessi alle precipitazioni del Novembre 2002 in Valtellina (Soil slips and debris flows triggered by the november 2002 storms in Valtellina, Italian Central Alps). International Symposium Interpraevent 2004, Riva/Trient, Italy, 11-20.
- Allen, S.K., Schneider, D., Owens, I.F., 2009. First approaches towards modelling glacial hazards in the Mount Cook region of New Zealand's Southern Alps. *Nat. Hazards Earth Syst. Sci.*, 9, pp. 481-499.
- Ancey, C., 2005. Monte Carlo calibration of avalanches described as Coulomb fluid flows. *Phil. Trans. R. Soc. A*, 363, 1529–1550, doi:doi:10.1098/rsta.2005.1593.
- Ancey, C., Gervasoni, C., Meunier, M., 2004. Computing extreme avalanches. *Cold Regions Science and Technology*, 39, 161– 180, doi:10.1016/j.coldregions.2004.04.004.
- Antiano, J.L. and Gosse, J., 2009. Large rockslides in the Southern Central Andes of Chile (32-34.5°S): Tectonic control and significance for Quaternary landscape evolution. *Geomorphology* 104 (3-4):117-133.
- Armento, M.C., Genevois, R., Tecca, P.R., 2008. Comparison of numerical models of two debris flows in the Cortina d' Ampezzo area, Dolomites, Italy. *Landslides* 5, pp. 143-150.
- Azzola, M., Tuia, T., 1983. Osservazione sui fenomeni franosi che hanno interessato i vigneti terrazzati a monte di Tresenda nel maggio 1983. *Geologia Tecnica*, 4:23-35.
- Barbolini, M., Cappabianca, F., Sailer, R., 2004. Empirical estimate of vulnerability relations for use in snow avalanche risk assessment. In: Brebbia, C. (Ed.): Risk analysis IV, WIT Press, Southampton, 533-542.
- Barbolini, M., Cappabianca, F., Savi, F., 2004. Risk assessment in avalanche-prone areas. *Annals of Glaciology* 38, 115–122.
- Barbolini, M., Biancardi, A., Cappabianca, F., Natale, L., Pagliardi, M., 2005. Laboratory study of erosion processes in snow avalanches. *Cold Regions Science and Technology* 43, pp. 1– 9.
- Bartelt, P., Salm, B., & Gruber, U., 1999. Calculating dense-snow avalanche runout using a Voellmy-fluid model with active/passive longitudinal straining. *Journal of Glaciology*, 45(150), 242-254.
- Beguieria, S., van Asch, Th.W.J., Malet, J.-P., Grondahl, S., 2009. A GIS-based numerical model for simulating the kinematics of mud and debris flows over complex terrain. *Nat. Hazards and Earth Syst. Sci.*, 9, pp. 1897-1909.

- Bell, R. and Glade, T., 2004. Quantitative risk analysis for landslides – Examples from Bildudalur, NW-Iceland. *Natural Hazards and Earth System Sciences*, 4: 117-131.
- Bertolo, P. and Bottino, G., 2008. Debris-flow event in the Frangerello Stream-Susa Valley (Italy)—calibration of numerical models for the back analysis of the 16 October, 2000 rainstorm. *Landslides*, 5(1): 19-30.
- Bertolo, P. and Wieczorek, G.F., 2005. Calibration of numerical models for small debris flows in Yosemite Valley, California, USA. *Nat. Hazards Earth Syst. Sci.*, 5, 993-1001.
- Bertrand, D., Naaim, M., Brun, M., 2010. Physical vulnerability of reinforced concrete buildings impacted by snow avalanches, *Nat. Hazards Earth Syst. Sci.*, 10, 1531-1545, doi:10.5194/nhess-10-1531-2010.
- Bisantino, T., Fischer, P., Gentile, F., 2010. Rheological characteristics of debris-flow material in South-Gargano watersheds. *Natural Hazards*, 54(2): 209-223.
- Blahut, J., van Westen, C.J., Sterlacchini, S., 2010a. Analysis of landslide inventories for accurate prediction of debris-flow source areas. *Geomorphology*, 119(1-2): 36-51.
- Blahut, J., Horton, P., Sterlacchini, S., Jaboyedoff, M., 2010b. Debris flow hazard modelling on medium scale: Valtellina di Tirano, Italy, *Nat. Hazards Earth Syst. Sci.*, 10, 2379-2390, doi:10.5194/nhess-10-2379-2010.
- Blahut, J., Poretti, I., De Amicis, M. and Sterlacchini, S., 2011. Database of geo-hydrological disasters for civil protection purposes. *Natural Hazards*, 60(3): 1065-1083.
- Blanc, T., 2008. Numerical simulation of debris flows with the 2D – SPH depth integrated model. *Memoire de Fin de D'études. F.I.F - AgroParisTech ENGREF.*
- Boniello, M.A., Calligaris, C., Lapasin, R., Zini, L., 2010. Rheological investigation and simulation of a debris-flow event in the Fella watershed, *Nat. Hazards Earth Syst. Sci.*, 10, 989-997, doi:10.5194/nhess-10-989-2010.
- Bouchut, F., Fernandez-Nieto, E.D., Mangeney, A., Lagree, P.-Y., 2008. On new erosion models of Savage-Hutter type for avalanches. *Acta Mech.* 199, pp. 181-208.
- Bozhinskiy, A.N., 2004. The Monte Carlo simulation of avalanche-type processes. *Annals of Glaciology*, 38(1): 351-356.
- Brunetti, M. T., Guzzetti, F., Rossi, M., 2009. Probability distributions of landslide volumes, *Nonlin. Processes Geo-phys.*, 16, 179-188, doi:10.5194/npg-16-179-2009.
- Brunetti M.T., Peruccacci, S., Rossi, M., Luciani, S., Valigi, D., Guzzetti, F., 2010. Rainfall thresholds for the possible occurrence of landslides in Italy. *Nat Hazards Earth Syst Sci* 10 (3):447-458.
- Calvo, B. and Savi, F., 2008. A real-world application of Monte Carlo procedure for debris flow risk assessment. *Computers & Geosciences*, 35(5), 967-977.
- Cancelli, A. and Nova, R., 1985. Landslides in soil debris cover triggered by rainstorms in Valtellina (Central Alps – Italy). In: *Proceedings of 4th International Conference and Field Workshop on Landslides*. The Japan Geological Society, Tokyo, pp. 267–272.

- Cannon, S.H. and Savage, W.Z., 1988. A mass change model for debris flow. *The Journal of Geology* 96, pp. 221–227.
- Cappabianca, F., Barbolini, M. and Natale, L., 2008. Snow avalanche risk assessment and mapping: A new method based on a combination of statistical analysis, avalanche dynamics simulation and empirically-based vulnerability relations integrated in a GIS platform. *Cold Regions Science and Technology*, 54(3), 193-205.
- CARG project, 1992. The New Italian 1:50 000 Geological Map, National Geological Survey, Rome, Italy.
- Castellanos Abella, E.A., 2008. Local landslide risk assessment. Multi-scale landslide risk assessment in Cuba. Utrecht, Utrecht University, ITC Dissertation 154, 193-226.
- Cepeda, J., 2007. The 2005 Tate's Cairn debris flow: Back-analysis, forward predictions and a sensitivity analysis. In: *The 2007 International Forum on Landslide Disaster Management*. Ho & Li (Eds.), ISBN 978-962-7619-30-7.
- Cepeda, J., 2009. Characterisation and risk management of rainfall-induced landslides. PhD Thesis.. University of Oslo.
- Ceriani, M., Lauzi, S., Padovan, N., 1992. Rainfall and landslides in the Alpine area of Lombardia Region, Central Alps, Italy. In: *Proceedings of the Internationales Symposium Interpraevent*. Bern, 2: 9-20.
- Cetina, M., Rajar, R., Hojnik, T., Zakrajsek, M., Krzyk, M., Mikos, M., 2006. Case study: Numerical simulation of debris flows below Stoze, Slovenia. *Journal of Hydraulic Engineering*, Vol. 132, No. 2, pp. 121-130.
- Cesca, M., 2008, Studi dei meccanismi di diposizione dei debris flow: Integrazioni tra esperienze di laboratorio, analisi di campo e modellazione numeriche. PhD Thesis. University of Padova.
- Chen, H. and Lee, C.F., 2000. Numerical simulation of debris flows. *Canadian Geotechnical Journal* 37, pp. 146–160.
- Chen, H. and Lee, C.F., 2003. A dynamic model for rainfall induced landslides on natural slopes. – *Geomorphology*, 51, pp. 269-288.
- Chen, J. and Lee, C.F., 2007. Landslide mobility analysis using Madflow. In: *The 2007 International Forum on Landslide Disaster Management*. Ho & Li (Eds.), ISBN 978-962-7619-30-7.
- Chen, H., Crosta, G.B., Lee, C.F., 2006. Erosional effects on runout of fast landslides, debris flows and avalanches: a numerical investigation. *Geotechnique* 56, No. 5, pp. 305–322.
- Chen, N. S., Yue, Z. Q., Cui, P., Li, Z. L., 2007. A rational method for estimating maximum discharge of a landslide-induced debris flow: A case study from southwestern China, *Geomorphology*, 84(1–2), 44–58, 2007.
- Christen, M., Bartlett, P., Kowalski, J., Stoffel, L., 2009. Calculation of dense snow avalanches in three-dimensional terrain with the numerical simulation program RAMMS. RAMMS User manual.
- Christen, M., Kowalski, J., Bartelt, P., 2010. RAMMS: Numerical simulation of dense snow avalanches in three-dimensional terrain. *Cold Regions Science and Technology* 63, pp. 1-14.
- Coe, J.A., Michael, J.A., Crovelli, R.A., Savage, W.Z., Laprade, W.T., Nashem, W.D., 2004. Probabilistic assessment of precipitation triggered landslides using historical records of landslide occurrence, Seattle, Washington. – *Environ. Eng. Geoscience*, 10, 103-122.

- Contreras, S.M. and Davies, T.R.H. 2000. Coarse-Grained Debris-Flows: Hysteresis and Time-Dependent Rheology. *Journal of Hydraulic Engineering*, 126(12): 938-941.
- Conway, S.J., Decaulne, A., Balme, M.R., Murray, J.B. and Towner, M.C., 2010. A new approach to estimating hazard posed by debris flows in the Westfjords of Iceland. *Geomorphology*, 114(4): 556-572.
- Corominas, J., 1996. The angle of reach as a mobility index for small and large landslides. *Canadian Geotechnical Journal* 33, pp. 260–271.
- Coussot P., 1997. *Mudflow Rheology and Dynamics*. IAHR monograph. Balkema: Rotterdam; 260.
- Coussot, P. and Piau, J.-M., 1995. A large-scale field coaxial cylinder rheometer for the study of the rheology of natural coarse suspensions. *Journal of Rheology*, 39(1): 105-124.
- Coussot, P., Proust, S.B., Ancey, C., 1996. Rheological interpretation of deposits of yield stress fluids. *Journal of Non-Newtonian Fluid Mechanics*, 66(1): 55-70.
- Crosta, G., 1990. A study of slope movements caused by heavy rainfall in Valtellina (Italy – July 1987). In: Cancelli, A. (Ed.): *Proceedings of ALPS90, Alpine Landslide Practical Seminar – 6th ICFL International Conference and Field Workshop on Landslides*, University of Milano, Milano, 247-258.
- Crosta, G., Marchetti, M., Guzzetti, F., Reichenbach, P., 1990. Morphological classification of debris-flow processes in South-Central Alps (Italy). *Proceedings of the 6th International IAEG Congress, Amsterdam*, 1565-1572.
- Crosta, G.B., Dal Negro, P., Frattini, P., 2003. Soil slips and debris flows on terraced slopes. *Natural Hazard and Earth System Sciences*, 3, 31-42.
- Crosta, G.B., Imposimato, S., Roddeman, D., 2003. Numerical modelling of large landslides stability and runout. *Nat. Hazards Earth Syst. Sci.* 3(6), pp. 523-538.
- Crosta, G.B., Fratinni, P., Fugazza, F., Caluzzi, L., Chen, J., 2005. Cost-benefit analysis for debris avalanche risk management. In: Hungr, O., Fell, R., Couture, R., Eberhardt, E. (Eds.): *Landslide Risk Management*. Taylor & Francis, London, 533-541.
- Crosta, G.B., Imposimato, S., Roddeman, D., 2009. Numerical modelling of entrainment-deposition in rock and debris-avalanches. *Engineering Geology*, 109 (1-2), pp. 135-145.
- Cruden, D., and Fell, R., (eds) 1997. *Landslide risk assessment*. Proc. of the International Workshop on Landslide Risk. Honolulu, USA, 19-21 February 1997, XI + 371 pp. ISBN: 90 5410 9149. A. Balkema.
- D'Ambrosio, D., Di Gregorio, S., Iovine, G., 2003. "Simulating debris flows through a hexagonal cellular automata: SCIDDICA S3-hex", *Natural Hazards and Earth System Sciences*, vol. 3, pp. 545-559.
- Dai, F.C., Lee C.F., Ngai Y.Y., 2002. Landslide risk assessment and management: an overview, *Engineering Geology*, Volume 64, Issue 1, Pages 65-87.
- DB2000, 2003. Database of the CM Valtellina di Tirano mapped at 1:2,000 scale. CM Valtellina di Tirano. CD-ROM. Available at: <http://www.cmtirano.so.it/sistemainformativo.php>

- De Blasio, F.V., Breien, H., Elverhøi, A., 2011. Modelling a cohesive-frictional debris flow: an experimental, theoretical, and field-based study. *Earth Surface Processes and Landforms*, 36(6): 753-766.
- DEI: Prezzi Tipologie Edilizie, 2006. DEI Tipografia del Genio Civile. CD-ROM., 2006.
- De Joode, A. and van Steijn, H., 2003. PROMOTOR-df: a GIS-based simulation model for debris flow hazard prediction. In: Rickenmann, D., Chen, C.L. (Eds.), "Debris-Flow Hazards Mitigation: Mechanics, Prediction, and Assessment," Proceedings 3rd International DFHM Conference, Davos, Switzerland, September 10–12, 2003. Millpress, Rotterdam, pp. 1173-1184.
- Deline, P., 2009. Interactions between rock avalanches and glaciers in the Mont Blanc massif during the late Holocene. *Quaternary Science Reviews*, Vol. 28, Issues 11-12, pp. 1070-1083.
- Denlinger, R.P. and Iverson, R.M., 2001, Flow of variably fluidized granular masses across three-dimensional terrain: 2. Numerical predictions and experimental tests, *Journal of Geophysical Research*, v. 106, no. B1, 553-566.
- Denlinger, R.P., and Iverson, R.M., 2004, Granular avalanches across irregular three-dimensional terrain: 1. theory and computation, *Journal of Geophysical Research*, v. 109, F01014, doi: 10.1029/2003JF000085. 14 p.
- Devoli, G., De Blasio, F., Elverhøi, A., Høeg, K., 2009. Statistical Analysis of Landslide Events in Central America and their Run-out Distance. *Geotechnical and Geological Engineering*, 27(1): 23-42.
- Douglas, J., 2007. Physical vulnerability modelling in natural hazard risk assessment. *Natural Hazards and Earth System Sciences*, 7, 283-288.
- DUSAF Project, 2003. Destinazione d'Uso dei Suoli Agricoli e Forestali, Lombardy Region, Milano, Italy.
- Duzgun, H.S.B. and Lacasse, S., 2005. Vulnerability and acceptable risk in integrated risk assessment framework. In: Hungr O, Fell R, Couture R, Eberhardt E (eds). *Landslide risk management*. Balkema, Rotterdam, 505–515.
- Egashira, S., Honda, N., Itoh, T., 2001 Experimental Study on the Entrainment of Bed Material into Debris Flow. *Phys. Chem. Earth (C)*, Vol. 26, No. 9, pp. 645-650.
- Eglit, M. and Demidov, K.S., 2005. Mathematical modeling of snow entrainment in avalanche motion. *Cold Regions Science and Technology* 43, pp.10– 23.
- EM-DAT: The CRED International Disaster Database, 2011. Natural Disasters Trends. From <http://www.emdat.be/natural-disasters-trends>
- Evans, S. G., 1989. "Rock avalanche run-up record". *Nature (London)* Vol. 340, pp. 271.
- Evans, S.G., Hungr, O., Enegren, E.G., 1994. "The Avalanche Lake rock avalanche, Mackenzie Mountains, Northwest Territories, Canada: description, dating, and dynamics". *Canadian Geotechnical Journal* Vol. 31 No. 5, pp. 749-768.
- Fell, R., 1994. Landslide risk assessment and acceptable risk. *Canadian Geotechnical Journal*, 31, 261-272.

- Fell, R. and Hartford, D., 1997. Landslide risk management. In: D. Cruden and R. Fell, Editors, *Landslide Risk Assessment*, Balkema, Rotterdam, pp. 51–109.
- Fell, R., Ho, K.K.S., Lacasse, S., Leroi, E., 2005. A framework for landslide risk assessment and management. . In: Hungr, O., Fell, R., Couture, R., Eberhardt, E. (Eds.): *Landslide Risk Management*. Taylor & Francis, London, 533-541.
- Fell, R., Corominas, J., Bonnard, C., Cascini, L., Leroi, E., Savage, W.Z., 2008. Guidelines for landslide susceptibility, hazard and risk zoning for land use planning. *Engineering Geology*, 102, 85-98.
- Flageollet, J.-C., Maquaire, O., Martin, B., Weber, D., 1999. Landslides and climatic conditions in the Barcelonnette and Vars basins (Southern French Alps, France). *Geomorphology*, 30: 65-78.
- FLO-2D: Reference manual, 2009. Available at: <http://www.flo-2d.com>.
- Froese, C.R., Jaboyedoff, M., Pedrazzini, A., Hungr, O., Moreno, F., 2009. Hazard mapping for the eastern face of Turtle Mountain, adjacent to the Frank Slide, Alberta Canada. In: J.P Malet, A, Remaitre, T. Boogard (eds), *Proceedings of the International Conference 'Landslide Processes, a Tribute to Theo van Asch'* Strasbourg, France.
- Fuchs, S., Heiss, K., Hübl, J., 2007. Towards an empirical vulnerability function for use in debris flow risk assessment. *Natural Hazards and Earth System Sciences*, 7, pp. 495-506.
- Galas, S., Dalbey, K., Kumar, D, Sheridan, M., Patra, A., 2007. Benchmarking titan2d mass flow model against a sand flow experiment and the 1903 frank slide. In: *The 2007 International Forum On Landslide Disaster Management*. Ho & Li (Eds.), ISBN 978-962-7619-30-7.
- Galli, M. and Guzzetti, F., 2007. Landslide Vulnerability Criteria: A Case Study from Umbria, Central Italy. *Environmental Management*, 40(4), 649-665.
- Gamma, P., 2000. DF-Walk: Ein Murgang-Simulationsprogramm zur Gefahrenzonierung (*Geographica Bernensia*, G66). University of Bern (in German).
- Gauer, P. and Issler, D., 2004. Possible erosion mechanisms in snow avalanches. *Annals of Glaciology*, Volume 38, Number 1, pp. 384-392.
- Gauer, P., Lied, K. and Kristensen, K., 2009. Analysis of avalanche measurements out of the runout area of NGI's full-scale test-site Ryggfonn. *Cold Regions Science and Technology*, 57(1): 1-6.
- GeoIFFI, 2006. The Regional Inventory (1:10.000) of Landslides and Hydrogeological Events, Lombardy Region, Italy, available at: <http://www.cartografia.regione.lombardia.it/GeoIFFI>
- Giacomelli, L., 1987. Speciale Valtellina 1987: Cronaca, storia, commenti. *Notiziario della Banca Popolare di Sondrio*, No. 45, Bergamo, 227 p
- Glade, T., 2003. Vulnerability assessment in landslide risk analysis. *Die Erde*, 134, 123-146.
- Glade, T., 2005. Linking debris-flow hazard assessment with geomorphology. *Geomorphology*, 66, 189–213.
- Glade, T., Anderson, M., Crozier, M.J. (eds). 2005. *Landslide Hazard and Risk*. John Wiley & Sons Ltd, Chichester, UK.
- Govi, M., Mortara, G., Sorzana, P., 1984. Eventi idrologici e frane. *Geologia Applicata e Idrogeologia*, XCVIII, 3 p.

- Grigorian, S.S., and Ostroumov, A.V., 1977. The Mathematical Model for Slope Processes of Avalanche Type (in Russian). Institute for Mechanics, Moscow State University, Moscow, Russia. Scientific report, 1955.
- Gumbel, E.J., 2004. Statistics of extremes. Reprint of the 1958 edition, Dover Publications, Mineola, 375 p.
- Guthrie, R.H., Evans, S.G., Catane, S., Zarco, M., Saturay, R., 2009. The 17 February 2006 rock slide-debris avalanche at Guinsaogon Philippines: a synthesis. *Bulletin of Engineering Geology and the Environment*. Vol. 68 No. 2, pp. 201-213.
- Guzzetti, F., Crosta, G., Marchetti, M., Reichenbach, P., 1992. Debris flows triggered by the July, 17–19, 1987 storm in the Valtellina area (Northern Italy). *International Symposium Interpraevent 1992*, Bern, Switzerland, pp. 193-203.
- Guzzetti F, Malamud B.D., Turcotte D.L., Reichenbach P., 2002. Power-law correlations of landslide areas in central Italy. *Earth and Planetary Science Letters* 195 (3- 4):169-183.
- Haddad, B., 2007. Modelización numerica mediante elementos finitos y SHP de los geomateriales fluidificados: aplicación a los deslizamientos rapidos de ladera. PhD Thesis. Universidad Complutense de Madrid.
- Haugen, E.D. and Kaynia, A.M., 2008. Vulnerability of structures impacted by debris flow. In Chen at al. (Eds.): *Landslides and Engineered Slopes*. Taylor & Francis, London, 381-387.
- HAZUS-MH, 2010. HAZUS – FEMAs Methodology for Estimating Potential Losses from Disasters, available at: <http://www.fema.gov/plan/prevent/hazus/index.shtm>.
- Heim, A., 1932. Bergsturz und Menschenleben. *Beiblatt zur Vierteljahrsschrift*. Fretz & Wasmuth Verlag, Zürich. 218 pp.
- Heinimann, H.R. 1999. Risikoanalyse bei gravitativen Naturgefahren. *Umwelt-Materialien* 107/1, 115 pp.
- Ho, K., Leroi, E., Roberts, B., 2000. Keynote lecture: quantitative risk assessment—application, myths and future direction. In: *Proceedings of the International Conference on Geotechnical and Geological Engineering, GEOENG 2000*, Melbourne, Australia vol. 1, Technomic, Lancaster, pp. 236–312.
- Hovius N, Stark C.P., Allen P.A., 1997. Sediment flux from a mountain belt derived by landslide mapping. *Geology* 25 (3):231-234.
- Horton, P., Jaboyedoff, M., Bardou, E., 2008. Debris flow susceptibility mapping at a regional scale, in: *4th Canadian Conference on Geohazards*, Universite Laval, Quebec, Canada.
- Hubl, J., and Steinwendtner, H., 2000. Estimation of rheological properties of viscous debris flow using a belt conveyor. *Physics and Chemistry of the Earth, Part B: Hydrology, Oceans and Atmosphere*, 25(9): 751-755.
- Huggel, C., Kaab, A., Haeberli, W., Krummenacher, B., 2003. Regional-scale GIS-models for assessment of hazards from glacier lake outbursts: evaluation and application in the Swiss Alps. *Natural Hazards and Earth System Sciences*, 3(6), 647-662.
- Hungr, O., 1995. A model for the runout analysis of rapid flow slides, debris flows, and avalanches. *Canadian Geotechnical Journal* 32, pp. 610–623.
- Hungr, O. and Evans S.G., 1996. Rock avalanche run out prediction using a dynamic model. In Senneset (ed.), *Landslides; Proc. intern. symp.*, Trondheim. Rotterdam: Balkema.

- Hungr, O. And Evans, S.G., 2004. "Entrainment of debris in rock avalanches: An analysis of a long run-out mechanism". GSA Bulletin Vol. 116.
- Hungr, O. and McDougall, S., 2009. Two numerical models for landslide dynamic analysis. *Computers & Geosciences* 35, pp. 978–992.
- Hungr, O., Evans, S.G., Bovis, M.J., Hutchinson, J.N., 2001. A review of the classification of landslides of the flow type. *Environmental & Engineering Geoscience*, VII (3), 221-238.
- Hungr, O., Corominas, J., Eberhardt, E., 2005. Estimating landslide motion mechanisms, travel distance and velocity. In *Landslide Risk Management*. O. Hungr, R. Fell, R. Couture and E. Eberhardt (Eds.). Taylor and Francis, London. pp.99-128.
- Hungr, O., McKinnon, M., McDougall, S., 2007. Two models for analysis of landslide motion: Application to the 2007 Hong Kong benchmarking exercises. In: *The 2007 International Forum on Landslide Disaster Management*. Ho & Li (Eds.), ISBN 978-962-7619-30-7.
- Hungr, O., Morgenstern, N., Wong, H.N., 2007. Review of benchmarking exercise on landslide debris runoff and mobility modelling. In: *The 2007 International Forum on Landslide Disaster Management*. Ho & Li (Eds.), ISBN 978-962-7619-30-7.
- Hürlimann, M., Rickenmann, D., Graf, C., 2003. Field and monitoring data of debris-flow events in the Swiss Alps. *Can. Geotech. J.* 40, pp. 161–175.
- Hürlimann, M., Copons, R., Altimir, J., 2006. Detailed debris flow hazard assessment in Andorra: A multidisciplinary approach. *Geomorphology*, 78(3-4): 359-372.
- Hürlimann, M., Medina, V., Bateman A., Copons, R., Altimir J., 2007. Comparison of different techniques to analyse the mobility of debris flows during hazard assessment-Case study in La Comella catchment, Andorra. In Chen & Majors (eds.) *Debris-Flow Hazard Mitigation : Mechanics, Prediction and Assessment*. Millpress, Netherlands, pp. 411-422.
- Hürlimann M., Rickenmann D., Medina V., Bateman A., 2008. Evaluation of approaches to calculate debris-flow parameters for hazard assessment, *Engineering Geology* 102, 152– 163.
- Hutchinson, J.N., 1986. A sliding-consolidation model for flow slides. *Canadian Geotechnical Journal* 23, pp. 115–126.
- Imran J., Harff P., Parker G., 2001. A numerical model of submarine debris-flow with graphical user interface. *Computer Geosciences* 27, pp. 717–729.
- Issler, D. and Johannesson, T., 2011. Dynamical Consistency Constraints on Entrainment and Deposition in Depth-Averaged Models of Snow Avalanches and Other Gravity Mass Flows. Technical Note 20110112-00-1-TN. Norwegian Geotechnical Institute (NGI).
- Iverson R.M., 2005. Debris flow mechanics. In: *Debris flows and related phenomena*. – Praxis, Chichester, 36-51.
- Iverson, R.M. and Denlinger, R.P., 2001. Flow of variably fluidized granular masses across three-dimensional terrain. 1. Coulomb mixture theory. *Journal of Geophysical Research* 106, pp. 537-552.
- Iverson, R., Reid, M., Lahusen, R., 1997. Debris flow mobilization from landslides. *Annu. Rev. Earth Planet. Sci.*, 25, pp. 85–138.

- Iverson, R.M., Schilling, S.P., Vallance, J.W., 1998. Objective delineation of lahar-inundation hazard zones. *Geological Society of America Bulletin*, 100: 972-984.
- Iverson, R.M., Logan N.M., Denlinger, R.P.. 2004. Granular avalanches across irregular three-dimensional terrain. 2: Experimental tests.–*J. Geophys. Res.*, 109, F01015.
- Iverson, R.M., Reid, M.E., Logan, M., LaHusen, R.G., Godt, J.W., Griswold, J.P., 2011. Positive feedback and momentum growth during debris-flow entrainment of wet bed sediment. *Nature Geoscience*, 4, pp.116–121.
- Jaiswal, P., van Westen, C.J., Jetten, V., 2010. Quantitative landslide hazard assessment along a transportation corridor in southern India. *Engineering Geology*, 116(3-4): 236-250.
- Jakob, M., Weatherly, H., 2005. Debris flow hazard and risk assessment, Jones Creek, Washington. In: Hungr, O., Fell, R., Couture, R., Eberhardt, E. (Eds.): *Landslide Risk Management*. Taylor & Francis, London, 533-541.
- Jakob, M., Anderson, D., Fuller, T., Hungr, O., Ayotte, D., 2000. "An unusually large debris flow at Hummingbird Creek, Mara Lake, British Columbia". *Canadian Geotechnical Journal* Vol. 37, pp. 1109-1125.
- Kaitna, R., Rickenmann, D., Schatzmann, M., 2007. Experimental study on rheologic behaviour of debris flow material. *Acta Geotechnica*, 2(2): 71-85.
- Kappes, M. S., Malet, J.-P., Remaitre, A., Horton, P., Jaboyedoff, M., Bell, R., 2011. Assessment of debris-flow susceptibility at medium-scale in the Barcelonnette Basin, France, *Nat. Hazards Earth Syst. Sci.*, 11, 627–641, doi:10.5194/nhess-11-627-2011.
- Karszenberg, D., Burrough, P. A., Sluiter, R., de Jong, K., 2001. The PCRaster Software and Course Materials for Teaching Numerical Modelling in the Environmental Sciences, *Transactions in GIS*, 5(2), 99–110.
- Kaynia, A.M., Papatoma-Köhle, M., Neuhäuser, B., Ratzinger, K., Wenzel, H., Medina-Cetina, Z.. 2008. Probabilistic assessment of vulnerability to landslide: Application to the village of Lichtenstein, Baden-Württemberg, Germany. *Engineering Geology*, 101(1-2), 33-48.
- Kelfoun, K. and Druitt, T.H., 2005. Numerical modeling of the emplacement of Socompa rock avalanche, Chile. *J Geophys Res* 110 : B12202.1-12202.13 DOI:10.1029/2005JB003758.
- Koch, T., 1998. Testing various constitutive equations for debris flow modeling. *Hydrology, Water Resources and Ecology in Headwaters* (Proceedings of the HeadWater'98 Conference held at Meran/Merano, Italy, April 1998). IAHS Publ. no. 248.
- Kowalski, J., 2008. Two-phase modeling of debris flows. PhD Thesis. ETH Zurich.
- Kuriakose, S.L.. 2010. Physically - based dynamic modelling of the effect of land use changes on shallow landslide initiation in the Western Ghats of Kerala. PhD Thesis. University of Twente Faculty of Geo-Information and Earth Observation ITC, 2010. ITC Dissertation 178, ISBN: 978-90-6164-298-5.
- Kuriakose, S.L., Quan Luna, B., Begueria Portugues, S., van Westen, C.J., 2009. Modelling the runoff of a debris flow of the Western Ghats, Kerala, India. In: *European Geosciences Union General Assembly* 19-24

- April 2009, Vienna. Austria : Geophysical research abstracts, 11(2009)EGU2009-4276.
- Kuriakose, S.L., van Beek, L.P.H., van Westen, C.J., 2009. Parameterizing a physically based shallow landslide model in a data poor region. *Earth Surface Processes and Landforms*, 34(6): 867-881.
- Kwan, J.S.H. and Sun, H.W., 2006. An improved landslide mobility model. *Canadian Geotechnical Journal*, vol. 43, 531-539.
- Kwan, J. and Sun, H.W., 2007. Benchmarking exercise on landslide mobility. Modelling – runout analyses using 3dDMM. In: *The 2007 International Forum on Landslide Disaster Management*. Ho & Li (Eds.), ISBN 978-962-7619-30-7.
- Leone, F., Asté, JP., Leroi, E., 1996. Vulnerability assessment of elements exposed to mass movements: working toward a better risk perception. In: Senneset K (ed) *Landslides- Glissements de Terrain*. Balkema, Rotterdam, 263–270.
- Leroi, E., Bonnard, Ch., Fell, R., McInnes, R. 2005. A framework for landslide risk assessment and management. In: Hungr, O., Fell, R., Couture, R., Eberhardt, E. (Eds.): *Landslide Risk Management*. Taylor & Francis, London, pp. 159-198.
- Li, Z., Huang, H., Nadim, F., Xue, Y., 2010. Quantitative Risk Assessment of Cut-Slope Projects under Construction. *Journal of Geotechnical and Geoenvironmental Engineering*, 136(12): 1644-1654.
- Li, Z., Nadim, F., Huang, H., Uzielli, M. and Lacasse, S., 2010. Quantitative vulnerability estimation for scenario-based landslide hazards. *Landslides*, 7(2), 125-134.
- Liu, X. and Lei, J., 2003. A method for assessing regional debris flow risk: an application in Zhaotong of Yunnan province (SW China). *Geomorphology*, 52(3-4), 181-191.
- Liu, X., Yue, Z. Q., Tham, L. G., Lee, C. F., 2002. Empirical assessment of debris flow risk on a regional scale in Yunnan province, southwestern China. *Environmental Management*, 30(2), 249-264.
- Lucas, A., Mangeney, A., Bouchut, F., Bristeau, M.O., Mege, D., 2007. Benchmarking exercises for granular flows. In: *The 2007 International Forum on Landslide Disaster Management*. Ho & Li (Eds.), ISBN 978-962-7619-30-7.
- Luino, F., 2005. Sequence of instability processes triggered by heavy rainfall in the northern Italy. *Geomorphology*, 66(1-4), 13-39.
- Luino, F., Nigrelli, G., Biddoccu, M., Cirio, C.G., Di Palma, M., Missaglia, M., Fassi, P., 2008. Definizione delle soglie pluviometriche d'innescio di frane superficiali e colate torrentizie: accorpamento per aree omogenee. IRER, Milano, 125 p.
- Ma, Y., 2011. Regional scale multi - hazard susceptibility assessment : a case study in Mtskheta - Mtianeti, Georgia, University of Twente Faculty of Geo-Information and Earth Observation ITC, Enschede, 65 pp.
- Major, J. J. and Pierson, T.C., 1992. Debris flow rheology: Experimental analysis of fine-grained slurries, *Water Resour. Res.*, 28(3), 841–857, doi:10.1029/91WR02834.
- Malamud B.D., Turcotte D.L., Guzzetti F, Reichenbach P., 2004. Landslide inventories and their statistical properties. *Earth Surface Processes and Landforms* 29(6):687-711.

- Malet, J.-P., 2010. OMIV Data Access - Barcelonnette area http://eost.u-strasbg.fr/omiv/data_access_Barcelonnette.html
- Malet, J.-P., Remaitre, A., Maquaire, O., Ancey, C., Locat, J., 2003. Flow susceptibility of heterogeneous marly formations. Implications for torrent hazard control in the Barcelonnette basin (Alpes-de-Haute-Provence, France). In: Rickenmann, D., Chen, C.-L. (Eds.): Proceedings of the Third International Conference on Debris-Flow Hazard Mitigation: Mechanics, Prediction and Assessment, Davos, Switzerland, Millpress, Rotterdam, pp. 351-362.
- Malet, J.-P., Remaitre, A., Maquaire, O., 2004. Runout modeling and extension of the threatened area associated with muddy debris flows. *Geomorphologie: relief, processus, environnement* n.3, pp. 195-210.
- Mangeney, A., Bouchut, F., Vilotte, J.P., Lajeunesse, E., Aubertin, A., Pirulli, M., 2005. On the use of Saint-Venant equations for simulating the spreading of a granular mass. *J. Geophys. Res.* 110, B09103, doi:10.1029/2004JB003161.
- Mangeney A., Bouchut, F., Thomas, N., Vilotte, J.P, Bristeau, M.O., 2007a. Numerical modeling of self-channeling granular flows and of their levee-channel deposits. *Journal of Geophysical Research* 112, F02017, doi: 10.1029/2006JF000469.
- Mangeney, A., Tsimring, L.S., Volfson, D., Aranson, I.S., Bouchut, F., 2007b. Avalanche mobility induced by the presence of an erodible bed and associated entrainment. *Geophysical Research Letters* Vol.34, L22401, 5 pp. doi:10.1029/2007GL031348.
- Mangeney, A., Roche, O., Hungr, O., Mangold, N., Faccanoni, G., Lucas, A., 2010. Erosion and mobility in granular collapse over sloping beds. *Journal of Geophysical Research*, vol. 115, F03040, 21 pp. doi:10.1029/2009JF001462.
- Mavrouli, O. and Corominas, J., 2010. Vulnerability of simple reinforced concrete buildings to damage by rockfalls. *Landslides*, 7(2), 169-180.
- McArdell, B.W.; Zanuttigh, B.; Lamberti, A.; Rickenmann, D., 2003. Systematic comparison of debris-flow laws at the Illgraben torrent, Switzerland. In: Rickenmann, D.; Chen, C.-I. (eds) *Debris-Flow Hazards Mitigation. Mechanics, Prediction, and Assessment*. Proc. of the third Int. Conf. on Debris-Flow Hazards Mitigation. Davos, Switzerland, September 10-12, 2003. Volume 1. Rotterdam, Millpress. pp. 647-657.
- McClung, D.M., 2001. Superelevation of flowing avalanches around curved channel bends. *Journal of Geophysical Research*, 106(B8), 16489-16498.
- McDougall, S., 2006. A new continuum dynamic model for the analysis of extremely rapid landslide motion across complex 3D terrain. PhD thesis, The University of British Columbia, 253 pp.
- McDougall, S. and Hungr, O., 2004. A model for the analysis of rapid landslide motion across three-dimensional terrain. *Canadian Geotechnical Journal*, 41(12), p. 1084-1097.
- McDougall, S. and Hungr, O., 2005. Dynamic modelling of entrainment in rapid landslides. *Can. Geotech. J.* 42, pp. 1437-1448.
- McDougall, S. and Hungr, O., 2006. Landslide dynamic analysis in 2D and 3D. *Sea to Sky Geotechnique*, the 59th Canadian Geotechnical Conference, Vancouver, 2006.

- McDougall, S., Boulton, N., Hungr, O., Stead, D., Schwab, J., 2006. "The Zymoetz River landslide, British Columbia, Canada; description and dynamic analysis of a rock slide-debris flow". *Landslides* Vol. 3, pp. 195.
- McKinnon, M., Hungr, O., McDougall, S., 2008. "Dynamic analyses of Canadian landslides". In : J. Locat, D. Perret, D. Turmel, D. Demers et S. Leroueil. *Comptes rendus de la 4e Conférence canadienne sur les géorisques: des causes à la gestion*. Proceedings of the 4th Canadian Conference on Geohazards : From Causes to Management. Presse de l'Université Laval, Québec, pp. 594.
- Medina, V., Hürlimann, M., Bateman, A., 2008. Application of FLATModel, a 2D finite volume code, to debris flows in the northeastern part of the Iberian Peninsula. *Landslides* 5, pp. 127–142.
- Mergili, M. 2008. Integrated modelling of debris flows with Open Source GIS - Numerical simulations of triggering, mobilization, and runout of debris flows for selected study areas along the Trans-Andean road corridor Mendoza, Valparaíso. PhD Thesis. University of Innsbruck, Austria.
- Metropolis, N., 1987. "The beginning of the Monte Carlo method". *Los Alamos Science* (1987 Special Issue dedicated to Stanisław Ulam): 125–130.
- Metropolis, N. and Ulam, S., 1949. "The Monte Carlo Method". *Journal of the American Statistical Association* (American Statistical Association) 44 (247): 335–341. doi:10.2307/2280232.
- Meunier, M. and Ancey, C., 2004. Towards a conceptual approach to predetermining long-return-period avalanche run-out distance, in *Journal of Glaciology*, IGS, vol. 50, num. 169, p. 268-278.
- Michael-Leiba, M., Baynes, F., Scott, G., Granger, K., 2003. Regional landslide risk to the Cairns community. *Natural Hazards*, 30(2): 233-249.
- Miller, D.J., Burnett, K.M., 2008. A probabilistic model of debris-flow delivery to stream channels, demonstrated for the Coast Range of Oregon, USA. *Geomorphology*, 94(1-2): 184-205.
- Mizuyama, T., Kobashi, S., Ou, G., 1992. Prediction of debris flow peak discharge. In: *International Symposium Interpraevent*. Bern, 99-108.
- Muir, I., Ho, K.S.S., Sun, H.W., Hui, T.H.H., Koo, Y.C., 2006. Quantitative risk assessment as applied to natural terrain landslide hazard management in a mid-levels catchment, Hong Kong. In: Nadim, F., Pöttler, R., Einstein, H., Klapperich, H., Kramer, S. (Eds.): "Geohazards", ECI Symposium Series, Volume P07, p. 1-8.
- Nadim, F. and Kjekstad, O., 2009. Assessment of global high-risk landslide disaster hotspots, in: *Disaster Risk Reduction*, edited by: Sassa, K. and Canuti, P., Springer-Verlag, Berlin, 213–222.
- Naef, D., Rickenmann, D., Rutschmann, P., and McArdell, B. W., 2006. Comparison of flow resistance relations for debris flows using a one-dimensional finite element simulation model. *Nat. Hazards Earth Syst. Sci.*, 6, pp. 155–165.
- O'Brien J.S. and Julien, P.Y. 1998. Laboratory analysis of mudflow properties. *Journal of Hydraulic Engineering*, 114(8), 877-887.
- O'Brien, J.S., Julien, P.Y., Fullerton, W.T., 1993. Two-dimensional water flood and mudflow simulation. *Journal of Hydraulic Engineering*, 119(2), 244-261.

- Papa, M., Egashira, S. and Itoh, T., 2004. Critical conditions of bed sediment entrainment due to debris flow. *Natural Hazards and Earth System Sciences* 4, pp. 469–474.
- Parsons, J.D., Whipple, K.X., Simoni, A., 2001. Experimental study of the grain-flow, fluid-mud transition in debris flows. *The Journal of Geology* 109, 427–447.
- Pascale, S., Sdao, F., Sole, A., 2010. A model for assessing the systemic vulnerability in landslide prone areas, *Nat. Hazards Earth Syst. Sci.*, 10, 1575–1590, doi:10.5194/nhess-10-1575-2010, 2010.
- Pastor, M., Blanc, M.J., Sanchez, M., Haddad, B., 2007. A SPH depth integrated model with pore pressure coupling for fast landslides and related phenomena. In: *The 2007 International Forum on Landslide Disaster Management*. Ho & Li (Eds.), ISBN 978-962-7619-30-7.
- Pastor, M., Haddad, B., Sorbino, G., Cuomo, S., Drempetic, V., 2009. A depth-intergrated, coupled SPH model for flow-like landslides and related phenomena. *Int. J. Numer. Anal. Meth. Geomech.* 33, pp. 143-172.
- Paudel, B. and Law, T., 2008. Case histories of landslide induced gravitative debris flows. In : J. Locat, D. Perret, D. Turmel, D. Demers et S. Leroueil. *Comptes rendus de la 4e Conférence canadienne sur les géorisques: des causes à la gestion*. Proceedings of the 4th Canadian Conference on Geohazards : From Causes to Management. Presse de l'Université Laval, Québec, 594 p.
- Petley, D.N., 2011. The landslide blog. <http://blogs.agu.org/landslideblog/>. Accessed 12 Oct 2011.
- Phillips, C.J. and Davies, T.R.H., 1991. Determining rheological parameters of debris flow material. *Geomorphology*, 4:101-110.
- Pirulli, M., Bristeau, M., Mangeney, A., Scavia, C., 2007. The effect of the earth pressure coefficients on the runout of granular material. *Environmental Modelling & Software* 22, pp. 1437-1454.
- Pirulli, M., and Mangeney, A., 2008. Results of back-analysis of the propagation of rock avalanches as a function of the assumed rheology. *Rock Mechanics and Rock Engineering*, 41 (1), pp 59-84.
- Pirulli, M., and Sorbino, G., 2008. Assessing potential debris flow run-out: a comparison of two simulation models. *Nat. Hazards Earth Syst. Sci.*, 8, 961–971.
- Pitman, B. E. and Le, L., 2005. A two-fluid model for avalanche and debris flow. *Phil. Trans. R. Soc. A.* 363, pp. 1573-1601.
- Poisel, R., Preh, A., 2007. Landslide detachment mechanisms. An overview of their mechanical models. In: *The 2007 International Forum on Landslide Disaster Management*. Ho & Li (Eds.), ISBN 978-962-7619-30-7.
- Poisel, R., Preh, A., Hungr, O., 2008. Run Out of Landslides – Continuum Mechanics versus Discontinuum Mechanics Models. *Geomechanik und Tunnelbau*, 1(5): 358-366.
- Prochaska, A., Santi, P., Higgins, J., Cannon, S., 2008. A study of methods to estimate debris flow velocity. *Landslides*, 5(4), 431-444.
- Pudasaini, S.P. and Hutter, K., 2007. *Avalanche dynamics - dynamics of rapid flows of dense granular avalanches*. Springer – Verlag, Berlin.
- Quan Luna, B., 2007. Assessment and modelling of two lahars caused by "Hurricane Stan" at Atitlan, Guatemala, October 2005, The University of Oslo, Oslo.

- Quan Luna, B., van Westen, C.J., Jetten, V., Cepeda, J., Stumpf, A., Malet, J.-P., Medina- Cetina, Z., van Asch, T.W.J., 2010. A preliminary compilation of calibrated rheological parameters used in dynamic simulations of landslide run - out. In: Mountain Risks: bringing science to society : proceedings of the Mountain Risks International Conference, Firenze, Italy, 24-26 November 2010 / ed. by J.-P. Malet, T. Glade and N. Casagli. - Strasbourg : CERG, 2010. ISBN 2-95183317-1-5. pp. 255-260.
- Quan Luna, B. Remaître, , A., van Asch, Th.W.J., Malet, J.-P., van Westen, C.J., 2011. Analysis of debris flow behavior with a one dimensional run - out model incorporating entrainment. In: Engineering geology, in press 13p.
- Quan Luna, B., Blahut, J., van Westen, C.J., Sterlacchini, S., van Asch, T.W.J., Akbas, S.O., 2011. The application of numerical debris flow modelling for the generation of physical vulnerability curves. Nat. Hazards Earth Syst. Sci., 11, 2047-2060, doi:10.5194/nhess-11-2047-2011.
- Remaître, A., Malet, J.-P., Maquaire, O., 2005. Morphology and sedimentology of a complex debris flow in a clay-shale basin. Earth Surf. Process. Landforms 30 pp.339-348.
- Remaître, A., Malet, J.-P., Maquaire, O., Ancey, C., Locat, J., 2005. Flow behaviour and runout nodelling of complex debris flow in a clay-shale basin. Earth Surf. Process. Landforms 30 pp.479-488.
- Remaître, A., 2006. Morphologie et dynamique des laves torrentielles: Applications aux torrents des Terres Noires du bassin de Barcelonnette (Alpes du Sud). Ph.D. thesis.
- Remaître, A., van Asch, Th.W.J., Malet, J.-P., Maquaire, O., 2008. Influence of check dams on debris flow run-out intensity. Nat. Hazards Earth Syst. Sci. 8, pp. 1403-1416.
- Remaître, A., Malet, J.-P., Maquaire, O., 2009. Sediment budget and morphology of the 2003 Faucon debris flow (South French Alps): scouring and channel-shaping processes. Proc. Landslide Processes: from geomorphological mapping to dynamic modelling, pp. 75-80.
- Remaître, A., Malet, J.-P., Maquaire, O., 2011. Geomorphology and kinematics of debris flows with high entrainment rates: A case study in the South French Alps. Comptes Rendus Geoscience, 343(11-12): 777-794.
- Remondo, J., Bonachea, J.,Cendrero, A., 2008. Quantitative landslide risk assessment and mapping on the basis of recent occurrences. Geomorphology, 94(3-4), 496-507.
- Revellino, P., Hungr, O., Guadagno, F., Evans, S., 2004. Velocity and runout simulation of destructive debris flows and debris avalanches in pyroclastic deposits, Campania region, Italy. Environmental Geology, 45(3): 295-311.
- Rickenmann, D., 1990. Debris flows 1987 in Switzerland: Modelling and Sediment Transport (IAHS Publication No. 194, 371–378), International Association of Hydrological Sciences, Christchurch, New Zealand.
- Rickenmann, D., 1999. Empirical relationships for debris flows. Natural Hazards 19 (1), 47–77.

- Rickenmann, D. and Zimmermann, M., 1993. The 1987 debris flows in Switzerland: documentation and analysis. *Geomorphology*, Vol. 8(2-3), pp. 175-189.
- Rickenmann, D. and Koch, T., 1997. Comparison of debris flow modeling approaches. In *Proceedings of the 1st International Conference on Debris-Flow Hazards Mitigation: Mechanics, Prediction, and Assessment*, San Francisco, Calif. Edited by C.L. Chen, American Society of Civil Engineers (ASCE). pp. 576–585.
- Rickenmann, D., Weber, D., Stepanov, B., 2003. Erosion by debris flows in field and laboratory experiments. In D. Rickenmann & C.L. Chen (eds), "Debris-Flow Hazards Mitigation: Mechanics, Prediction, and assessment", *Proceedings 3rd International DFHM Conference*, Davos, Switzerland, September 10-12, 2003: 883-894. Rotterdam: Millpress.
- Rickenmann, D., Laigle, D. McArdell, B.W., Hübl, J., 2006. Comparison of 2D debris-flow simulation models with field events. *Computat Geosci*, 10, pp. 241-264.
- Salm, B., 1993. Flow transition and runout distances of flowing avalanches. *Annals of Glaciology*, 18, 221-226.
- Sassa, K., Kaibori, M., Kitera, N., 1985. Liquefaction and undrained shear of torrent deposits as the cause of debris flows. *Proc. Inter. Symp. On Erosion, Debris flows and Disas. Prev.*, pp. 231-236.
- Sassa, K., 1988. Geotechnical model for the motion of landslides. *Proc. Vth ISL, Lausanne*, pp. 37-55.
- Sassa, K., Wang, F., 2000. A modified geotechnical simulation model for the areal prediction of landslide motion. *Annuals of Disas. Prev. Res. Inst., Kyoto Univ.*, No. 43 B-1.
- Sassa, K., Wang, G.H., 2005. Mechanism of landslide-triggered debris flows: Liquefaction phenomena due to the undrained loading of torrent deposits. In Jakob, K. and Hungr, O. (eds.) *Debris Flow hazards and Related Phenomena. Praxis*. Springer Berlin Heidelberg. 2005. pp. 81-104.
- Savage, S.B. and Hutter, K., 1991. The dynamics of avalanches and granular material from initiation to run-out. Part I : Analysis. *Acta Mech.*, 86, 201-223.
- Schatzmann, M., Fischer, P. Bezzola, G.R., 2003. Rheological Behavior of Fine and Large Particle Suspensions. *Journal of Hydraulic Engineering*, 129(10): 796-803.
- Scheidegger, A., 1973. On the prediction of the reach and velocity of catastrophic landslides. *Rock Mech.*, 5, 231-236.
- Scheidl, C., and Rickenmann, D., 2010. Empirical prediction of debris-flow mobility and deposition on fans. *Earth Surface Processes and Landforms*, 35(2): 157-173.
- Schilling, S.P., 1998. LAHARZ; GIS programs for automated mapping of lahar-inundation hazard zones: U.S. Geological Survey Open-File Report, 98-638.
- Scotto di Santolo, A., Pellegrino, A. M., Evangelista, A., 2010. Experimental study on the rheological behaviour of debris flow, *Nat. Hazards Earth Syst. Sci.*, 10, 2507-2514, doi:10.5194/nhess-10-2507-2010.
- Skempton, A.W., 1954. The pore-pressure coefficients A and B. *Geotechnique* 4, pp. 143-147.

- Soeters, R. and van Westen, C.J. 1996. Slope instability recognition, analysis, and zonation. In: Landslides, investigation and mitigation / ed. by. A.K. Turner and R.L. Schuster. Washington, D.C. National Academy Press, 1996. ISBN 0-309-06151-2. (Transportation Research Board, National Research Council, SpecialReport ; 247) pp. 129 - 177.
- Sosio, R., Crosta, G.B., Frattini, P., 2007. Field observations, rheological testing and numerical modelling of a debris-flow event. *Earth Surface Processes and Landforms*, 32(2): 290-306.
- Sovilla, B., Burlando, P., Bartelt, P., 2006. Field experiments and numerical modeling of mass entrainment in snow avalanches. *J. Geophys. Res.*, 111(F3): F03007, 16 pp. doi:10.1029/2005JF000391.
- Sovilla, B., Margreth, S., Bartelt, P., 2007. On snow entrainment in avalanche dynamics calculations. *Cold Regions Science and Technology* 47 pp. 69–79.
- Stark, C.P. and Guzzetti, F., 2009. Landslide rupture and the probability distribution of mobilized debris volumes. *Journal of Geophysical Research*, Vol. 114, F00A02, 16 pp. doi:10.1029/2008JF001008.
- Strimbu B., 2011. Modeling the travel distances of debris flows and debris slides: quantifying hillside morphology. *Ann. For. Res.* 54(1): 119-134, 2011.
- Sun, H.W., Lam, T.T.M., Tsui, H.M., 2003. Design basis for standardized modules of landslide debris-resisting barriers. GEO Report No. 174. Geotechnical Engineering Office, Hong Kong.
- Takahashi, T., 1978. Mechanical characteristics of debris flows. *Journal of the Hydraulics Division, ASCE*, 104 (HY8), 1153-1169.
- Takahashi, T., 2001. Mechanics and simulation of snow avalanches, pyroclastic flows and debris flows. *Spec. Publs. Int. Ass. Sediment.* 31, pp. 11 – 43.
- Takahashi, T., 2009. A Review of Japanese Debris Flow Research. *International Journal of Erosion Control Engineering, ASCE, Volume 2, No.1*, pp 1-14.
- Tang, C., Zu, J., Chang, M., Ding, J., Xin, Q., 2011. An empirical-estastistical model for predicting debris-flow runout zones in the Wenchuan earthquake area. *Quaternary International*, doi:10.1016/j.quaint.2010.11.020.
- Thiery, Y., Malet, J.-P., Sterlacchini, S., Puissant, A., Maquaire, O., 2007. Landslide susceptibility assessment by bivariate methods at large scales: Application to a complex mountainous environment. *Geomorphology*, 9(1-2): 38-59.
- Toyos, G., Oramas Dorta, D., Oppenheimer C., Pareschi M.T., Sulpizio R., Zanchetta G., 2008. GIS-assisted modelling for debris flow hazard assessment based on the events of May 1998 in the area of Sarno, Southern Italy: II. Velocity and dynamic pressure. *Earth Surface Processes and Landforms*, 33(11): 1693-1708.
- Uzielli, M., Nadim, F., Lacasse, S., Kaynia, A.M., 2008. A conceptual framework for quantitative estimation of physical vulnerability to landslides. *Engineering Geology*, 102(3-4), 251-256.
- van Asch, Th., Malet, J.-P., Remaitre, A., Maquaire, O., 2004. Numerical modelling of the runout of a muddy debris-flow. The effect of rheology on velocity and deposit thickness along the run-out track. In *Proceedings*

- of the 9th International Symposium on Landslides, edited by: Lacerda, W., Rio de Janeiro, Brazil, 1, pp. 1433–1438.
- van Asch, Th.W.J., Malet, J.-P., van Beek, L.P.H., Amitrano, D., 2007. Techniques, issues and advances in numerical modelling of landslide hazard. *Bull. Soc. géol. Fr.*, 2007, t. 178, no 2, pp. 65-88.
- van Asch, Th.W.J., Daehne, A., Spickermann, A., Travelletti, J., Remaitre, A., Malet, J.-P., Quan Luna, B., 2010. A comparison of two run - out models and a preliminary evaluation of their potentials for regional hazard and risk assessment. In: *Mountain risks : bringing science to society : proceedings of the Mountain Risks International Conference, Firenze, Italy, 24-26 November 2010* / ed. By J.-P. Malet, T. Glade and N. Casagli. - Strasbourg : CERG, 2010. ISBN 2-95183317-1-5. pp. 129-133.
- van Westen, C.J. (ed.), 2009. Multi-hazard risk assessment, Guide book. Distance education course, Faculty of Geo-Information Science and Earth Observation (ITC), University of Twente.
- van Westen, C.J., Rengers, N., Terlien, M.T.J, Soeters, R., 1997. Prediction of the occurrence of slope instability phenomena through GIS-based hazard zonation. *Geologische Rundschau* 86, pp. 404–414
- van Westen, C.J., van Asch, Th. J.W., Soeters, R., 2006. Landslide hazard and risk zonation --why is it still so difficult? – *Bull. Eng.Geol. Env.*, 65, pp. 167-184.
- van Westen, C.J., Castellanos Abella, E.A., Sekhar, L.K., 2008. Spatial data for landslide susceptibility, hazards and vulnerability assessment: an overview. In: *Engineering geology*, 102 (3-4), 112-131.
- van Westen, C.J., Quan Luna, B., Vargas Franco, R.D., Malet, J.P., Jaboyedoff, M., Horton, P., Kappes, M., 2010. Development of training materials on the use of geo - information for multi - hazard risk assessment in a mountainous environment. In: *Mountain risks : bringing science to society : proceedings of the Mountain Risks International Conference, Firenze, Italy, 24-26 November 2010* / ed. by J.-P. Malet, T. Glade and N. Casagli. - Strasbourg : CERG, 2010. ISBN 2-95183317-1-5. pp. 469-475.
- Vandine, D.F. and Bovis, M., 2002. History and goals of Canadian debris-flow research, a review. *Natural Hazards* 26, pp. 69–82.
- Voellmy, A., 1955. Über die Zerstorungskraft von Lawinen (On breaking force of avalanches). *Schweizerische Bauzeitung* 73, pp. 212–285.
- Vulliet, L., 2000. Natural slopes in slow movement. In: *Modeling in geomechanics*. – Wiley & Sons, Chichester, pp. 653-676.
- Wang, F., and Sassa, K., 2007. Landslide simulation by geotechnical model adopting a model for variable apparent friction coefficient. In: *The 2007 International Forum on Landslide Disaster Management*. Ho & Li (Eds.), ISBN 978-962-7619-30-7.
- Wesseling, C. G., Karssenberg, D., Van Deursen, W., Burrough, P. A., 1996. Integrating dynamic environmental models in GIS: the development of a Dynamic Modelling language, *Transactions in GIS*, 1, 40–48.
- Whipple, K.X., 1992. Predicting debris-flow runout and deposition on fans: the importance of the flow hydrograph. In: Walling, D., Davies, T., Hasholt, B. (Eds.), *Erosion, Debris-Flows and Environment in Mountain Regions: Proceedings of the Chengdu Symposium*. International Association of Hydrological Sciences, vol. 209, 337– 345.

References

- Wieczorek, G.F., 1984. Preparing a detailed landslide-inventory map for hazard evaluation and reduction. *Bulletin of the Association of Engineering Geologists* 21 3, pp. 337–342.
- Wilhelm, C., 1998. Quantitative risk analysis for evaluation of avalanche protection projects. In: *Proceedings of the 25 Years of Snow Avalanche Research*, Oslo, Norway, 288–293.
- Wong, H.N., Ko, F.W.Y. 2005. *Landslide Risk Assessment - Application and Practice (SPR 4/2005)*. Geotechnical Engineering Office, Hong Kong, 311 p.
- Wu, T.H., Tang W.H., Einstein H.H..1996. Landslide hazard and risk assessment. In: A.K. Turner and R.L. Schuster, Editors, *Landslides: Investigation and Mitigation*, Special Report 247, Transportation Research Board, National Research Council, National Academy Press, Washington, DC., pp. 106–120.
- Zanuttigh, B. and Lamberti, A., 2004. Numerical modelling of debris surges based on shallow-water and homogeneous material approximations. *Journal of Hydraulic Research*, 42(4): 376-389.
- Zêzere, J.L., Garcia, R.A.C., Oliveira, S.C. and Reis, E., 2008. Probabilistic landslide risk analysis considering direct costs in the area north of Lisbon (Portugal). *Geomorphology*, 94(3-4), 467-495.
- Zimmerman, M.N., 2005. Analysis and management of debris-flow risks at Sörenberg, Switzerland. In: Jakob, M., Hungr, O. (Eds.): *Debris-Flow Hazards and Related Phenomena*, Praxis, Springer, Berlin, Heidelberg, pp. 305–324.

Curriculum Vitae



Byron Quan Luna was born on 30th of March of 1975. He obtained his Bachelor degree in Environmental Engineering at the Rafael Landivar University in Guatemala. During the period of 1999 to 2005, he worked as a technical advisor in a private sector company in Guatemala (SEPINSA - Incorporated Professional Services) where his main activities were to plan, develop and evaluate agricultural, forestry and environmental projects. In 2007, Byron Quan Luna received a Master of Science in Environmental Geology and Geohazards from the Department of Geosciences, University of Oslo, Norway with the thesis: "Assessment and modelling of two lahars caused by Hurricane Stan at Atitlan, Guatemala, October 2005". From 2007 to 2008, he did an internship at the International Centre of Geohazards (ICG) in the Norwegian Geotechnical Institute (NGI) on numerical analysis and computer modelling of mass movements (landslides, debris flows and snow avalanches).

In 2008, Byron Quan Luna started his PhD research in The Netherlands at ITC-University of Twente (UT) as a part of the Mountain Risk project as an Early Stage Researcher inside the Marie Curie Research Training Network. The project main focus is research and training in all aspects of mountains hazards and risks assessment and management. The network intended to develop an advanced understanding of how mountain hydro-geomorphological processes behave and to apply this understanding to living with the hazards in the long-term. In 2012, he was involved in the last part of the SafeLand project "Living with landslide risk in Europe: Assessment, effects of global change, and risk management strategies"

Since his start at ITC-UT in 2008, he has been involved as participant or lecturer in different topical workshops and intensive courses that has taken place in different countries such as Italy, Spain, Austria, Nicaragua, France, The Netherlands, Switzerland and Germany. He was a participant in the LARAM 2008 summer school (International School on "Landslide Risk Assessment and Mitigation") in Ravello, Italy. He has been advisor in several master thesis carried out by ITC-UT students.

List of publications

ISI Journal Articles

- Quan Luna, B.**, Remaitre, A., van Asch, Th.W.J., Malet, J.-P., van Westen, C.J., 2011. Analysis of debris flow behavior with a one dimensional run - out model incorporating entrainment. In: Engineering geology, (2011) in press 13 p.
- Quan Luna, B.**, et al., 2011. The application of numerical debris flow modeling for the generation of physical vulnerability curves. In: Natural hazards and earth system sciences (NHESS), 11 (2011) 7 pp. 2047-2060.
- Quan Luna, B.**, Kuriakose, S., Begueria, S., van Westen, C.J., van Asch, T.W.J., 2012. Comparison of two dimensional physically-based landslides run-out models that include the entrainment process. A case study in the Western Ghats of Kerala, India. (Under preparation).
- Hussin, H.Y., **Quan Luna, B.**, van Westen, C.J., Christen, M., Malet, J.-P., van Asch, T.W.J., 2012. Spatial frequency assessment of debris flow run-out using the RAMMS model. A parameterization analysis on a reference event in the French Alps. (Under review in Natural Hazards and Earth System Sciences).
- Quan Luna, B.**, Blahut, J., Camera, C., van Westen, C.J., Apuani, T., Jetten, V., Sterlacchini, S., 2012. Quantitative risk assessment for debris flows based on physically-based dynamic run-out modelling. A case study in Tresenda, Northern Italy. (under review in Landslides).

Conference Proceedings (full papers)

- van Asch, Th.W.J., Daehne, A., Spickermann, A., Travelletti, J., Remaitre, A., Malet, J.-P. and **Quan Luna, B.**, 2010. A comparison of two run - out models and a preliminary evaluation of their potentials for regional hazard and risk assessment. In: Mountain risks : bringing science to society : proceedings of the Mountain Risks International Conference, Firenze, Italy, 24-26 November 2010 / ed. by J.-P. Malet, T. Glade and N. Casagli. - Strasbourg : CERG, 2010. ISBN 2-95183317-1-5. pp. 129-133.
- van Westen, C.J., **Quan Luna, B.**, Vargas Franco, R.D., and et al., 2010. Development of training materials on the use of geo - information for multi - hazard risk assessment in a mountainous environment. In: Mountain risks : bringing science to society : proceedings of the Mountain Risks International Conference, Firenze, Italy, 24-26 November 2010 / ed. by J.-P. Malet, T. Glade and N. Casagli. - Strasbourg : CERG, 2010. ISBN 2-95183317-1-5. pp. 469-475.
- Quan Luna, B.**, van Westen, C.J. and et al., 2010. From deterministic hazard modelling to risk and loss estimation. In: Mountain risks : bringing science to society : proceedings of the Mountain Risks International Conference, Firenze, Italy, 24-26 November 2010 / ed. by J.-P. Malet, T. Glade and N. Casagli. - Strasbourg : CERG, 2010. ISBN 2-95183317-1-5. pp. 373-380.
- Quan Luna, B.**, van Westen, C.J., Jetten, V.G. and et al. (2010). A preliminary compilation of calibrated rheological parameters used in dynamic simulations of landslide run - out. In: Mountain risks : bringing science to society : proceedings of the Mountain Risks International Conference, Firenze, Italy, 24-26 November 2010 / ed. by J.-P. Malet, T. Glade and N. Casagli. - Strasbourg : CERG, 2010. ISBN 2-95183317-1-5. pp. 255-260.
- Quan Luna, B.**, Cepeda, J., Stumpf, A., van Westen, C.J. and et al., 2011. Analysis and uncertainty quantification of dynamic run - out model parameters for landslides. Presented at the Second World Landslide Forum, 3-9 October 2011, Rome, Italy. 4 p.

Samenvatting

Aardverschuivingen en modder/puinstromen zijn geomorfologische gebeurtenissen die een gevaar op kunnen leveren voor leefgemeenschappen in berggebieden. Dit gevaar komt niet alleen voort uit de aard van de processen, maar ook uit de interactie met menselijke systemen en hun gerelateerde gevoeligheid. Onderzoek naar de voorspelling en beheersing van de gevaren die met deze processen samenhangen is nog steeds van empirische aard, en vereist een combinatie van kwalitatieve en kwantitatieve analysemethoden. De ontwikkeling van numerieke dynamische modellen voor het bepalen van de "run-out" (uitstroomgebied en afstand) heeft een dramatische verandering teweeg gebracht in het onderzoek naar dit soort processen, omdat deze de mogelijkheid bieden om toekomstige scenario's te simuleren, vooral die waarvoor geen historisch vergelijkbare gebeurtenissen bekend zijn. Dynamische computermodellen bieden de mogelijkheid om dergelijke geomorfologische processen met een redelijke mate van nauwkeurigheid te simuleren. Daardoor kunnen een aantal toekomstige scenario's geanalyseerd worden, en de resultaten kunnen worden gebruikt om de lokale autoriteiten en bevolking te informeren zodat ze beter voorbereid zijn en de risico's kunnen verminderen. Daarom is het van belang om de betrouwbaarheid en consistentie van deze dynamische modellen verder te onderzoeken, met name die welke een fysieke beschrijving van de massabewegingprocessen integreren in een numerieke analyse, gekoppeld aan een Geografisch Informatie Systeem (GIS).

Er bestaat een grote variatie in het aantal modellen voor het simuleren van massabeweging- fenomenen, en het gevaar daarvan. Dynamische run-out modellen zijn in staat tot het voorspellen van de hellingafwaartse stroming van materialen na hun bezwijking, en het bepalen van de gebieden waar risico-elementen (zoals de fysieke infrastructuur) beschadigd kunnen worden met een zekere intensiteit. De resultaten van deze modellen vormen een belangrijke invoer voor het bepalen van de fysieke gevoeligheid (vulnerability) en het risico. Een belangrijk aspect in het gebruik van run-out modellen is de mogelijkheid om voorspellingen te doen over toekomstige gevaren en de veranderingen daarin. Het meeste onderzoek met betrekking tot de kalibratie van deze modellen vindt echter plaats door middel van de analyse van historische scenario's. De parameterisatie van run-out modellen is problematisch, gegeven het aantal onbekende parameters en het feit dat de meeste van de rheologische parameters niet in het laboratorium bepaald kunnen worden. Vandaar dat de meeste toepassingen van run-out modellen gericht zijn op het numeriek reconstrueren van historische modderstromen. Het gebruik van deze modellen voor het voorspellen van toekomstige gevarensenario's wordt gehinderd door de grote onzekerheid van de invoer parameters.

Het hoofddoel van dit onderzoek was het optimaliseren van dynamische run-out modellen voor kwantitatieve risicoanalyse van modderstromen, door middel van het kwantificeren van de onzekerheid van de invoergegevens. Aangezien er een groot aantal van dit soort modellen ontwikkeld is voor het simuleren van stromingsprocessen en het ruimtelijk bepalen van de intensiteit daarvan, is het van belang om na te gaan welke het beste functioneren, en de onzekerheid in de benodigde invoergegevens te verminderen. Dit maakt de analyse van gevarencurves beter en zorgt ook voor meer betrouwbare gegevens die gebruikt worden in gevoeligheidscurves en uiteindelijk in een betere bepaling van de risicocurves en de kwantificering van het risico.

Dit onderzoek beschrijft de huidige stand van zaken in dynamisch run-out modelleren, met een specifieke focus op zogenaamde "continuüm depth-averaged" modellen, waarbij de stroom wordt beschouwd als een continu medium met een gemiddelde stroomsnelheid over de diepte. Drie ruimtelijke dynamische run-out modellen (MassMov2D, DAN3D and RAMMS) werden gebruikt voor het maken van een gevoeligheidsanalyse van de weerstandsparameters die gebruikt worden in de Voellmy rheologie. De methodes werden toegepast in drie test gebieden: Barcelonnette in de Franse Alpen, Valtellina di Tirano in Noordwest Italië, en een klein gebied in de staat Kerala in India.

Speciale aandacht werd in dit onderzoek gegeven aan het mechanisme van erosie van materialen door modder- en puinstromen tijdens het transport. De toename van het volume tussen het bezwijken en de uiteindelijke afzetting van de materialen vanwege erosie tijdens het transport heeft een grote invloed op de grootte van het gebied dat uiteindelijk getroffen wordt. Om dit effect te onderzoeken werd een 1-D run-out model gepresenteerd waarin de effecten van deze erosie zijn geïntegreerd met behulp van "limit equilibrium" (eindig evenwicht) analyse en het ontstaan van wateroverspanning in de poriën van het stroombedmateriaal door niet gedraineerde belasting.

Een bestand met rheologische parameters (Voellmy en Bingham rheologieën) werd gemaakt op basis van een groot aantal publicaties over de toepassing van run-out modellen in verschillende milieus, met verschillen in beginvolume, type beweging en andere karakteristieken. Deze database werd gebruikt om de variabiliteit van de rheologische parameters weer te geven met behulp van waarschijnlijkheidsverdelingen (probability density functions). Deze werden vervolgens toegepast in een waarschijnlijkheidsanalyse met behulp van Monte Carlo simulatie voor het doorrekenen van de effecten van de onzekerheid van de invoergegevens op de eindresultaten. Een groot aantal steekproeven (5000) werden genomen uit de gecombineerde waarschijnlijkheidsverdelingen van de Voellmy en

Bingham rheologieën. Deze werden vervolgens gebruikt als invoergegevens voor de model run-out simulaties. De resultaten vertoonden een Gamma-verdeling van de mogelijke hoogte en snelheid van de gemodelleerde stroomscenario's voor een aantal specifieke punten, welke gebruikt werden om de kans op de mate van intensiteit (impact) te bepalen.

De waarschijnlijkheidsverdelingen werden ook toegepast in een nieuw ruimtelijk run-out model voor analyse op middelgrote schalen. Dit 2-D één fase continuüm model (AschFlow) simuleert het transport, de erosie en de afzetting van aardverschuivingen en modderstromen. Het werd toegepast op een middelgrote schaal in de testgebieden in de Franse Alpen en Noordwest Italië.

Eén van de meeste complexe aspecten is de interactie tussen de intensiteiten die met de run-out modellen worden bepaald, en de karakteristieken van de risico-elementen die beschadigd kunnen worden (bijv. gebouwen). In dit onderzoek werden drie gevoeligheidscurven gegenereerd voor het voorspellen van de schade aan gebouwen, door gebruikt te maken van de resultaten van de run-out modellen en de fysieke schade aan de gebouwen tijdens een recente modderstroom in het testgebied in Italië.

In een naburig testgebied werden deze gevoeligheidscurven vervolgens gebruikt voor een kwantitatieve risicoanalyse voor modderstromen, gebaseerd op dynamische run-out modellering. Op basis van historische gegevens en bestaande gevarenkaarten werden drie mogelijke ontstaansgebieden van modderstromen geïdentificeerd. Het dynamische run-out model FLO-2D werd vervolgens toegepast om de mogelijke overstroomde (impact) gebieden te bepalen voor drie terugkeerperiodes van de regenval die verantwoordelijk is voor het ontstaan van deze modderstromen (10, 50 en 100 jaar). De methode had verschillende componenten, waaronder de regenvalanalyse, het modelleren van de regenval-afvoer relatie, de analyse van bodemonsters in het laboratorium, de analyse van terreinkenmerken, het modelleren van de modderstromen, de bepaling van de mogelijke hoogte en snelheid en de daaruit afgeleide intensiteit (impact) voor de toepassing van de gevoeligheidscurves, en de uiteindelijke bepaling van de te verwachten economische schade door middel van zogenaamde risicocurven.

Dit onderzoek heeft bijgedragen aan een beter begrip met betrekking tot het gebruik van run-out modellen voor modderstromen, en heeft nieuwe mogelijkheden onderzocht waardoor de onzekerheid van de invoergegevens beter geanalyseerd kan worden, om uiteindelijk een betere schatting te maken van de te verwachten economische schade. De resultaten kunnen worden toegepast in kosten-baten analyse voor het ontwerpen van risico verminderende maatregelen.

Samenvatting

Het grootste deel van dit onderzoek werd uitgevoerd als zogenaamde “Early Stage Researcher” binnen een Marie Curie Actions Research Training Network genaamd “Mountain Risks: from prediction to management and governance” binnen het 6^e Kaderprogramma van de Europese Commissie (<http://mountain-risks.eu/>). Het laatste onderdeel van dit onderzoek werd gefinancierd vanuit het “SafeLand” project binnen het 7^e Kaderprogramma voor onderzoek en technologische ontwikkeling van de Europese Commissie (<http://www.safeland-fp7.eu/>).

Appendices

Appendix 1

Database for Voellmy model

Case number	Case	Author
1	Avalanche Lake rockslide in the Mackenzie Mountains (CANADA)	Evans et al. 1994
2	Jonas Creek, Alberta	McKinnon, 2006
3	Jonas Creek, Alberta	McKinnon, 2006
4	Coal Mine Waste Flow Slides, British Columbia	Hungr, 1995
5	Frank Slide, Canada	McDougall 2006
6	Frank Slide, Canada	Quan Luna 2007
7	Frank Slide, Canada	Quan Luna 2007
8	Shuwan slide (Hong Kong)	Quan Luna 2007
9	Shuwan slide (Hong Kong)	Quan Luna 2007
10	Vall Pola (Italy)	Hungr & Evans 1996
11	Vall Pola (Italy)	Haddad 2007
12	Zymoetz River landslide, British Columbia, Canada	McDougall 2004
13	Zymoetz River landslide, British Columbia, Canada	McDougall 2004
14	Hummingbird Creek, British Columbia	Jakob et al. 2000.
15	Hummingbird Creek, British Columbia	Jakob et al. 2000
16	Eagle Pass, British Columbia	Hungr and Evans 2004
17	Eagle Pass, British Columbia	Hungr and Evans 2004
18	Nomash River Slide, British Columbia	Hungr, 2004
19	Nomash River Slide, British Columbia	Hungr, 2004
20	Nomash River Slide, British Columbia	Hungr, 2004
21	1248 Mt Granier, Isere and Savoie, France	Cruden, 1972 - McKinnon 2008
22	Pandemonium Creek, British Columbia, Canada (1959)	Evans 1989
23	Pandemonium Creek, British Columbia, Canada (1959)	Evans 1989
24	2006 Guinsaungon, Philippines	Guthrie et al., 2007
25	2006 Guinsaungon, Philippines	Guthrie et al., 2008
26	2006 Guinsaungon, Philippines	Guthrie et al., 2009
27	2006 Guinsaungon, Philippines	Guthrie et al., 2010
28	1717 Triolet Glacier, Italy	Deline, 2009
29	1717 Triolet Glacier, Italy	Deline, 2010
30	1959 Madison Canyon Rockslide, Montana, USA	McKinnon, 2008
31	1959 Madison Canyon Rockslide, Montana, USA	McKinnon, 2008
32	1959 Madison Canyon Rockslide, Montana, USA	McKinnon, 2008
33	Rockslide Pass, Northwest Territories, Canada	Hungr and Evans 1996
34	Brazeau Lake, Alberta, Canada	McKinnon, 2008
35	Brazeau Lake, Alberta, Canada	McKinnon, 2008

Appendices

36	1991 Mt Cook, New Zealand	McKinnon, 2008
37	Rockslide Pass, Northwest Territories, Canada	McKinnon, 2008
38	Rockslide Pass, Northwest Territories, Canada	McKinnon, 2008
39	2001 Las Colinas, El Salvador	McKinnon, 2008
40	2002 Las Colinas, El Salvador	McKinnon, 2008
41	2002 McAuley Creek, BC	Hungr, 2004
42	2003 McAuley Creek, BC	Hungr, 2004
43	1982 Mt. Sale, China	McKinnon, 2008
44	1983 Mt. Sale, China	McKinnon, 2008
45	Schipfenbach 2000, Switzerland	Hurlimann,2003
46	Font de la Llum torrent, Montserrat,2000	Medina,2008
47	Cardemeller torrent, Pal, Andorra.1982	Medina,2008
48	Jou torrent, La Guingueta. Spain, 1982	Medina,2008
49	Panabaj, Guatemala 2005	Quan Luna 2007
50	San Juan, Guatemala, 2005	Quan Luna 2007
51	Coal Mine Waste Flow Slide (case1), British Columbia	Hungr, 2002
52	Coal Mine Waste Flow Slide (case2), British Columbia	Hungr, 2002
53	Six des Eaux Froides Rock Avalanche, Switzerland 1946	McDougall,2006
54	Cervinara,Campania, Italy, 2004	McDougall,2006
55	Cervinara,Campania, Italy, 2005	Revellino, 2004
56	Sham Tseng San Tsuen, Hong Kong, 1999	Blanc, 2008
57	Tsing Shan, Hong Kong, 1990	Blanc, 2008
58	Tsing Shan, Hong Kong, 2000	Blanc, 2008
59	Tsing Shan, Hong Kong, 2000	Blanc, 2008
60	Lei Pui Street Lanslide, Hong Kong, 2001	Paudel and Law 2008
61	Lei Pui Street Lanslide, Hong Kong, 2001	Paudel and Law 2008
62	Lei Pui Street Lanslide, Hong Kong, 2001	Paudel and Law 2009
63	Lei Pui Street Lanslide, Hong Kong, 2001	Sun, 2003
64	Kamikamihori Valley, Japan, 1976	Koch, 1998
65	Kamikamihori Valley, Japan, 1979	Koch, 1998
66	Illgraben, Switzerland, 2000	Zanuttigh and Lamberti,2004
67	Illgraben, Switzerland, 2005	Kowalski, 2008
68	Kamikamihori Valley, Japan, 1976	Naef, 2006
69	Mendoza, Argentina,	Mergili, 2007
70	Tates Cairn, Hong Kong, 2005	Cepeda, 2007
71	Tates Cairn, Hong Kong, 2005	Cepeda, 2007
72	1991 Mt Cook, New Zealand	Allem and Schneider, 2009
73	Picacho landslide, 1982, El Salvador	Cepeda, 2008
74	Turnoff Creek, 1992, Canada	Begueria, 2009
75	Turnoff Creek, 1992, Canada	Begueria, 2009
76	Turtle Mountain, Canada (scenario)	Froese, 2009
77	Tates Cairn, Hong Kong, 2005	Wang, 2007

78	Tates Cairn, Hong Kong, 2005	Hurlimann, 2007
79	Tates Cairn, Hong Kong, 2005	Hurlimann, 2007
80	Tates Cairn, Hong Kong, 2005	Kwan, 2007
81	Tates Cairn, Hong Kong, 2005	Pastor, 2007
82	Tates Cairn, Hong Kong, 2005	Pirulli, 2007
83	Fei Tsui Road, 1995, Kong Kong	Wang, 2007
84	Fei Tsui Road, 1995, Kong Kong	Cheng, 2007
85	Fei Tsui Road, 1995, Kong Kong	Kwan, 2007
86	Fei Tsui Road, 1995, Kong Kong	Mangueney, 2007
87	Fei Tsui Road, 1995, Kong Kong	Hungr, 2007
88	Fei Tsui Road, 1995, Kong Kong	Pastor, 2007
89	Fei Tsui Road, 1995, Kong Kong	Sassa, 2007
90	Fei Tsui Road, 1995, Kong Kong	Pirulli, 2007
91	Fei Tsui Road, 1995, Kong Kong	Pirulli, 2007
92	Shuwan slide (Hong Kong)	Wang, 2007
93	Shuwan slide (Hong Kong)	Cheng, 2007
94	Shuwan slide (Hong Kong)	Crosta, 2007
95	Shuwan slide (Hong Kong)	Kwan, 2007
96	Shuwan slide (Hong Kong)	Kwan, 2007
97	Shuwan slide (Hong Kong)	Mangueney, 2007
98	Shuwan slide (Hong Kong)	Hungr, 2007
99	Shuwan slide (Hong Kong)	Hungr, 2007
100	Shuwan slide (Hong Kong)	Pastor, 2007
101	Shuwan slide (Hong Kong)	Pastor, 2007
102	Frank Slide, Canada	Crosta, 2007
103	Frank Slide, Canada	Kwan, 2007
104	Frank Slide, Canada	Mangueney, 2007
105	Frank Slide, Canada	Hungr, 2007
106	Frank Slide, Canada	Pastor, 2007
107	Frank Slide, Canada	Pastor, 2007
108	Frank Slide, Canada	Pirulli, 2007
109	Frank Slide, Canada	Sheridan, 2007
110	Sham Tseng San Tsuen, Hong Kong, 1999	Quan Luna 2007
111	Sham Tseng San Tsuen, Hong Kong, 1999	Quan Luna 2007
112	Sham Tseng San Tsuen, Hong Kong, 1999	Kwan, 2007
113	Sham Tseng San Tsuen, Hong Kong, 1999	Hungr, 2007
114	Sham Tseng San Tsuen, Hong Kong, 1999	Hungr, 2007
115	Sham Tseng San Tsuen, Hong Kong, 1999	Pastor, 2007
116	Tsing Shan, Hong Kong, 2000	Wang, 2007
117	Tsing Shan, Hong Kong, 2000	Hurlimann, 2007
118	Tsing Shan, Hong Kong, 2000	Hurlimann, 2008
119	Tsing Shan, Hong Kong, 2000	Chen, 2007

Appendices

120	Tsing Shan, Hong Kong, 2000	Pastor, 2007
121	Thurweiser rock avalanche, Italy, 2004	Cheng, 2007
122	Thurweiser rock avalanche, Italy, 2005	Crosta, 2007
123	Thurweiser rock avalanche, Italy, 2006	Hungr, 2007
124	Thurweiser rock avalanche, Italy, 2007	Kwan, 2007
125	Thurweiser rock avalanche, Italy, 2008	Pastor, 2007
126	Lo Wai debris flow, 2005, Hong Kong	Wang, 2007
127	Peringalam, India, 2001	Quan Luna 2008
128	di Fiames debris flow, 2006, Italy	Cesca, 2008
129	Aquabona debris flow, Italy	Armento, 2008
130	Aquabona debris flow, Italy	Armento, 2008
131	Aquabona debris flow, Italy	Armento, 2008
132	K109 debris flow, Italy	Armento, 2008
133	K109 debris flow, Italy	Armento, 2008
134	K109 debris flow, Italy	Armento, 2008
135	Thurweiser rock avalanche, Italy, 2005	Sosio, 2008
136	Yosemite valley, USA	Bertolo 2005
137	Yosemite valley, USA	Bertolo 2005
138	Yosemite valley, USA	Bertolo 2005
139	Mount Cayley 1983, Canada	Hungr, 2005
140	Mount Cayley 1983, Canada	Hungr, 2005
141	Mount Cayley 1983, Canada	Hungr, 2005
142	Mount Steele, Canada, 2007	McKinnon, 2008
143	1915 Great Fall, England	McKinnon, 2008
144	1988 Abbot' Cliff, England	McKinnon, 2008
145	1850 Seaford England	McKinnon, 2008
146	1850 Seaford England	McKinnon, 2008
147	Mid-levels Dlow Hong Kong (scenario)	Muir 2006
148	Mid-levels Dlow Hong Kong (scenario)	Muir 2006
149	Ceppo Morelli Landslide, Italy (scenarios)	Castelli, 2007
150	Rosone Landslide, Italy (scenario)	Castelli, 2007
151	Frangerello stream-Susa valley. Italy 2000	Bertolo & Botino, 2009
152	Campanian Apennines	Revellino et al. 2004
153	Campanian Apennines	Revellino et al. 2004
154	Campanian Apennines	Revellino et al. 2004
155	Campanian Apennines	Revellino et al. 2004
156	Campanian Apennines	Revellino et al. 2004
157	Campanian Apennines	Revellino et al. 2004
158	Campanian Apennines	Revellino et al. 2004
159	Campanian Apennines	Revellino et al. 2004
160	Campanian Apennines	Revellino et al. 2004
161	Campanian Apennines	Revellino et al. 2004

162	Campanian Apennines	Revellino et al. 2004
163	Campanian Apennines	Revellino et al. 2004
164	Campanian Apennines	Revellino et al. 2004
165	Campanian Apennines	Revellino et al. 2004
166	Campanian Apennines	Revellino et al. 2004
167	Campanian Apennines	Revellino et al. 2004
168	Campanian Apennines	Revellino et al. 2004

Case number	Type	Volume (cubic m)	Height	Runout (m)	Fahrböschung	Velocity (m/s)	Friction angle	Turbulent Coefficient (m/s ²)
1	Rock avalanche	200,000,000	1,200	2,900	22.30	82	0.02	250
2	Rock avalanche	4,000,000	880	3250	15.11	7	0.15	500
3	Rock avalanche	4,000,000	880	3250	15.11	7	0.36	1500
4	Debris Flows	3,000,000	560	1220	24.7	45	0.36	1500
5	Rock avalanche	36000000	770	3500	12.4	30	0.1	500
6	Rock avalanche	36000000	770	3500	12.4	30	0.1	700
7	Rock avalanche	36000000	770	3500	12.4	30	0.24	1500
8	Debris Flows	26000	82	245	18.26	15	0.3	500
9	Debris Flows	26000	82	245	18.26	15	0.62	1500
10	Rock avalanche	34000000	356	800	24	80	0.1	500
11	Rock avalanche	34000000	356	800	24	80	0.32	1500
12	Debris flow	7200000	425	1390	17	54	0.12	500
13	Debris flow	7200000	425	1390	17	67	0.26	2000
14	Debris Flows	25,000	162	560	16.17	20.7	0.36	2000
15	Debris Flows	25,000	162	560	16.17	20.7	0.08	200
16	Rock avalanche	250,000	520	1200	23.26	8	0.57	1500
17	Rock avalanche	250,000	520	1200	23.26	8	0.05	400
18	Rock avalanche	300,000	560	2234	14	40	0.19	1500
19	Rock avalanche	300,000	560	2282	13.5	35	0.05	800
20	Rock avalanche	300,000	560	2500	12.62	22	0.04	500
21	Rock avalanche	200,000,000	1,620	7300	12	90	0.1	500
22	Rock avalanche	5,000,000	2,000	8610	13	89	0.07	1200
23	Rock avalanche	5,000,000	2,000	8631	13	96	0.08	2000
24	Rock avalanche	20,000,000	810	3914	11.64	70	0.17	2000
25	Rock avalanche	20,000,000	810	3630	12	70	0.18	2000
26	Rock avalanche	20,000,000	810	3630	12	72	0.07	500
27	Rock avalanche	20,000,000	810	4100	11.14	80	0.2	2000
28	Rock avalanche	9,800,000	1,860	7250	14.35	44	0.05	850

Appendices

29	Rock avalanche	9,800,000	1,860	7100	14.68	44	0.1	2100
30	Rock avalanche	21,000,000	2,200	8461	14.6	38	0.3	2000
31	Rock avalanche	21,000,000	2,200	8461	14.6	41	0.28	500
32	Rock avalanche	21,000,000	2,200	8461	14.6	42	0.3	100
33	Rock avalanche	370,000,000	600	4000	8.5	30	0.03	450
34	Rock avalanche	4,500,000	893	2750	18	65	0.1	100
35	Rock avalanche	4,500,000	893	2750	18	80	0.34	1500
36	Rock avalanche	11,000,000	2,660	7084	20.55	55	0.05	1000
37	Rock avalanche	30,000,000	860	5760	8.5	35	0.07	500
38	Rock avalanche	30,000,000	860	8000	5.71	65	0.05	700
39	Landslide	102,500	160	731	12.3	25	0.21	2000
40	Landslide	102,500	160	709	12.6	25	0.15	1000
41	Rock avalanche	7,400,000	750	1600	25.07	62	0.57	2000
42	Rock avalanche	7,400,000	750	1600	25.07	62	0.1	500
43	Rock avalanche	30,000,000	320	1526	13.22	36	0.19	2000
44	Rock avalanche	30,000,000	320	1594	11.3	32	0.15	900
45	Debris flow	5,500	1,315	2450	28.19	7	0.175	125
46	Debris flow	10,000	550	1375	21.8	15.6	0.13	100
47	Debris flow	500	640	1150	28.81	7.2	0.22	144
48	Debris flow	30,000	1,150	3300	19.18	6	0.1	100
49	Debris flow	55,000	1,440	4900	16.3	15	0.04	450
50	Debris flow	57,600	230	800	16.01	16	0.04	450
51	Debris flow	700,000	420	750	29.24	32	0.1	500
52	Debris flow	700,000	420	1650	14.25	44	0.05	200
53	Rock avalanche	5,000,000	715	2500	16	87	0.13	450
54	Debris flow	3,750	820	1550	27.47	10.5	0.57	1500
55	Debris flow	3,750	820	1550	27.47	10.5	0.07	200
56	Debris flow	600	90	210	23.2	4.4	0.3	1000
57	Debris flow	350	404	1035	21.32	16.5	0.24	1500
58	Debris flow	150	360	754	25.5	5.5	0.18	500
59	Debris flow	150	360	588	31.47	5.7	0.18	500
60	Landslide	250	139	235	26	18	0.48	2000
61	Landslide	250	139	120	26	9	0.48	200
62	Landslide	250	139	130	47	11	0.48	500
63	Landslide	680	139	320	23	14	0.2	500
64	Debris flow	6,500	460	1900	13.6	8	0.06	120
65	Debris flow	14,800	460	1900	13.6	6	0.08	120

66	Debris flow	35,000	458	2600	10	4	0.043	480
67	Debris flow	140,000	458	2600	10	4	0.1	330
68	Debris flow	6,400	460	2200	11.81	9	0.06	120
69	Debris flow	7,000	515	1315	21.38	28	0.6	1500
70	Debris flow	1,200	140	332	23	7.3	0.26	1000
71	Debris flow	1,200	140	332	23	3.6	0.36	500
72	Rock avalanche	11,000,000	2,660	7084	20.55	55	0.15	2900
73	Debris flow	425,000	1280	4600	15.53	4.4	0.05	500
74	Rock avalanche	4,000,000	535	2000	15	18.3	0.09	300
75	Rock avalanche	4,000,000	535	2000	15	7	0.2	300
76	Rock avalanche	6,590,000	600	3200	10.61	50	0.36	1500
77	Debris flow	1,200	140	332	23	11	0.45	2000
78	Debris flow	1,200	140	332	23	7	0.42	400
79	Debris flow	1,200	140	332	23	11	0.46	1000
80	Debris flow	1,200	140	332	23	8	0.26	500
81	Debris flow	1,200	140	332	23	6.27	0.3	500
82	Debris flow	1,200	140	332	23	1.28	0.46	1000
83	Landslide	14,000	35	72	24.72	11	0.57	1000
84	Landslide	14,000	35	72	24.72	18.5	0.4	1000
85	Landslide	14,000	35	72	24.72	5.7	0.7	1000
86	Landslide	14,000	35	72	24.72	68	0.48	1000
87	Landslide	14,000	35	72	24.72	3.6	0.7	1500
88	Landslide	14,000	35	72	24.72	8	0.5	1500
89	Landslide	14,000	35	72	24.72	5.5	0.39	1000
90	Landslide	14,000	35	72	24.72	4.8	0.51	1500
91	Landslide	14,000	35	72	24.72	4.8	0.46	1000
92	Debris Flows	26000	82	245	18.26	12.25	0.28	1000
93	Debris Flows	26000	82	245	18.26	8.16	0.36	1500
94	Debris Flows	26000	82	245	18.26	4.9	0.4	2000
95	Debris Flows	26000	82	245	18.26	8.75	0.26	1500
96	Debris Flows	26000	82	245	18.26	10.2	0.26	500
97	Debris Flows	26000	82	245	18.26	10	0.32	1500
98	Debris Flows	26000	82	245	18.26	25	0.36	2000
99	Debris Flows	26000	82	245	18.26	16	0.19	200
100	Debris Flows	26000	82	245	18.26	9	0.3	1000
101	Debris Flows	26000	82	245	18.26	10	0.34	1500
102	Rock avalanche	36000000	770	3500	12.4	38.8	0.23	2000
103	Rock avalanche	36000000	770	3500	12.4	58.33	0.13	1500

Appendices

104	Rock avalanche	36000000	770	3500	12.4	35	0.11	1800
105	Rock avalanche	36000000	770	3500	12.4	120	0.1	500
106	Rock avalanche	36000000	770	3500	12.4	49.29	0.21	1500
107	Rock avalanche	36000000	770	3500	12.4	29	0.7	2500
108	Rock avalanche	36000000	770	3500	12.4	58	0.09	700
109	Rock avalanche	36000000	770	3500	12.4	63	0.24	1500
110	Debris flow	600	90	210	23.2	22	0.35	2000
111	Debris flow	600	90	210	23.2	9	0.25	450
112	Debris flow	600	90	210	23.2	4	0.21	500
113	Debris flow	600	90	210	23.2	9	0.3	500
114	Debris flow	600	90	210	23.2	19	0.3	2000
115	Debris flow	600	90	210	23.2	23	0.36	1500
116	Debris flow	1,600	360	754	25.5	18.9	0.24	2000
117	Debris flow	400	360	754	25.5	22	0.2	64
118	Debris flow	400	360	754	25.5	22	0.15	400
119	Debris flow	1,600	360	754	25.5	30	0.19	500
120	Debris flow	150	360	754	25.5	9.3	0.18	500
121	Rock avalanche	1,800,000	1250	2900	23.31	57	0.36	500
122	Rock avalanche	2,200,000	1250	2900	23.31	62.5	0.4	2000
123	Rock avalanche	2,200,000	1250	2900	23.31	60	0.1	1000
124	Rock avalanche	2,200,000	1250	2900	23.31	32	0.5	2000
125	Rock avalanche	2,200,000	1250	2900	23.31	33.8	0.39	1000
126	Debris flow	550	62	450	7.8	16	0.15	2000
127	Debris flow	1,435	320	1280	14	8	0.5	250
128	Debris flow	11,241	360	800	24	9	0.18	500
129	Debris flow	16,393	530	1632	18	14	0.163	400
130	Debris flow	16,604	530	1632	18	13	0.12	300
131	Debris flow	16,407	530	1632	18	10.6	0.133	100
132	Debris flow	13,973	328	774	23	12.1	0.233	400
133	Debris flow	13,932	328	774	23	10.5	0.191	200
134	Debris flow	13,906	328	774	23	8.4	0.17	100
135	Rock avalanche	2,200,000	1250	2900	23.31	55	0.14	1500
136	Debris Flow	750	525	1295	21.8	26	0.12	500
137	Debris Flow	750	525	1459	19.29	20	0.1	600
138	Debris Flow	750	525	644	38	38	0.12	500
139	Rock avalanche	740,000	1180	5000	12	68	0.1	500
140	Rock	740,000	1180	3460	19	70	0.2	1500

	avalanche							
141	Rock avalanche	740,000	1180	3460	19	65	0.12	2000
142	Rock avalanche	30,000,000	1860	5760	18	39	0.6	600
143	Rock avalanche	1,250,000	150	628	13		0.17	600
144	Rock avalanche	280,000	145	442	18	18	0.18	400
145	Rock avalanche	153,000	68	121	28		0.4	100
146	Rock avalanche	153,000	68	121	28		0.34	1000
147	Debris flow	10,000,000	310	570	28		0.36	1000
148	Debris flow	10,000,000	310	570	28		0.23	1000
149	Rock avalanche	1,000,000	485	1170	23		0.32	1500
150	Rock avalanche	1,800,000	420	1268	17.5	46.57	0.23	1000
151	Debris flow	18,000	1587	3500	24	23	0.14	400
152	Debris flow	260	775	1003	38		0.07	200
153	Debris flow	1,745	750	1923	22	14.2	0.07	200
154	Debris flow	327	475	518	42		0.08	200
155	Debris flow	6,831	740	3280	13	10.2	0.05	200
156	Debris flow	10,573	735	2591	16		0.07	200
157	Debris flow	1,226	735	1995	21		0.1	200
158	Debris flow	1,130	730	1890	22		0.07	200
159	Debris flow	953	740	2074	20		0.07	200
160	Debris flow	1,300	755	1589	26	9.4	0.01	200
161	Debris flow	2,552	780	2069	21		0.09	200
162	Debris flow	6,311	645	2077	18		0.08	200
163	Debris flow	2,200	440	1145	21		0.07	200
164	Debris flow	579	435	1170	20		0.11	200
165	Debris flow	2,703	730	2058	19		0.08	200
166	Debris flow	938	740	2990	14	6.2	0.05	200
167	Debris flow	717	755	1250	31	13.9	0.07	200
168	Debris flow	157	570	760	36	14.2	0.07	200

Case number	Method used	Environment (Koppen classification)	Type of movement	Source sediment
1	Back-calibration	Polar-Tundra. Glacial	Unchanneled	Dolostone/Carbonite
2	Back-calibration	Continental subartic, glacial	Unchanneled	Quartzite
3	Back-calibration	Continental subartic, glacial	Unchanneled	Quartzite
4	Back-calibration	Continental subartic, glacial	Channeled	Sandstone, siltstone and shale
5	Back-calibration	Continental subartic, glacial	Unchanneled	Fragmented limestone
6	Back-calibration	Continental subartic, glacial	Unchanneled	Fragmented limestone

Appendices

7	Back-calibration	Continental subartic, glacial	Unchanneled	Fragmented limestone
8	Back-calibration	subtropical	Unchanneled	Weathered tuff and clay
9	Back-calibration	subtropical	Unchanneled	Weathered tuff and clay
10	Back-calibration	Alpine	Unchanneled	Gneiss/Diorite
11	Back-calibration	Alpine	Unchanneled	Gneiss/Diorite
12	Back-calibration	Continental subartic, glacial	Channeled	Volcanic tuff
13	Back-calibration	Continental subartic, glacial	Channeled	Volcanic tuff
14	Back-calibration	Continental subartic, glacial	Channeled	Sandstone
15	Back-calibration	Continental subartic, glacial	Channeled	Sandstone
16	Back-calibration	Continental subartic, glacial	Unchanneled	Gneiss
17	Back-calibration	Continental subartic, glacial	Unchanneled	Gneiss
18	Back-calibration	Continental subartic, glacial	Unchanneled	Marble and basaltic sills
19	Back-calibration	Continental subartic, glacial	Unchanneled	Marble and basaltic sills
20	Back-calibration	Continental subartic, glacial	Unchanneled	Marble and basaltic sills
21	Back-calibration	Alpine	Unchanneled	Limestone
22	Back-calibration	Continental subartic, glacial	Unchanneled	Gneiss/ quartz diorite
23	Back-calibration	Continental subartic, glacial	Unchanneled	Gneiss/ quartz diorite
24	Back-calibration	Tropical-Volcanic	Unchanneled	Breccia/Mudstones
25	Back-calibration	Tropical-Volcanic	Unchanneled	Breccia/Mudstones
26	Back-calibration	Tropical-Volcanic	Unchanneled	Breccia/Mudstones
27	Back-calibration	Tropical-Volcanic	Unchanneled	Breccia/Mudstones
28	Back-calibration	Alpine/glacier	Unchanneled	Granite/morainic rocks
29	Back-calibration	Alpine/glacier	Unchanneled	Granite/morainic rocks
30	Back-calibration	Continental subartic	Unchanneled	Gneiss/schist
31	Back-calibration	Continental subartic	Unchanneled	Gneiss/schist
32	Back-calibration	Continental subartic	Unchanneled	Gneiss/schist
33	Back-calibration	Polar-Tundra. Glacial	Unchanneled	Dolostone/limestone
34	Back-calibration	Continental subartic	Unchanneled	Dolostone/limestone
35	Back-calibration	Continental subartic	Unchanneled	Dolostone/limestone
36	Back-calibration	Alpine	Unchanneled	Morainic sandstone/volcanic rock
37	Back-calibration	Polar-Tundra. Glacial	Unchanneled	Dolostone/limestone
38	Back-calibration	Polar-Tundra. Glacial	Unchanneled	Dolostone/limestone
39	Back-calibration	Tropical-Volcanic	Unchanneled	Pyroclastic material
40	Back-calibration	Tropical-Volcanic	Unchanneled	Pyroclastic material
41	Back-calibration	Continental subartic	Unchanneled	Gneiss
42	Back-calibration	Continental subartic	Unchanneled	Gneiss
43	Back-calibration	Alpine	Unchanneled	Loess
44	Back-calibration	Alpine	Unchanneled	Loess
45	Back-calibration	Alpine	Channeled	Limestone/granite/gneiss
46	Back-calibration	Alpine	Channeled	Sandstones and lutites
47	Back-calibration	Alpine	Channeled	Limestones/phyllites/slates

48	Back-calibration	Alpine	Channeled	Shale
49	Back-calibration	Tropical-Volcanic	Channeled	Pyroclastic material
50	Back-calibration	Tropical-Volcanic	Channeled	Pyroclastic material
51	Back-calibration	Continental subartic, glacial	Channeled	Sandstone, siltstone and shale
52	Back-calibration	Continental subartic, glacial	Channeled	Sandstone, siltstone and shale
53	Back-calibration	Alpine	Unchanneled	Limestone
54	Back-calibration	Mediterranean/Alpine	Channeled	Pyroclastic material
55	Back-calibration	Mediterranean/Alpine	Channeled	Pyroclastic material
56	Back-calibration	subtropical	Channeled	Decomposed granite
57	Back-calibration	subtropical	Channeled	Decomposed granite/volcanic rocks
58	Back-calibration	subtropical	Channeled	Decomposed granite/volcanic rocks
59	Back-calibration	subtropical	Channeled	Decomposed granite/volcanic rocks
60	Back-calibration	subtropical	Channeled	Colluvium/saprolites
61	Back-calibration	subtropical	Channeled	Colluvium/saprolites
62	Back-calibration	subtropical	Channeled	Colluvium/saprolites
63	Back-calibration	subtropical	Channeled	Colluvium/saprolites
64	Back-calibration	Subtropical/Volcanic	Channeled	Pyroclastic material
65	Back-calibration	Subtropical/Volcanic	Channeled	Pyroclastic material
66	Back-calibration	Alpine	Channeled	Quartzites/calcareous dep./dolomites
67	Back-calibration	Alpine	Channeled	Quartzites/calcareous dep./dolomites
68	Back-calibration	Subtropical/Volcanic	Channeled	Pyroclastic material
69	Back-calibration	Mediterranean/Alpine	Channeled	Gypsum/volcanic rocks
70	Back-calibration	subtropical	Channeled	Hornfels/rhyolite/granite
71	Back-calibration	subtropical	Channeled	Hornfels/rhyolite/granite
72	Back-calibration	Alpine	Unchanneled	Morainic sandstone/volcanic rock
73	Back-calibration	Tropical	Channeled	Fractured lava/tephra deposits
74	Back-calibration	Continental subartic, glacial	Unchanneled	Shale/sandstone
75	Back-calibration	Continental subartic, glacial	Unchanneled	Shale/sandstone
76	Scenario	Continental subartic, glacial	Unchanneled	Fragmented limestone
77	Back-calibration	subtropical	Channeled	Hornfels/rhyolite/granite
78	Back-calibration	subtropical	Channeled	Hornfels/rhyolite/granite
79	Back-calibration	subtropical	Channeled	Hornfels/rhyolite/granite
80	Back-calibration	subtropical	Channeled	Hornfels/rhyolite/granite
81	Back-calibration	subtropical	Channeled	Hornfels/rhyolite/granite
82	Back-calibration	subtropical	Channeled	Hornfels/rhyolite/granite
83	Back-calibration	subtropical	Unchanneled	Kaolinite/decomposed tuff
84	Back-calibration	subtropical	Unchanneled	Kaolinite/decomposed tuff
85	Back-calibration	subtropical	Unchanneled	Kaolinite/decomposed tuff
86	Back-calibration	subtropical	Unchanneled	Kaolinite/decomposed tuff
87	Back-calibration	subtropical	Unchanneled	Kaolinite/decomposed tuff

Appendices

88	Back-calibration	subtropical	Unchanneled	Kaolinite/decomposed tuff
89	Back-calibration	subtropical	Unchanneled	Kaolinite/decomposed tuff
90	Back-calibration	subtropical	Unchanneled	Kaolinite/decomposed tuff
91	Back-calibration	subtropical	Unchanneled	Kaolinite/decomposed tuff
92	Back-calibration	subtropical	Unchanneled	Weathered tuff and clay
93	Back-calibration	subtropical	Unchanneled	Weathered tuff and clay
94	Back-calibration	subtropical	Unchanneled	Weathered tuff and clay
95	Back-calibration	subtropical	Unchanneled	Weathered tuff and clay
96	Back-calibration	subtropical	Unchanneled	Weathered tuff and clay
97	Back-calibration	subtropical	Unchanneled	Weathered tuff and clay
98	Back-calibration	subtropical	Unchanneled	Weathered tuff and clay
99	Back-calibration	subtropical	Unchanneled	Weathered tuff and clay
100	Back-calibration	subtropical	Unchanneled	Weathered tuff and clay
101	Back-calibration	subtropical	Unchanneled	Weathered tuff and clay
102	Back-calibration	subtropical	Unchanneled	Weathered tuff and clay
103	Back-calibration	Continental subartic, glacial	Unchanneled	Fragmented limestone
104	Back-calibration	Continental subartic, glacial	Unchanneled	Fragmented limestone
105	Back-calibration	Continental subartic, glacial	Unchanneled	Fragmented limestone
106	Back-calibration	Continental subartic, glacial	Unchanneled	Fragmented limestone
107	Back-calibration	Continental subartic, glacial	Unchanneled	Fragmented limestone
108	Back-calibration	Continental subartic, glacial	Unchanneled	Fragmented limestone
109	Back-calibration	Continental subartic, glacial	Unchanneled	Fragmented limestone
110	Back-calibration	subtropical	Channeled	Colluvium/decomposed granite
111	Back-calibration	subtropical	Channeled	Colluvium/decomposed granite
112	Back-calibration	subtropical	Channeled	Colluvium/decomposed granite
113	Back-calibration	subtropical	Channeled	Colluvium/decomposed granite
114	Back-calibration	subtropical	Channeled	Colluvium/decomposed granite
115	Back-calibration	subtropical	Channeled	Colluvium/decomposed granite
116	Back-calibration	subtropical	Channeled	Decomposed granite/volcanic rocks
117	Back-calibration	subtropical	Channeled	Decomposed granite/volcanic rocks
118	Back-calibration	subtropical	Channeled	Decomposed granite/volcanic rocks
119	Back-calibration	subtropical	Channeled	Decomposed granite/volcanic rocks
120	Back-calibration	subtropical	Channeled	Decomposed granite/volcanic rocks
121	Back-calibration	Alpine	Unchanneled	Dolostone/black limestone
122	Back-calibration	Alpine	Unchanneled	Dolostone/black limestone
123	Back-calibration	Alpine	Unchanneled	Dolostone/black limestone
124	Back-calibration	Alpine	Unchanneled	Dolostone/black limestone
125	Back-calibration	Alpine	Unchanneled	Dolostone/black limestone
126	Back-calibration	subtropical	Channeled	Man-made slope

127	Back-calibration	Tropical	Channeled	Sparolite sands/lithomargic clays
128	Back-calibration	Alpine	Channeled	Dolomite
129	Back-calibration	Alpine	Channeled	Dolomite
130	Scenario	Alpine	Channeled	Dolomite
131	Scenario	Alpine	Channeled	Dolomite
132	Back-calibration	Alpine	Channeled	Dolomite
133	Scenario	Alpine	Channeled	Dolomite
134	Scenario	Alpine	Channeled	Dolomite
135	Back-calibration	Alpine	Unchanneled	Dolostone/black limestone
136	Back-calibration	Subtropical-Dry	Channeled	Granites/plutonic rocks
137	Back-calibration	Subtropical-Dry	Channeled	Granites/plutonic rocks
138	Back-calibration	Subtropical-Dry	Channeled	Granites/plutonic rocks
139	Back-calibration	Continental subartic, glacial	Unchanneled	Pyroclastic tuff
140	Back-calibration	Continental subartic, glacial	Unchanneled	Pyroclastic tuff
141	Back-calibration	Continental subartic, glacial	Unchanneled	Pyroclastic tuff
142	Back-calibration	Continental subartic, glacial	Unchanneled	
143	Back-calibration	Oceanic	Unchanneled	Chalk
144	Back-calibration	Oceanic	Unchanneled	Chalk
145	Back-calibration	Oceanic	Unchanneled	Chalk
146	Back-calibration	Oceanic	Unchanneled	Chalk
147	Scenario	Subtropical	Unchanneled	Saprolites/Vitric tuff
148	Scenario	Subtropical	Unchanneled	Saprolites/Vitric tuff
149	Scenario	Alpine	Unchanneled	Gneiss
150	Scenario	Alpine	Unchanneled	Gneiss
151	Back-calibration	Alpine	Channeled	Dolomite
152	Back-calibration	Pyroclastic/appenines	Channeled	Pyroclastic
153	Back-calibration	Pyroclastic/appenines	Channeled	Pyroclastic
154	Back-calibration	Pyroclastic/appenines	Channeled	Pyroclastic
155	Back-calibration	Pyroclastic/appenines	Channeled	Pyroclastic
156	Back-calibration	Pyroclastic/appenines	Channeled	Pyroclastic
157	Back-calibration	Pyroclastic/appenines	Channeled	Pyroclastic
158	Back-calibration	Pyroclastic/appenines	Channeled	Pyroclastic
159	Back-calibration	Pyroclastic/appenines	Channeled	Pyroclastic
160	Back-calibration	Pyroclastic/appenines	Channeled	Pyroclastic
161	Back-calibration	Pyroclastic/appenines	Channeled	Pyroclastic
162	Back-calibration	Pyroclastic/appenines	Channeled	Pyroclastic
163	Back-calibration	Pyroclastic/appenines	Channeled	Pyroclastic
164	Back-calibration	Pyroclastic/appenines	Channeled	Pyroclastic
165	Back-calibration	Pyroclastic/appenines	Channeled	Pyroclastic
166	Back-calibration	Pyroclastic/appenines	Channeled	Pyroclastic
167	Back-calibration	Pyroclastic/appenines	Channeled	Pyroclastic
168	Back-calibration	Pyroclastic/appenines	Channeled	Pyroclastic

Database for Bingham model

Case number	Case	Author
1	Charmaix - Modane	Malet and Remaitre, 2010
2	Saint-Gervais	Malet and Remaitre, 2010
3	Ravoire de Pontamafrey	Malet and Remaitre, 2010
4	Ravoire de Pontamafrey	Malet and Remaitre, 2010
5	Ravoire de Pontamafrey	Malet and Remaitre, 2010
6	Ravoire de Pontamafrey	Malet and Remaitre, 2010
7	Ravoire de Pontamafrey	Malet and Remaitre, 2010
8	Ravoire de Pontamafrey	Malet and Remaitre, 2010
9	Ravoire de Pontamafrey	Malet and Remaitre, 2010
10	Ravoire de Pontamafrey	Malet and Remaitre, 2010
11	Ravoire de Pontamafrey	Malet and Remaitre, 2010
12	Claret	Malet and Remaitre, 2010
13	Claret	Malet and Remaitre, 2010
14	Claret	Malet and Remaitre, 2010
15	Claret	Malet and Remaitre, 2010
16	Claret	Malet and Remaitre, 2010
17	Claret	Malet and Remaitre, 2010
18	Claret	Malet and Remaitre, 2010
19	Claret	Malet and Remaitre, 2010
20	Claret	Malet and Remaitre, 2010
21	Claret	Malet and Remaitre, 2010
22	Claret	Malet and Remaitre, 2010
23	Claret	Malet and Remaitre, 2010
24	Claret	Malet and Remaitre, 2010
25	Claret	Malet and Remaitre, 2010
26	Claret	Malet and Remaitre, 2010
27	Claret	Malet and Remaitre, 2010
28	Claret	Malet and Remaitre, 2010
29	Rieu-Sec	Malet and Remaitre, 2010
30	Rieu-Sec	Malet and Remaitre, 2010
31	Rieu-Sec	Malet and Remaitre, 2010
32	Rieu-Sec	Malet and Remaitre, 2010
33	Rieu-Sec	Malet and Remaitre, 2010
34	Rieu-Sec	Malet and Remaitre, 2010
35	Pousset	Malet and Remaitre, 2010
36	Pousset	Malet and Remaitre, 2010
37	Pousset	Malet and Remaitre, 2010
38	Pousset	Malet and Remaitre, 2010
39	Pousset	Malet and Remaitre, 2010

40	Pousset	Malet and Remaitre, 2010
41	Pousset	Malet and Remaitre, 2010
42	Pousset	Malet and Remaitre, 2010
43	Pousset	Malet and Remaitre, 2010
44	Sainte-Elisabeth	Malet and Remaitre, 2010
45	Sainte-Elisabeth	Malet and Remaitre, 2010
46	Sainte-Elisabeth	Malet and Remaitre, 2010
47	Sainte-Elisabeth	Malet and Remaitre, 2010
48	Verdarel	Malet and Remaitre, 2010
49	Verdarel	Malet and Remaitre, 2010
50	Verdarel	Malet and Remaitre, 2010
51	Verdarel	Malet and Remaitre, 2010
52	Boscodon - Bragouse	Malet and Remaitre, 2010
53	Boscodon - Bragouse	Malet and Remaitre, 2010
54	Boscodon - Bragouse	Malet and Remaitre, 2010
55	Boscodon - Bragouse	Malet and Remaitre, 2010
56	Salso Moreno - Le Pra (Tinée)	Malet and Remaitre, 2010
57	Salso Moreno - Le Pra (Tinée)	Malet and Remaitre, 2010
58	Salso Moreno - Le Pra (Tinée)	Malet and Remaitre, 2010
59	Salso Moreno - Le Pra (Tinée)	Malet and Remaitre, 2010
60	Manival	Malet and Remaitre, 2010
61	Manival	Malet and Remaitre, 2010
62	Manival	Malet and Remaitre, 2010
63	Manival	Malet and Remaitre, 2010
64	Merdaret	Malet and Remaitre, 2010
65	Saint-Martin	Malet and Remaitre, 2010
66	Saint-Martin	Malet and Remaitre, 2010
67	Saint-Martin	Malet and Remaitre, 2010
68	Saint-Martin	Malet and Remaitre, 2010
69	Saint-Martin	Malet and Remaitre, 2010
70	Saint-Martin	Malet and Remaitre, 2010
71	Saint-Martin	Malet and Remaitre, 2010
72	Saint-Martin	Malet and Remaitre, 2010
73	Saint-Martin	Malet and Remaitre, 2010
74	Saint-Martin	Malet and Remaitre, 2010
75	Arbonne	Malet and Remaitre, 2010
76	Arbonne	Malet and Remaitre, 2010
77	Arbonne	Malet and Remaitre, 2010
78	Arbonne	Malet and Remaitre, 2010
79	Faucon	Malet and Remaitre, 2010
80	Faucon	Malet and Remaitre, 2010
81	Raja - Chapieux	Malet and Remaitre, 2010

Appendices

82	Popocatepl	Haddad, 2007
83	Popocatepl	Haddad, 2007
84	Popocatepl	Haddad, 2007
85	Popocatepl	Haddad, 2007
86	Popocatepl	Haddad, 2007
87	Popocatepl	Haddad, 2007
88	Font de la Llum torrent, Montserrat,2000	Medina et al. 2008
89	Madison Canyon, Montana, USA 1959	Hungr,1995
90	Wartschenbach, Austria 1997	Begueria et al, 2009
91	Facuon, 2003. France	Begueria et al, 2009
92	Kamikamihori Valley, Japan, 1976	Koch, 1998
93	Kamikamihori Valley, Japan, 1979	Koch, 1998
94	Illgraben, Switzerland, 2000	Zanuttigh and Lamberti,2004
95	Kamikamihori Valley, Japan, 1976	Naef et al, 2006
96	Pink mountain, 2002, Canada	Geerstema, 2005
97	Boite River, Dolomites, Italy (scnari)	Armento et al., 2009
98	Lo Wai debris flow, 2005, Hong Kong	Pastor et al., 2007
99	Yosemite valley, USA	Betolo and Weiczoreck, 2005
100	Yosemite valley, USA	Betolo and Weiczoreck, 2005
101	Yosemite valley, USA	Betolo and Weiczoreck, 2005
102	Mount Cayley 1983, Canada	Hungr, 2005
103	Stoze, 2000, Slovenia	Cetina et al., 2006
104	Frangerello stream-Susa velley. Italy 2000	Bertolo & Botino, 2008
105	Frangerello stream-Susa velley. Italy 2001	Bertolo & Botino, 2008

Case number	Run-out Distance	Source Sediment	Volume	Yield stress	Viscosity
1	7.2	Fine grained marls	145000 - 160000	45 - 51 - 60	67 - 91 - 87
2	12.2	Clays & fine grained sandstones	80000	81 - 102	54 - 89
3	7.2	Clays & fine grained limestones	100000	62 - 74	51 - 78
4	7.2	Clays & fine grained limestones	65000	51 - 57	64 - 89
5	7.2	Clays & fine grained limestones	40000	45 - 67	62 - 79
6	7.2	Clays & fine grained limestones	70000 - 80000	30 - 36 - 38	62 - 85 - 76
7	7.2	Clays & fine grained limestones	30000	47 - 61	58 - 91
8	7.2	Clays & fine grained limestones	50000	26 - 28	72 - 86
9	7.2	Clays & fine grained limestones	35000	31 - 48	55 - 70
10	7.2	Clays & fine grained limestones	250000 - 300000	55 - 61 - 63 - 67	71 - 79 - 67 - 74
11	7.2	Clays & fine grained limestones	160000 - 170000	40 - 43	49 - 63
12	1.6	Clays & limestones & evaporites	25000	30 - 34	20 - 34
13	1.6	Clays & limestones & evaporites	30000 - 35000	28 - 39	24 - 32

14	1.6	Clays & limestones & evaporites	15000	29 - 44	29 - 41
15	1.6	Clays & limestones & evaporites	10000	21 - 34	21 - 39
16	1.6	Clays & limestones & evaporites	25000	20 - 32	24 - 49
17	1.6	Clays & limestones & evaporites	14000	26 - 39 - 31 - 28	19 - 30 - 23 - 21
18	1.6	Clays & limestones & evaporites	18000	28 - 42	28 - 35
19	1.6	Clays & limestones & evaporites	40000 - 50000	27 - 34	20 - 28
20	1.6	Clays & limestones & evaporites	40000	29 - 37	40 - 51
21	1.6	Clays & limestones & evaporites	20000	15 - 31 - 25	27 - 39 - 21
22	1.6	Clays & limestones & evaporites	35000	44 - 56	21 - 27
23	1.6	Clays & limestones & evaporites	40000	19 - 27	28 - 38
24	1.6	Clays & limestones & evaporites	50000 - 60000	26 - 36 - 29	15 - 34 - 17
25	0.9	Clays & limestones & evaporites	18000	27 - 41	21 - 39
26	1.6	Clays & limestones & evaporites	20000	20 - 24	25 - 39
27	1.6	Clays & limestones & evaporites	30000	21 - 26 - 22	39 - 51 - 49
28	0.9	Clays & limestones & evaporites	12000	28 - 39 - 42	31 - 48 - 56
29	1.9	Clays & evaporites	15000	45 - 57	58 - 69
30	1.9	Clays & evaporites	25000	56 - 63	72 - 89
31	1.9	Clays & evaporites	20000	60 - 71	78 - 89
32	1.3	Clays & evaporites	15000	54 - 63	50 - 79
33	1.9	Clays & evaporites	10000	68 - 72 - 73	62 - 69 - 61
34	1.9	Clays & evaporites	20000	65 - 69 - 66	72 - 94 - 76
35	2.1	Clay shales & schistoses	30000	35 - 41	25 - 37
36	1.2	Clay shales & schistoses	15000	39 - 54	31 - 42
37	2.1	Clay shales & schistoses	10000 - 12000	30 - 41	28 - 40
38	1.3	Clay shales & schistoses	17000	29 - 34	24 - 51
39	1.8	Clay shales & schistoses	22000	30 - 43	26 - 38
40	2.1	Clay shales & schistoses	25000	42 - 49	40 - 52
41	1.7	Clay shales & schistoses	12000	26 - 34 - 28 - 31	34 - 47 - 39 - 35
42	1.8	Clay shales & schistoses	35000	34 - 41	38 - 46
43	2.1	Clay shales & schistoses	30000 - 35000	32 - 41 - 38	31 - 53 - 39
44	1.8	Clay schales & limestones & moraines	10000	54 - 59	50 - 62
45	1.8	Clay schales & limestones & moraines	25000	60 - 69	64 - 72
46	1.3	Clay schales & limestones & moraines	20000	67 - 81 - 71	61 - 93 - 72
47	1.8	Clay schales & limestones & moraines	30000	59 - 63 - 62	49 - 69 - 53
48	3.7	Clay schales & limestones & moraines	40000	35 - 56	35 - 48
49	2.8	Clay schales & limestones & moraines	15000	34 - 48	39 - 56
50	3.7	Clay schales & limestones & moraines	30000	45 - 51	42 - 53
51	3.7	Clay schales & limestones & moraines	20000	45 - 60 - 47	41 - 60 - 57

Appendices

52	3.9	Clays & cagneules & moraines	40000	61 - 70	56 - 71
53	3.9	Clays & cagneules & moraines	50000	60 - 72	72 - 81
54	2.6	Clays & cagneules & moraines	10000	65 - 79 - 68	78 - 96 - 81
55	3.9	Clays & cagneules & moraines	25000	80 - 85	101 - 127
56	3.2	Fined grained marls	40000 - 50000	85 - 90	60 - 81
57	3.2	Fined grained marls	50000	70 - 78	62 - 92
58	2.5	Fined grained marls	15000	62 - 74 - 72	58 - 67 - 66
59	3.2	Fined grained marls	40000	69 - 81 - 70	54 - 62 - 62
60	7	Clay shales & schistoses	60000	78 - 92	79 - 91
61	7	Clay shales & schistoses	15000	65 - 81	86 - 95
62	7	Clay shales & schistoses	12000	60 - 78	65 - 81
63	7	Clay shales & schistoses	6000	71 - 79 - 72	69 - 89 - 67
64	3.1	Clay shales	25000	74 - 79	86 - 103
65	6.8	Clay schales & limestones & moraines	10000 - 15000	56 - 70	101 - 132
66	6.8	Clay schales & limestones & moraines	45000	54 - 62	105 - 116
67	4.2	Clay schales & limestones & moraines	15000 - 20000	57 - 61	81 - 97
68	4.7	Clay schales & limestones & moraines	20000	49 - 59	79 - 92
69	6.8	Clay schales & limestones & moraines	50000	60 - 64	75 - 105
70	6.8	Clay schales & limestones & moraines	20000 - 25000	48 - 54	102 - 119
71	6.8	Clay schales & limestones & moraines	12000	54 - 61 - 57	72 - 89 - 79
72	3.1	Clay schales & limestones & moraines	6000	50 - 71	74 - 96
73	2.9	Clay schales & limestones & moraines	5000	51 - 64	84 - 106
74	4.1	Clay schales & limestones & moraines	20000 - 25000	62 - 74 - 63 - 67	78 - 96 - 89 - 91
75	6.6.	Clay shales & schistoses	180000	36 - 39	45 - 61
76	6.6	Clay shales & schistoses	350000	32 - 44	62 - 71
77	6.6	Clay shales & schistoses	300000	41 - 52 - 51	46 - 73 - 67
78	6.6	Clay shales & schistoses	35000	35 - 39 - 35	35 - 55 - 46
79	4.5	Clays-shales & Sandstones & Moraine	100,000	22 - 35	13 - 25
80	3.8	Clays-shales & Sandstones & Moraine	70,000	33 - 47	20 - 43
81	2.8	Clay-shales & sandstones	15000	35 - 39	26 - 39
82	12	Lahar -Volcanic	1600000	60	45
83	12	Lahar -Volcanic	1600000	500	45
84	12	Lahar -Volcanic	1600000	130	210
85	12	Lahar -Volcanic	1600000	240	810
86	12	Lahar -Volcanic	1600000	4794	958
87	12	Lahar -Volcanic	1600000	38	2.1
88	1.375	Sandstones and lutites	10,000	450	750
89	8.461	Gneiss/schist	21,000,000	300000	40000
90	0.15	Gneiss/schist	24000	2500	525

91	0.215	Clay-shales/sandstones	11000	400	67
92	1.9	Pyroclastic material	6,500	1000	800
93	1.9	Pyroclastic material	14,800	800	400
94	2.6	Quartzites/calcareous dep./dolomites	35,000	100	130
95	2.185	Pyroclastic material	6,400	200	3200
96	1.95	Sandstone/shale	740,000	2000	5000
97	0.774	Dolomites	9,000	218	88
98	0.45	Man-made slope	550	150	400
99	1.295	Granites/plutonic rocks	750	240	1000
100	1.459	Granites/plutonic rocks	750	150	800
101	0.644	Granites/plutonic rocks	750	300	1000
102	3.46	Pyroclastic tuff	1,080,000	1800	1000
103	0.98	Dolomite	1,200,000	2000	1000
104	3.5	Dolomite	18,000	400	1500
105	3.5	Dolomite	18,000	240	900

Appendix 2

MassMov2D with entrainment Model

2.1) Model theory

MassMov2D is implemented in the PCRaster environmental modeling language (Wesseling *et al.*, 1996; Karszenberg *et al.*, 2001) and based on the classical Savage-Hutter theory (Savage and Hutter, 1989), which assumes a one-phase homogeneous material with rheological properties. The flow was modeled as a 2-D continuum medium using a depth integrated approximation of the flow dynamics equations. Contrary to depth-integrated models that use a local reference frame linked to the topography, the equations governing MassMov2D are referenced in a 2-D Euclidean space with Cartesian coordinates x , y . The mass (Eq. 1) and momentum (Eq. 2) balance equations were developed with a new state variable h_s , representing the thickness of the soil and regolith base (m), and added to the mass and momentum equations (Begueria *et al.*, 2009).

$$\frac{\partial h}{\partial t} + c_x \frac{\partial(hu)}{\partial x} + c_y \frac{\partial(hv)}{\partial y} - \frac{\rho_s}{\rho} \frac{\partial h_s}{\partial t} = 0 \quad (1)$$

$$\begin{aligned} \frac{\partial u}{\partial t} + c_x u \frac{\partial u}{\partial x} + c_y v \frac{\partial u}{\partial y} &= -c_x g \left(S_x + k \frac{\partial(c_x h)}{\partial x} + S_f q_x \right) - \frac{u}{h} \frac{\partial h_s}{\partial t} \\ \frac{\partial v}{\partial t} + c_y v \frac{\partial v}{\partial x} + c_x u \frac{\partial v}{\partial y} &= -c_y g \left(S_y + k \frac{\partial(c_y h)}{\partial y} + S_f q_y \right) - \frac{v}{h} \frac{\partial h_s}{\partial t} \end{aligned} \quad (2)$$

where h is the flow thickness in the direction normal to the bed; (u,v) are the x and y components of the velocity vector along the bed; the coefficients $c_x = \cos\alpha_x$ and $c_y = \cos\alpha_y$ are the direction cosine of the bed (geometry factors to correct from local to global reference systems); and α_x and α_y are the values of the angle between the bed and the horizontal plane in the x and y directions, which take a negative value if the down slope direction is towards positive x and y , respectively. The ratio between the soil and flowing mass

densities is determined by $\frac{\rho_s}{\rho}$. The term $\frac{\partial h_s}{\partial t}$ is the entrainment rate due to scouring, and it affects both the mass and the momentum equations. The mass balance equation for h_s can be calculated in a number of different ways. In MassMov2D it is made proportional to the flow momentum (Eq.3):

$$\frac{\partial h_s}{\partial t} = E h \sqrt{u^2 + v^2} \quad (3)$$

where E is an average entrainment rate which can be approximated from observational data as (McDougal and Hungr 2004) (Eq.4):

$$E_s = \frac{1}{S} \ln \left(\frac{V_f}{V_o} \right) \quad (4)$$

where V_o and V_f are respectively the volume of the flowing mass before and after entrainment and S is the approximate average path length of the entrainment zone.

The momentum equation is expressed in terms of acceleration, where g is the acceleration due to gravity. The second and third terms on the left side of Eq. (2) represent the convective acceleration, i.e. the time rate of change due to change in position in the spatial field. The right side of the equation represents the local or time acceleration, expressing the time rate of change at a fixed position. The first term between the brackets represents the acceleration due to gravity, and $S_x = \tan\alpha_x$ and $S_y = \tan\alpha_y$ are the bed slope gradient in the x and y directions, respectively. The spatial derivative in the second term is the pressure acceleration, i.e. the time rate of change due to pressure differences within the flow. S_f is the flow resistance gradient, which accounts for momentum dissipation within the flow due to frictional stress with the bed. The term k in Eq. (2) is the earth pressure coefficient, i.e. the ratio between the tangential and normal stresses. It has a value of 1 for a perfect fluid, but can vary greatly for plastic materials (Savage and Hutter,

1989) and ranges between two extreme values corresponding to the active and passive states in the Rankine theory (Eq. 5):

$$\begin{aligned} K_a &= \frac{1 - \sin \phi}{1 + \sin \phi} \\ K_p &= \frac{1 + \sin \phi}{1 - \sin \phi} \end{aligned} \quad (5)$$

The flow term Sf in Eq. (2) represents the bed shear stress of the flow. This variable describes the rheological properties of the flow, which control flow behavior. The model defined by Eqs. (1) and (2) is therefore valid for different types of flows, depending on the formulation of Sf . Two different rheology laws are implemented inside MassMov2D: a Coulomb-viscous rheology (Eq. 6) and the Voellmy rheology (Eq. 7).

$$Sf = g \tan \phi' + \frac{1}{\rho h} \left(\frac{3}{2} \tau_c + \frac{3\eta}{h} u \right) \quad (6)$$

where ρ is the material density; u is the internal pore fluid pressure; ϕ' is the basal friction angle of the flow; g is the gravitational force; τ_c is a constant yield strength due to cohesion; and η is the viscosity of the flow which is related to the percent concentration of solids (Begueria et al., 2009).

$$Sf = g \left(\tan \phi' + \frac{U^2}{\xi h} \right) \quad (7)$$

where, Sf is the unit base resistance, g is the gravitational acceleration, ϕ' is the apparent friction angle, U is the flow velocity, h is the flow thickness and ξ is the turbulent coefficient. The parameters μ and ξ are constants whose magnitudes depend, respectively, on the flow properties and the roughness of the flow surface.

2.2) Numerical solution method

The model was implemented in an explicit finite difference (Eulerian) mesh, i.e. the flow was described by variation in the conservative variables at points of fixed coordinates (i, j) as a function of time (n). The mesh is defined as a regular grid with size $s = \Delta x = \Delta y$, in accordance with the grid format common to most GIS platforms. Equations (11) and (12) are written in more compact vector notation, in order to describe the numerical solution (Eq.8) and solved numerically using a central difference forward scheme (Eq.9).

$$\frac{\partial}{\partial t}(w) + k_1 \frac{\partial}{\partial x} f + k_2 \frac{\partial}{\partial y} g + k_3 (q - s) = 0 \quad (8)$$

$$w_{i,j}^{n+1} = W(w_{i,j}^n) - \Delta \left(k_{1i,j}^n (f_{i+1,j}^n - f_{i-1,j}^n) + k_{2i,j}^n (g_{i,j+1}^n - g_{i,j-1}^n) + k_{3i,j}^n (q_{i,j}^n + s_{i,j}^{n+1/2}) \right) \quad (9)$$

where Δt is the time step duration (s), and the pressure gradient term in q is computed by central differences.

An underlying assumption of the finite difference solution is that of continuity and smoothness of the spatial domain. Although this generally holds true, in some cases the basal topography presents horizontal discontinuities or singularities such as channels (artificial or natural), which are very relevant to the correct simulation of the flow. Such structures can not be adequately represented in a finite differences mesh, as the central difference scheme requires a continuous surface. Specification of topographical discontinuities was incorporated into the model such that they are treated as no-flow boundaries unless the flow thickness becomes larger than the difference in height at both sides of the discontinuity. Whenever this occurs, flow is automatically allowed between the two sides of the topographical discontinuity by applying Eq. (19) to the fraction of h that exceeds the height of the obstacle (Begueria *et al.*, 2009)

2.3) Model requirements

The model requires four input files in form of DEM (digital elevation models) comprising the topography of the bed, the soil depth of the terrain and the locations of the inlet and outlet cells. The DEM defines not only the basal boundary of the flow, but also the spatial computation domain and the mesh size. These files have to be converted into raster maps to be linked together in the PCRaster environment. In addition to these maps, the model requires specification of the input discharge at the cells defined in the inlet map during the simulation time. This can be set either as a constant inflow rate for a specified time interval or as a transient flow by creating a text file containing three columns that indicate the time variation of the state variables (h , u , v) at the inlet. MassMov2D requires model parameter for the respective rheological parameter that have been chosen, either ϕ' , τ_c and η for the coulomb-viscous models; or μ and ξ for the Voellmy-fluid type. The erosion rate is also need when simulating the ersoion process.

Appendix 3

DAN3D Model

DAN3D model is implemented using a numerical method adapted from smoothed particle hydrodynamics (McDougall and Hungr, 2005). The model features include:

- (i) the ability to simulate flow across complex three-dimensional terrain;
- (ii) the ability to allow non-hydrostatic and anisotropic internal stress distributions, coupled with strain changes through frictional relationships;
- (iii) the ability to simulate material entrainment;
- (iv) a choice of different rheological kernels (at the moment including frictional- and Voellmy-type);

- (v) a meshless solution, which eliminates problems with mesh distortion during long displacements

3.1) Model theory

The 2-dimensional set of governing equations is

$$\frac{\partial h}{\partial t} + h \frac{\partial u_x}{\partial x} + \frac{\partial u_y}{\partial y} = \frac{\partial b}{\partial t} \quad (1)$$

$$\rho h \frac{\partial u_x}{\partial t} = \rho h g_x + k_x \sigma_z \left(\frac{\partial h}{\partial x} \right) + k_{yx} \sigma_z \left(-\frac{\partial h}{\partial y} \right) + \tau_{zx} - \rho u_x \frac{\partial b}{\partial t} \quad (2)$$

$$\rho h \frac{\partial u_y}{\partial t} = \rho h g_y + k_y \sigma_z \left(\frac{\partial h}{\partial y} \right) + k_{xy} \sigma_z \left(-\frac{\partial h}{\partial x} \right) + \tau_{zy} - \rho u_y \frac{\partial b}{\partial t} \quad (3)$$

where

- h is the flow height,
- u_x velocity component in x-direction,
- u_y velocity component in y-direction,
- g gravitational acceleration,
- k_x, k_y, k_{xy}, k_{yx} , tangential stress coefficients, dependent on the tangential strain state,

$$\sigma_z = \rho h \left(g \cos \varphi + \frac{u^2}{r} \right)$$

is the normal stress r the radius of the track and \bar{u} the depth-averaged speed,

$$\frac{\partial b}{\partial t} = E h \bar{u}$$

is the erosion rate, E is an empirical constant.

Bed entrainment is simulated after defining an entrainment zone, a maximum depth of supply material and an average growth or erosion rate, E_s , defined as:

$$E_s = \frac{\ln \left(\frac{V_f}{V_o} \right)}{S}$$

where V_o and V_f are respectively the estimated total volume of the flowing mass before and after entrainment and S is the approximate average path length of the entrainment zone.

Two rheological kernels implemented for the shear stresses τ_{zx}, τ_{zy}

(i) Coulomb friction type

$$\tau_{zi} = -\frac{u_i}{|u|} \sigma_z \tan \phi_b, \quad (\phi_b \text{ is the bed friction angle})$$

(ii) Voellmy fluid type

$$\tau_{zi} = -\left(\sigma_z f + \frac{\rho g u_i^{-2}}{\xi} \right), \quad f (\tan \phi_b) \text{ and } \xi \text{ are friction parameters.}$$

3.2) Numerical solution method

The model uses a meshless interpolation technique, based on Smoothed Particle Hydrodynamics (SPH), which satisfies continuity implicitly. The total volume of the slide mass is divided into a number of elements, known as “smooth particles.” Each particle has a finite volume, which may only increase due to entrainment, and remains centered at one of the moving reference columns. Since the density of the material is assumed constant, the flow depth at each reference column location is proportional to the volume of material in the area, which is given by the proximity of nearby particles. Thus, the flow depth at reference column i can be estimated using the summation interpolant (Wang and Shen 1999):

$$h_i = \sum_{j=1}^N V_j W_{ij} \quad (4)$$

where W_{ij} is an interpolating kernel (weighting factor for proximity) and V_j is the volume of particle j . Figure 1 gives an illustration of this procedure. Other parameters are calculated in a similar manner (McDougall and Hungr, 2004).

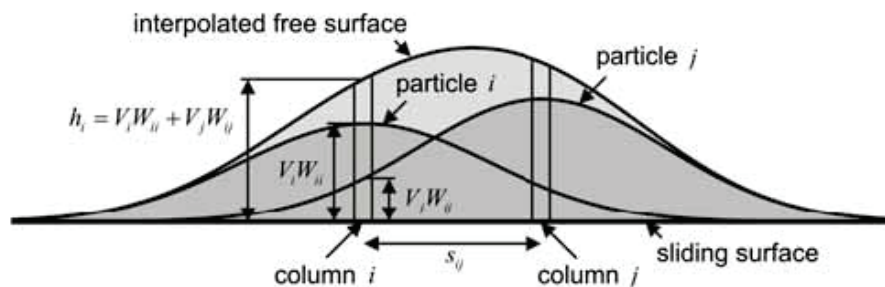


Figure.1: A physical interpretation of SPH in a depth-averaged framework (McDougall and Hungr, 2004). When the interpolating kernel is Gaussian, the particles can be visualized as bell-shaped objects. The total depth and depth gradient at any location are determined by superposition of the particles.

1.3) Model requirements

Both input and output of DAN3D is in the form of three-dimensional surfaces. All the files are defined on the same rectangular grid, described by an origin, a grid spacing and a number of grid points in the x and y direction. Three input are necessary: -*Path surface DTM*: a grid file describing the ground surface in the problem area, with the slide material removed and the rupture surface exposed. It can be constructed by subtracting the source thickness file from the DTM of the area before the slide. - *Source thickness file*: In the source area, this represents the difference in elevations of the grid between the ground surface before and after the slide. In the deposition area, the source thickness file must be zero. There must be no negative values. - *Erosion thickness file*: If no entrainment is specified, this must be a zero grid. Otherwise, entrainment areas have values corresponding to the prescribed entrainment depth. These areas can extend outside the prospective landslide path. Entrainment will occur only where the area is over-run by the slide.

The model requires model parameter for the respective rheological parameter, i.e. either ϕ_b for the Coulomb type friction model or f and ξ for the Voellmy-fluid type. If erosion is enabled also an parameter for the erosion rate is needed.

Appendix 4

The RAMMS model

The RAMMS model is a generalization of the quasi one-dimensional model as discussed by Bartelt *et al.* (1999). RAMMS uses the Voellmy-Salm fluid flow continuum model (Salm, 1993) based on the Voellmy-fluid flow law and describes the debris flow as a hydraulic-based depth-average continuum model. The flow resistance is divided into a dry-Coulomb friction and a viscous resistance turbulent friction as will be explained in the next section. RAMMS further contains an entrainment model discussed by Sovilla *et al.* (2006). The model solves the governing mass and momentum equations using a second-order, cell-centered, positivity conserving HLLC (Harten, Lax, van Leer and Einfeldt) finite volume scheme, which is a numerical method to solve a Riemann problem (Christen *et al.*, 2010) Time integration within the model is given by the Runge-Kutta-Heun method (Christen *et al.*, 2010) which is an extension of the Euler's method into a two-stage Runge-Kutta method and is a numerical procedure for approximating differential equations.

The RAMMS environment is based on three dimensions: x and y are the directions of the mass movement flowing down the surface and the elevation

is given by $z(x,y)$ which is perpendicular to the profile. Based on this three component coordinate system used on the surface, the gravitational acceleration vector in the three directions is $g=(g_x,g_y,g_z)$ and the time component is defined as t (Christen *et al.*, 2010). RAMMS moves the flow in an unsteady and non-uniform motion and is characterized by two main flow parameters which are the flow height $H(x,y,t)$ (m) and the mean velocity $U(x,y,t)$ (m/s) (Christen *et al.*, 2010):

$$U(x,y,t)=(U_x(x,y,t),U_y(x,y,t))^t \quad (1)$$

where U_x and U_y are the velocities in the x and y directions respectively, and T is used to transpose the matrix of the mean velocity. The magnitude of the velocity is given by:

$$\|U\| = \sqrt{U_x^2 + U_y^2} \quad (2)$$

where the double lines ($\|\cdot\|$) indicate the norm on the velocity U , making it a strictly positive velocity with a certain size in a vector space, which is the Cartesian coordinate system. The direction of the flow velocity is given by a unit vector :

$$\eta_u = \frac{1}{\|U\|} (U_x, U_y)^T \quad (3)$$

The Voellmy-Salm model uses the following mass balance equation:

$$\partial_t H + \partial_x (HU_x) + \partial_y (HU_y) = Q(x, y, t) \quad (4)$$

where H is the flow height (m) and $Q(x,y,t)$ ($\text{kg}/\text{m}^2\text{s}$) is the mass production source term, also called the entrainment rate ($Q>0$) or deposition rate ($Q<0$) (Christen *et al.*, 2010). $Q = 0$ if there is neither entrainment nor deposition of mass. The depth-averaged momentum balance equations in the x and y directions are respectively given by:

$$\partial_t (HU_x) + \partial_x \left(c_x HU_x^2 + g_z k_a \frac{H^2}{2} \right) + \partial_y (HU_x U_y) = S_{gx} - S_{fx} \quad (5)$$

and

$$\partial_t(\mathbf{H}\mathbf{U}_y) + \partial_y\left(c_y\mathbf{H}\mathbf{U}_y^2 + g_z k_{\frac{a}{p}} \frac{\mathbf{H}^2}{2}\right) + \partial_x(\mathbf{H}\mathbf{U}_x\mathbf{U}_y) = S_{gy} - S_{fy} \quad (6)$$

where C_x and C_y are profile shape factors and g_z is the gravitational acceleration in the vertical direction. The vertical information within the Voellmy-Salm model is given by an anisotropic Mohr-Coulomb relation, using the earth pressure coefficient as a proportionality factor for the vertical and normal stresses (Christen *et al.*, 2010). The earth pressure coefficient is given by the following equation:

$$k_{\frac{a}{p}} = \tan^2\left(45^\circ \mp \frac{\varphi}{2}\right) \quad (7)$$

where φ (degrees) is the angle of internal friction of the debris flow. The earth pressure coefficient can be either active:

$$k_{\frac{a}{p}} = \tan^2\left(45^\circ - \frac{\varphi}{2}\right) \quad (8)$$

where the flow is dilatant and contracting causing an increase in the change of the velocity ($\nabla \cdot \mathbf{U} \geq 0$), or passive:

$$k_{\frac{a}{p}} = \tan^2\left(45^\circ + \frac{\varphi}{2}\right) \quad (9)$$

where the flow is compressive and the change in velocity of the flow decreases ($\nabla \cdot \mathbf{U} < 0$). The earth pressure coefficient in the RAMMS software is given the name "Lambda", which is the name that will be further used in this thesis. The right hand side of Equations 8 and 9 give the effective accelerations, and are noted as:

$$S_{gx} = g_x H \quad (10)$$

and

$$S_{gy} = g_y H \quad (11)$$

where S_{gx} and S_{gy} are the driving gravitational accelerations in the x and y directions, respectively. Equations 8 and 9 further contain on the right hand side frictions that add up to a total friction (Sf):

$$S_f = (S_{fx}, S_{fy})^T \quad (12)$$

where S_{fx} and S_{fy} are the frictions in the x and y directions respectively and are given by:

$$S_{fx} = \eta_{U_x} \left[\mu g_z H + \frac{g \|U\|^2}{\xi} \right] \quad (13)$$

and

$$S_{fy} = \eta_{U_y} \left[\mu g_z H + \frac{g \|U\|^2}{\xi} \right] \quad (14)$$

where η_{ux} and η_{uy} are the velocity directional unit vectors in the x and y directions respectively. The total basal friction in the Voellmy-Salm model is split into a velocity independent dry-Coulomb friction coefficient μ (Mu) and a velocity dependent turbulent friction coefficient ξ (Xi) (m/s^2) (Christen *et al.*, 2010). For the sake of simplicity μ is named the “friction coefficient” and ξ the “turbulent coefficient”.

RAMMS uses a rate-controlled entrainment method which regulates the mass being up taken by the incoming debris flow and regulates the time delay to accelerate this mass to the debris flow velocity. The entrainment rate $Q(x,y,t)$ is given by (Christen *et al.*, 2010)

$$Q(x, y, t) = \begin{cases} 0 & \text{for } \left[h_s(x, y, 0) - \int_0^t Q(x, y, t) dt \right] = 0 \\ \frac{\rho_i^s}{\rho} K_i U & \text{for } \left[h_s(x, y, 0) - \int_0^t Q(x, y, t) dt \right] > 0 \end{cases} \quad (15)$$

where ρ (kg/m^3) is the density of the initiated debris flow, τ is the shear stress and $h_s(x, y, 0)$ (m) is the initial height of the entrainment layer given by the total height of the debris cover at position (x,y) and time $t=0s$. The total height of the entrainment layer in RAMMS can be divided into three separate entrainment layers: $i \{1,2,3\}$, Finally, K_i is the dimensionless entrainment coefficient for each layer. However, if a single entrainment layer is chosen, K_i can be simply defined as K .

Appendix 5

FLO-2D model

FLO-2D is a Eulerian two-dimensional finite difference model that is able to route non-Newtonian flows in a complex topography based on a volume conservation model. The flow volume is routed through a series of tiles that simulates overland flow (2D flow), or through line segments for channel routing (1D flow). Flow in two dimensions is accomplished through a numerical integration of the equations of motion and the conservation of fluid volume.

The governing equations -originally presented by O'Brien *et al.*, (1993) - are the continuity equation

$$\frac{\partial h}{\partial t} + \frac{\partial h V_x}{\partial x} + \frac{\partial h V_y}{\partial y} = i \quad (1)$$

and the two-dimensional equations of motion

$$S_{fx} = S_{ox} - \frac{\partial h}{\partial x} - \frac{V_x}{g} \frac{\partial V_x}{\partial x} - \frac{V_y}{g} \frac{\partial V_x}{\partial y} - \frac{I}{g} \frac{\partial V_x}{\partial t} \quad (0)$$

$$S_{fy} = S_{oy} - \frac{\partial h}{\partial y} - \frac{V_y}{g} \frac{\partial V_y}{\partial y} - \frac{V_x}{g} \frac{\partial V_y}{\partial x} - \frac{I}{g} \frac{\partial V_y}{\partial t} \quad (3)$$

in which h is the flow depth and V_x and V_y are the depth-averaged velocity components along the horizontal x- and y-coordinates. The excess rainfall intensity (i) may be nonzero on the flow surface. The friction slope components S_{fx} and S_{fy} are written as function of bed slope S_{ox} and S_{oy} , pressure gradient and convective and local acceleration terms.

FLO-2D software models the shear stress as a summation of five shear stress components: the cohesive yield stress, the Mohr-Coulomb shear, the viscous shear stress, the turbulent shear stress and the dispersive shear stress. All these components can be written in terms of shear rates giving a quadratic rheological model function of sediment concentration, adding a turbulent and dispersive term to the Bingham equation (FLO-2D Users Manual, 2007).

The depth-integrated rheology is expressed (after dividing the shear stresses by the hydrostatic pressure at the bottom of the flow $\gamma_m h$) as:

$$S_f = \frac{\tau_y}{\gamma_m h} + \frac{K \eta V}{8 \gamma_m h^2} + \frac{n_{td}^2 V^2}{h^{4/3}} \quad (4)$$

where S_f is the friction slope (equal to the shear stress divided by $\gamma_m h$); V is the depth-averaged velocity; τ_y and η are the yield stress and viscosity of the fluid, respectively, which are both a function of the sediment concentration by volume; γ_m is the specific weight of the fluid matrix; K is a dimensionless resistance parameter that equals 24 for laminar flow in smooth, wide, rectangular channels, but increases with roughness and irregular cross section geometry; and n_{td} is an empirically modified Manning n value that takes into account the turbulent and dispersive components of flow resistance.

The Bingham parameters τ_y and η are defined as exponential functions of sediment concentration which may vary over time. The resistance coefficient n accounts for both for collisional (inertial grain shear) and turbulent frictional losses. The friction slope is determined separately for both orthogonal flow directions.

The yield stress, the viscosity, and the empirically modified Manning n value are calculated as follows:

$$\tau_y = \alpha_1 e^{\beta_1 C_v} \quad (5)$$

$$\eta = \alpha_2 e^{\beta_2 C_v} \quad (6)$$

$$n_{td} = n_t b e^{m C_v} \quad (7)$$

where α_1 , β_1 , α_2 , and β_2 are empirical constants, C_v is the fine sediment concentration (silt- and clay-size particles) by volume of the fluid matrix, n_t is the turbulent n -value, b is a coefficient (0.0538) and m is an exponent (6.0896).

The differential equations of motion are solved using a central difference scheme. The boundary conditions are specified as follows: the inflow condition is defined in one or more upstream grid elements with a hydrograph (water discharge vs. time) and values of C_v for each point in the hydrograph; the outflow condition is specified in one or more downstream grid elements. Time steps vary according to the Courant-Friedrich-Lewy stability condition.

The model requires the specification of the terrain surface as a uniformly spaced grid. Within the terrain surface grid, a computational grid, i.e. a domain for the calculations, must be specified. The Manning n values should be assigned to each grid element to account for the hydraulic roughness of

the terrain surface. The values can be spatially variable to account for differences in surface coverage.

ITC Dissertation List

http://www.itc.nl/Pub/research/Graduate-programme/Graduate-programme-PhD_Graduates.html